TNT 2013
Trends in NanoTechnology

September 09-13, 2013
Seville (Spain)

Abstracts

Verios™ XHR SEM

Discover the world of Extreme High Resolution SEM

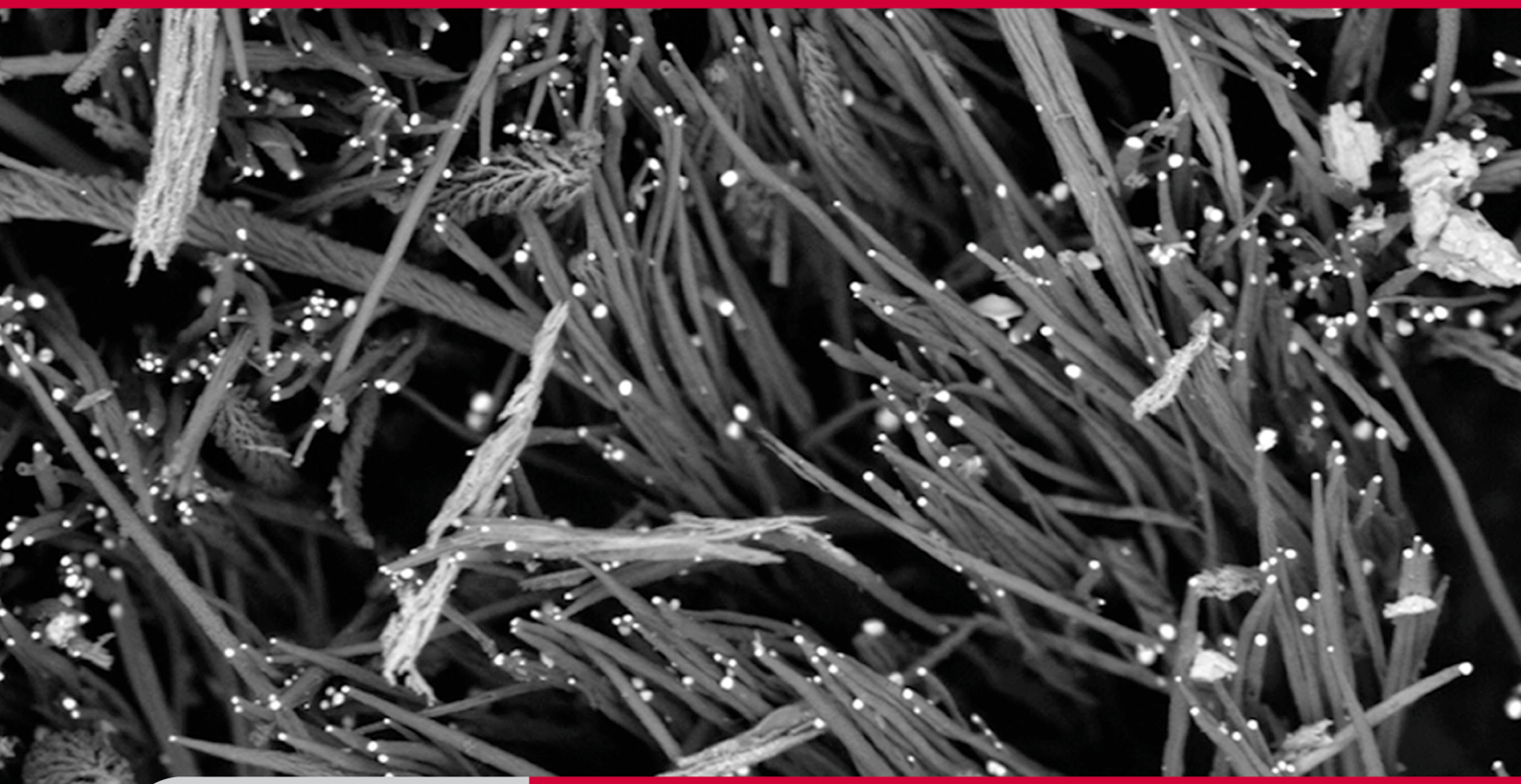

The Verios is the second generation of FEI's leading XHR SEM family. It offers sub-nanometer resolution over the full 500 eV to 30 keV energy range with excellent materials contrast. The Verios' extraordinary low-voltage performance provides extremely precise, surface-specific information that has been previously unavailable from other techniques.

Learn more at FEI.com/Verios

High resolution SEM with excellent materials contrast to visualize the catalyst particles on top of each nanotube. Horizontal field width 14 µm. *Sample courtesy of ICN.*

FEI™ Explore. Discover. Resolve.

TNT2013 index

Image credit: Experimental deep-subwavelength imaging of the optical local density of state in a nanostructured photonic membrane. Riccardo Sapienza (Kings College, London, UK)

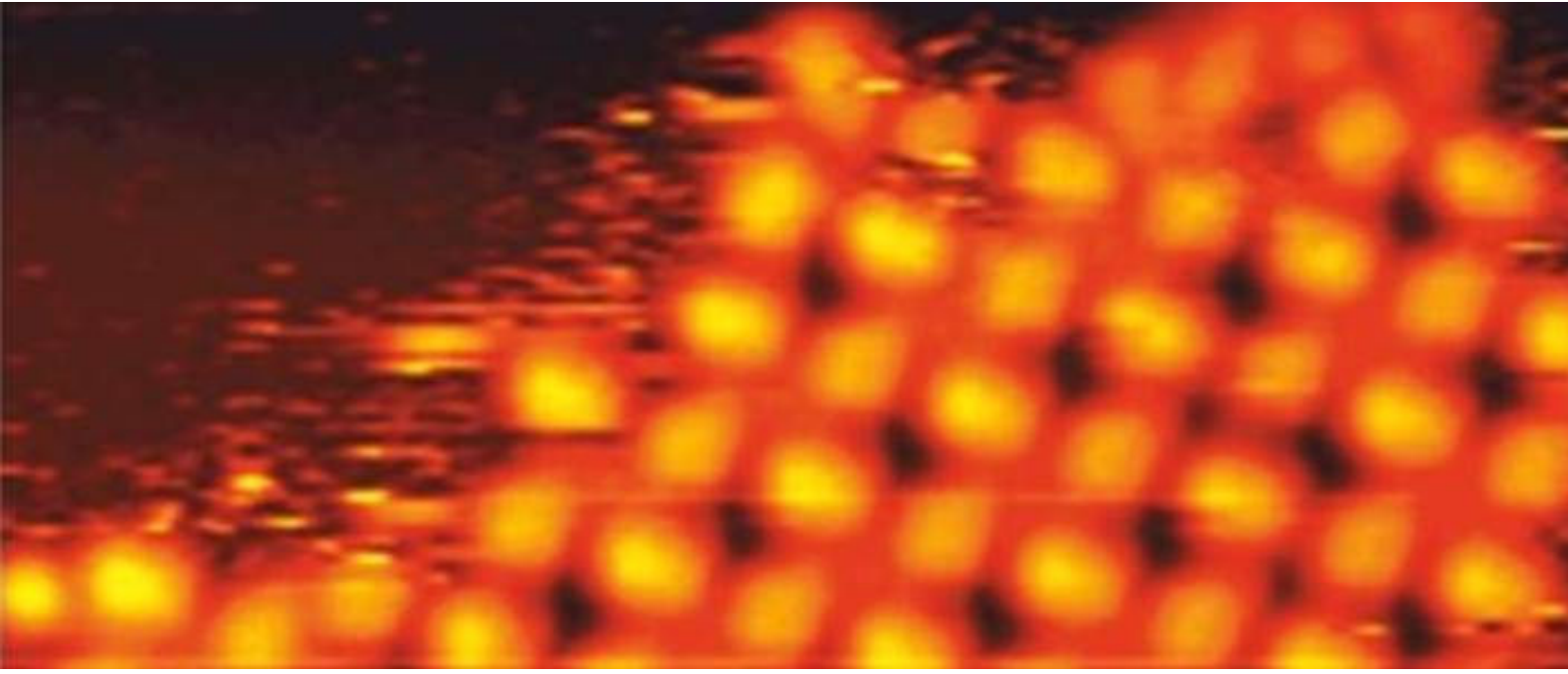

On behalf of the International, Local and Technical Committees, we take great pleasure in welcoming you to Seville (Spain) for the 14th "Trends in NanoTechnology" International Conference (TNT2013).

TNT2013 is being held in large part due to the overwhelming success of earlier TNT Nanotechnology Conferences.

This high-level scientific meeting series aims to present a broad range of current research in Nanoscience and Nanotechnology worldwide, as well as initiatives such as EU/ICT/FET, MANA, CIC nanoGUNE Consolider, IBEC, DIPC, etc. TNT events have demonstrated that they are particularly effective in transmitting information and promoting interaction and new contacts among workers in this field. Furthermore, this event offers visitors, exhibitors and sponsors an ideal opportunity to interact with each other.

In particular, this year, a Graphene one-day Symposium will be organized within TNT2013 in collaboration with ICN2 (Spain).

The Graphene Day will entail a plenary session during the morning and the afternoon session will be divided in track A (Graphene science driven oral contributions) and track B (Graphene driven applications Keynotes & Graphene Flagship dedicated session).

One of the main objectives of the Trends in Nanotechnology conference is to provide a platform where young researchers can present their latest work and also interact with high-level scientists. For this purpose, the Organising Committee provides every year around 40 travel grants for students. In addition, this year, 7 awards (1400 Euros in total) will be given to young PhD students for their contributions presented at TNT. More than 40 senior scientists are involved in the selection process. Grants and awards are funded by the TNT Organisation in collaboration with private bodies and several governmental/research institutions.

TNT is now one of the premier European conferences devoted to nanoscale science and technology.

We are indebted to the following Scientific Institutions, Companies and Government Agencies for their financial support: Phantoms Foundation, Donostia International Physics Center (DIPC), Universidad Autónoma de Madrid (UAM), NIMS (Nanomaterials Laboratory) and MANA (International Center for Materials and Nanoarchitectonics), Institute for Bioengineering of Catalonia (IBEC), Institut Català de Nanociencia I Nanotecnologia (ICN2), Materials Physics Center (CFM), FEI, American Elements, European Physical Society (EPS), Thermo Scientific, AtMol Integrated Project (EU/ICT/FET) and Viajes El Corte Inglés.

We would also like to thank the following companies and institutions for their participation: Raith, IOP Publishing and Institut Català de Nanociencia I Nanotecnologia (ICN2).

In addition, thanks must be given to the staff of all the organising institutions whose hard work has helped planning this conference.

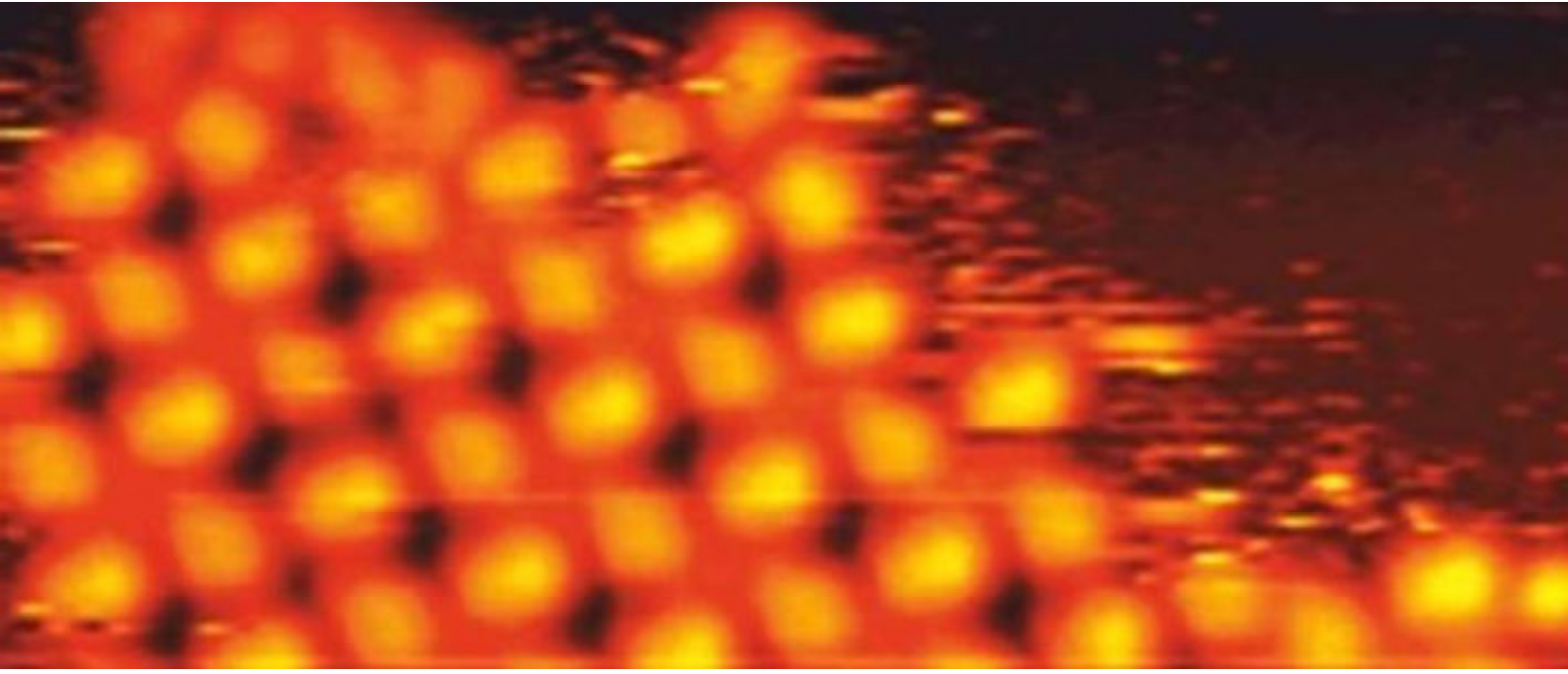

Image credit: STM image of the self-assembled structure obtained by depositing DCNQI molecules with the substrate held at 120 K. Roberto Otero (IMDEA-Nano, Spain)

TNT2013 Organising Committee

TNT2013 Committees

Organising Committee

Jose-Maria Alameda (Universidad de Oviedo, Spain)
Masakazu Aono (MANA, NIMS, Japan)
Robert Baptist (CEA / DRT / LETI, France)
Xavier Cartoixa (UAB, Spain)
Antonio Correia (Phantoms Foundation, Spain) – Conference Chairman
Gianaurelio Cuniberti (TUD, Germany)
Pedro Echenique (DICP / UPV, Spain)
Jose Maria Gonzalez Calbet (UCM, Spain)
Uzi Landman (Georgia Tech, USA)
Jose Manuel Perlado Martin (IFN-ETSII / UPM, Spain)
Jose Maria Pitarke (CIC nanoGUNE Consolider, Spain)
Ron Reifenberger (Purdue University, USA)
Jose Rivas (INL, Portugal)
Juan Jose Saenz (UAM, Spain)
Josep Samitier (IBEC - Universitat de Barcelona, Spain)
Frank Scheffold (University of Fribourg, Switzerland)
Didier Tonneau (CNRS-CINaM, France)

International Scientific Committee

Masakazu Aono (MANA / NIMS, Japan)
Emilio Artacho (CIC nanoGUNE Consolider, Spain)
Andreas Berger (CIC nanoGUNE Consolider, Spain)
Fernando Briones (IMM / CSIC, Spain)
Remi Carminati (Ecole Centrale Paris, France)
Jose-Luis Costa Kramer (IMM / CSIC, Spain)
Antonio Garcia Martin (IMM / CSIC, Spain)
Raquel Gonzalez Arrabal (IFN-ETSII / UPM, Spain)
Pierre Legagneux (Thales, France)
Annick Loiseau (ONERA - CNRS, France)
Stefan Roche (ICN and CIN2, Spain)
Josep Samitier (IBEC - Universitat de Barcelona, Spain)

Technical Committee

Carmen Chacón Tomé (Phantoms Foundation, Spain)
Viviana Estêvão (Phantoms Foundation, Spain)
Maite Fernández Jiménez (Phantoms Foundation, Spain)
Paloma Garcia Escorial (Phantoms Foundation, Spain)
Pedro Garcia Mochales (UAM, Spain)
Adriana Gil (Nanotec, Spain)
Conchi Narros Hernández (Phantoms Foundation, Spain)
Joaquin Ramon-Laca (Phantoms Foundation, Spain)
Jose-Luis Roldan (Phantoms Foundation, Spain)

TNT2013 Poster awards

Funded by		Award
	European Physical Society	250 Euros
	Phantoms Foundation	Tablet
	Phantoms Foundation	Tablet
	Phantoms Foundation	Tablet
David Prize	Private donation	300 US Dollars
Keren Prize	Private donation	300 US Dollars
	TNT 2013 Organisation	Free registration to the 2014 Conference

TNT2013 Sponsors

TNT2013 Exhibitors

Raith is a leading provider and manufacturer of electron and ion beam lithography systems for nanofabrication. Founded in 1980 and headquartered in Dortmund, Germany, the company offers solutions for researchers and engineers in both academic and industry settings. With approximately 120 employees supporting customers in Europe, the Americas, Asia and the Pacific region, Raith provides a professional support infrastructure that delivers added value to customers. Raith includes high level universities, academic institutions as well as companies from high technology business among its clientele. For more information please visit www.raith.com

Effective February 15, 2013 Raith and Vistec Lithography announce that they unite their worldwide activities for electron and ion beam lithography and nanofabrication instruments to form one solution provider. Raith has agreed to acquire Vistec Lithography from private equity firm Golden Gate Capital.

Raith GmbH
Exhibit Contact: Andreas REMSCHEID
Konrad-Adenauer-Allee 8
44263 Dortmund- Germany
Phone: +49 (0)231 / 95004 - 0
Fax: +49 (0)231 / 95004 - 460
E-mail: sales@raith.com / remscheid@raith.de
Web: www.raith.com

Phantoms Foundation, based in Madrid, is a non-profit organization which focus its activities on Nanoscience & Nanotechnology (N&N), bringing together and coordinating the efforts of Spanish and European universities groups, research institutes and companies through the organization of major scientific and technological networks and events, such as ImagineNano or Graphene. Today, the Phantoms Foundation is a key player in structuring and promoting European excellence and improving collaborations in N&N. It is also essential as a platform for spreading excellence on funded projects and for establishing new networks of collaboration.

Web: www.phantomsnet.net

IOP Publishing provides publications through which leading-edge scientific research is distributed worldwide. Since launch we have expanded rapidly to become one of the leading international STM publishers. We have a global reach, with offices in Philadelphia, Washington DC, Mexico City, Munich, Moscow, St. Petersburg, Wroclaw, Beijing and Tokyo as well as Bristol and London in the UK

Web: http://publishing.iop.org/

The Catalan Institute of Nanoscience and Nanotechnology (ICN2) is a private foundation created on 11 July 2003 with the objective of becoming a world-renowned centre for nanoscience and nanotechnology research. It is part of CERCA, the network of Research Centres launched by the Catalan Government as a cornerstone of its long-term strategy to foster development of a knowledge-based economy.

ICN2's research lines focus on the newly discovered physical and chemical properties that arise from the fascinating behaviour of matter at the nanoscale.

Much of our work is devoted to studying and understanding fundamental physical phenomena associated to state variables as regards electrons, phonons, photons, plasmons, etc.; investigating new properties derived from tailored nanostructures; and establishing new processes for the conception and fabrication of new nanodevices.

This work enables functionalisation of nanoparticles, encapsulation of active agents and creation of new nanodevices and nanosensors, through frontier science that has direct implications for various sectors (health, food, energy, the environment, etc.).

Campus de la UAB,
Edifici ICN2 08193 Bellaterra, Spain
E-mail: info@icn2.cat
Web: www.icn.cat

TNT2013 Speakers

Index alphabetical order

TNT2013 Speakers

Keynotes

TNT2013 Speakers

Oral - Seniors (plenary session)

TNT2013 Speakers

Oral - Seniors (parallel session)

TNT2013 Speakers

Orals - PhD (parallel session)

Electrical and Mechanical Properties of Atomically Thin Layers of MoS_2

Nicolás Agraït, Andrés Castellanos and Gabino Rubio-Bollinger

Dpto. de Física de Materiales, Universidad Autónoma de Madrid, 28049 Madrid, Spain
Instituto Madrileño de Estudios Avanzados en Nanociencia (IMDEA-Nano), Madrid, Spain

nicolas.agrait@uam.es

Two-dimensional crystals are promising materials for next-generation flexible electronic devices. Although graphene is by far the most studied two-dimensional crystal, its lack of a bandgap hampers its application in semiconducting and photonic devices. A large bandgap is a requirement, for instance, to fabricate field-effect transistors with a large current on/off ratio and low power consumption. In contrast to graphene atomically thin MoS_2 crystals show a large intrinsic bandgap making it a potentially interesting material for electronic devices and sensors.

In this talk I will present our recent results on the mechanical and electrical properties of this material. In particular, we have studied the elastic properties of MoS_2 in freely suspended nanosheets, with thicknesses ranging from 5 to 25 layers using atomic force microscopy [1] and the electrostatic screening by single and few-layer MoS_2 sheets by means of electrostatic force microscopy [2].

References

[1] Andres Castellanos-Gomez, Menno Poot, Gary A. Steele, Herre S. J. van der Zant, Nicolás Agraït, and Gabino Rubio-Bollinger, Elastic Properties of Freely Suspended MoS2 Nanosheets, Adv. Mater. 24, (2012) 772–775.

[2] Andres Castellanos-Gomez, Emmanuele Cappelluti, Rafael Roldán, Nicolás Agraït, Francisco Guinea and Gabino Rubio-Bollinger, Electric field screening in atomically thin layers of MoS2: the role of interlayer coupling, Adv. Mater. 25, (2013) 899–903.

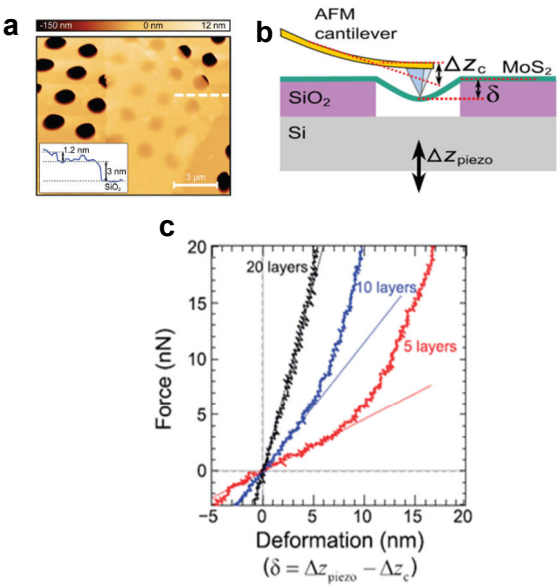

Figure 1. a) AFM topography of a 3-4.2-nm-thick (5-7 layers) MoS_2 flake deposited on top of a 285 nm SiO_2/Si substrate pre-patterned with an array of holes 1.1 µm in diameter. Inset: Topographic line profile acquired along the dashed line. b) Schematic diagram of the nanoscopic bending test experi¬ment carried out on a freely suspended MoS_2 nanosheet. c) Force versus deformation traces measured at the center of the suspended part of MoS_2 nanosheets with 5, 10, and 20 layers in thickness.

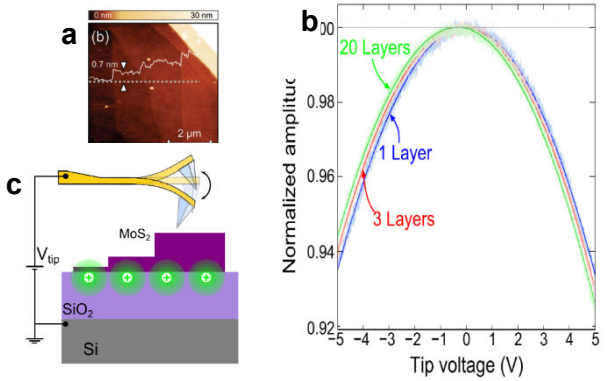

Figure 2. a) Topographic AFM image of the region studied showing regions of 1,2 and 3 layers. b) Normalized cantilever oscillation amplitude as a function of the applied tip-sample bias voltage, measured in the 3 regions. c) Schematic of the EFM measurement setup.

BioInspired Nanotechnology & High Speed AFM Instrumentation

Jean-Pierre Aimé

jp.aime@cnanogso.org

IECB-CBMN CNRS -University Bordeaux
Ave Geoffroy St Hilaire Bât 14 Pessac 33600 France

DNA based nanostructures built on a long single stranded DNA scaffold, known as DNA origamis, offer the possibility to organize various molecules at the nanometer scale in one pot experiments. The folding of the scaffold is guaranteed by the presence of short, single stranded DNA sequences (staples), that hold together separate regions of the scaffold. In this paper, we first consider simple structures made of three single-stranded oligonucleotides. Based on experimental (UV absorption) and numerical (replica exchange molecular dynamics simulations) data, we show that cooperativity is key to understand the thermodynamics of these constructions. In a second part, we derive a model of the annealing-melting properties of DNA origamis. The model captures important features such as the hysteresis between melting and annealing, as well as the dependence upon the topology of the scaffold. We also obtain temperature dependent average conformations that compare well to AFM images of quenched states of the partially folded origamis.

References

[1] “Nanoscale liquid interfaces” Edts T. Ondarçuhu & JP Aimé. 2013. 19 Chapters. http://www.amazon.com/Nanoscale-Liquid-Interfaces-Patterning-Microscopy/dp/9814316458

[2] “Cooperativity in the annealing of DNA origamis", JM Arbona, JP Aimé, J. Elezgaray. J. Chem. Phys. 138, 015105 (2013);

[3] “Modeling the mechanical properties of DNA nanostructures.” Jean Michel Arbona, Jean-Pierre Aimé, and Juan Elezgaray. PHYSICAL REVIEW E 86, 051912 (2012)

[4] “Modelling the folding of DNA origami. “ J. M. Arbona, J. Elezgaray and J. P. Aimé Eur. Phys. Let., 100 (2012) 28006

[5] “Direct Visualisation of Transient Thermal response of a DNA Origami” J. Song, J.M. Arbona, Z. Zhang, Lei Liu, E. Xie, J. Elezgaray, JP Aimé, K. V. Gothelf, F. Besenbacher, and M. Dong JACS 134, 9844-9847 (2012).

[6] “Carbon nanotubes adhesion and nanomechanical behavior from peeling force spectroscopy” J. Buchoux, L. Bellon, S. Marsaudon, and J.-P. Aimé Eur. Phys. J. B 84, 69–77 (2011)

Ultrasensitive DNA detection in biological systems using Magnetic fluorochrome nanoparticles

David Alcantara[1], Hoonsung Cho[2], Yanyan Guo[2], Lee Josephson[2] and Maria L. Garcia-Martin[1]

[1]Andalusian Center for Nanomedicine and Biotechnology (BIONAND), Parque Tecnológico de Andalucía, c/ Severo Ochoa, 35, 29590 Campanillas, Málaga, Spain
[2]Center For Translational Nuclear Medicine and Molecular Imaging, MGH-Harvard Medical School, 149 13th Street, Charlestown, MA 02129, USA.

dalcantara@bionand.es

We hypothesized that a magnetic nanoparticle (NP) surface functionalized with multiple DNA binding fluorochromes might react with DNA through a multivalent, avidity-type reaction and yield a highly sensitive method for detecting DNA by the T2 relaxation time of water protons measured by Magnetic Resonance (MR) techniques. Although oligonucleotides have been used to target NP's to specific sequences on nucleic acids, the considerable literature on fluorochrome/nucleic acid interactions has not been mined for potential nanoparticle (NP) targeting strategies. Our studies showed how a NP displaying a DNA-binding fluorochrome, bind in a multivalent fashion to yield a highly sensitive, T2-based method of detecting DNA. Furthermore, fluorochrome-functionalized NPs are a novel class of nanomaterials which, based on their recognition of DNA in biological systems, can serve as vital fluorochromes.

We synthesized the DNA-binding NPs by attachment of the DNA-binding fluorochrome TO-PRO 1 to the Feraheme (FH) NP using a "TO- PRO1 NHS ester". TO-PRO 1 fluoresces when bound to DNA by intercalation. The resulting NPs, termed FH-TO, had variable TO-PRO 1's per NP attached through a 6-carbon, flexible linker. FH-TO NPs had r_1 and r_2 relaxivities between 23.3 and 122 $(mM\ Fe\ sec)^{-1}$, and a size between 18.2 and 42 nm. The parent FH nanoparticle had a zeta potential of -37.8±3 mV (pH 6) that was largely preserved with the attachment of TO-PRO 1 to the NPs.

A PCR reaction was monitored by MR using FH-TO NPs as intercalant agent. Either light scattering or relaxometry can be used to determine aggregate formation in the low DNA concentration range. However, relaxometry has two advantages: T_2 is a hyperbolic function of DNA concentration (no hook effect) and T_2 is a radiofrequency-based method (no light based interferences). With light scattering and hook effects, some aggregate sizes (e.g. 200 nm) can reflect low or high concentrations and additional measurements with diluted samples are required. The estimated sensitivity of DNA detection by T2 was 27 fM DNA per a T_2 change of 2.6 msec [1].

On the other hand fluorochrome-functionalized NPs have a series of properties that make them far different from vital fluorochromes. First, fluorochrome-functionalized NPs are far larger than DNA binding fluorochromes. TO-FHs with different numbers of fluorochromes attached had diameters of 18 to 42 nm, corresponding to proteins with molecular weights in excess of 750 kDa, while vital fluorochromes have molecular weights of less than about 1000 Da. Second, when injected, TO-FH had a blood half-life similar to the parent Feraheme NP, rather than the far more rapid clearance seen with low molecular weight materials. Third, fluorochrome-functionalized NPs have superparamagnetic cores that allowed their reaction with DNA to be determined by relaxometry (or potentially by MRI). Finally, the conjugation of fluorochromes to NP surfaces provides a means of synthesizing DNA binding materials with valencies far above the divalency obtained with fluorochromes like TO-TO. High valency fluorochrome-functionalized NPs exhibit strong multivalent effects when binding DNA.

Attaching multiple DNA binding fluorochromes to magnetic nanoparticles provides a way of generating DNA binding NPs that can be used to detect DNA by microaggregate formation in vitro, for imaging the DNA of necrotic cells in culture, and for imaging the DNA of a tumor treated with a chemotherapeutic agent. Fluorochrome functionalized NPs are a multimodal (magnetic and fluorescent), highly multivalent (n ≈ 10 fluorochromes/NP) nanomaterials useful for imaging the DNA of biological systems [2].

References

[1] Alcantara, D.; Guo, Y.; Yuan, H.; Goergen, C. J.; Chen, H. H.; Cho, H.; Sosnovik, D. E.; Josephson, L. Angewandte Chemie International Ed, 2012, 51, 6904.

[2] Cho, H.; Alcantara, D.; Yuan, H.; Sheth, R. A.; Chen, H. H.; Huang, P.; Andersson, S. B.; Sosnovik, D. E.; Mahmood, U.; Josephson, L. ACS nano 2013, 7, 2032.

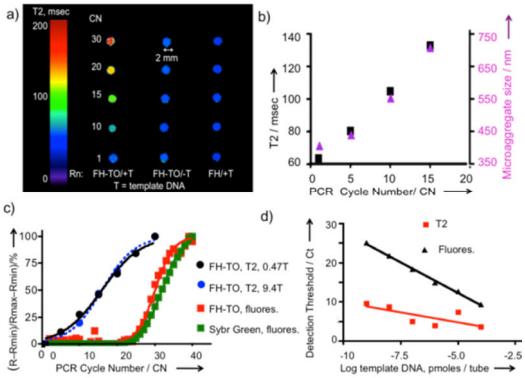

Figure 1. (a) PCR reactions with FH-TO added were run in sealed PCR tubes and imaged by MR at 9.4T. Omission of template DNA or use of FH yielded no changes in T2. (b) PCR reaction checked by relaxometry and DLS. (c) Comparison of the response by T2 and fluorescence. (d) Comparison of threshold cycle (Ct) by fluorescence and T2.

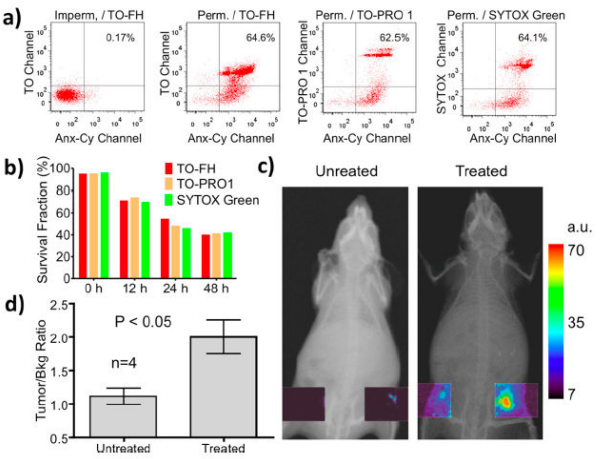

Figure 2. Interaction of TO-FH with HT-29 cells after permeabilization or after exposure to 5-FU/oxaliplatin treatment to induce cell death. (a) Normal or permeabilized cells were reacted with Anx-Cy and TO-FH or TO-PRO 1 or Sytox Green. (b) Cells were treated with 5-FU/oxaliplatin and exposed to Anx-Cy plus the indicated fluorochrome. Data are plotted as the survival fraction versus time of expose. Survival fraction is the percent of cells failing to bind both Anx-Cy and a second fluorochrome, i.e., the lower left-hand quadrant of the scatter plot. With an increasing duration of treatment, the survival fraction falls. Survival fraction falls similarly with Anx-Cy and any of the three vital fluorochromes, TO-FH, TO-PRO 1, Sytox Green. (c) Tumor surface fluorescence after TO-FH injection with untreated and treated (5-FU/oxaliplatin) HT-29 xenografts. (d) Tumor fluorescence, measured as tumor/bkg fluorescence ($p < 0.05$), $n = 4$.

Resonant Photocurrent Generation in Dye-Sensitized Periodically Nanostructured Photoconductors by Optical Field Confinement Effects

M. Anaya, M. Calvo, J.M. Luque and H. Míguez

miguel.anaya@csic.es

Instituto de Ciencia de Materiales de Sevilla, Américo Vespucio 49, Sevilla, 41092, Spain

Herein we show experimental evidence of resonant photocurrent generation in dye sensitized periodically nanostructured photoconductors. These materials were attained by the alternating deposition of layers of TiO_2 nanoparticles with different porosity to produce a spatial modulation of the refractive index in one dimension of the space [1]. We have built both periodic and broken symmetry nanostructured photoconducting TiO_2 multilayers with enough number of periods as to display different types of photon resonances that confine the field within the material in different ways. The resonant photocurrent finds their foundations in light confinement effects that were achieved by spectral matching of the sensitizer absorption band to different types of localized photon modes present in either periodical or broken symmetry structures. Results are explained in terms of the calculated spatial distribution of the electric field intensity within the configurations under analysis [2]. Such simulations were performed using a code written in MatLab and based on the transfer matrix method. A direct relation between resonant photon modes and photon-to-electron conversion peaks can be established. We foresee this sort of structures could allow the development of photo-electro-chemical devices with finer spectral control over light absorption.

References

[1] Calvo, M.E.; Colodrero, S.; Rojas, T.C.; Anta, J.A.; Ocaña, M.; Míguez,H.; Adv. Func. Mater., 18 (2008), 2708-2715.

[2] Anaya, M.; Calvo, M.E.; Luque, J.M.; Míguez, H., J. Am. Chem. Soc. (2013), DOI: 10.1021/ja401096k

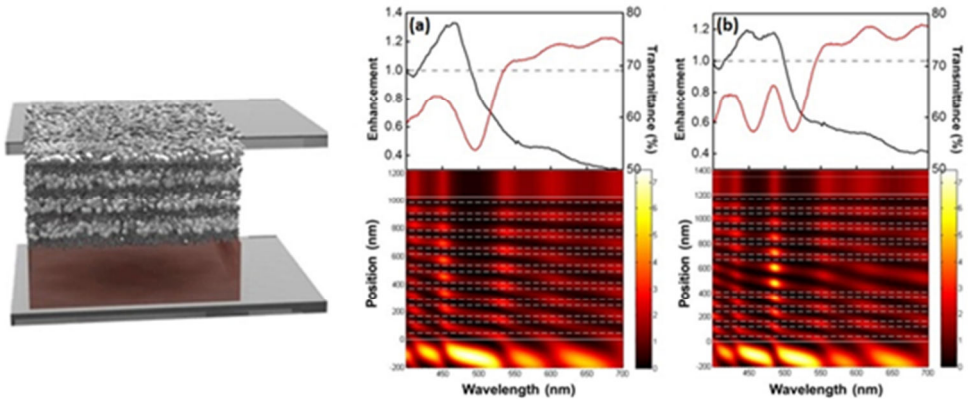

Figure 1. Left: System design. Right: Spectral variation of the photocurrent enhancement factors for (a) periodic arrangement of layers and (b) a resonator built by depositing a thicker middle layer within a periodic multilayer (black solid lines). The respective transmittance spectra are also plotted (red solid lines). In the bottom panels, the calculated spatial distribution of the electric field along a cross section of both types of structures is plotted as a function of the incident wavelength.

Edge states and flat bands in graphene nanoribbons with arbitrary geometries

W. Jaskólski[1], **A. Ayuela**[2], M. Pelc[1], H. Santos[3] and L. Chico[3]

[1]Instytut Fizyki UMK, Grudziadzka 5, PL-87-100 Toruń, Poland
[2]Centro de Física de Materiales CFM-CPM CSIC-UPV/EHU, Departamento de Física de Materiales (Facultad de Química, UPV) and Donostia International Physics Center, ES-20080 San Sebastián/Donostia, Spain
[3]Instituto de Ciencia de Materiales de Madrid, CSIC, Cantoblanco, ES-28049 Madrid, Spain

We prescribe general rules to predict the existence of edge states and zero-energy flat bands in graphene nanoribbons and graphene edges of arbitrary shape [1]. No calculations are needed. For the so-called *minimal* edges, the projection of the edge translation vector into the zigzag direction of graphene uniquely determines the edge bands. By adding nodes to minimal edges, arbitrary modified edges can be obtained; their corresponding edge bands can be found by applying hybridization rules of the extra states with those belonging to the original edge. Our prescription correctly predicts the localization and degeneracy of the zero-energy bands at one of the graphene sublattices, confirmed by tight-binding and first-principles calculations. It also allows us to qualitatively predict the existence of E≠0 bands appearing in the energy gap of certain edges and nanoribbons.

We also apply these rules to graphene nanoribbons and carbon nanotubes containing ordered defect lines built of octagonal rings [2]. We show that octagonal defect lines are a robust source of state localization at the Fermi energy, in some cases leading to spontaneous magnetization. We also prove that the localization at chains of octagons is a consequence of the zigzag nature of the graphene edges forming the defect lines.

References

[1] W. Jaskólski, A. Ayuela, M. Pelc, H. Santos, and L. Chico, Phys. Rev. B 83, 235424 (2011).
[2] M. Pelc, L. Chico, A. Ayuela, and W. Jaskólski, Phys. Rev. B 87, 165427(2013).

Transition voltage spectroscopy scrutinized

Ioan Bâldea

Theoretische Chemie, Universit ¨ at Heidelberg, Im Neuenheimer Feld 229, D-69120 Heidelberg, Germany

ioan.baldea@pci.uni-heidelberg.de

In the first part of this contribution I will report on recent [1-8] theoretical work of the author on transition voltage spectroscopy (TVS). In the second part several new results will be presented.

TVS is a method proposed by the groups of Kushmerick and Frisbie [9] to estimate the energy offset ε_0 =min ($E_F - E_{HOMO}$; $E_{LUMO} - E_F$) relative to the electrodes' Fermi energy E_F of the frontier molecular orbital (HOMO or LUMO), which dominates the charge transport through a single-molecule junction.

ε_0 is a key quantity, because it determines the charge transfer efficiency. Unfortunately, ε_0 can not be determined from low (ohmic) conductance G alone, which is commonly measured experimentally; in the case wherein the transport is determined by a single molecular orbital, G depends not only on ε_0, but also on the broadening functions $\Gamma_{L;R}$ caused by the couplings to (say,) left and right electrodes, $\Gamma = \Gamma_L = \Gamma_R$, assumed equal for simplicity. So, *I-V* -transport measurements beyond the linear regime are necessary. In principle, ε_0 could be "easily" determined from a full *I-V* curve; this curve should display current steps (abrupt if $\Gamma \ll \varepsilon_0$) at voltages $V = V_r$ where the molecular level becomes resonant with the Fermi energy of one electrode. For symmetric potential profiles (voltage division factor γ= 0), this occurs at voltages satisfying $eV_r = \pm 2\ \varepsilon_0$. Practically, this is impossible, because molecular junctions can hardly withstand such high voltages.

Typical transport measurements yield *I-V* -curves without structure (no maximum, no inflection point, *etc*), not seldom with substantial noise, which do not straightforwardly suggest how to determine ε_0.

Beebe et al [9] suggested that the energy offset can be estimated from the so-called transition voltage V_t, which is defined as the source-drain voltage at the minimum of the Fowler-Nordheim (FN) plot, *i. e.*, the curve $\log(I/V^2)$ *vs:* $1/V$. According to the initial claim,[9] a transition from direct tunneling to field-emission (FN) tunneling occurs at V_t, which corresponds to a change in the shape of the tunneling barrier from trapezoidal to triangular. Although such a change is not essential, [8,10,11], this "barrier-shape conjecture" [4] turned out to yield a reasonable estimate ($\varepsilon_0 \approx eV_t$).

To give support to the "barrier-shape conjecture", TVS initially invoked results based on the Simmons model. The interpretation of TVS within the Simmons model has been challenged [10]. However, that approach turned out to have serious drawbacks, as demonstrated in a series of works [4-7]. *E. g.*, it ignored the lateral constriction and exaggerated the image effects by using an approximate image potential proposed by Simmons, which is in error by a factor of two.

As recently shown by the author [1-3,8], a variety of *I-V* -curves measured in molecular junctions can be excellently reproduced within the Newns-Anderson model; an example is presented in Fig. 1. Pleasantly for the experimentalist colleagues, simple analytical expressions can be deduced, which conveniently allow to deduce both the MO energy offset and the voltage division factor from the measured transition voltages V_{t+} and V_{t-} at positive and negative biases[2]

$$|\varepsilon_0| = 2\frac{e|V_{t+}V_{t-}|}{\sqrt{V_{t+}^2 + 10|V_{t+}V_{t-}|/3 + V_{t-}^2}},$$

$$\gamma = \frac{\mathrm{sign}\varepsilon_0}{2}\frac{V_{t+} + V_{t-}}{\sqrt{V_{t+}^2 + 10|V_{t+}V_{t-}|/3 + V_{t-}^2}}.$$

The above formula holds for realistic cases, where $\Gamma \ll |\varepsilon_0|$. The leading corrections to the above results, which are of the order $O(\Gamma/\varepsilon_0)^2$, can also expressed in closed analytical form [3]

$$V_{t+} = \frac{2}{3}\frac{\sqrt{4\gamma^2+3}+4\gamma}{1-4\gamma^2}\varepsilon_0 + \frac{99+192\gamma\sqrt{4\gamma^2+3}\left[\left(\gamma^2-\frac{1}{3}\right)^2+\frac{191}{144}\right]+624\gamma^2+112\gamma^4-384\gamma^6}{(1-4\gamma^2)\left\{\sqrt{4\gamma^2+3}\left[\frac{63}{256}+\left(\gamma^2-\frac{3}{16}\right)^2\right]-2\gamma\left(\gamma^4-\frac{9}{16}\right)\right\}}\frac{\Gamma_a^2}{96\varepsilon_0},$$

$$V_{t-} = -\frac{2}{3}\frac{\sqrt{4\gamma^2+3}-4\gamma}{1-4\gamma^2}\varepsilon_0 - \frac{99-192\gamma\sqrt{4\gamma^2+3}\left[\left(\gamma^2-\frac{1}{3}\right)^2+\frac{191}{144}\right]+624\gamma^2+112\gamma^4-384\gamma^6}{(1-4\gamma^2)\left\{\sqrt{4\gamma^2+3}\left[\frac{63}{256}+\left(\gamma^2-\frac{3}{16}\right)^2\right]+2\gamma\left(\gamma^4-\frac{9}{16}\right)\right\}}\frac{\Gamma_a^2}{96\varepsilon_0}.$$

Whatever the fabrication method, stochastic fluctuations are inherent, and they play an essential role in the interpretation of the transport data in single-molecule junctions. In an important experimental work [12], relying upon an impressive statistics (thousands of junctions), simultaneous *G*- and V_t-measurements have demon strated that the *G* and V_t-histograms are affected in a completely different manner by stochastic fluctuations. On the basis of the above results, the different impact of fluctuations observed [12] can be quantitatively explained [1]. These results also demonstrate that, unlike *G*, V_t represents a molecular signature [1].

In the second part of this presentation I will present some new results demonstrating the usefulness of TVS for quantifying solvent effects and to interpret recent transport data in redox metalloproteins [13].

Financial support for this work provided by the Deutscheforschungsgemeinschaft (grant BA 1799/2-1) is gratefully acknowledged.

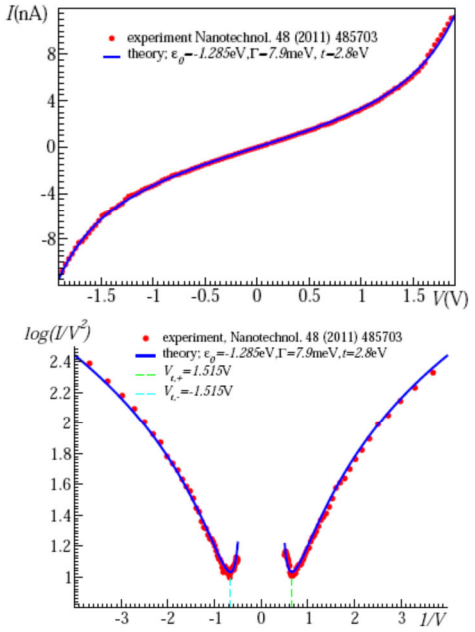

Figure 1. An example demonstrating that the Newns-Anderson model is able to excellently reproduce full *I-V* transport data in general and the TVS in particular (after Ref. 3).

References

[1] I. Bâldea, J. Am. Chem. Soc., 134 (2012) 7958.
[2] I. Bâldea, Phys. Rev. B, 85 (2012) 035442.
[3] I. Bâldea, Chem. Phys., 400 (2012) 65–71.
[4] I. Bâldea and H. Köppel, Phys. Lett. A 376 (2012) 1472.
[5] I. Bâldea, Europhys. Lett., 98 (2012) 17010.
[6] I. Bâldea and H. Köppel, Phys. Stat. Solidi (b), 249 (2012) 1791.
[7] I. Bâldea, J. Phys. Chem. Solids, 73 (2012) 1151.
[8] I. Bâldea, Chem. Phys., 377 (2010) 15.
[9] J. M. Beebe, B. Kim, J. W. Gadzuk, C. D. Frisbie and J. G. Kushmerick, Phys. Rev. Lett., 97 (2006) 026801.
[10] E. H. Huisman, C. M. Guédon, B. J. van Wees and S. J. van der Molen, Nano Letters, 9 (2009) 3909.
[11] M. Araidai and M. Tsukada, Phys. Rev. B 81 (2010) 235114.
[12] S. Guo, J. Hihath, I. Diez-Pérez and N. Tao, J. Am. Chem. Soc., 133 (2011) 19189.
[13] I. M. Artes, M. Lopez-Martinez, A. Giraudet, I. Diez-Pérez, F. Sanz, and P. Gorostiza, J. Am. Chem. Soc., 134 (2013) 20218.

Synthesis and Characterization of Nano-materials (ultra-thin Fe, FeS nano-sheets and single crystalline Fe nano-cubes) Via Mustard Oil Mediated Solution Phase Process and Their Applications in Sensing and Photo-Thermal ablation

Ankur Baliyan, Yoshikata Nakajima, Takahiro Fukuda, Tatsuro Hanajiri and Toru Maekawa.

ankurbaliyan@gmail.com

Bio-Nano Electronics Research Centre, Toyo University, 2100 Kujirai, Kawagoe, Saitama 350-8585, Japan.

We report a facile synthesis of ultra-thin Fe, FeS nano-sheets and single crystalline Fe nanocubes using mustard oil. Nano-materials were studied in detailed and characterized by using HRTEM, HRSEM, EDS, SAED, XRD, AFM, U-Vis, FTIR, Raman, XPS, and Auger spectroscopy. We have also investigated the mechanism involved for the formation of such nano-structures. It is an inexpensive, efficient, convenient, and ultra fast process to synthesis varieties of nano-materials. In addition, their possible sensing and photo-thermal ablation ability have been highlighted.

References

[1] Y.Y. Xu, D. Zhao, W.T. Jin, P. Kashkarov and H. Zhang. Physica E, 41, 806, (2009).

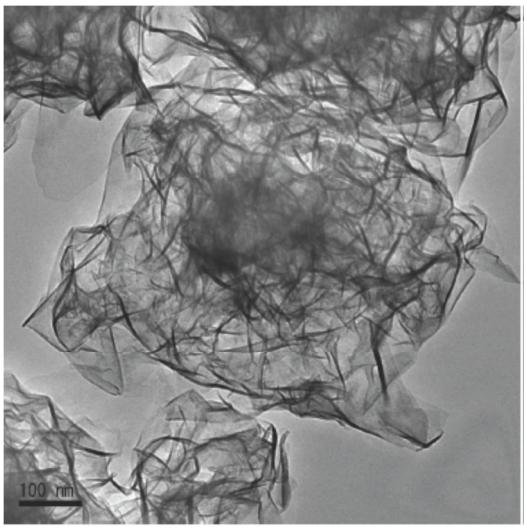

Figure 1. TEM image of ultra-thin Fe Nano-sheets.

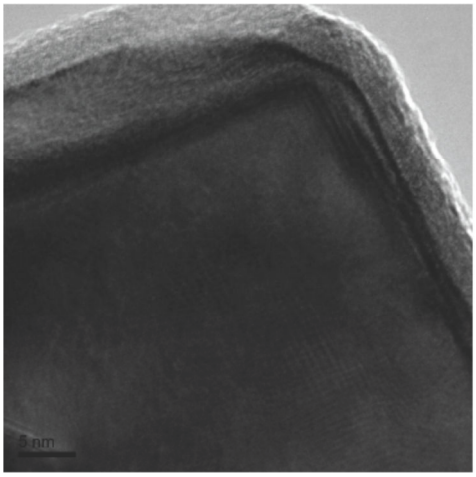

Figure 2. TEM image of Fe Nano-cube.

Sensing with Schottky barrier based silicon nanowires FET

Larysa Baraban, Felix Zoergiebel, Lotta Roemhildt, Sebastian Pregl and Gianaurelio Cuniberti

Institute for Materials Science and Max Bermann Center of Biomaterials, Technische Universität Dresden, Budapesterstr.27, 01069 Dresden, Germany

larysa.baraban@nano.tu-dresden.de

Nanomaterials have entered the phase of commercial applications [1] in medicine as drug carriers or labels [2], contrast agents for magnetic resonance imaging [3], and convenient tool for biodetection. Some of the prominent examples are the use of nanoparticles in combination with fluorescent labels for large number of biochemical tests or a new class of biological sensors, relying on semiconducting nanowires [5], for detection of biological molecules or of products of biologically catalyzed reactions. In contrast to already conventional optics-related biodetection methodology, the alternative concept utilizes the measurements of the electrical signals, *i.e*. electrical resistance [6]. For instance, conductance of the nanometer sized field effect transistors can be affected by an electric field of the target molecule adsorbed on its surface [5]. This novel approach offers advantage of the real-time and label-free detection of the analytes in liquid samples, whereas most of standard biochemical methods require the use of labels.

Here we introduce the first bottom-up grown Schottky barrier silicon nanowire field effect transistors for liquid sensing applications (see Figure 1). As a first application, the sensing effect is demonstrated for changing pH values. In particular, we are addressing three main issues: (i) bottom-up fabrication of high-quality silicon nanowire (SiNW) FETs, which allow an integration into non-silicon systems; (ii) high-current sensing for low-cost electronic measurements of ion-sensitive field effect transistors (ISFETs) devices by assembling large numbers of nanowires [7] into a single ISFET; (iii) investigations of charge sensing sensitivities, allowing quantitative statements on the sensor quality and pH values, which can be further developed to sensing concentrations of biological molecules. A novel type of online measurement for the determination of threshold voltage and other parameters during the experiment is introduced.

References

[1] O. Salata, “Applications of nanoparticles in biology and medicine,” J. Nanobiotechnol., 2, (2004), p. 1.

[2] D. Bechet, et al., “Nanoparticles as vehicles for delivery of photodynamic therapy agents”, Trends in Biotechnology, 26 (11), (2008), p. 612.

[3] C.W. Lai, et al., “Iridium-complex-functionalized Fe3O4/SiO2 core/shell nanoparticles: a facile three-in-one system in magnetic resonance imaging, luminescence imaging, and photodynamic therapy”, Small, 4 (2), (2008), p. 218.

[4] J.M. Nam, et al., “Nanoparticles-based bio-barcodes for the ultrasensitive detection of proteins”, Science, 301, (2003), p. 1884.

[5] G. Zheng, et al., “Multiplexed electrical detection of cancer markers with nanowire sensor arrays” Nature Biotechnology, 23, (2005), p.1294.

[6] I. Moench, et al., “Rolled-up magnetic sensor: nanomembrane architecture for in-flow detection of magnetic objects”, ACS Nano, 5, (2011), p. 7436.

[7] S. Pregl, et al., “Parallel arrays of Schottky barrier nanowire field effect transistors: Nanoscopic effects for macroscopic current output”, Nano Research, (2013), DO: 10.1007/s12274-013-0315-9.

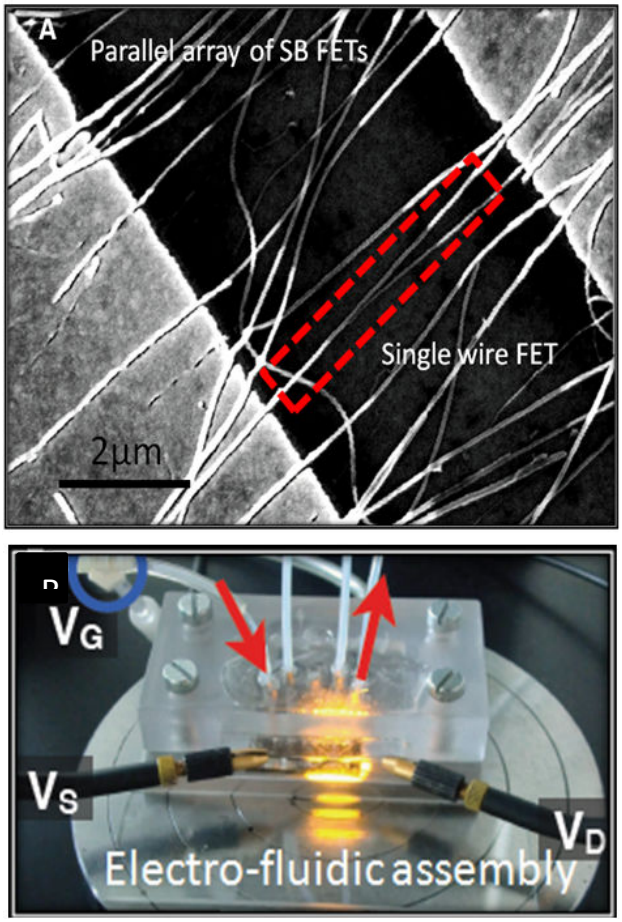

Figure 1. Sensor platform based on silicon nanowires FETs: (a) device consisting ofparallel array of undoped silicon nanowires and nanosized Schottky junctions; (b) Microlfuidic chip for sensing measurements.

Dendron-Carbon Nanotubes for Therapeutic Applications

Alessia Battigelli, Julie Tzu-Wen Wang, Tatiana Da Ros, Khuloud T. Al-Jamal, Maurizio Prato and Alberto Bianco

CNRS, UPR 3572, Laboratoire d'Immunopathologie et Chimie Thérapeutique, Strasbourg, France

a.battigelli@ibmc-cnrs.unistra.fr

In the last decade, carbon nanotubes (CNTs) attracted great interest in the biomedical field, beside their potential applications in nanoelectronics or composite materials.[1] The ability of CNTs to passively enter into cells and their low cytotoxicity render them a good candidate as drug delivery system. In particular, it was observed that functionalization of the sidewall or the tips of CNTs gives significant advantages, modulating their cytotoxicity[2] and permitting to anchor different molecules, like drugs or targeting agents.[3] Moreover, the functionalization of CNTs with positively charged groups permits to obtain a promising carrier for genetic material.[4,5]

In this communication, the design and synthesis of a new series of cationic dendron-CNTs of first and second generation will be described.[6] The dendrons were synthesized inserting at their termini ammonium or guanidinium groups in order to obtain an efficient gene delivery system and at the same time to shed new light on the differences between these two functionalities once present on the CNT scaffold.

To further investigate the potential of this nanomaterial, a targeting peptide for mitochondria was coupled to cationic CNTs. The effective subcellular localization of the material inside the desired organelle was proved by microscopic techniques, highlighting the promising use of these conjugates as drug delivery systems in the treatment of mitochondrial diseases.

The characterization techniques, the cytotoxicity and the complexation studies with genetic material will be also discussed.

References

[1] A. Jorio, G. Dresselhaus, M. S. Dresselhaus, in Carbon nanotubes: advanced topics in the synthesis, structure, properties and applications, Springer-Verlag, Berlin, Heidelberg (2008).

[2] H. Ali-Boucetta, A. Nunes, R. Sainz, M. A. Herrero, B. Tian, M. Prato, A. Bianco, K. Kostarelos, Angew. Chem. Int. Ed., 52 (2013) 2274.

[3] G. Lamanna, A. Battigelli, C. Ménard-Moyon, A. Bianco, Nanotechnology Rev., 1 (2012), 17.

[4] J. E. Podesta, K. T. Al-Jamal, M. A. Herrero, B. Tian, H. Ali-Boucetta, V. Hedge, A. Bianco, M. Prato, K. Kostarelos, Small, 5 (2009) 1176.

[5] M. A. Herrero, F. M. Toma, K. T. Al-Jamal, K. Kostarelos, A. Bianco, T. Da Ros, F. Bano, L. Casalis, G. Scoles, M. Prato, J. Am. Chem. Soc., 131 (2009) 9843.

[6] A. Battigelli, J. Tzu-Wen Wang, J. Russier, T. Da Ros, K. Kostarelos, K. T. Al-Jamal, M. Prato, A. Bianco, Small (2013) DOI: 10.1002/smll.201300264.

E.M. Attenuation Performance of Exfoliated Graphite Composites for Microwave Applications

Stefano Bellucci[1], Alain Celzard[2], Jan Macutkevic[3] and Polina Kuzhir[4]

bellucci@lnf.infn.it

[1]INFN-Laboratori Nazionali di Frascati, Via Enrico Fermi 40, 00044 Frascati, Rome, Italy
[2]IJL – UMR CNRS 7198 AND LERMAB – ENSTIB,France
[3]Vilnius University, Lithuania
[4]Research Institute for Nuclear Problems, Belarusian State University

The latest trends, techniques and applications of microwave radiation in wireless network technologies, cellular phones, targeting radars, vehicle speed detection, and electron spin resonance apparatus, etc stimulate searching of new materials with desirable mechanical and thermal properties providing high electrical conductivity and electromagnetic interference shielding effectiveness (EM SE). For that purpose, a series of composite samples were prepared, based on epoxy resin (Epikote 828), a curing agent called A1 (a modified TEPA) and up to 2.0 wt.% content of exfoliated graphite (EG). EG was obtained by intercalation of natural graphite flakes, subsequently submitted to a thermal shock. Accordion-like particles were thus produced, leading to a material of low packing density, around 3 g/L [1]. The complex dielectric permittivity $\varepsilon^* = \varepsilon' - i\varepsilon''$ was measured by a LCR meter HP4284A in the frequency range 20 Hz–1 MHz at room temperatures. The spectra of S–parameters of epoxy/EG composites were measured in microwave range (26-37 GHz) with scalar network analyzer. The average value of power transmitted through the samples is 60%, 30%, and close to 0 for 0.25, 1 and 2 wt.% of EG embedded, respectively. Along with high EM performance in microwave range, graphene platelets are much more easily processable than composites filled with CNTs. Concluding, giving the benefit of being lightweight, using EG leads to exceptionally good EM attenuation ability, along with high dielectric permittivity in low frequency range (see Fig.1).

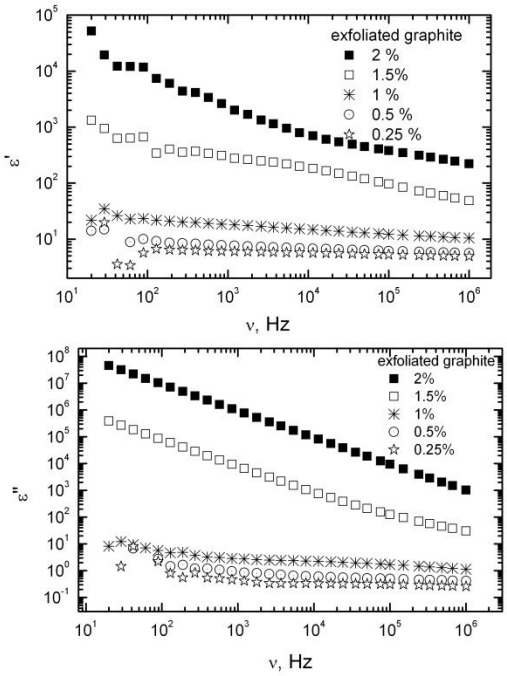

Figure 1. Dielectric permittivity of epoxy/EG in low frequency range.

Keynote

Nanoelectromechanical Systems for Proteomics

Robert H. Blick

Universitaet Hamburg - Angewandte Physik
Sprecher der Angewandten Physik
Germany

robert.blick@uni-hamburg.de

Mechanical resonators realized on the nano-scale by now offer applications in mass-sensing of biomolecules with extraordinary sensitivity. The general idea is that perfect mechanical biosensors should be of extremely small size to achieve zepto-gram sensitivity in weighing single molecules similar to a balance. However, the small scale and long response time of weighing biomolecules with a cantilever restricts their usefulness as a high-throughput method. Commercial mass spectrometry (MS), such as electro-spray ionization (ESI)-MS and matrix-assisted laser desorption/ionization (MALDI)-time of flight (TOF)-MS are the gold standards to which nanomechanical resonators have to live up. These two methods rely on the ionization and acceleration of biomolecules and the following ion detection after a mass selection step, such as time-of-flight (TOF). Hence, the spectrum is typically represented in m/z, i.e. the mass to ionization charge ratio. In this presentation I will describe the feasibility and mass range of detection of a new mechanical approach for ion detection in time-of-flight mass spectrometry. The principle of which is that the impinging ion packets excite mechanical oscillations in a semiconductor nanomembrane. Ion detection is demonstrated in MALDI-TOF analysis over a broad range with angiotensin, bovine serum albumin (BSA), equimolar protein mixtures of insulin, BSA, Immunoglobulin G (IgG), and IgM. We find an unprecedented mass range of operation of the nanomembrane detector.

Graphene related materials for non-volatile resistive memories: a review

Paolo Bondavallli

paolo.bondavalli@thalesgroup.com

Head of the nanomaterial team,
Joint research unit Thales/CNRS,
Thales Research and Technology, Palaiseau, France

In electronics, graphene is rapidly becoming the great hope for replacing and improving silicon semiconductors for future high performance devices. Since silicon semiconductors remain the basis of most commercial electronics (especially computing), the challenge for the next generation materials really becomes a great challenge. The graphene potentialities are attracting a lot of research funding, which in turn attracts researchers to probe opportunities in a number of directions such as novel graphene based transistors or spintronics. Another approach currently under development by some teams, is to employ graphene and other related nanomaterials to achieve non-volatile memories exploiting their "memresistive" behaviour. Indeed for e.g. computer high density storage memory, transistors work by storing an electrical charge. Thanks to "memresistive" materials we can store electrical resistance. That is, when a current is passed through these materials, their level of resistance to electricity (in Ohms) changes in a non-volatile and in an energetically "friendly" way. Resistive memory exploits the electric field responsive resistive switching of materials as an information write/erase principle for non-volatile data storage. The reading of resistance states is nondestructive, and the memory devices can be operated without transistors in every cell, thus making a cross-bar structure feasible. A large variety of solid-state materials have been found to show these resistive switching characteristics including solid electrolytes such as GeSe and Ag_2S, perovskites such as $SrZrO_3$, $Pr_{0.7}Ca_{0.3}MnO_3$, and $BiFeO_3$, binary transition metal oxides such as NiO, TiO_2, ZrO_2, and ZnO, organic materials, amorphous silicon (a-Si), and amorphous carbon (a-C). The main advantages of graphene related materials are not only that they seem to show extremely promising performances, but also that these materials provide more flexibility (physically) and potentially can lower the final cost of the devices, if scalable fabrication methods will be developed in parallel. Moreover we need only a two terminal device, which dramatically reduces the circuitry and allows the implementation of 3D architectures. Finally, this type of circuit commonly used for computer memory could be potentially easily printed or deposited (e.g. by spray-gun) on plastic sheets and used wherever flexibility is needed, such as in wearable electronics.

This contribution deals with the main scientific results and the potential market for graphene related materials in case of resistive non-volatile memories. Non-volatile memories are identified as key device for the future of computational system considering the reduced energy consumption compared to volatile-memories. However a specific new technology as not been identified up to now considering the issues related to scalability and cost. Graphene related materials offer an interesting and extremely promising alternative to existing technologies. In this contribution, we show the main works dealing with graphene layers, graphene-oxide and reduced graphene oxide. These works are quite recent but show impressing results especially in term of writing time and endurance/cyclability compared to common flash memories. The other main advantage of these materials is the potential of developing a CMOS compatible technology highly scalable. Moreover the carbonaceous materials are easily available compared to rare earths and also compatible with flexible applications and can open new field of innovation.

Source	Material and configuration	On/Off max	Switching time	Cyclability	Retention time	Character	Energy consumption to write (J)
[Li08]	Graphitic layers on nanowire (planar)	10^7	1µs	at less 1000 with no variation	1 day at less (15 days of consecutive switching)	Unipolar	~4 10^{-15}
[Stadley08]	Graphene (planar)	10^2	100ms	10^5 without visible changes in signals	To be performed on more than 24 hours	Unipolar	Not clear
[Sinitski09]	Graphene (planar)	10^7	1µs (tested limit)	at less 22000 with no variation	Not specified, even if the device is defined very stable	Unipolar	~8 10^{-17}
	Carbon (vertical)	10^6	1µs (tested limit)	at less 200	Not specified, even if the device is defined very stable	Unipolar	~7 10^{-17}
[He09]	GO (vertical)	20	No data	at less 100	10^4seconds	Bi-polar	No switching time
[Jeong10]	GO (vertical)	10^3	No data	at less 100	10^5seconds	Bi-polar	No switching time
[Hong11]	GO (vertical)	10^3	No data	100 and failure	Not specified, even if the device is defined very stable	Bi-polar	No switching time
[Panin11]	GO (planar)	10^3	No data	No data	No data	Bi-Polar and Uni-polar	No switching time
[Vasu11]	RGO (vertical)	10^5	10µs	Few hundreds	Not specified, even if the device is defined very stable	Unipolar	~ 10^{-13}

Table 1. Table summarizing all the main characteristics of the main works on graphene based non-volatile memories

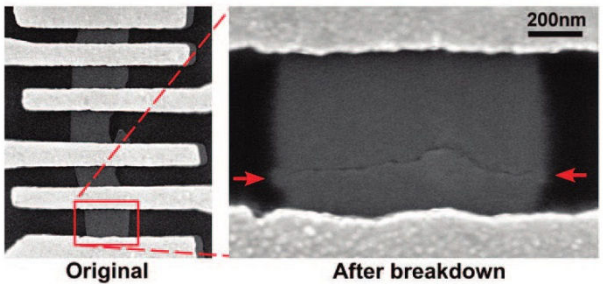

Figure 1. SEM image of the device before (left panel) and after breakdown of the graphene layers (right panel). The arrows indicate the edges of the nanoscale gap [Stadley08].

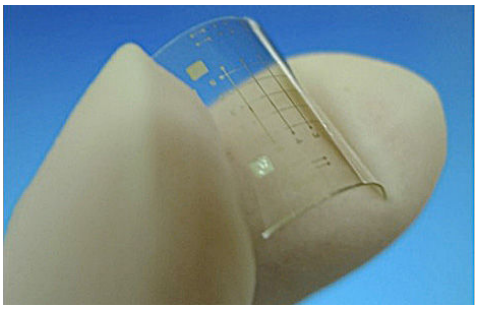

Figure 2. Real crossbar memory devices based on Graphene Oxide on flexible substrate [Jeong10] [IEEE10].

Graphene-enabled innovative solutions for consumer electronics

Stefano Borini, Di Wei, Alan Colli, Samiul Haque, Richard White, Michael Astley, Nadine Harris, Elisabetta Spigone, Jani Kivioja, Tapani Ryhanen

Nokia Research Center, Cambridge UK

New technology enablers - such as new functional materials – may allow the mass scale production of innovative electronic devices with outstanding performance and new form factors, driving innovation in mobile industry. In particular, graphene and other 2D materials have already demonstrated a great potential for radical technological innovations in a plenty of R&D fields, offering new opportunities in electronics and optoelectronics.

We'll report a few examples to illustrate how the development of graphene technology may impact on the field of flexible electronics, providing solutions for sensing and energy storage. Highly sensitive graphene-based sensors have been demonstrated in various fields, spanning from chemical sensors to photodetectors, and 2D materials are ideal candidates for the actual achievement of flexibility and stretchability. In addition, the unique 2D nature of these materials can lead to unprecedented sensing performances, paving the way to new applications in various fields such as consumer electronics, mobile health and environmental monitoring.

Furthermore, graphene is an ideal material for the development of portable energy storage components, thanks to the high specific surface area, the superior electrical conductivity, a high chemical tolerance and a broad electrochemical window. Graphene technology can enable a combination of flexible components with low-cost and low-power sensors, thus opening new avenues in the field of portable electronic devices. Also, scalability to mass production together with compatibility with low cost manufacturing processes, such as printing and roll-to-roll techniques, are major advantages of this technology. Therefore, graphene may represent an important technological platform for the next generation of mobile devices.

Production of silver nanoparticles by continuous wave laser in water

M. Boutinguiza, R. Comesaña, F. Lusquiños, A. Riveiro, J. del Val and J. Pou

mohamed@uvigo.es

Dpt. Física Aplicada, E.T.S.I. Industriales, Universidade de Vigo, Lagoas-Marcosende 9, 36280 Vigo, Spain

Silver nanoparticles have attracted much attention as a subject of investigation due to their well known properties, such as good conductivity [1], antibacterial and catalytic effects [2-4], etc. They are used in many different areas, medicine [5-6], industrial applications [7], and scientific investigation [8], etc. The size as well as the shape is very important for certain applications. There are different techniques for producing Ag nanoparticles, chemical, electrochemical, sonochemical, etc. These methods often lead to impurities together with nanoparticles or colloidal solutions. Laser ablation of solids in liquids (LASL) enables obtaining nanoparticles with no need of chemical precursors. In almost all publications reporting synthesis of nanoparticles by LASL a pulsed laser is used, especially nanosecond and femtosecond lasers. Nevertheless nanoparticles can be obtained in liquid media using long pulse lasers and continuous wave (CW) lasers. In previous works we have already reported the formation of nanporticles by LASL using CW lasers [9,10]. In this work silver nanoparticles are obtained in water using CW laser. The obtained particles are analysed and the nanoparticles formation mechanism is discussed.

Targets plates of Ag were cleaned and sonicated to be attached to a bottom of a glass vessel and filled with water up to 1 mm over the upper surface of the Ag plate. The laser source system used was a monomode Ytterbium doped fiber laser (YDFL). This laser works in CW mode delivering a maximum average power of 200 W. Its high beam quality allowed setting the irradiance range between 2×10^5 and 10^6 W/cm^2. The laser beam was coupled to an optical fiber of 50 µm core diameter and focused on the upper surface of the target. The laser beam was kept in relative movement with respect to the metallic plate at a scanning speed of 5 mm/s. After each experiment, the obtained colloidal suspensions were dropped on carbon coated copper microgrids substrates for examination of particle morphology and microstructure, while as prepared colloidal solutions were used for UV–vis absorption tests.

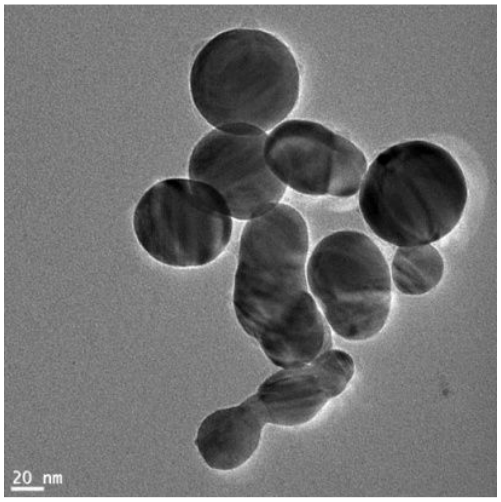

Figure 1. TEM micrograph showing Ag nanoparticles obtained by CW laser in water.

Taking into account that the used laser works in continuous regime, the interaction between the laser beam ant the silver target is governed by thermal effect. Several parameters depending on the laser radiation and the target nature are involved. When a laser beam strikes a silver target submerged in liquid, delivering irradiance of around 10^6 W/cm^2, a thin layer of metal is heated up above its melting point leading to a combination and boiling which give place to nanoparticle formation. According to the collected material, the obtained particles exhibit rounded shape with certain tendency to agglomeration, as can be seen from figure 1. This confirms that the main formation mechanism is melting and rapid solidification in the surrounding water. Several EDS microanalysis performed on individual particles confirmed that

the obtained particles are metallic Ag. The HRTEM images of obtained nanoparticles revealed that they are crystalline, as can be seen from figure 2 which shows clearly visible lattice fringes and their corresponding Fast Fourier Transform (FFT). The calculated interplanar distances from the FFT for particle obtained in water are compared with those of Ag in table 1.

Measured d- (nm)	Ag, d_{hkl} (nm)
0.2353	0.1359
0.2118	0.2044

Table 1. Measured interplanar distances from the FFT of figure 2 compared to those of Ag.

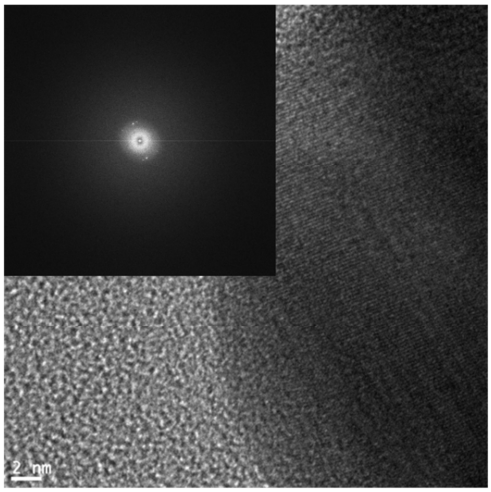

Figure 2. HRTEM image of the obtained nanoparticles in water with clearly visible lattice fringes and their corresponding FFT.

The use of the CW laser with at moderate irradiance contributes to control the size distribution of the obtained nanoparticles, since the CW mode doesn't produce high peaks power which can provoke deep holes. Furthermore, the laser beam was kept in movement relative to the target in order to reduce the thickness of the melted layer. The reduction of the interaction time by increasing the scanning speed can lead to a reduction of the extracted layer from the metal plate and the formation of smaller particles.

In conclusion, we have obtained colloidal nanoparticles of Ag in de-ionized water a CW laser to ablate metallic Ag target. The size distribution can be controlled by the scanning speed with mean diameter ranging from 5 to 80 nm. The obtained nanoparticles exhibit rounded shape.

The research leading to these results has received funding from ERDF through Atlantic Area Transnational Cooperation Programme Project MARMED (2011-1/164).

References

[1] R. Lesyuk, W. Jillek, Y. Bobitski, B. Kotlyarchuk, Microelectronic Engineering, 88 (2011) 318–321.
[2] A. Petica, S. Gavriliu, M. Lungu, N. Buruntea and C. Panzaru, Materials Science and Engineering: B, 152 (2008) 22-27.
[3] P. Gupta, M. Bajpai and S. K. Bajpai, Journal of Cotton Science, 12 (2008) 280-286.
[4] Z.L. Jiang, C. Y. Liu and L. W. Sun, The Journal of Physical Chemistry B, 109 (2005) 1730-1735.
[5] I.M. Hamouda, J. Biomed. Res.26 (2012) 143–151.
[6] Albrecht, M.; Janke, V.; Sievers, S.; Siegner, U.; Schüler, D.; Heyen, J. Magn. Magn. Mater. 290–291 (2005) 269–271.
[7] El-Rafie, M.H. Shaheen, T.I. Mohamed, A.A. Hebeish, Carbohydr. Polym. 90 (2012) 915–920.
[8] J. Yang Pan, Acta Mater., 60 (2012) 4753–4758.
[9] M. Boutinguiza, B. Rodríguez-González, J. del Val, R. Comesaña., F. Lusquiños, J. Pou. Nanotechnology 22 (2011) 195606
[10] [M. Boutinguiza, B. Rodriguez-Gonzalezb, J. del Val, R. Comesaña, F. Lusquiñosa J. Pou, Applied Surface Science 258 (2012) 9484-9486

Measuring magnetic anisotropy in a single-molecule spin transistor

E. Burzuri[1], A.S. Zyazin[1], A. Cornia[2] and H.S.J. van der Zant[1]

[1]Kavli Institute of Nanoscience, Delft University of Technology, Lorentzweg 1, Delft, The Netherlands
[2]Department of chemistry and INSTM, University of Modena and Reggio Emilia, via G. Campi 183, I-41100 Modena, Italy

E.BurzuriLinares@tudelft.nl

Spintronics, which aims to use the spin state of the electrons to process information, is a promising technology to supplement conventional electronics based on the control of the electrical charge of the electrons. The field is rapidly evolving into molecular spintronics where transport takes place through individual molecules advancing in miniaturization and spin-state preservation. The versatility of molecular synthesis allows to introduce built-in properties such as magnetism in molecules. As a result, the molecule possess intrinsic spin and therefore a spin polarized current is no longer needed. But, under what conditions this molecular spin-state can be read, controlled or written? The viability of molecular spintronics rest in the ability to discern and control the spin state of this magnetic molecule.

We study three-terminal charge transport through individual Fe_4 single-molecule magnets [1]. The Fe4 molecule is linked to two gold electrodes fabricated by self-breaking electromigration of a gold nanowire [2,3]. A third gate electrode is used to access different redox states of the molecule.

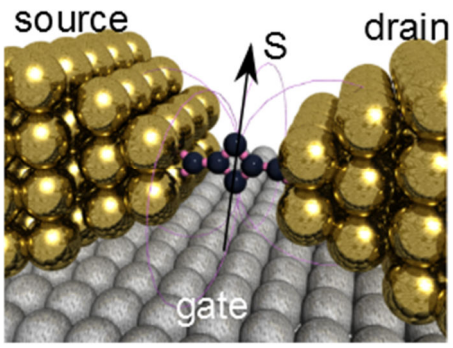

Figure 1.

We directly observe for the first time [4] the magnetic anisotropy of the single molecule by introducing a spectroscopy technique based on measuring the position of the zero-bias degeneracy-point (see figure) as a function of gate voltage and applied magnetic field.

Our measurements reveal an increase of the magnetic anisotropy and a decrease of the ground state spin upon reduction of the molecule. Moreover, the sensitivity of this method allows to detect small changes in the orientation and magnitude of the anisotropy in different charge states. We find that the easy axes of the molecule in adjacent charge states are (almost) collinear.

The sensitivity of the technique will allow to study quantum properties of the Fe_4 such as the quantum tunneling of the magnetization at the single-molecule scale.

This work was supported by FOM and the EU FP7 program under the Grant Agreement ELFOS.

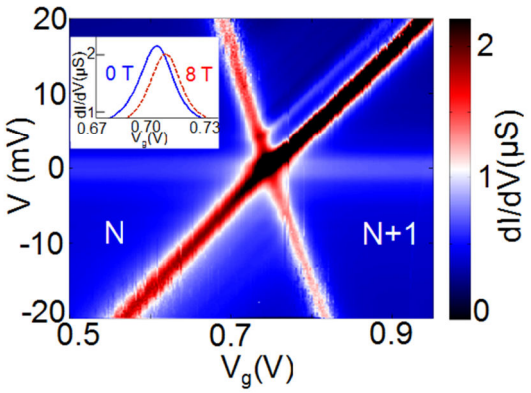

Figure 2. Differential conductance map of a single Fe4 SMM showing two different charge states.

References

[1] S. Accorsi et al., J. Am. Chem. Soc., 128 (2006) 4742.
[2] H. Park et al., Appl. Phys. Lett. 75 (1999) 301.
[3] K. O'Neil et al., Appl. Phys. Lett. 90 (2007) 133109.
[4] E. Burzuri et al., Phys. Rev. Lett. 109 (2012) 147203.

Functional polymer nanofibers for photonics, nanoelectronics and biotechnology

A. Camposeo[1,2,3], V. Fasano[2,4], G. Morello[1,2], M. Moffa[2], L. Persano[1,2,3], D. Pisignano[1,2,4]

andrea.camposeo@nano.cnr.it

[1]National Nanotechnology Laboratory of Istituto Nanoscienze-CNR, Lecce, Italy
[2]Center for Biomolecular Nanotechnologies @ UNILE, Istituto Italiano di Tecnologia Via Barsanti, Arnesano (LE), Italy
[3]Soft Materials and Technologies S.r.l. (SM&T S.r.l.), I-73100, Lecce, Italy
[4]Dipartimento di Matematica e Fisica "Ennio De Giorgi", Università del Salento via Arnesano, Lecce, Italy

Functional polymer micro- and nanofibers are novel structures, exhibiting smart physico-chemical properties, with applications ranging from liquid and air filtration, tissue engineering, regenerative medicine, sensing, photonics, nanoelectronics. Technologies for producing polymer fibers are rapidly evolving from the production of inert nanofibers materials to more specialized, functional and multi-functional nanofibers. The nanostructure capabilities range from conduction properties to light-sensing, from promoted cellular differentiation to enhanced mechanical, thermal and anisotropy properties. Here results and perspectives of our research on functional fibers are presented, focusing on hybrid fabrication approaches (electrospinning, nanoimprinting, soft lithography, two-photon lithography and together with novel perspectives opened by biomineralization) and complementary applications of polymeric and biological fibers. Demonstrators include field-effect transistors, polarized light-emitters, lasers, smart controllable surfaces, waveguides and bioactive systems.

The financial support from the FIRB Contract RBFR08DJZI "Futuro in Ricerca" and the FIRB Projects RBNE08BNL7 "Merit" is acknowledged.

References

[1] D. Tu, S. Pagliara, A. Camposeo, G. Potente, E. Mele, R. Cingolani, D. Pisignano, Adv. Funct. Mater., 21 (2011) 1140.
[2] S. C. Laza, M. Polo, A. A. R. Neves, R. Cingolani, A. Camposeo, D. Pisignano, Adv. Mater., 24 (2012) 1304.
[3] A. Camposeo, L. Persano, D. Pisignano, Macromol. Mater. Eng., 298 (2013) 487-503.
[4] L. Persano, A. Camposeo, C. Tekmen, D. Pisignano, Macromol. Mater. Eng., 298 (2013) 504-520.
[5] G. Morello, A. Polini, S. Girardo, A. Camposeo, D. Pisignano, Appl. Phys. Lett. in press 2013. DOI: 10.1063/1.4807894.

A microfluidic sensor that maps the velocity field around an oscillating microsphere

S. Carretero-Palacios, S. Nedev, S. R. Kirchner, F. Jäckel & J. Feldmann

carretero.palacios@lmu.de

Photonics and Optoelectronics Group, Physics Department and Center for NanoScience (CeNS), Ludwig-Maximilians-Universität München,
Amalienstr. 54, 80799 Munich, Germany

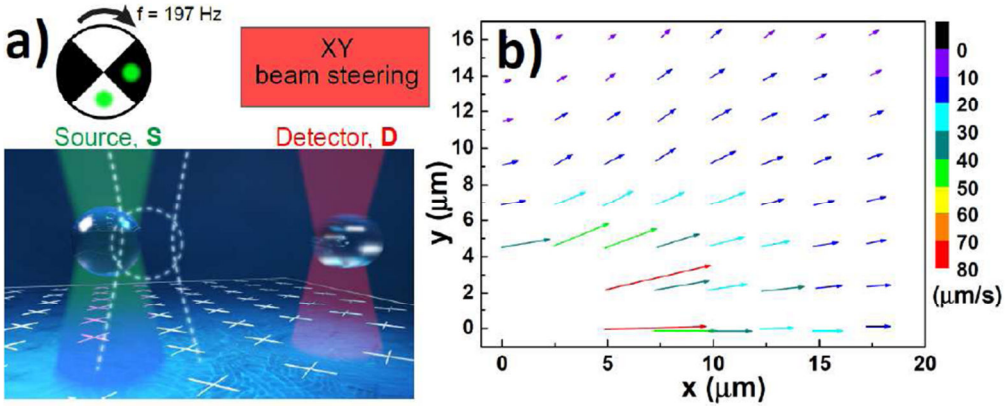

Figure 1. a) Schematic of our experiment: 2 SiO_2 particles of 0.88 μmm radius in water are trapped in 2 independently controlled optical traps. The source oscillates with f = 197 Hz. b) Direction and magnitude of the velocity field measured experimentally.

Optical trapping is a well established technique that has been widely used to noninvasively manipulate micro- and nano-sized objects [1-4]. Its combination with microfluidics provides novel analytical and sensing capabilities [5-9].

Here we show a novel experimental and theoretical approach on how an optically trapped microsphere can be used as an ultrasensitive detector for the induced motion of the medium surrounding a second oscillating microparticle. Fluidic vibrations created by the source (an optically trapped silica particle set to oscillate in a dipole-type mode) are detected by another twin silica particle independently trapped and located in the vicinity of the source (Fig.1a). Fourier analysis of the motion of the detecting particle at different points in space and time renders the velocity map around the oscillating microsphere (Fig.1b). The combination with acoustic and microfluidic theoretical models reveal that the measured fields are dominated by microfluidic contributions. The concept introduced here opens the way for new detection methods (i.e. Nano-Position System (NPS)) able to provide location and recognition (due to the field pattern) of moving sources that may be applied to artificial micro-objects and also to living organisms, like cells and bacteria.

References

[1] A. Ashkin, Phys. Rev. Lett. 24, 156 (1970).
[2] H. Misawa et al., Chemistry Letters 20, 469 (1991).
[3] K. Svoboda et al., Opt. Lett. 19, 930 (1994).
[4] M. E. J. Friese, et al., Phys. Rev. A 54, 1593 (1996).
[5] D. Psaltis et al., Nature 442, 381 (2006).
[6] Y.-F. Chen et al., Nanoscale 4, 4839 (2012).
[7] B. S. Schmidt et al., Optics Express 15, 14322 (2007).
[8] G. Boer et al., Review of Scientific Instruments 78, 116101 (2007).
[9] C. Liberale et al., Scientific reports 3 (2013).

Carbon Nanotubes as Directional probes for Magnetic Resonance Imaging

Daniel Calle
and **Sebastián Cerdán**

scerdan@iib.uam.es

Instituto de Investigaciones Biomédicas "Alberto Sols" CSIC/UAM,
c/ Arturo Duperier 4, Madrid 28029, Spain

Magnetic Resonance Imaging (MRI) has become one of the most powerful tools in modern medical diagnosis because of its non-invasive character, high inherent spatial resolution and the possibility to enhance locally and specifically image intensity using appropriate paramagnetic or superparamagnetic contrast agents (CAs). Most of the MRI CAs currently available are chelates of paramagnetic metals of the rare earth series or superparamagnetic iron oxide nanoparticles, the Gd(III) chelates being the most widely used [1]. In all these cases, the induced relaxation of the water molecules surrounding the probe is isotropic precluding the encoding of directionality in many fundamental biological processes already detectable by molecular imaging [2, 3]. On these grounds, it would entail considerable relevance to develop CAs in which the predominant molecular orientation of the probe with respect to the external magnetic field can be inferred from the non-invasive MRI measurement.

In this lecture we shall describe the use of Single-Wall and Multi-Wall Carbon Nanotubes as directional probes for MRI. SWCNT suspensions are excellent candidates for this purpose, since they orient parallel to the external magnetic field Bo and are able to induce anisotropic relaxivity [4] and anisotropic diffusion [5] of water molecules in a way in which the orientation of the nanotube can be predicted from the MRI measurement. We shall discuss the production, shortening and characterization of these arrangements using Atomic Force Microscopy, Transmission Electron Microscopy (+Energy Dispersive Spectroscopy), SQUID, VSM and MRI. Our measurements provide for the first time to our knowledge a sound basis for the magnetic properties of these preparations and allow their decoration with customized reporter molecules for improved imaging or therapeutic performance.

References

[1] A. E. Merbach, and E. Tóth, The chemistry of contrast agents in medical magnetic resonance imaging (Wiley Chichester (W. Sx.) etc., 2001).
[2] S. Aime et al., Accounts of chemical research 42, 822 (2009).
[3] D. Pan et al., Future medicinal chemistry 2, 471 (2010).
[4] A. Cerpa et al., MedChemComm 4, 669 (2013).
[5] V. Negri et al., Angewandte Chemie 122, 1857 (2010).

Large anisotropic conductance and band gap fluctuations in nearly-round-shape Bismuth nanoparticles

Ori Cheshnovsky

School of Chemistry, Tel Aviv University, Tel Aviv 69978, Israel

Unlike their bulk counterpart, nanoparticles often show spontaneous fluctuations in their crystal structure at constant temperature. This phenomenon takes place whenever the net gain in the surface energy of the particles outweighs the energy cost of internal strain. The configurational space is then densely populated due to shallow free-energy barriers between structural local minima. Here we report that in the case of bismuth (Bi) nanoparticles (BiNPs), due to the high anisotropy of the mass tensor of their charge carriers, structural fluctuations result in substantial dynamic changes in their electronic and conductance properties. Transmission electron microscopy (TEM) is used to probe the stochastic dynamic structural fluctuations of selected BiNPs. The related fluctuations in the electronic band structure and conductance properties are studied by scanning tunneling spectroscopy (STM) and are shown to be temperature dependent. Continuous probing of the conductance of individual BiNPs reveals corresponding dynamic fluctuations (as high as 1eV) in their apparent band gap. At 80K, upon freezing of structural fluctuations, conductance anisotropy in BiNPs is detected as band gap variations as a function of tip position above individual particles.

We have also tested the role of the capping agents on these dynamics. Bismuth nanoparticles, protected by two types of capping ligands, 1-dodecanethiol and ethylene di-amine tetra-acetate (EDTA) were probed by TEM and STM at 80K and 300K. We show that the different capping ligands dramatically alter the mechanism of structural dynamics in these particles. This finding suggests that molecular control of structural and consequently electronic switching in anisotropic nano-systems is feasible.

BiNPs offer a unique system to explore anisotropy in zero-dimension conductors as well as the dynamic nature of nanoparticles.

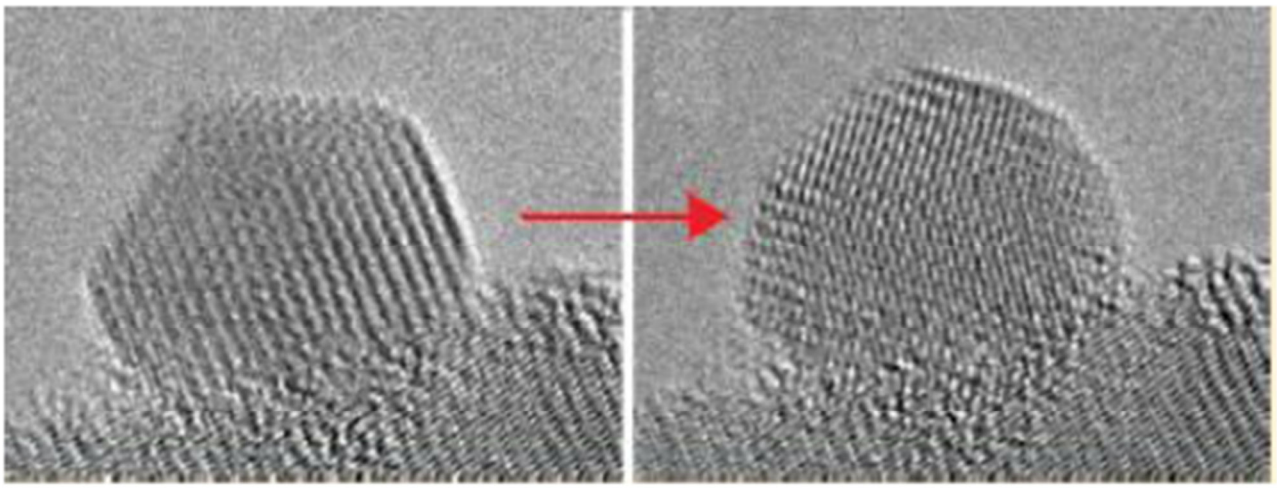

Graphene Planar Plasmonic Waveguide Devices

Choon-Gi Choi

cgchoi@etri.re.kr

Creative Research Center for Graphene Electronics,
Electronics and Telecommunications Research Institute (ETRI), Daejeon, 305-700, Korea

Graphene has attracted great attention due to its extraordinary electronic, thermal, mechanical, and optical properties [1]. In photonics, graphene have been exhibited outstanding properties such as transparency, wavelength-independent optical absorption, satuable absorption, electron-hole pair generation, third-order nonlinearity, and electro-absorption. Graphene has been used as a transparent conductor for photovoltaics, light emitting diodes, and touch panels [2]. In optical data communication applications, graphene has been considered as a versatile photonic material to modulate, detect, control, and even guide light [3-5].

Recent theoretical investigations on graphene-based photonic devices exhibited that graphene embedded in a homogenous dielectric can serve as a lightwave guiding medium [6–8]. For further development of graphene based on-chip PICs, planar-lightwave-circuit (PLC)-compatible integrations of the graphene-based optoelectronic devices is being consistently demanded, thereby novel PIC platform such as plasmonic waveguide and modulator have been proposed [9-10].

In this talk, we demonstrated recent progress in graphene-based plasmonic devices such as thermo-optic mode extinction modulator and planar lightwave-type photodetector based on graphene plasmonic waveguides for all graphene photonic integrated circuits [11-12].

This work was supported by the Creative Research Program of the ETRI (13ZE1110) of Korea and by a grant (Code No. 2011-0031660) from the Center for Advanced Soft Electronics under the Global Frontier Research Program of the Ministry of Science, ICT and Future Planning of Korea.

References

[6] A. K. Geim and K. S. Novoselov, Nat. Mater. 6 (2007) 183.

[7] F. Bonaccorso, Z. Sun, T. Hasan, and A. C. Ferrari, Nat. Photon. 4(9) (2010) 611.

[8] M. Liu, X. Yin, E. Ulin-Avila, B. Geng, T. Zentgraf, L. Ju, F. Wang, and X. Zhang, Nature 474 (2011) 64.

[9] T. Mueller, F. Xia and P. Avouris, Nat. Photon. 4(5) (2010) 297.

[10] Q. Bao, H. Zhang, B. Wang, Z. Ni, C. H. Y. X. Lim, Y. Wang, D. Y. Tang, and K. P. Loh, Nat. Photon. 5(7) (2011) 411.

[11] S. A. Mikhailov and K. Ziegler, Phys. Rev. Lett. 99(1) (2007) 016803.

[12] G. W. Hanson, J. Appl. Phys. 103(6) (2008) 064302.

[13] M. Jablan, H. Buljan, and M. Soljacic, Phys. Rev. B 80(24) (2009) 245435.

[14] Jin Tae Kim, Jaehyeon Kim, Hongkyw Choi, Choon-Gi Choi and Sung-Yool Choi, Nanotechnology 23(34) (2012) 344005.

[15] Jin Tae Kim and Choon-Gi Choi, Optics Express, 20(4) (2012) 3556.

[16] Jin Tae Kim, Kwang Hyo Chung, and Choon-Gi Choi, Optics Express (2013) in revision.

[17] Jin Tae Kim, Young-Jun Yu, Hongkyw Choi, and Choon-Gi Choi, in preparation.

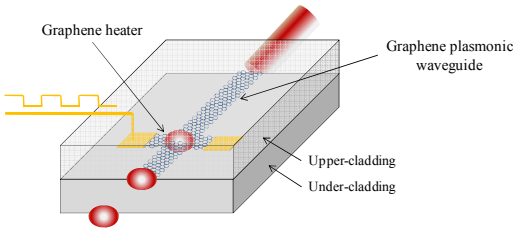

Figure 1. (a) Schematic view of the proposed graphene-based thermo-optic mode extinction modulator.

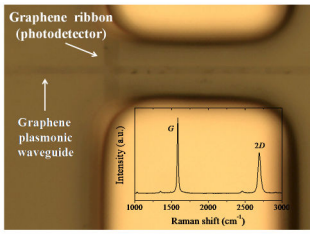

Figure 2. Picture of the fabricated planar lightwave-type graphene photodetector. The inset shows the Raman spectrum from the graphene ribbon.

Creating Molecularly-Reconfigurable Plasmonic Surfaces for Biosensing

Alasdair W. Clark, J.M. Cooper

University of Glasgow, School of Engineering, Glasgow, UK

Alasdair.clark@glasgow.ac.uk

Abstract

We report a new plasmonic manipulation technique which employs biomolecular interactions as active building blocks in the construction of novel surfaces which gains optical functionality due to individual molecular binding events. We demonstrate two novel biosensors which combine direct-write fabrication with molecular nanopatterning to position individual nanoparticles around single, complex plasmonic nanostructures due to molecular binding. In doing so, we demonstrate both an extremely sensitive naked-eye biosensor which relies on a plasmonic colour-shift to report on antibody-binding events, and a surfaceenhanced Raman sensor which relies on the completion of a simple plasmonic circuit by a DNA-conjugated nanoparticle to detect an individual DNA-hybridisation event.

Method

To create the molecularly-reconfigurable plasmonic surfaces we use a novel combination of electron-beam lithography and molecular surface nanopatterning, which allows us to control individual molecular interactions such that we can dictate, with proteinscale resolution (~5 nm), the placement of single nanoparticles (NPs) around individual nanostructures, Figure 1. After defining a nanostructure using electron-beam lithography, a second electron-beam step is carried out in order to define a “window” at a particular point around the structure. The surface beneath this window can then be molecularly modified and the polymer resist material removed, leaving a nanophotonic surface that has been molecularly patterned at specific points. Molecularly conjugated NPs can then be bound to these areas in a controlled manner (the initial surface modification is large enough such that only a single particle can bind to any one area).

Naked-eye detection of antibody-binding

Our understanding of biological systems is dependent on our ability to visualise and measure biomolecules and biological events with high spatial and temporal resolution. Plasmonic colorimetry is a biosensing technique which relies on visible plasmon resonance shifts in nanostructures due to some biological event or process. Scattered plasmonic colours are highly sensitive to environmental changes surrounding the nanostructures, making the effect ideal for sensing applications. Any metallic nano-object brought into proximity with the array will influence its resonance, shifting the plasmon frequency and causing a change in structural colour, which can be observed by eye.

To date, biosensors based on plasmonic colour shifts have relied on random, molecularly driven aggregation of chemically synthesized colloid, or blanket binding of NPs to pre-fabricated structures [1-4] and thus have demonstrated little or no control over the number and location of binding events. Although there has been great progress in recent years in molecular lithography techniques, there remains significant problems in terms of the control, placement and spacing of individual particles in order to create arbitrary structures. Here, we bridge the gap between the versatility of direct-write nanolithography, and the resolution and selectivity of molecular self-assembly, combining both techniques for the first time. Precise positioning of single particles around pre-fabricated plasmonic structures allows us to manipulate the plasmon supported by the resultant structure, altering the colour of the light scattered by the surface in an engineered fashion. In large arrays (>100µm, comprising of several thousand structures) the homogeneous colour-shifts can be seen with the nakedeye, without the need for any spectroscopy or microscopy equipment (Figure 2(a)).

Completing a plasmonic bowtie with a DNA nanoparticle for extreme Raman detection

The use of metallic NPs in surface enhanced resonance Raman spectroscopy (SERRS) applications is well-known[5]. By aggregating discrete NPs, exceptionally large field enhancement values can be realised due to interparticle plasmonic-coupling, creating electromagnetic "hot-spots" in the nanometre gaps between particles.[6] However, controlling this coupling is problematic; common NP aggregation techniques produce randomly coupled particles, where neither the hot-spot number, location or resonance can be controlled. This leads to non-repeatable spectra, and requires large amounts of NPs and analyte to ensure a signal is obtained.

We describe a novel, molecularly reconfigurable plasmonic structure capable of detecting single DNA-binding events via SERRS. By positioning single NPs within plasmonic bowties (Figure 2(b)) we can generate intense hot-spots at known locations and known plasmonic frequencies. This novel approach to DNA-driven plasmonic tuning directly addresses one of the fundamental challenges of NP SERRS; control over the localization and frequency of EM-hotspots in NP assemblies. Using NPs modified with both DNA and a Raman reporter, we show an improvement of 2 orders of magnitude *above* the existing SERRS effect, allowing us to pinpoint and measure single DNA-NP binding events.

References

[1] R. Elghanian, J. J. Storhoff, R. C. Mucic, R. L. Letsinger and C. A. Mirkin, Selective colorimetric detection of polynucleotides based on the distance-dependent optical properties of gold nanoparticles, Science, 5329, (1997) 1078-1081

[2] W. P. Hall, S. N. Ngatia and R. P. Van Duyne, LSPR Biosensor Signal Enhancement Using Nanoparticle-Antibody Conjugates, Journal of Physical Chemistry C, 5, (2011) 1410-1414

[3] H. X. Li and L. Rothberg, Colorimetric detection of DNA sequences based on electrostatic interactions with unmodified gold nanoparticles, Proceedings of the National Academy of Sciences of the United States of America, 39, (2004) 14036-14039

[4] J. R. Waldeisen, T. Wang, B. M. Ross and L. P. Lee, Disassembly of a Core-Satellite Nanoassembled Substrate for Colorimetric Biomolecular Detection, Acs Nano, 7, (2011) 5383-5389

[5] M. C. Daniel and D. Astruc, Gold nanoparticles: Assembly, supramolecular chemistry, quantum-size-related properties, and applications toward biology, catalysis, and nanotechnology, Chemical Reviews, 1, (2004) 293-346

[6] L. Guerrini and D. Graham, Molecularly-mediated assemblies of plasmonic nanoparticles for Surface-Enhanced Raman Spectroscopy applications, Chemical Society Reviews, 21, (2012) 7085-7107

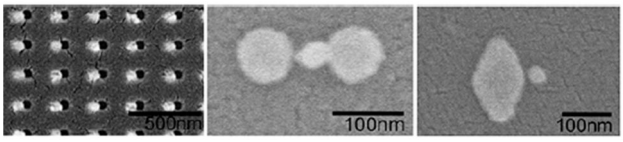

Figure 1. From left; SEM of Au plasmonic structures aligned to resist "windows" which allow molecular surface modification; Individual NP molecularly bound between 2 discs; Individual NP bound at specific point around nano-diamond structure.

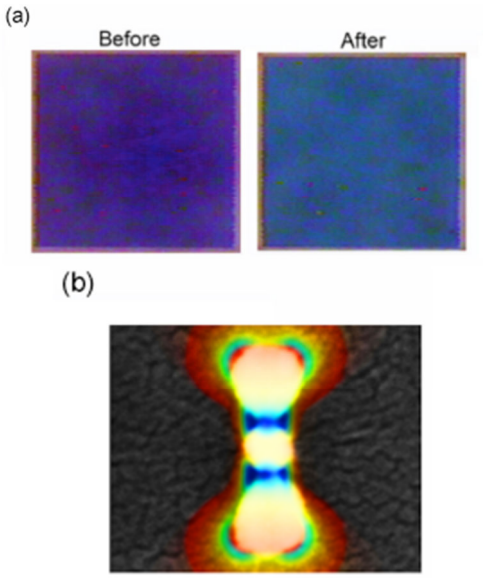

Figure 2. (a) Bright-field images of a plasmonic sensor array before and after antibody affinity binding. (b) A superimposition of an SEM and a finite-element simulation of localized electricfield for a nanoplasmonic bowtie structure with a DNA bound NP in its centre.

Single Molecule Bioelectronics

Departments of Physics, Chemistry, and Molecular Biology and Biochemistry, University of California at Irvine, Irvine, California 92697, USA

Y. Choi, P.C. Sims, T. Olsen, O.T. Gul, B.L. Corso, M. Iftikhar, G.A. Weiss, and **P.G. Collins**

collinsp@uci.edu

Nanoscale electronic devices like field-effect transistors have long promised to provide sensitive, labelfree detection of biomolecules. In particular, single-walled carbon nanotubes have the requisite sensitivity to detect single molecule events, and they have sufficient bandwidth to directly monitor single molecule dynamics in real time. Recent measurements have demonstrated this premise by monitoring the dynamic, single-molecule processivity of three different enzymes: lysozyme (Fig. 2) [1, 2], protein Kinase A (Fig. 3) [3], and the Klenow fragment of DNA polymerase I (Fig. 4) [4]. With all three enzymes, single molecules were electronically monitored for 10 or more minutes, allowing us to directly observe rare transitions to chemically inactive and hyperactive conformations. The high bandwidth of the nanotube transistors further allow every individual chemical event to be clearly resolved, providing excellent statistics from tens of thousands of turnovers by a single enzyme. Besides establishing values for processivity and turnover rates, the measurements revealed variability, dynamic disorder, and the existence of intermediate states. Initial success with three different enzymes indicates the generality and attractiveness of the nanotube devices as a new tool to complement other single molecule techniques. Furthermore, our focused research on transduction mechanisms provides the design rules necessary to further generalize this architecture [5]. This presentation will summarize these rules, and demonstrate how the purposeful incorporation of just one amino acid is sufficient to fabricate effective, single molecule nanocircuits from a wide range of enzymes or proteins (Fig. 1).

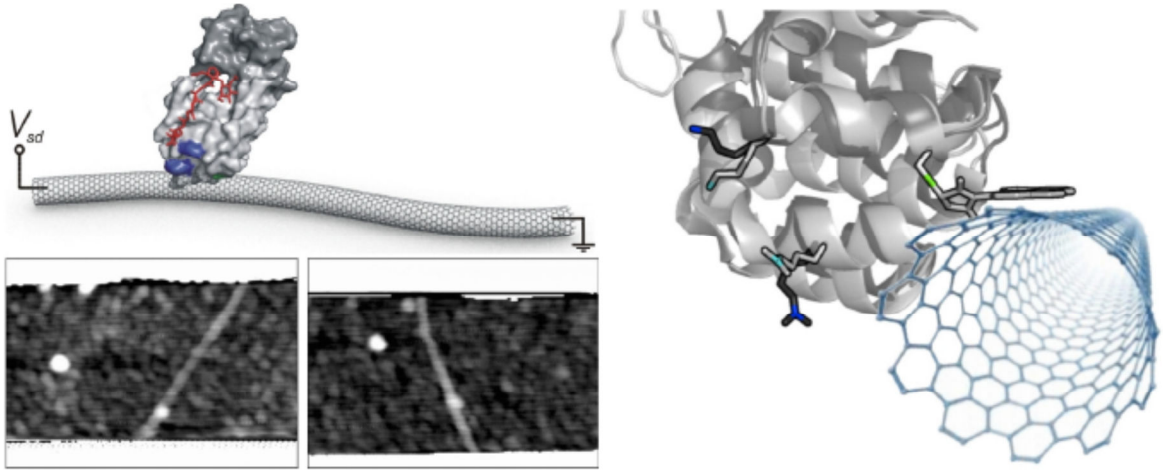

Figure 1. **Single biomolecule nanocircuits**. (left) Schematic representation of a device, showing the relative size of a carbon nanotube to lysozyme. Lysozyme's two active domains (light and dark grey) move with respect to each other when processing substrate (red). Example AFM images show carbon nanotube transistors labeled with single T4 lysozyme molecules. (right) Detail of a pyrene-maleimide linker molecule attaching a protein to the nanotube sidewall. A cysteine (C90) has been introduced to a cysteine-free variant of T4 lysozyme to provide a single and reproducible attachment site. Charged amino acids K83 and R119 are highlighted because they move substantially during catalytic processing and are believed to play important roles affecting the SWNT device.

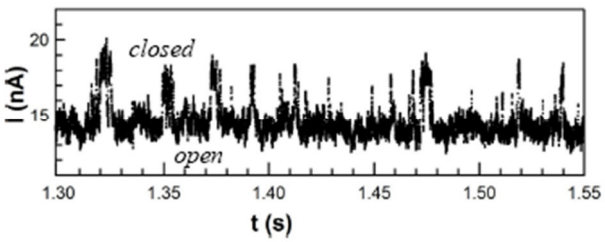

Figure 2. Lysozyme activity. Electronic signals transduced by a single T4 lysozyme molecule during processing of its substrate, peptidoglycan. The device current fluctuates between two levels in sync with the enzyme domains opening and closing on substrate, producing a real-time electrical recording of the enzyme's activity.

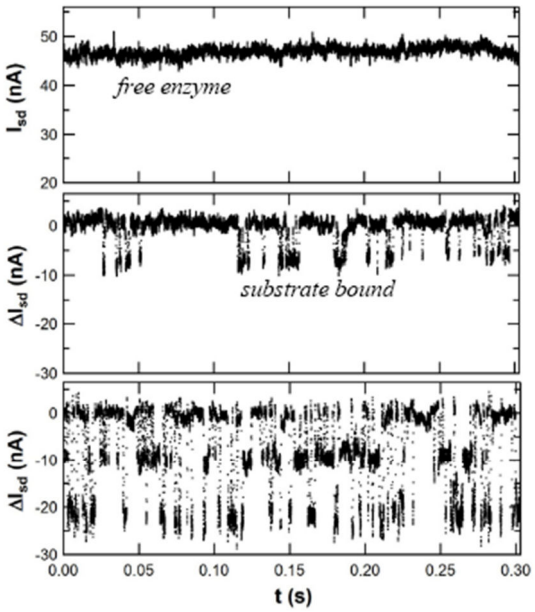

Figure 3. Protein Kinase A activity. Electronic signals transduced by a single PKA molecule without substrate (top), with Kemptide substrate (middle), and with both substrate and ATP present (bottom). The current difference ΔI in the bottom two panels is relative to the free enzyme level of the top panel. When both substrate and ATP are present, two independent binding events produce a three-molecule complex that allows for substrate phosphorylation. The electronic signal easily distinguishes the intermediate state with substrate bound from the fully closed state when phosphorylation can occur.

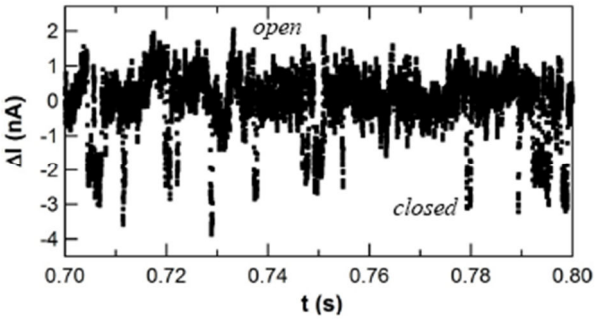

Figure 4. Klenow fragment activity. Electronic signals transduced by a single molecule of the Klenow fragment of DNA polymerase I. When measured in the presence of homopolymeric, single-stranded DNA ($poly(dT)_{42}$) and complementary dATP nucleotides, brief current excursions below the baseline ΔI=0 correspond to single nucleotide incorporation events.

References

[1] Y. Choi, I. Moody, P. Sims, S. Hunt, B. Corso, G. Weiss, P. Collins, Science 335 (2012) 319.

[2] Y. Choi, I. Moody, P. Sims, S. Hunt, B. Corso, D. Seitz, L. Blaszcazk, P. Collins, G. Weiss, J. Am. Chem. Soc. 134 (2012) 2032.

[3] P. Sims, I. Moody, Y. Choi, C. Dong, M. Iftikhar, B. Corso, O. Gul, P. Collins, G. Weiss, J. Am. Chem. Soc. 135 (2013) 7861.

[4] T. Olsen, Y. Choi, P. Sims, O. Gul, B. Corso, C. Dong, W. Brown, P. Collins, G. Weiss, J. Am. Chem. Soc. 135 (2013) 7855

[5] Y. Choi, T. Olsen, P. Sims, I. Moody, B. Corso, M. Dang, G. Weiss, P. Collins, Nano Lett. 13 (2013) 625.

Grain Boundary Resistivity in Polycrystalline Graphene

Aron W. Cummings[1], Dinh Van Tuan[1], Jani Kotakoski[2,3] and Stephan Roche[1,4]

[1]ICN2 - Institut Catala de Nanociencia i Nanotecnologia,Campus UAB, Barcelona, Spain
[2] Department of Physics, University of Vienna, Boltzmanngasse 5, 1090 Wien, Austria
[3] Department of Physics, University of Helsinki, 00014 University of Helsinki, Finland
[4] ICREA - Institucio Catalana de Recerca i Estudis Avançats, 08010 Barcelona, Spain

aron.cummings@icn.cat

In recent years, graphene has emerged as a favorable material for a wide range of technological applications [1]. In particular, its high room-temperature mobility, unique dispersion relation, and advantageous mechanical properties make graphene an exciting substance for the realization of next-generation electronic devices [2,3]. While single-crystal graphene would be an ideal choice, the most promising approach for the mass production of large-area graphene is chemical vapor deposition (CVD), which usually results in a material that is polycrystalline [4,5]. This polycrystallinity arises due to the nucleation of growth sites at random positions and orientations during the CVD process. In order to accommodate the lattice mismatch between misoriented grains, the grain boundaries in polycrystalline graphene are made up of a variety of non-hexagonal carbon rings, which can serve as a source of scattering during charge transport [6,7]. Indeed, several experimental works have demonstrated that grain boundaries add an extra resistance compared to single-grain samples [8-10]. Thus, in order to understand the large-scale transport properties of polycrystalline graphene, it is important to understand the scattering mechanisms associated with the grain boundaries.

In this work, we use numerical simulations to examine the role that grain boundaries play in charge transport through polycrystalline graphene. We find that the presence of grain boundaries increases the sheet resistance of graphene samples, and by employing a simple scaling law we can extract the intrinsic grain boundary resistivity from our simulations. A comparison to experiment reveals that the calculated grain boundary resistivity is 1-2 orders of magnitude smaller than what is obtained from experimental measurements. This suggests that scattering due to the non-hexagonal structure of the grain boundaries is relatively small, and that another mechanism must be responsible for most of the experimentally-measured grain boundary resistivity.

To calculate the sheet resistance of polycrystalline graphene, we use a real-space order-N quantum wave packet approach to compute the Kubo-Greenwood conductivity [7]. In this approach, the zero-frequency conductivity for charge carriers is given by

$$\sigma_{\infty}(E) = \frac{e^2}{4}\rho(E)\lim_{t\to\infty}\frac{\partial}{\partial t}\Delta X^2(E,t), \quad (1)$$

where $\rho(E)$ is the density of states and $\Delta X^2(E,t)$ 2 is the mean-square spreading of the wave packet. From this, we can calculate the sheet resistance of a polycrystalline graphene sample as $R_S = 1/\sigma_{DC}$. By doing this calculation for samples of varying grain size, we can extract the grain boundary resistivity according to a simple scaling law,

$$R_S = R_S^0 + \frac{\rho_{GB}}{l_G}, \quad (2)$$

where R_S^0 is the sheet resistance of an individual grain, ρ_{GB} is the grain boundary resistivity, and l_G is the average diameter of each grain.

The results of these simulations can be seen in Fig. 1, where we plot the sheet resistance of polycrystalline graphene as a function of the average grain size. The blue squares are from our simulations, and the blue dotted line is a fit to this data using Eq. (2) and assuming that $R_S^0 = 0$. From this fit we extract a grain boundary resistivity of $\rho_{GB}^{sim} = 0.064$ kΩ- µm . For comparison, we also plot the sheet resistance of polycrystalline graphene measured by Duong et al [8]. The red circles

indicate their measurements, and the red dotted line is the fit to Eq. (2). From this fit, we extract R_S^0 = 130 Ω and ρ_{GB}^{exp} = 1.4 kΩ- µm, which is 20x larger than the theoretical value. Table 1 shows a summary of the values of ρ_{GB} extracted from a variety of experimental measurements. In all cases, the experimental value is 1-2 orders of magnitude larger than our calculated value.

These results suggest that the scattering due to the non-hexagonal structure of the grain boundaries is relatively small, and that another mechanism must be responsible for most of the experimentally-measured grain boundary resistivity. It has been shown experimentally that the grain boundaries tend to be highly reactive compared to pristine graphene [4,8,11,12], resulting in a great deal of functionalization between individual grains. Therefore, our future work involves a study of the effect that grain boundary functionalization has on the charge transport properties of polycrystalline graphene.

References

[1] A. K. Geim, Science 324 (2009), 1530-1534.
[2] K. S. Novoselov, Rev. Mod. Phys. 83 (2011), 837-849.
[3] A. H. Castro Neto et al., Rev. Mod. Phys. 81 (2009), 109-162.
[4] P. Y. Huang et al., Nature 469 (2011), 389-392.
[5] K. Kim et al., ACS Nano 5 (2011), 2142-2146.
[6] O. V. Yazyev and S. G. Louie, Nat. Mater. 9 (2010), 806-809.
[7] D. van Tuan et al., Nano Lett. 13 (2013), 1730-1735.
[8] D. L. Duong et al., Nature 11 (2012), 235-240.
[9] Q. Yu et al., Nat. Mater. 10 (2011), 443-449.
[10] A. W. Tsen et al., Science 336 (2012), 1143-1146.
[11] P. Nemes-Incze et al., Appl. Phys. Lett. 99 (2011), 023104.
[12] A. Salehi-Khojin et al., Adv. Mater. 24 (2012), 53-57.

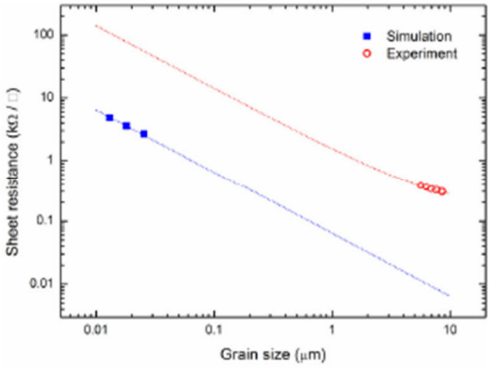

Figure 1. Sheet resistance of polycrystalline graphene as a function of average grain size. The blue squares are the results of numerical simulations and the red circles are measurements from Ref. [8]. The dotted lines are fits using the scaling law in Eq. (2).

Source	Grain size	ρ_{GB}(kΩ - µm)	$\rho_{GB}^{exp}/\rho_{GB}^{sim}$
This work	13 – 25 nm	0.064	1
Duong et al. [8]	5 – 9 µm	1.4	22
Yu et al. [9]	5 – 10 µm	8	125
Tsen et al. [10]	1 µm	0.5 – 4	8 – 63

Table 1. Comparison of theoretical and experimental grain boundary resistivity. The first row shows our numerical results, and the subsequent rows show the experimental results.

Graphene based tunable nano-plasmonic infrared tweezers

Mohammad Danesh[1,2], Cheng-Wei Qiu[2] and Er-Ping Li[1]

danesh@nus.edu.sg

[1]Institute of High Performance Computing (A*STAR), 1 Fusionopolis Way #16-16 Connexis, Singapore
[2]National University of Singapore, 21 Lower Kent Ridge Road, Singapore

Since the pioneer work by Ashkin, diffraction-limited focused beams have become a powerful method for manipulating micrometer sized objects [1]. Further extending this concept to effectively manipulate and control nanometer sized particles introduces new challenges. A major issue can be the large reduction of the total force with size which requires higher field intensities and smaller spot sizes. Fundamental limitations in focusing beams and practical limitations in increasing laser intensities make obtaining such highly confined fields in the nanoscale difficult [2]. An approach to elevate this issue is to apply well engineered structures to confine evanescent electromagnetic fields way beyond the diffraction limit [3]. In this work we are focusing on engineering nanostructured material to effectively control nanoparticles. The choice of Graphene as the material interface, in addition to supporting plasmons in the infrared spectrum adds a new tunability dimension to the nano-tweezers. In standard trapping apparatuses control of the position of the particle requires steering or changing the polarization of the incident beam. In plasmonic tweezers this is more difficult due to the dependence of the trapping process on the geometry [4]. However in this design Graphene's inherent tunability allows localized control over the trapping forces via electrostatic gates embedded on the structure. It is shown that the highly confined plasmons on the Graphene aperture allow a low powered beam (0.18 nW/μm^2) to exert forces up to 50 pN on the particle. In addition by slightly detuning the incident light from the resonance frequency of the aperture, the structure has been optimized to have a self-induced back action feature (SIBA) effect to further reduce the intensity requirements [5]. We believe this design shows the capability of Graphene based nanoplasmonic structures to extend optical nanotweezers further for advanced multipurpose nanoscale functions such as ultra-accurate positioning and trapping, particle sorting, self assembly and maybe someday an integrated carbon based lab-on-a-chip.

References

[1] Ashkin, A., et al., Observation of a single-beam gradient force optical trap for dielectric particles. Opt. Lett., 11 (1986) p. 288-290.
[2] Juan, M.L., M. Righini, and R. Quidant, Plasmon nano-optical tweezers. Nat Photon, 5(6) (2011) p. 349-356.
[3] Kern, J., et al., Atomic-Scale Confinement of Resonant Optical Fields. Nano Letters, 12(11) (2012) p. 5504-5509.
[4] Kang, J.-H., et al., Low-power nano-optical vortex trapping via plasmonic diabolo nanoantennas. Nat Commun, 2: (2011) p. 582.
[5] Juan, M.L., et al., Self-induced back-action optical trapping of dielectric nanoparticles. Nature Phys., 5: (2009) p. 915-919.

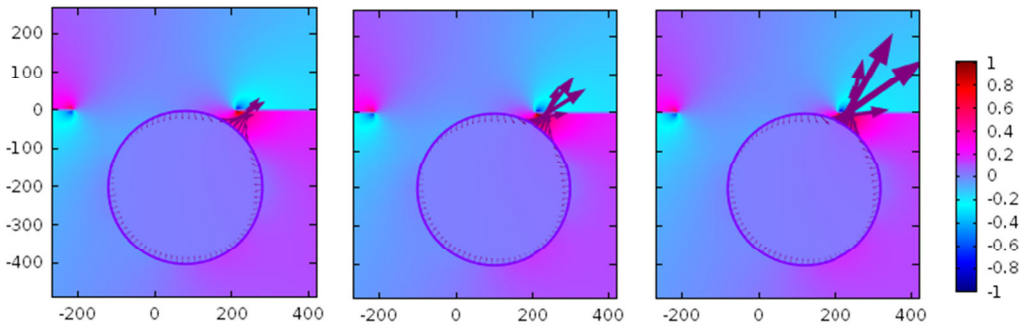

Figure 1. Trapping of dielectric particle in Graphene aperture trap. The particles position progresses from 80 to 120 nm. Background is intensity (normalized) of electric field perpendicular to the Graphene sheet. Arrows are total time averaged electromagnetic force exerted on the particles surface.

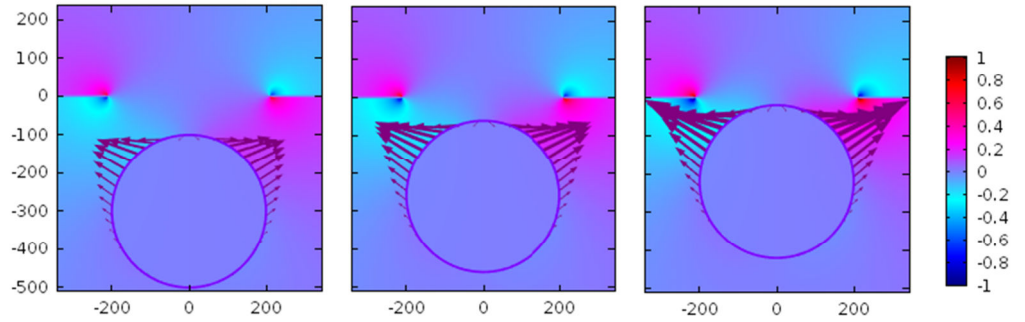

Figure 2. Trapping of the dielectric particle in the plasmonic near-field as it converses in the y direction from -300 to -220 nm. Here it is assumed the particle is moving along the x=0 line. The total force is upwards, opposite to the direction of the incident wave and the scattering force.

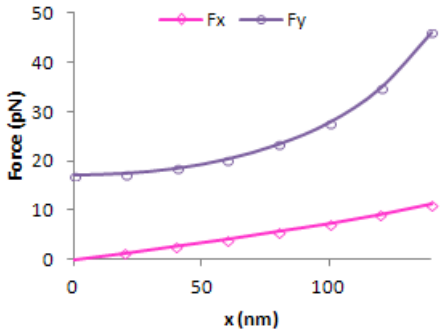

Figure 3. Total force on particle as it traverses in the x direction below the aperture. The power intensity P is 0.18 (nW/μm^2). In the x direction a linear behavior can be observed with a stiffness of 0.44 (pN/nm/P). In the y direction the force shows a second order behavior with an averaged stiffness of approximately 2.5 (pN/nm/P).

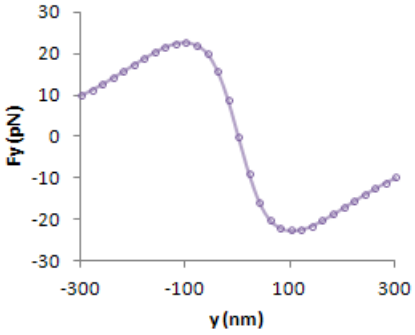

Figure 4. Total force on particle as it moves along the x = 0 line. The power intensity P is 0.18 (nW/μm^2). In the -100 to 100 nm range an average stiffness of 3.37 (pN/nm/P) is achieved. When the particle is above the aperture in respect to the incident beam, a pushing force is observed and when the particle is below the aperture a pulling force of equal magnitude exists

Nanoparticles and Occupational Risks Prevention

Mª Nieves de la Peña

osalantpr16ba@ej-gv.es

Lan Segurtasun eta Osasunerako Euskal Erakundea - Osalan – Basque Institute for Occupational Health and Safety
Dinamita bidea, z/g, 48903 Barakaldo, Spain

Manufactured or enigneered nanoparticles show some properties, due to its so small size, quite different from the ones that the same material at a higher scale has. These new properties are a key factor in generating new materials or materials with others properties, new medical cures, new products, fabrics, etc. However, these properties have created a worry about their effect on the human organism and environment. At the workplace Occupational Risks Prevention management has to give an answer to this situation and implement the means to prevent the effects over the workers' health. In order to do that, it seems that the engineering controls, personal protection measures, used up to now, with new work procedures considering the presence of nanoparticles could be enough, although, nowadays, the information in this area is not definitive, sometimes contradictory or not existent: effects? parameter to measure? measurement equipment? exposure reference value? laws or standards? –we have REACH and CLP, but…- . Besides, the European Commission has included in its definition of nanoparticles any nanosized particle, not only the engineered ones. This definition suggests that any nanosized particle has to be considered in a workplace and that is a great change for the Occupational or Industrial Hygiene and perhaps could explain the effects of some occupational exposures…

References

[1] Brouwer, Derk (TNO) "Nano Release & Exposure Scenarios" Lecture SENN 2012

[2] Berges, Markus (IFA – Institut für Arbeitsschutz der Deutschen Gesetzlichen Unfallversicherung) "Field measurements of nanoparticles" Lecture SENN 2012

[3] Muir, Robert (Naneum Limited) "Measurement of Health Risk from Exposure to ENP and Recent Instruments Developments" Lecture SENN 2012

[4] Golanski, Luanna (Comissariat à l'Energie Atomique – CEA), Guillot, Aranaud (CEA), Tardif François (CEA) "Are Conventional protective devices such as fibrous filter media, cartridge for respirators, protective clothing and gloves also efficient for nanoaerosols? Efficiency of fibrous filters and personal protective equipments against aerosol." Dissemination Report January 2008, DR325/326-200801-1 Project ID NMP2-CT-2005-515843

[5] Tardif, François (CEA), Sicard, Yves (CEA), Shakesheff, Alan (QNL), Moehlmann, (HVBG-BGIA), Backman, Ulrika (VTT) "Is it possible to easily measure the engineered nanoparticles at workplaces? An essential step for exposure evaluation in case of potential nanotoxicity" Dissemination report June 2008 DR115/121 June 200806-3 Project ID NMP2-CT-2005-515843

[6] Hoet, P (KUL), Bois, F (Ineris) "What is nanotoxicology? How to estimate the potential hazard related to nanoparticles?" Dissemination report October 2008 DR-225 200810-5 Project ID NMP2-CT-2005-515843

[7] Paik, Samuel Y (Lawrence Livermore National Laboratory –LLNL), Zalk, David M (LLNL) and Swuste, Paul (Safety Science Group, Delft University of Technology) "Application of a Pilot Control Banding Tool for Risk Level Assement and Control of Nanoparticle Exposures" Ann Occup. Hyg Vol 52 No6 (2008), pp419-428

[8] Communication from the Commission to the European Parliament, the Council and the European Economic and Social Committee.

Second Regulatory Review on Nanomaterials. Brussels, 3.10.2012. COM(2012) 572 final

[9] Gulumian, Mary "Wide approach to nanotechnology, safety, health exposure and its assessment, and monitoring devices" Keynote 1 SENN 2012

[10] Keller, M, Kreck G, Holzapfel, Y "Monitoring Method for Carbon Nanotubes (CNT): Personal Sampler and Corresponding Reading Device " Oral Free Communication SENN 2012

[11] Fierz, M, Meier, D, Steigmeier P, Burtscher M " A nanoparticle dosimeter for workplace exposure monitoring" Oral Free Communication SENN 2012

[12] Cheatham B.J. " Optical Observation and Hyperspectral Characterization of Nanomaterials in-situ" Oral Free Communication SENN 2012

[13] Pagels J, Nilsson P.T., Eriksson A, Isaxon C., Messing M.E., Deppert K., Hedmer M "Method for highly time and resolved detection of metal nanoparticles" Oral Free Communication SENN 2012

[14] Burdett G., Bard D,, Kelly A., Staff J. "The use of online aerosol measurement instruments for the dustiness testing of nanopowders" Oral Free Communication SENN 2012

[15] Hämeri, Kaarle "Characteristics of nanoparticles – particles composition and properties for exposure studies" Keynote 3 SENN 2012

[16] Geraci, Charles "Exposure Assessment: A key element in setting effective occupational exposure limits for nanomaterials" Keynote 4 SENN 2012

[17] Kasper, Gerhard "Detection and Monitoring of ENP in Air: Devices, Techniques, Strategies – A Perspective." Keynote 5 SENN 2012

[18] Endo, Morinobu "Carbon nanotubes: promises for the future" Keynote 6 SENN 2012

[19] Shvedova, Anna A " Redox interactions and inflammation in Pulmonary Toxicity of Carbonaceus Nanoparticles" keynote 7 SENN 2012

[20] Tinke, Sally "Controlling risks of nanotechnology/ engineered nanoparticles" Keynote 8 SENN 2012

[21] Kuhlbusch, Thomas "Bridging the gap between exposure and effects –from concentration to dose" Keynote 9 SENN 2012

[22] Industrial Forum IMAGINENANO 2013. Bilbao. EHS Advance Conferences organised by NANOBASQUE

Luminescent Core–Shell Imprinted Nanoparticles Engineered for Targeted Förster Resonance Energy Transfer-Based Sensing

Ana B. Descalzo[1], Clara Somoza[1], María C. Moreno-Bondi[2] and Guillermo Orellana[1]

ab.descalzo@quim.ucm.es

Dpmts. of [1]Organic Chemistry and [2]Analytical Chemistry, Faculty of Chemistry, Complutense University of Madrid (UCM), Av. Complutense s/n, 28040, Madrid, Spain

Molecularly imprinted polymers (MIPs) are regarded as synthetic analogues of antibodies in that they bear cavities which are complementary in size, shape, and chemical functions to a target molecule [1]. Such biomimetic materials can be employed as adsorbents for selective binding of the latter, making them useful as stationary phases for smart chromatography-based analysis. However, alternative analytical methods based on fluorescent detection are needed to enable fast, sensitive, user-friendly, affordable sensing devices for health care, food, and environmental testing.

The task of coupling a binding event in a MIP with an optical signal is not straightforward. Here we show how this is possible to benefit from a *Förster resonance energy transfer* (FRET) process for signaling binding of our target analyte, enrofloxacin –a broad spectrum antibiotic– to a MIP layer. FRET is a photochemical distance-dependent process that can reveal the proximity of two species, an energy donor (D)–acceptor (A) pair, by way of their luminescence. An efficient electronic energy transfer from the photoexcited D to ground state A dyes occurs if D and A approach enough ($R < 10$ nm) and if there is significant spectral overlap between the emission of D and the absorption of A [2].

The approach described herein involves FRET between near-infrared (NIR) labeled analyte molecules and *luminescent core–shell nanoparticles* (NPs). A cyanine-labeled enrofloxacin (NIR-ENR) has been chosen as the FRET acceptor and the $[Ru(phen)_3]^{2+}$ (phen: 1,10-phenantroline) complex is the energy donor (Figure 1).[3] In addition to detection in the NIR region, another advantage of this D–A pair is the long emission lifetime of the Ru(II) dye. Furthermore, the D molecules are encapsulated into silica NPs to bring about signal intensification [4] and minimize luminescence quenching by dissolved oxygen.[5] Finally, a thin polymer shell, imprinted with our target analyte, is grown around the silica NP core, providing selective binding sites for the antibiotic.

In order to optimize the FRET signal output, we had to consider two parameters: i) the distribution of D dye molecules in the NPs –location of the dye in the NP can be controlled at will by adjusting the *time* elapsed before the luminophore is added to the reaction mixture;[6] and ii) the MIP shell *thickness*, that should not be too large in order to allow the adequate FRET to the bound acceptor. The last can be regulated by adjusting the concentration of monomers and cross-linkers in the polymerization mixture.[7]

The resulting core–shell NPs were evaluated in a competitive assay between NIR-ENR and ENR itself, and changes on the FRET signal were employed for determining the extent of enrofloxacin binding (Figure 2).

The *nanoanalytical platform* engineered in this way can be tuned to virtually any analyte to benefit from background-free emission intensity and lifetime measurements, the brightness of dyed nanoparticles, the fast kinetics of the assay and, remarkably, the advantage of performing the biomimetic assay in rich aqueous (buffered) media at neutral pH. In this way, the artificial system might become a cheaper more robust alternative to competitive fluorescence immunoassays.

References

[1] a) L. Ye, Mosbach, K. Chem. Mater. 20 (2008) 859; b) S.-W. Lee, T. Kunitake, Eds. Handbook of Molecular Imprinting: Advanced Sensor Applications; Pan Stanford: Singapore (2013); c) K. Haupt, Ed. Molecular Imprinting, Topics in Current Chemistry; Springer: Berlin Heidelberg, 325 (2012).

[2] a) T.W.J. Gadella, Ed. FRET and FLIM Techniques, Laboratory Techniques in Biochemistry and Molecular Biology; Elsevier: Amsterdam, 33 (2009); b) B. Valeur, M.-N. Berberán-Santos, In Molecular Fluorescence: Principles and Applications, 2nd ed.; Wiley-VCH: Weinheim (2012) 231–261.

[3] A.B. Descalzo, C. Somoza, M.C. Moreno-Bondi, G. Orellana, Anal. Chem. 2013 DOI: 10.1021/ac400520s.

[4] a) S. Zhu, T. Fischer, W. Wan, A.B. Descalzo, K. Rurack, Topics Curr. Chem. 300 (2011) 51; b) S. Bonacchi, D. Genovese, R. Juris, M. Montalti, L. Prodi, E. Rampazzo, N. Zaccheroni, Angew. Chem. Int. Ed. 50 (2011) 4056; (c) L. Wang, K. Wang, S. Santra, X. Zhao, L.R. Hilliard, J.E. Smith, Y. Wu, W. Tan, Anal. Chem. 78 (2006) 646.

[5] J. López-Gejo, D. Haigh, G. Orellana, Langmuir 26 (2010) 2144.

[6] D. Zhang, Z. Wu, J. Xu, J. Liang, J. Li, W. Yang, Langmuir, 26 (2010) 6657.

[7] D. Gao, Z. Zhang, M. Wu, C. Xie, C. Guan, D. Wang, J. Am. Chem. Soc. 129 (2007) 7859.

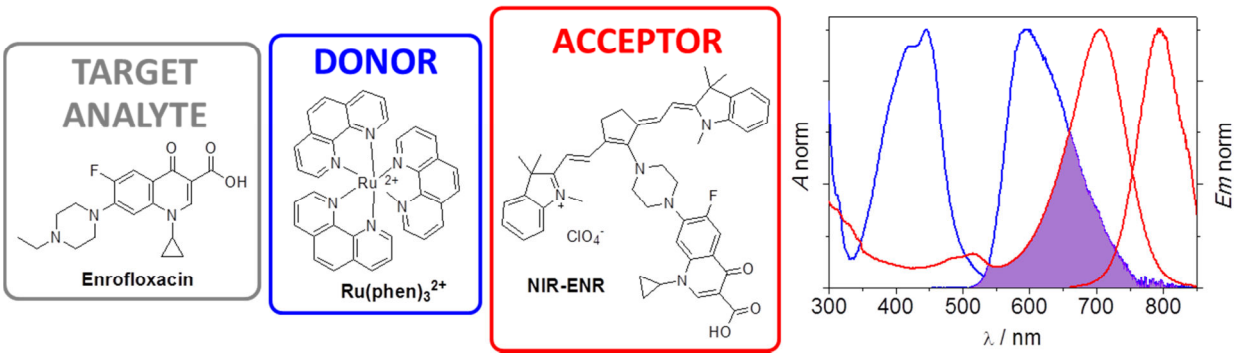

Figure 1. Chemical structures of the enrofloxacin (ENR) analyte, the FRET donor ($Ru(phen)_3^{2+}$), and the FRET acceptor fluorophore (NIR-ENR). The graph shows the absorption and emission spectra of D (blue) and A (red) in ethanol, with the region of the spectral overlap in violet.

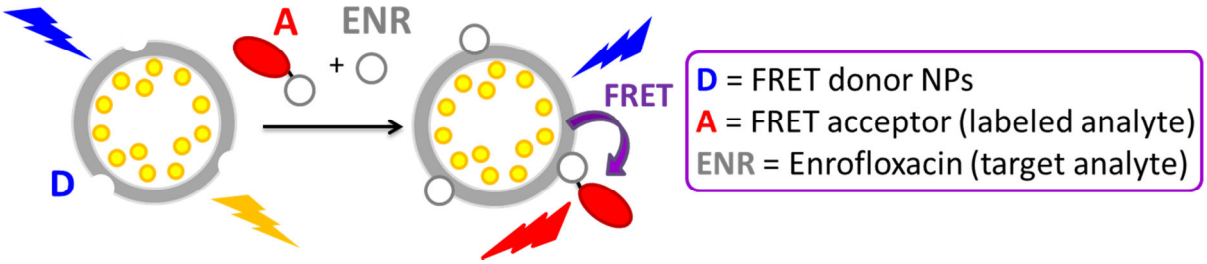

Figure 2. Schematic representation of the NPs FRET assay described here. In this assay, the target analyte ENR competes for the binding sites of the MIP shell in the NPs with the FRET acceptor dye. Consequently, the higher the concentration of ENR, the weaker the FRET signal.

Keynote

Nitrogen atoms and molecules landing, reacting, and rebounding at metal surfaces

Ricardo Díez Muiño

rdm@ehu.es

Centro de Física de Materiales, Centro Mixto CSIC-UPV/EHU, San Sebastián, Spain
and Donostia International Physics Center DIPC, San Sebastián, Spain

Advances in gas-surface dynamics are largely triggered by the quest for systems and conditions under which reactivity can be controled, enhanced or inhibited. Nitrogen on metal surfaces is a common subject of studies in this field. The closed shell nature of molecular N_2, as well as its high binding energy, makes the molecule quite inert. In contrast, atomic N is generally reactive, recombines easily with other atoms, and strongly adsorbs at surfaces. This dichotomy turns the Nitrogen dynamics at surfaces into a rich and intriguing problem.

Here we review recent theoretical work on elementary reactive processes taking place when Nitrogen atoms and molecules interact with clean and decorated metal surfaces [1-4]. The theoretical framework relies on ab-initio built potential energy surfaces and full-dimensional classical dynamics. Energy exchange with the surface is included through the excitation of electron-hole pairs and phonons. We actually evaluate the role of these two energy dissipation channels in the scattering and adsorption of N_2 on W(110) and N on Ag(111) [1-2]. We show that, in atomic N adsorption, phonons are responsible for determining the adsorption probability but electronic excitations are relevant at a later stage to fix the atoms to the adsorption positions. In the case of N atoms incident on N-covered Ag(111), we show that the Eley-Rideal recombination process between gas-phase N atoms and N adsorbates is a highly efficient mechanism for N_2 formation [3]. Finally, we show that strain can be a useful tool to promote reactivity: N_2 molecules adsorb and dissociate with higher rates at the strained Fe/W(110) surface than at the Fe(110) surface [4]. We conclude that relatively small variations in interaction energies can lead to drastic changes in the dynamics and thus to modifications in the final output of the scattering process.

References

[1] L. Martin-Gondre, M. Alducin, G. A. Bocan, R. Díez Muiño, and J. I. Juaristi Phys. Rev. Lett. 108, 096101 (2012).
[2] L. Martin-Gondre, G. A. Bocan, M. Alducin, J. I. Juaristi, and R. Díez Muiño Computational and Theoretical Chemistry 990, 126 (2012).
[3] M. Blanco-Rey, E. Díaz, G. A. Bocan, R. Díez Muiño, M. Alducin, and J. I. Juaristi (submitted, 2013).
[4] I. Goikoetxea, M. Alducin, R. Díez Muiño, and J. I. Juaristi (submitted, 2013)

Spin-dependent transport in graphene-based nanostructures

F. Domínguez-Adame[1], J. Munárriz[1], C. Gaul[1], A. V. Malyshev[1], P. A. Orellana[2] and C. A. Müller[3]

[1]GISC, Departamento de Física de Materiales, Universidad Complutense, Madrid, Spain
[2]Departamento de Física, Universidad Técnica Federico Santa María, Valparaíso, Chile
[3]Centre for Quantum Technologies, National University of Singapore, Singapore

adame@ucm.es

The occurrence of large spin-coherence lengths [1] has spurred the interest in graphene as a material of choice for spintronic devices. In this contribution we show the occurrence of a spin-dependent transport and negative differential resistance (NDR) in quantum rings and superlattices based on armchair graphene nanoribbons. We consider nanoribbons with a set of ferromagnetic insulating stripes, like EuO, grown on top of it (Figure 1). The ferromagnets induce the exchange splitting of the electronic levels in the regions of the ribbon located just below the stripes. This results in a spin-dependent potential profile. One can choose the system geometry to produce a resonant mode close to the energy of the band edge for spin up electrons, paving the way for obtaining spin-dependent NDR.

Numerical simulations were carried out using the standard tight-binding model, taking into account up to the third nearest neighbor interaction and the hydrogenation of carbon atoms in the edge of the nanoribbon. We used the quantum transmission boundary method (see Refs. [2,3] for details) to obtain the spin-dependent transmission coefficient for a given energy and source-drain voltage. In the case of superlattices, results were compared to those obtained by the Dirac approach [4], valid at energies close to the Fermi level. Using the Landauer-Buttiker formalism we calculated the current-voltage characteristics.

We show that due to the exchange splitting induced by the magnetic ion of the ferromagnetic layer, the transmission coefficient in quantum rings, shown in left panel of Figure 1, is different for spin up and spin down electrons, giving rise to the polarization of the conductance and the electric current [3]. We demonstrated that both the current and its polarization can be controlled by a side-gate voltage. Predicted effects are shown to be robust under a moderate edge disorder and other fabrication imperfections, such as the asymmetry of the ring.

We found that the current-voltage curves show regions of well-defined NDR in the case of the superlattice shown in the right panel of Figure 1. The spin dependence of the transmission spectrum leads to different voltage intervals at which highly transmitting channels are open, which makes the NDR be spin-dependent too, as shown in Figure 2. We note that in a spintronic device the degree of freedom that carries information is the polarization of the current rather than its magnitude. We show that the current polarization is also a non-monotonic function of the source-drain voltage, suggesting that it can be used as resonant tunnel device. This opens a possibility to design a whole new class of true spintronic circuits such as spin oscillators, amplifiers and triggers.

References

[1] C. L. Kane and E. J. Mele, Phys. Rev. Lett. 95 (2005) 226801.
[2] J. Munárriz, F. Domínguez-Adame and A. V. Malyshev, Nanotechnology. 22 (2011) 365201.
[3] J. Munárriz, F. Domínguez-Adame, P. A. Orellana and A. V. Malyshev, Nanotechnology 23 (2012) 205202.
[4] J. Munárriz, C. Gaul, A. V. Malyshev, P. A. Orellana, C. A. Müller and F. Domínguez-Adame (2013, submitted for publication).

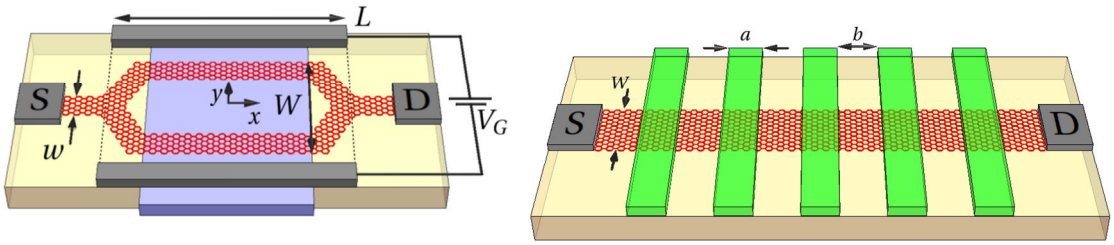

Figure 1. Schematic views of the nanodevices (quantum ring with side-gate voltage [3] at the left and superlattice [4] at the right), with ferromagnetic insulating stripes grown on top of them. The devices are connected to source (S) and drain (D).

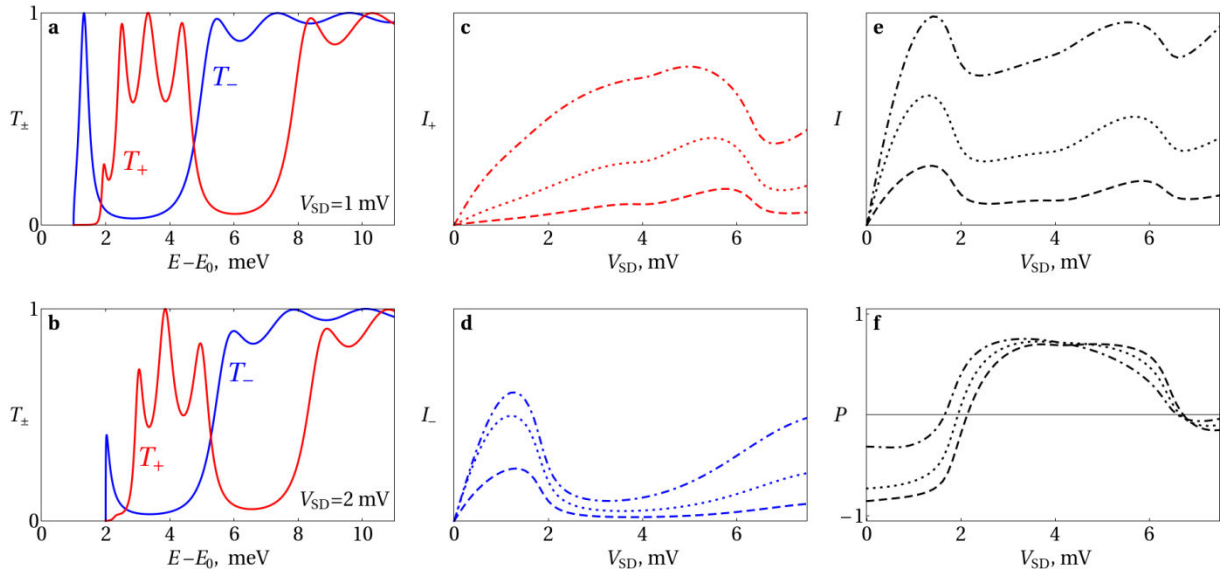

Figure 2. Panels a) and b) show the transmission bands in the superlattice for both spins at finite bias. Panels c) and d) display the spin-polarized currents $I_\pm$ as functions of the bias V_{SD}, for T = 4 K and different values of the chemical potential. Finally, panels e) and f) show the total current $_I = I_+ + I_-$ and the current polarization $P = (I_+ + I_-)/I$ for the same parameters. All the intensity plots use the same arbitrary scale.

Keynote

Heat transport in graphene and three-dimensional nanostructured carbon

Davide Donadio

donadio@mpip-mainz.mpg.de

MPI for Polymer Research
Ackermannweg 10
55128 Mainz - Germany

Carbon presents a wealth of allotropic forms with a wide range of thermo-mechanical properties. For example diamond is the bulk material with the highest lattice thermal conductivity, which is exceeded only by the thermal condcutivity of carbon nanostructures, such as graphene and nanotubes.

Combining atomistic molecular dynamics simulations and lattice dynamics calculations we investigate the phonon processes that make carbon nanostructures so versatile in either efficiently conducting or blocking heat. To this aim we compare phonon transport properties of carbon nanotubes, suspended graphene, negatively curved three-dimensional graphene and diamond at different conditions.

Synthesis of Nanographene Fragments

Antonio M. Echavarren, Pilar Calleja, and Ruth Dorel

Institute of Chemical Research of Catalonia (ICIQ),
Av. Països Catalans 16, 43007 Tarragona, Spain

aechavarren@iciq.es

As part of a program on the synthesis of large polyarenes for their application in molecular electronics [1], our group is developing new strategies for the rational synthesis of well-defined molecular-sized sections of graphite single layers (nanographenes) and linear acenes (tetracene, pentacene, and the like) based on the use of Au(I)-catalyzed reactions. To limit the problems of handling insoluble materials, the transformations leading to planarization will be delayed until the last step(s) of the synthesis.

Thus, we have synthesized dihydrotetracene **2** by cyclization synthesis of functionalized acenes by gold(I)-catalyzed [4+2] cycloaddition of 1,7-enynes, a powerful synthetic method developed in our group [2].

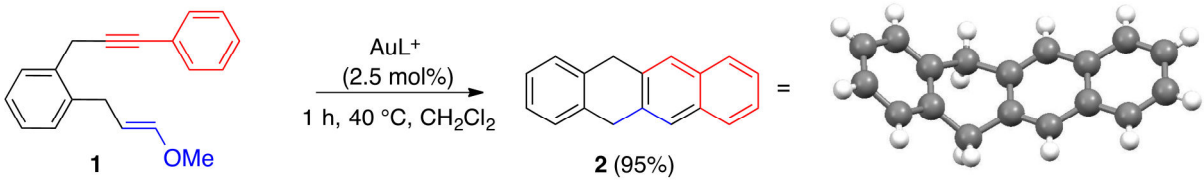

In addition, we will discuss our work aimed at the preparation of larger polyarenes such as planar C54 derivative **5** from 1,7-enyne **3** using a Lego-type approach. The Diels-Alder reaction of **5** at the bay regions could lead to a C66 nanographene [3]. Using this and related strategies, nanoribbons o non-symmetrical nanographenes could be also be obtained.

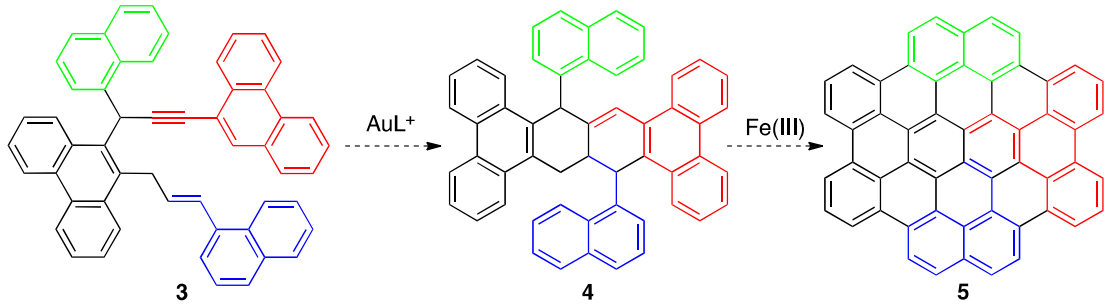

Acknowledgements. We thank the MICINN (CTQ2010-16088/BQU), AtMol (Contract No. ICT-270028), European Research Council (Advanced Grant No. 321066), the AGAUR (2009 SGR 47), PFU fellowship to P. C., and the ICIQ Foundation for financial support.

References

[1] (a) Soe, W.-H.; Manzano, C.; Sarkar, A. D.; Ample, F.; Chandrasekhar, N.; Renaud, N.; de Mendoza, P.; Echavarren, A. M.; Hliwa, M.; Joachim, C. Phys. Rev. B 2011, 83, 155443. (b) Soe, W.-H.; Manzano, C.; Renaud, N.; de Mendoza, P.; Sarkar, A. D.; Ample, F.; Hliwa, M.; Echavarren, A. M.; Chandrasekhar, N.; Joachim, C. ACS Nano 2011, 5, 1436.

[2] (a) Nieto-Oberhuber, C.; López S.; Echavarren, A. M. J. Am. Chem. Soc. 2005, 127, 6178. (b) Nieto-Oberhuber, C.; Pérez-Galán, P.; Herrero-Gómez, E.; Lauterbach, T.; Rodríguez, C.; López, S.; Bour, C.; Rosellón, A.; Cárdenas, D. J.; Echavarren, A. M. J. Am. Chem. Soc. 2008, 130, 269.

[3] (a) Fort, E. H.; Donovan, P. M.; Scott, L. T. J. Am. Chem. Soc. 2009, 131, 16006. (b) Fort, E. H.; Scott, L. T. Angew. Chem. Int. Ed. 2010, 49, 6626.

Electron dynamics at surfaces, nanostructures, graphene and topological insulators

P. M . Echenique

Dpto. de Física de Materiales UPV/EHU,
Donostia International Physics Center (DIPC) and Material Physics Center (CFM).
Pº Manuel Lardizabal 4, 20018 Donostia - San Sebastián, Basque Country, Spain

Femtosecond and subfemtosecond time scales typically rule electron dynamics at metal surfaces. In this talk we shall analyze electron dynamics at surfaces and nanostructures, including graphene and topological insulators. Condensed matter effects on attophysics will also be discussed.

Ultra-Short Carbon Nanotubes as Novel Biotracers

R. Faes[1], L. Cognet[2], C. Jaillet-Bartholome[1], B. Lounis[2], L. Oudjedi[2] and P. Poulin[1]

[1]Centre de Recherche Paul Pascal CNRS UPR 8641, France
[2]Laboratoire Photonique Numérique et Nanoscience, Université de Bordeaux, France

faes@crpp-bordeaux.cnrs.fr

Ideal optical tracers for bioimaging should be nanosized, biocompatible and visualizable in nearIR wavelengths that can penetrate within biological tissues. Conventional fluorescent molecular labels are not active in the nearIR spectrum. Carbon nanotubes exhibit suitable optical properties and also strongly absorb nearIR irradiation. They can therefore be visualized via photothermal effects [1] in addition to photoluminescence. Unfortunately available nanotubes are generally too long (length>100nm) for bioimaging applications. In this context, ultra-short carbon nanotubes (CNTs) would offer a unique opportunity to become a novel type of highly efficient biolabels. We develop in this work ultra-short CNTs and their biofunctionalization, for a use as nearIR nanolabels. We target in particular the achievement of nanotubes shorter than 100 nm that can be visualized by photothermal spectroscopy [1] or photoluminescence. Ultrashort nanotubes are prepared by strong sonication treatments known to be efficient at cutting CNTs [2], chemical treatments [3] and sorted by length using Density Gradient Ultracentrifugation (DGU) [4].

The UV-vis-NIR absorption spectra of several fractions are shown in Fig. 1. The absorption peaks in 900-1300 nm range are due to the lowest E_{11} subband transitions. Multiple peaks corresponding to various semiconducting SWNTs are present in the sample. Both first and second subband absorption peaks show blue shifts as the average nanotube length is reduced. The shift is monotonic: shorter fractions show stronger blue shift. We can attribute the observed length-dependent spectra blue shifts of SWCNTs to finite length effects, that are due to quantum confinement along the SWCNT length [5].

The spectral shifts ΔE_{11} can be calculated using the following expression:

$$E = \frac{h_c}{\lambda} \; thus \; \Delta E(eV) = \frac{1240}{\lambda_2} - \frac{1240}{\lambda_1}$$

where ΔE is the spectral shift in electron-volts, and λ_2 and λ_1 are the wavelengths associated CNTs of a given chirality. We found high spectral shifts for the upper fractions of the vial after DGU process as shown in Fig. 2. This can be correlated to the theoretical estimation of the length :

$$\Delta E = \frac{\hbar^2 \times k_{zl}^2}{2m^*} = \frac{\hbar^2}{2m^*} \times \frac{\pi^2}{L^2}$$

with ħ the reduced Planck constant, m*the mass of the exciton, k_{zl} the quantization of wave vector along the length of the tube and *L* the length of the tube.

This theoretical estimation is confirmed by qualitative tapping mode AFM images of different fractions (Fig. 3). The shortened SWCNTs are identified as less than 15 nm for the fraction F, whereas their original length was approximately 1-2 µm. The CNTs showed an average length of 45 nm for the fraction F, whereas the average length for the fraction N was 812 nm.

Different approaches are used to functionalize ultra-short CNTs: on one hand the covalent functionalization for photothermic spectroscopy, and on the other hand the non-covalent functionalization, with molecules such as pyrene butyric succinimide, for the preservation of the luminescence properties.

Finally, biological tests will be performed by the “Laboratoire de la Synapse” at Bordeaux to image the plasticity of synapsis of glutamate receptors.

References

[1] Berciaud S., Cognet. L., Poulin P., Weisman B., Lounis B., Nano Letters, 7 (2007) 1203-1207.

[2] Lucas A., Zakri C., Maugey M., Pasquali M., Van der Schoot P., Poulin P., The Journal of Physical Chemistry C, 113 (2009) 20599-20605.

[3] Price B. K., Lomeda J.R., and Tour J.M., Chemistry of Materials, 21 (2009) 3917-3923.

[4] Sun X., Zaric S., Daranciang D., Welsher K., Lu Y., Li X. and Dai H., The Journal of the American Chemical Society, 130 (2008) 6551-6555.

[5] Wu, J.; Duan, W. H.; Gu, B. L.; Yu, J. Z.; Kawazoe, Y. Appl. Phys. Lett., 77 (2000) 2554–2556.

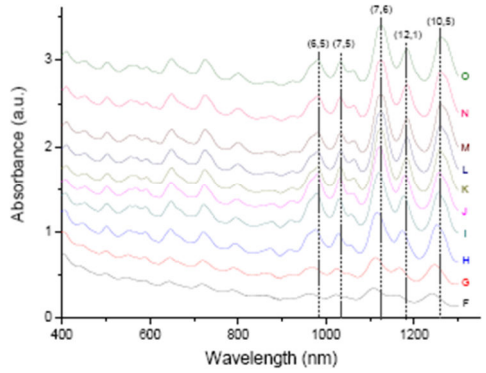

Figure 1. UV-Vis-IR measurements of different fractions of CNTs sorted by DGU. The CNT length is increasing from the bottom (F) to the top (O).

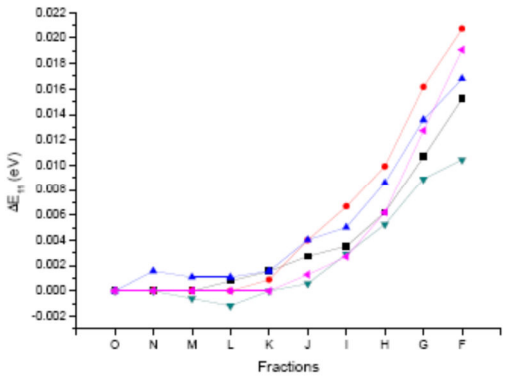

Figure 2. Spectral shifts ΔE11 for the upper fractions, calculated from the different CNTs chiralities ((10,5) in black, (12,1) in red, (7,6) in blue, (7,5) in Green and (6,5) in pink).

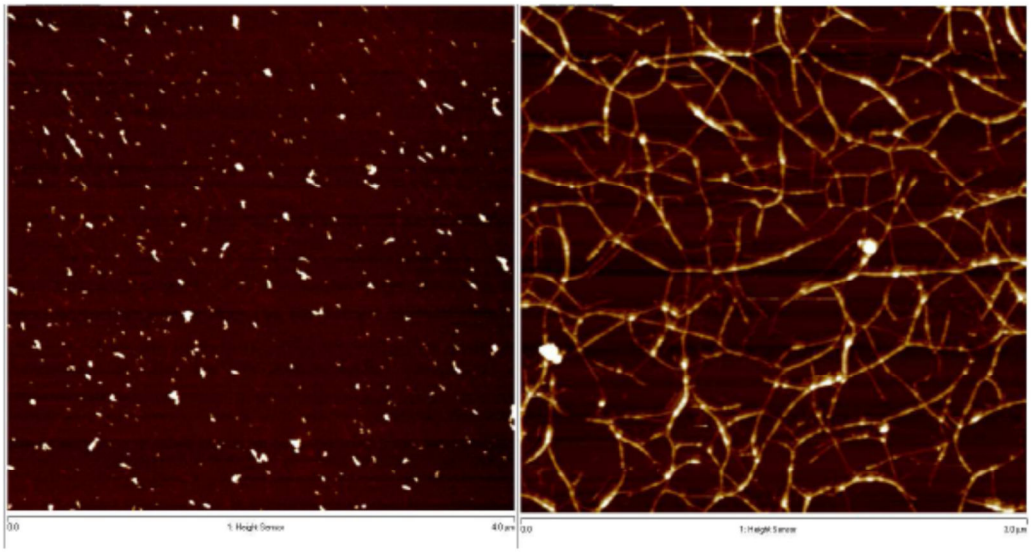

Figure 3. AFM image of spin-coated CNTs fraction F (left) and fraction N (right) onto mica substrate.

Electrons in graphene heterostructures with hexagonal crystals

John Wallbank,
M Mucha-Kruczynski,
Vladimir I. Falko

v.falko@lancaster.ac.uk

Department of Physics, Lancaster University, Lancaster, LA1 4YB, United Kingdom

We analyze the transformation of the spectrum of electrons in monolayer graphene and bilayer graphene due to the influence of a tightly bound insulating or semiconducting layer with a slightly incommensurate highly oriented hexagonal lattice, such as boron nitride, or InAs/GaSb. We present a symmetry-based classification and quantitative analysis of generic miniband structures for electrons in graphene heterojunction with 2D crystals with the hexagonal lattice which has the period almost matching the period of graphene lattice or the period of √3x√3 enlarged cell of graphene. We identify conditions for which the first moire miniband is separated from the rest of the spectrum, either by one or a group of three isolated mini Dirac point (not obscured by dispersion surfaces coming from other minibands), or by a well-developed gap. In such cases the Hall coefficient exhibits two distinct alternations of its sign as a function of charge carrier density. Then, we study the Hofstadter spectrum of electrons in such moire superlattice in a magnetic field.

Stepwise method to fabricate conductive molecular wires characterized by scanning tunneling microscopy

Quirina Ferreira[1], Ana Margarida Bragança[1], Luís Alcácer[1] and Jorge Morgado[1,2]

quirina.ferreira@lx.it.pt

[1]Instituto de Telecomunicações, Avenida Rovisco Pais, P-1049-001 Lisboa, Portugal
[2]Department of Bioengineering, Instituto Superior Técnico, Avenida Rovisco Pais, Portugal

Long, conductive molecular wires have attracted great interest due to their promising potential for single molecule devices.[1] Usually, long synthesized molecules are used as molecular wires but their syntheses are complicate and expensive.[2] Stepwise methods, based on self-assembly properties of molecules, can provide a simpler and reproducible solution to prepare supramolecular structures with molecular control. The scanning tunneling microscope (STM) is a versatile tool to fabricate and control the molecular assemblies at molecular scale. In particular, when it is operated at the solid/liquid interface, placing a solvent droplet between the STM tip and the substrate, it is possible to add molecules in order to create organized structures.[3]

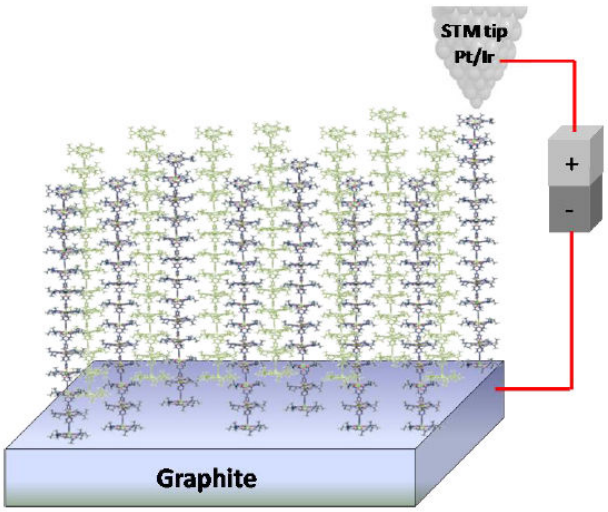

Figure 1. Scheme of a graphite substrate functionalized with molecular wires composed by alternating zinc octaetylporphyrins and 4,4' bypiridines.

We have been applying a stepwise method to built long molecular wires composed by zinc-octaethylporphyrins separated by 4,4'-bipyridines, as illustrated in Figure 1.[4,5] STM at solid/liquid interface was used to assembly the molecules on Highly Oriented Pyrolitc Graphite (HOPG). Each molecule is deposited individually, where each step is controlled in real time using molecular resolution images obtained by STM. Figure 2 shows a STM image of the 4th monolayer composed by bypiridines whit a darker region corresponding to the porphyrins of the previous monolayer. With this method, we fabricated wires composed by up to 25 individual molecules arranged in a well-defined sequence and assembled via bonding of the central metal of the porphyrin to the nitrogen atom of bipyridine. The final structure is a molecular wire with 14.29 nm in length (as determined by density functional theory using a SPARTAN software).

In addition, we have also measured the conductivity of each molecular wire using scanning tunneling spectroscopy (STS), where hundreds of I/V curves were recorded at each wire growth step. The length dependence of the molecular wires resistance was analyzed to assess the relative importance of tunneling and hopping processes. The results showed that these molecular wires are highly conductive with an ultralow attenuation factor (β) [5]. Similar low β values have been reported for other, though different, porphyrin-based systems.[6]

References

[1] S. H. Choi, C. D. Frisbie, "Enhanced hopping conductivity in low band gap donor-acceptor molecular wires Up to 20 nm in length". Journal of the American Chemical Society, 132(45), 16191–201, 2010.

[2] G. A. Ashwell, B. Urasinska, C. Wang, M. R. Bryce, I. Grace, C. J. Lambert, "Single-molecule electrical studies on a 7 nm long molecular wire", Chem. Commun. 4706-4708 (2006).

[3] Q. Ferreira, A. M. Bragança, N. M. M. Moura, M. A. F. Faustino, L. Alcácer, J. Morgado, "Dynamics of porphyrin adsorption on highly oriented pyrolytic graphite monitored by scanning tunnelling microscopy at the liquid/solid interface", Applied Surface Science, 273(2013), 220.

[4] Q. Ferreira, L. Alcácer, J. Morgado, "Stepwise Preparation and Characterization of Molecular Wires made of Zinc octaethylporphyrin complexes bridged by 4,4'-bipyridine on HOPG, Nanotechnology, 22 (2011), 435604,

[5] Q. Ferreira, Ana Margarida Bragança, L. Alcácer, J. Morgado, "Conductance of well-defined porphyrin self-assembled molecular wires up to 14 nm in length", submitted

[6] G. Sedghi, L. J. Esdaile, H. L. Anderson, S. Martin, D. Bethell, S. J. Higgins, R. J. Nichols, "Comparison of the Conductance of Three Types of Porphyrin-Based Molecular Wires: β, meso, β-Fused Tapes, meso-Butadiene-Linked and Twisted meso-meso Linked Oligomers", Advanced Materials, 24, 653-657, 2012

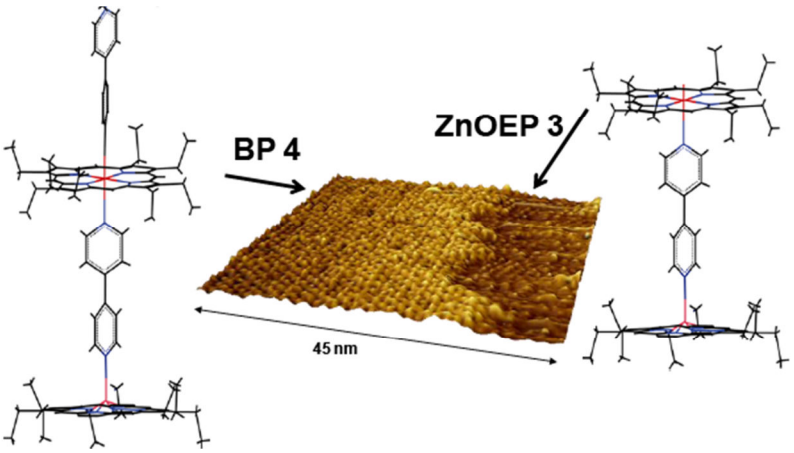

Figure 2. STM image (45x45nm^2) of the 4th monolayer composed by bypiridine molecules (BP4) where the darker region is composed by zinc octatethylporphyrin molecules from the previous monolayer (ZnOEP3)

Growth of Self-Assembled Monolayers directly on a ferromagnetic metal surface

S. Tatay[1,2], **A. Forment-Aliaga**[1], M. Mattera[1], M. Galbiati[2],P. Seneor[2], R. Mattana[2], E. Coronado[1]

alicia.forment@uv.es

[1]Unidad de Investigación de Materiales Moleculares, Instituto de Ciencia Molecular, 46980 Paterna, Spain
[2]Unité Mixte de Physique CNRS/Thales associée à l'Université Paris-Sud, 91767 Palaiseau, France

Introduction

Spin-Electronics (spintronics),is a relatively new field of research based on the utilization in electronic transport of the spin of the electrons in addition to their charge. Traditionally, inorganic metals, insulators and semiconductors have been used as the main components in spintronic devices. However, this situation is currently evolving and a new field called Organic Spintronics is rapidly emerging. When compared to traditional inorganic materials, molecules not only have the traditional advantages inherited from organic electronics field: monodispersity, variability, low-density, flexibility, transparency, large scale processability and low-cost, but also the inherent weak spin–orbit coupling and hyperfine interactions found in organic systems that offers the possibility of preserving spin–coherence over times much longer than in conventional metals or semiconductors. Moreover, molecular materials should not be considered as a simple spin transmission media. In fact, as it has been very recently shown, they can also offer spintronics tailoring opportunities unachievable or unthinkable with inorganic materials. The molecular structure, the local geometry at the molecule/electrode interface and, more importantly, the ferromagnetic molecule/metal hybridization can strongly influence interfacial spin properties, for example, going from spin polarization enhancement to its sign control [1].

Self-Assembled Monolayers (SAMs) are formed by molecules including functional groups (anchoring groups) displaying high affinities for a specific surface [2]. The directing force for the assembly is in most cases the formation of covalent bonds between the molecules and the solid surface; the assembly can be further stabilized by secondary intermolecular interactions within the monolayer being the final film thickness (some nanometers) determined by the size of the molecules.

SAMs as Spintronic Barriers

Recently we have developed the protocols for the grafting of SAMs over ferromagnetic oxide $La_{1/3}Sr_{2/3}MnO_3$ (LSMO) and has successfully integrated them into spintronics devices with the structure Co/SAM//LSMO [3]. Spin valves (SVs) and magnetic tunnel junctions (MTJs) are the simplest and most representative among the spintronics structures. A SV is a layered structure of two ferromagnetic (FM) electrodes separated by a nonmagnetic metallic or semiconducting spacer. The spacer allows spin polarized carriers to travel through it without much relaxation. In MTJs the two ferromagnetic-metallic electrodes sandwich a thin insulating layer that electrons must cross by tunnelling. Depending on their electronic structures SAMs can be used either in SVs or MTJs. As spacer SAMs MAIN ADVANTAGES are:

i) Can be easily engineered: Are modular and their parts can be exchanged while keeping the others unchanged.
ii) Are intrinsically nanometer thick: Film thickness will be determined by molecule size and SAM structure.
iii) Have defined structures: SAM formation is a self-assembly process, structure is preprogrammed.
iv) Can work at high bias voltage [4].

However, as LSMO's surface Curie temperature (T_c) is close to room temperature, spintronics effects in LSMO-based devices are expected only at low temperature. So, in order to obtain spintronics effects at room temperature it will be desirable to substitute LSMO by a ferromagnet of higher T_c, as

for example ferromagnetic metals or alloys, like cobalt (Co) or permalloy (Py).

Unlike LSMO, ferromagnetic metals readily oxidize and is not surprisingly that SAM grafting protocols over FM electrodes are missing. The formation of SAMs on bare magnetic metals is a challenging task since surface oxidation (which suppresses surface ferromagnetic properties) during SAMs grafting has to be avoid. In this communication, we present our first results towards the integration of SAM into room temperature spintronics devices.

We have developed the grafting protocols necessary for the integration of SAMs on 3d ferromagnetic metals. We will present evidence that bare metal surface (Co, Py) remains un-oxidized under glove box conditions. Moreover, we have developed the methods to selective etch metal oxide under glove box environment in order to remove native oxide from oxidized surfaces (Figure 1).

Finally, we have tested SAMs grafting with thiols or phosphonic acids anchoring group on bare metal (Co, Py) and intentionally oxidized surfaces (Figure 2).

In fine, standard characterizations like contact angle measurements shows that only thiol group can be successfully grafted on ferromagnetic surfaces whereas phoshonic acids group works with oxidized metal surfaces.

References

[1] C. Barraud, P. Seneor, R. Mattana, S. Fusil, K. Bouzehouane, C. Deranlot, P. Graziosi, L. Hueso, I. Bergenti, V. Dediu, F. Petroff, A. Fert, Nat. Phys. 6 (2010) 615.

[2] A. Ulman, An Introduction to Ultrathin Organic Films: From Langmuir-Blodgett to Self-Assembly, Academic Press, 1991.

[3] S. Tatay, C. Barraud, M. Galbiati, P. Seneor, R. Mattana, K. Bouzehouane, C. Deranlot, E. Jacquet, A. Forment-Aliaga, P. Jégou, A. Fert, F. Petroff, ACS Nano 6 (2012) 8753.

[4] M. Galbiati, C. Barraud, S. Tatay, K. Bouzehouane, C. Deranlot, E. Jacquet, A. Fert, P. Seneor, R. Mattana, F. Petroff, Adv. Mater. 24 (2012) 6429.

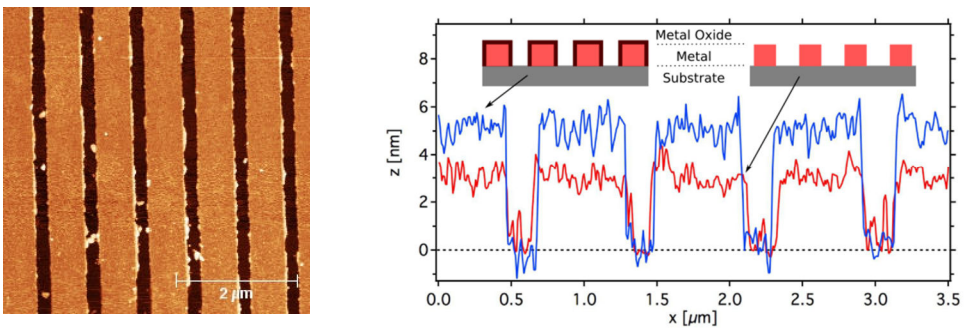

Figure 1. AFM image of a serie of Co lines made using the microcontact printing technique (left). Topographic profile of the lines before and after oxide etching (right). The difference in height corresponds to the oxide thickness.

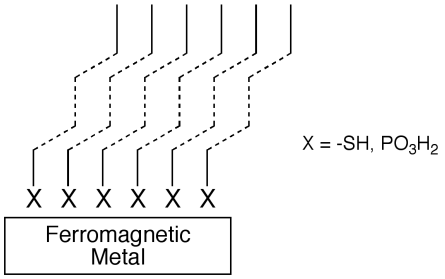

Figure 2.

Simulation of the mechanical response of encapsulated individual cells during normal force spectroscopy measurements

Katerina Foteinopoulou and Manuel Laso

kfoteinopoulou@etsii.upm.es

Institute for Optoelectronics and Microsystems (ISOM) and ETSII, Universidad Politécnica de Madrid, Spain

The atomic force microscope (AFM) [1] is a useful tool for investigating individual cells. Material properties of individual mammalian cells and bacteria have been investigated by using AFM to measure forces, a technique known as force spectroscopy. In a force spectroscopy measurement, cantilever deflection is measured as a function of sample position and is subsequently converted into force using appropriate calibrations giving the force curve (i.e. a plot of force versus sample position). However, interpreting measured force curves can be complicated because forces arising from material deformation (elastic and hydrodynamic forces) may not be distinguishable from other forces (surface forces, steric forces etc). Accurate interpretation relies on understanding the contribution of all invoked elements in the measured force curve.

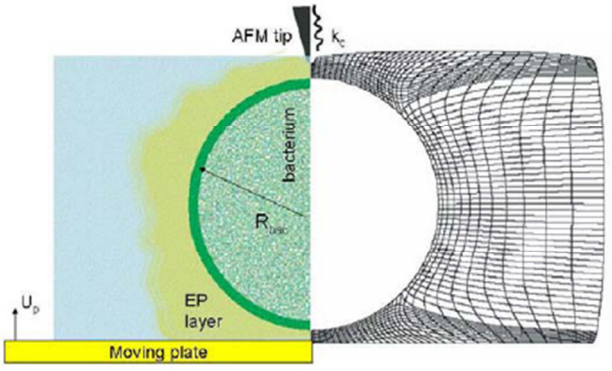

Figure 1. Schematic view of the problem geometry (left) together with the mesh generated for its finite element numerical solution (right).

In the work presented here, the mechanical response, the force-indentation relationship, in normal force spectroscopy measurements carried out on individual polysaccharide encapsulated bacteria is modelled, considering the elastic response of the bacterium and cantilever in combination with a fluid (hydrodynamic) model for the polysaccharide layer. For the hydrodynamic description of the polysaccharide layer a two-dimensional, axisymmetric, fully viscoelastic description is adopted, incorporating multi-modal Phan-Thien-Tanner (PTT) or Giesekus models. For the problem solution, viscoelastic, axisymmetric 2D time-dependent complex flow finite element (FE) calculations were carried out, taking into consideration the viscoelastic character of the polysaccharide liquid incorporating all elements of the system: AFM tip, bacterium stage and the surrounding extracellurar polysaccharide (EP) layer. Figure 1 shows a schematic representation of the problem geometry. The flow FE calculations are coupled with an adaptive remeshing strategy which is based on mapping the physical time-varying domain onto a simpler computational mesh and solving subsequently a set of elliptic partial differential equations for the physical coordinates.

In all studied cases the simulation model rigorously considers the time dependent rheologicalmechanical coupling between the elastic and fluid viscoelastic physical components of the experimental setup. Effects of inherent variability in geometrical and material properties of the bacterium and polysaccharide layer on the measurable response are quantified [1]. Calculations are used to predict and explain the mechanical response in an AFM experiment of single encapsulated bacteria which are conducted to provide physical insight into the pathology of certain diseases and the development of novel therapeutics [1]. The FE results are compared with experimentally obtained curves on Staphylococcus aureus without incorporating any adjustable parameters. Rheological data for the surrounding

polysaccharide layer (i.e. relaxation time and zero-shear rate viscosity) are considered from steady-state rheological measurements on bacterium polysaccharide extracted from its native environment. It is demonstrated that experimental results can be accurately described by the FE solutions of the viscoelastic fluid model [3]. Furthermore results are presented and compared for the force curve and time-dependent deformation of the physical domain (defined by the bacterium, the cantilever deflection and the EP fluid layers surrounding the bacterium). The viscoelastic fluid parameters invoked were equal to published parameters for advanced multimode constitutive equations of PTT and Giesekus as resulted from fittings of the above models to experimental rheological data of various EP viscoelastic fluids [4]. Representative results are shown in figure 2.

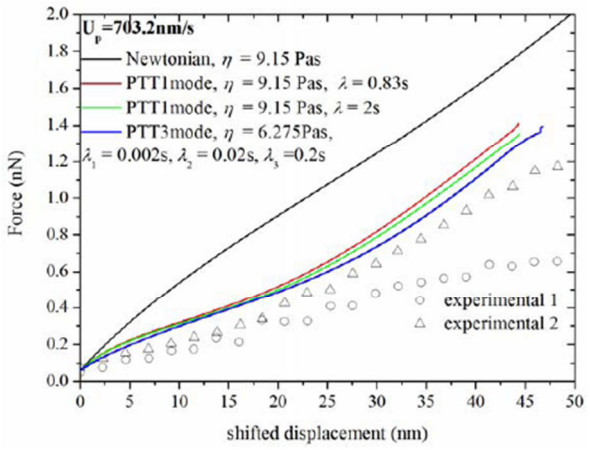

Figure 2. Representative simulation results adopting different models (Newtonian, 1mode PTT, 3mode PTT) for the description of the EP fluid and their comparison the experimental results under the same operative conditions.

Our numerical method can accurately predict and describe the mechanical response of isolated encapsulated cells during a force spectroscopy measurement without the need of any adjustable parameter since all the intrinsic bacterial and EP layer parameters serve as input parameters of the model. However the EP production is an intrinsically variable property of bacteria with possible variation of the EP inherent properties (layer thickness, viscosity, relaxation time) within a population of cells. Bacterial properties (radius and stiffness) are also subject to significant variations. Therefore achieving high reproducibility in experimental measurements of single encapsulated bacteria is extremely difficult [3]. Supported by model calculations, we also point the way to methods of *in vivo* rheological characterization of the extracellular polysaccharide as a preferable alternative to characterization after its removal from the native environment.

References

[1] Binnig, G., Quate, C.F., Gerber, C. Phys. Rev. Lett. 56, (1986) 930.
[2] F. M. Coldren, K. Foteinopoulou, D. L. Carroll, M. Laso, Langmuir 24 (2008) 9575.
[3] F. M. Coldren, K. Foteinopoulou, W. M. H. Verbeeten, D. L. Carroll, M. Laso, Langmuir 24 (2008) 9588.
[4] W.M.H. Verbeeten, J. of Rheology 54 (2010) 447.

Flat optics and generalized reflection and refraction laws

Zeno Gaburro[1,2,3]

zeno.gaburro@iit.it

[1]Center of Neuroscience and Cognitive Systems, Istituto Italiano di Tecnologia, Italy
[2]Department of Physics, University of Trento, Italy
[3]School of Engineering and Applied Science, Harvard University, Cambridge, MA, USA

We have recently proposed a structure that generalizes classical Snell and Fresnel laws, based on "phase discontinuities" [1]. The discontinuities in the wave propagation allow for the introduction of the idea of “flat optics”, a way to squeeze the thickness of optical devices by four orders of magnitude or more, with dramatic implications for mobile optical applications and for novel medical devices. I provide a newer outlook on this concept, from four basic, different, and complementary points of view, referred to classical Huygens, Fermat, Bragg, and Fresnel laws.

Generalized Fresnel coefficients can be formulated as the solution of a 1D equivalent circuit of a 3D flat optic device (Fig. 1). The tangential components of electromagnetic fields are not conserved across interfaces loaded with our structures.

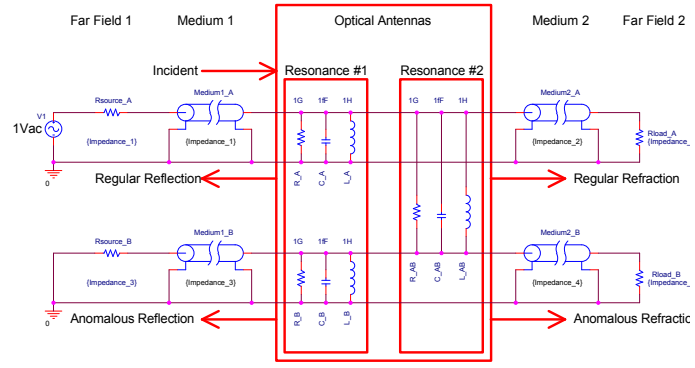

Figure 1. Equivalent circuit, with coexisting lumped and distributed impedances, of the metainterface that generalizes reflection and Snell’s laws [1]. The figure is a snapshot from Spice, the well-known electronic simulator, which has been used to simulate the Fresnel coefficients (results are not shown here, but will be discussed in the presentation).

The Bragg's approach [2] shows a generalization of the concept of “systematic absence”, a known effect of natural crystals. Here, a novel concept of "metacrystal" can be introduced, where systematic absences can be originated from form factors of meta-atoms (Fig. 2), in contrast with natural absences, which are based on geometrical structure factors only. Strategies for broadband operation will be presented. Implications in optomechanics will be discussed.

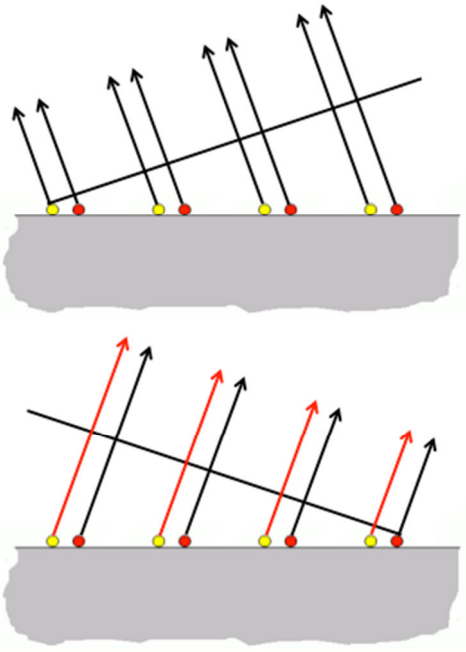

Figure 2. Example of systematic absence due to form factor. Yellow and red dots represent simultaneously excited meta-atoms of a 1D crystal. Meta-atoms are designed in such a way that amplitude of scattered waves is the same for all meta-atoms, whereas phase response of red dots is ahead ¼ of time period from yellow dots. Red dots are displaced by ¼ of space period from yellow dots. Resulting interference of first Bragg order is fully constructive to the left (top panel) and fully destructive to the right (bottom panel). Hence, this structure provides a net photonic momentum as a collective interference effect.

An update on applications, including vortex generators, polarizers and flat lenses, will be also presented [3].

Mechanical Deformation of graphene and graphene-based nanocomposites

C. Galiotis[1,2,3], G. Tsoukleri[2,3], Ch. Androulidakis[1,2], D. Sfyris[2], I. Polyzos[2], J. Parthenios[2] and K. Papagelis[1,2]

[1]Department of Materials Science, University of Patras, 26504 Patras, Greece
[2]Institute of Chemical Engineering and High Temperature Chemical Processes - Foundation of Research and Technology Hellas, 26504 Patras, Greece
[3]Interdepartmental Programme in Polymer Science and Technology, University of Patras, Greece

c.galiotis@iceht.forth.gr

Graphene has received a lot of attention nowadays due to the fact that as a single, virtually defect-free crystal is predicted to have an intrinsic tensile strength higher than any other known material [1] and tensile stiffness similar to graphite [2]. In this work, we have been subjecting a single layer of graphene -embedded into the upper surface of a PMMA cantilever or 4-point-bend bars and covered by a ~100nm thickness polymeric film to tension and compression, while its Raman spectrum is recorded simultaneously (Fig.1). The beams can be flexed up or down by means of adjustable screws subjecting the flake to compressive or tensile loads, respectively. Graphene's strain value at each deflection level is estimated using the results of Timoshenko's theory of beams [3]. Except the significant information on the monolayer deformation - stress uptake, we determine the compression buckling strain in single graphene flakes of different geometries. In all cases the mechanical response is monitored by the shift of the G and 2D Raman lines with strain, using two different excitation laser wavelengths (514.5nm and 785nm) [4,5].

In tension, the embedded flakes seem to sustain strains up to 1.3% in a reversible manner [4]. The position of the 2D peak shifts linearly to the applied uniaxial strain using the 514.5nm excitation line having a rate of ~52 cm^{-1}/% in agreement with recent results [6]. In compression, the G and 2D band response is non-linear. The corresponding $\partial\omega_{G,2D}/\partial\varepsilon$ values decrease with strain till the eventual turn-over of the slope, which is indicative of progressive buckling that precedes the final collapse of the flake [5] (Fig.2). Pertinent analytical expressions for the critical buckling strain, ε_c^{emb}, have been developed by considering the Euler classical analysis and/or a Winker type of approach to account for the resistance to buckling provided by the surrounding matrix. Despite the infinitely small thickness of the monolayers, the results show that graphenes embedded in plastic beams exhibit remarkably high compression bucking strain compared to that of the suspended ones, due to the effect of the lateral support provided by the polymer matrix, which is indeed dramatic and increases the effective flexural rigidity of graphene. The experimental finding that one atom thick monolayers embedded in polymers can provide reinforcement in compression to high values of strain is very significant for the development of nanocomposites for structural applications [5].

Finally, in graphene/ polymer composites the stress transfer distribution was extracted in as-prepared flakes and then at various levels of applied strain. Important parameters such as the stress-transfer length and the maximum value of interfacial shear that is developed in each case were determined [6]. In the case of a monolayer graphene (1LG) supported on a SU8/ PMMA bar, evidence is provided that the peeling procedure during graphite exfoliation induces a compressive, shear-generated, residual stress distribution. The related stress-transfer lengths from the graphene edges were found to be in the submicron range and hence much smaller than originally thought. Upon application of external tensile load to the substrate, the stress appears to be transferred to 1LG not through interfacial shear but by direct normal forces. The extension of this work to fully embedded graphene/ polymer composites and related analytical modeling will be discussed.

References

[1] Q.Z. Zhao, M. B. Nardelli, J. Bernholc, Phys. Rev. B , 65 (2002) 144105.
[2] C. Lee, X. D. Wei, J. W. Kysar, J. Hone, Science, 321 (2008) 385.
[3] S. P. Timoshenko, J.M. Gere, Theory of Elastic Stability, McGraw-Hill, New York, 1961.
[4] G. Tsoukleri, J. Parthenios, K. Papagelis, R. Jalil, A.C. Ferrari, A.K. Geim, K.S. Novoselov, C. Galiotis, Small, 5 (2009) 2397.
[5] O. Frank, G. Tsoukleri, J. Parthenios, K. Papagelis, K.S. Novoselov, A.K. Geim, C. Galiotis, ACS Nano, 6 (2010) 3131.
[6] T.M.G Mohiuddin, A. Lombardo, R.R. Nair, A. Bonetti, G. Savini, R. Jail, N. Bonini, D.M. Basko, C. Galiotis, N. Marzari, K.S. Novoselov, A.K. Geim, A.C. Ferrari, Phys. Rev. B, 79 (2009) 205433.
[7] G. Tsoukleri, J. Parthenios, I. Polyzos, K. Papagelis and C. Galiotis, in press (2013).

Electronic phase transitions in thin magnetite films

I. Bernal and **S. Gallego**

sgallego@icmm.csic.es

Materials Science Institute of Madrid (CSIC)
c/ Sor Juana Inés de la Cruz 3, 28049 Madrid, Spain

Fe oxides are versatile materials present in a large number of applications from disparate fields, and in particular in emergent nanotechnologies related to environmental protection, bio-medicine or spintronics. Among them, magnetite (Fe_3O_4) occupies a relevant position. It is a half-metallic ferrimagnet with high magnetic moment and moderate conductivity, that undergoes a complex metal-insulator transition (the so-called Verwey transition) at low temperatures involving a structural transformation from the inverse spinel structure to a monoclinic symmetry, and the emergence of charge- and orbitalordered patterns [1]. This transition is ultimately governed by electron-phonon couplings in the presence of strong electron correlations [2]. Interestingly, it has been shown that similar metal-insulator transitions can be induced by application of external electric fields in nanostructures, under hydrostatic pressure or strain, and at surfaces, eventhough much remains to be understood about the detailed microscopic characteristics of these induced transitions [3,4].

A large effort is currently devoted to the investigation of magnetite thin films. Magnetite-oxide heterostructures are currently under scrutiny for the design of novel devices that exploit magnetism, electron correlation effects and interface phenomena: spin valves controlled by charge-orbital order [5] or non-volatile resistance switching driven by ferroelastic strain [6] have been proposed. All these phenomena rely on the control of the properties of magnetite in thin film form. However, the effect of reduced dimensionality on the metal-insulator transition, and on the relative stability with respect to other Fe oxide phases with different stoichiometry, magnetism and conductivity is not clear.

Here we will address the study of thin magnetite films based on first-principles calculations. These calculations provide a unique tool to disentangle interface and bulk effects, and allow to simulate nonequilibrium conditions difficult to achieve in the experiments. We will focus on the effect of boundaries (both with the vacuum and with the substrate) and film thickness on the electronic and magnetic properties of different films. We will show how the emergence of charge and orbital order is intimately related to the symmetry of the film, and how it affects to magnetism and conductivity. Our results indicate the universality of the surface electronic gap, and its consequences on the existence of a threshold thickness to recover a Verwey-like transition. Finally, we will also provide a detailed description of the magnetic order and how it is much less affected by the thickness of the films. These results support the ability to exploit electronic transitions involving magnetic order in novel devices based on ultrathin magnetite films.

References

[1] Hoesch et al., Phys. Rev. Lett. 110 (2013) 207204.
[2] M.S. Senn, J.P. Wright, and J.P. Attfield, Nature 481 (2012) 173.
[3] S. Lee et al., Nature materials 7 (2008) 130.
[4] Z. Lodziana, Phys. Rev. Lett. 99 (2007) 206402.
[5] H.-C. Wu et al., Scientifc reports 3 (2013) 1830.
[6] M. Liu et al., Scientifc reports 3 (2013) 1876.

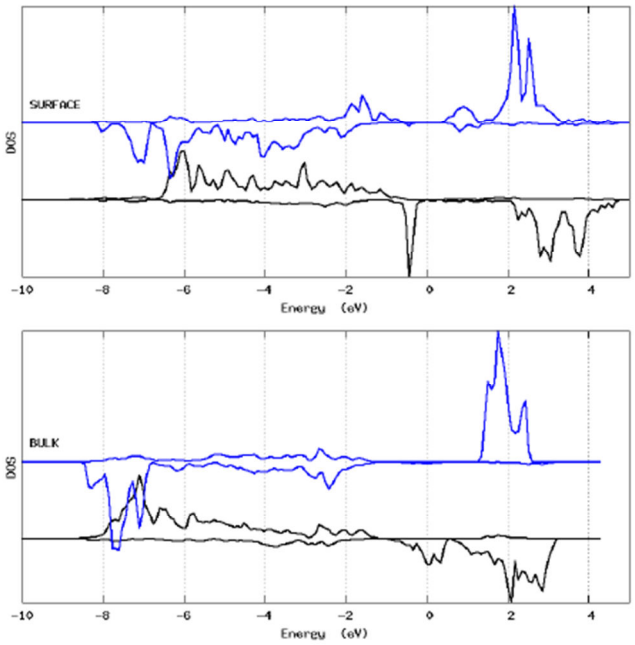

Figure 1. Spin-resolved density of states of Fe in an ultrathin magnetite film compared to the bulk, showing tetrahedral (blue) and octahedral (black) sites.

On the Formation of Carbon Nanotube Serpentines: A Multi-Million Fully Atomistic Molecular Dynamics Investigation

D. S. Galvão[1], L. D. Machado[1], S. B. Legoas[2], J. S. Soares[3], N. Shadmi[4], A. Jorio[3], and E. Joselevich[4]

galvao@ifi.unicamp.br

[1]State University of Campinas, 13083-970, Campinas-SP, Brazil
[2]Federal University of Roraima, 69304-000, Boa Vista-RR, Brazil
[3]Federal University of Minas Gerais, 30123-970, Belo Horizonte-MG, Brazil
[4]Weizmann Institute of Science, 76100, Rehovot, Israel

Carbon nanotubes (CNTs) have been subject of intense research in the last decades, mainly due to their unique mechanical and electronic properties. However, their disseminated use in many different applications has been limited by the experimental difficulties in producing large amounts of CNTs with specific diameters and chiralities.

One possible solution to overcome these limitations could be the use of carbon nanotube serpentines (CNSs) [1]. CNSs are S-like shaped nanostructures, composed of a series of straight, parallel, and regularly spaced segments, connected by U-shaped turns (Figure 1).

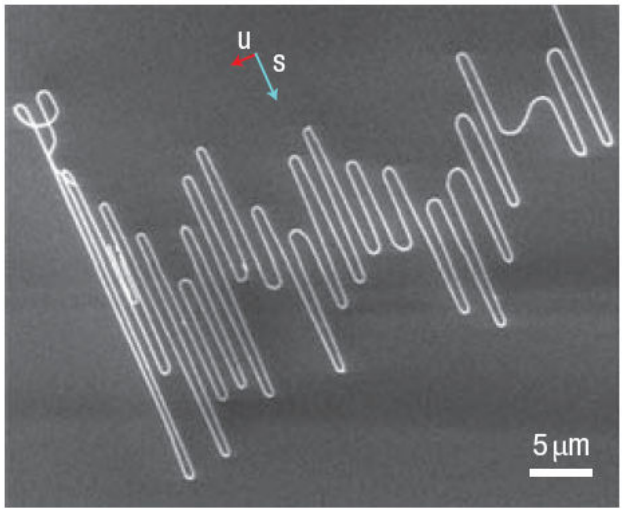

Figure 1. Example of a carbon nanotube serpentine formed on silicon oxide substrate. Figure adapted from reference [1].

CNS formation has been qualitatively explained based on the "falling spaghetti mechanism" [1,2]. The serpentines would be formed in a two-step process, where the isolated nanotubes are grown standing up from the stepped substrates. The tube would then fall down, preferentially along the steps, as a result of the van der Waals interactions between the tubes and the substrates. These movements can create oscillatory patterns, like spaghetti falling on a tilted bamboo mat [1.2], thus leading to the spontaneous formation of the serpentines.

In this work we present the first modeling of the dynamics of CNS formation. We have carried out multi-million fully atomistic molecular dynamics simulations (MD) using the well-known and tested CHARMM force field, as implemented in the NAMD computer code [3]. We have considered long carbon tubes (about 1 micron in length) and stepped substrates of silicon oxide (used in the experiments [1,2]) and graphite. The graphite substrates were also used to test the dependence of the dynamics of CNS formation on the type and composition of the substrates. Typical systems (nanotube plus substrate) contain up to 2 million atoms.

In order to simulate the formation of the CNSs we considered a CNT placed over the substrate with a significant part of the tube initially perpendicular to the substrate. An external forward force (mimicking the gas flow used in the experiments) was applied to the suspended part of the tube and the system is then set to freely evolve in time.

Our results [4] show that these conditions are sufficient to form robust serpentines. From the simulations and force profile analysis, it is possible to explain how the serpentines are formed. The process involves a balance of different kind of

forces, elastic deformations, and stress-strain force distributions modulated by the materials and format of the substrate steps. As the forward force is applied, the tube starts to move forward, but at the same time the interactions with the substrate (mainly van der Waals forces) pulls it down toward the substrate. As the tube segments start to interact with the substrate, elastic waves (deformations) are generated and propagate through the tube, which tends to align it with the substrate steps. This continues until the elastic limit (maximum stress) is reached (which depends on multiple factors, such as kind of substrate, temperature, applied external force, catalytic particle, etc.) and the forward tube force or velocity overcomes the elastic deformation, leading to a Uturn formation. The repetition of these processes leads to serpentine formation. From the simulations we observed that, as far as the top part of the tube continues to be ahead of its main body, serpentinelike structures can be formed. When this condition is not satisfied, the tube falls on itself, producing looped or ill-formed serpentines. Interestingly, the simulations showed that, although complex and involving many factors, the qualitative general trends of the serpentine formation are basically the ones of the proposed ‘‘falling spaghetti mechanisms’’ [1-2], thus validating the general features of this model. A typical snapshot from MD simulations, showing a well-formed CNS is shown in Figure 2.

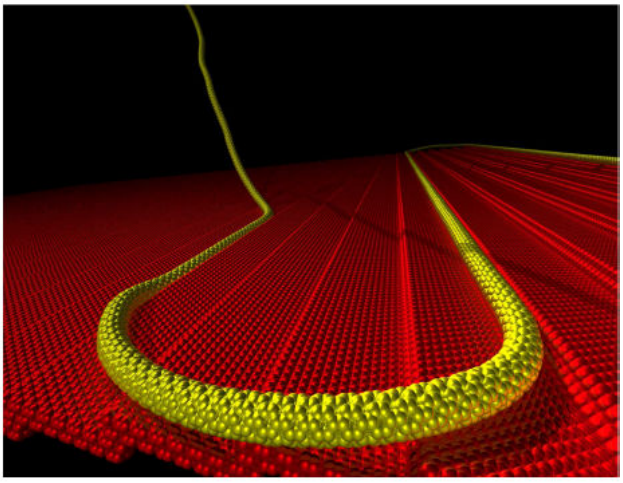

Figure 2. Typical snapshot from molecular dynamics simulations showing a well-formed carbon nanotube serpentine. Figure adapted from reference [4].

References

[1] N. Geblinger, A. Ismach, and E. Joselevich, Nature Nanotechnology 3 (2008) 195.

[2] E. Joselevich, Nano Res. 2 (2009) 743.

[3] J. C. Phillips, R. Braun, W.Wang, J. Gumbart, E. Tajkhorshid, E. Villa, C. Chipot, R. D. Skeel, L. Kale, and K. Schulten, J. Comp. Chem. 26 (2005) 1781. www.ks.uiuc.edu/Research/namd/.

[4] L. D. Machado, S. B. Legoas, J. S. Soares, N. Shamdi, A. Jorio, E. Joselevich, and D. S. Galvao, Phys. Rev. Lett. 110 (2013) 105502.

Magneto-optical activity in interacting magnetoplasmonic nanodisks

Gaspar Armelles[1], Alfonso Cebollada[1], Fernando García[1], **Antonio García-Martín**[1], María Ujué González[1], David Meneses[1], Nuno de Sousa[2] and Luis S. Froufe-Pérez[3]

a.garcia.martin@csic.es

[1]IMM-Instituto de Microelectrónica de Madrid (CNM-CSIC), Tres Cantos, Madrid, Spain
[2]Departamento de Física de la Materia Condensada, UAM, Madrid, Spain
[3]Instituto de Estructura de la Materia, CSIC, Madrid, Spain

Metal-dielectric plasmonic nanodisks show a rich optical behaviour with the appearance of two modes of magnetic and electric dipolar character due to the interaction between the disks. These modes couple to the incident light in a different way, giving rise to regions with low and high optical extinction, respectively [1]. Moreover, the insertion of a ferromagnetic component inside the structure introduces magneto-optical activity in the system. As a consequence, metaldielectric magnetoplasmonic nanodisks exhibit a rich optical and MO spectral phenomenology. It has previously been shown that, in Au/Co/Au nanodisks where a SiO_2 layer is inserted, it is possible to obtain nanodisk configurations for which low optical absorption and large MO activity occur at the same spectral range. This is basically achieved by an adequate positioning of the dielectric component within the structure[2].

Here we present our study on the influence that the dielectric spacer thickness has on the interaction between the disks, and as a consequence, on the optical and MO properties of such structures.

The structures consist of a pure Au nanodisk separated by a SiO_2 spacer from a MO component constituted by a 4nmAu/2nmCo multilayer nanodisk, which exhibits perpendicular magnetic anisotropy, reducing the required magnetic field to achieve saturation in polar configuration.

It will be shown that these structures exhibit the expected magnetic and electric dipolar modes, both in the optical and MO spectra. The position of the magnetic-like mode strongly depends on the SiO_2 thickness, while that of the electric like one remains basically unaltered.

As the SiO_2 thickness is increased, the strength of the MO activity of the magnetic-like dipolar mode increases much more strongly than the corresponding extinction peak. On the other hand, the MO activity of the electric-like mode decreases as the SiO_2 thickness increases, while the corresponding extinction peak remains nearly unaffected.

References

[1] A. Dmitriev, T. Pakizeh, M. Käll, and D.S. Sutherland, Small 3, 294 (2007).
[2] J.C. Banthí et al., Adv. Mater. 24, OP36 (2012).

Universal Distance-Scaling of Nonradiative Energy Transfer to Graphene

L. Gaudreau, K. J. Tielrooij, G. E. D. K. Prawiroatmodjo, J. Osmond, J. Garia de Abajo and F. Koppens

ICFO - The Institute of Photonic Sciences, Spain

louis.gaudreau@icfo.es

The near-field interaction between an emitter and a purely two-dimensional material is of great interest since it allows for the exploration of new limits of light-matter interactions. Graphene becomes thus an ideal platform to study these types of interactions [1]. Through lifetime measurements of emitters placed at a distance d from a graphene flake, we observe that due to the two-dimensionality and gapless character of graphene, the near-field nonradiative coupling at distances below 30 nm is greatly enhanced [2]. This enhancement is demonstrated by the strongly modified decay rate of the emitters when placed near the graphene flake, reaching up to 90 times their decay rate in vacuum. Moreover, by measuring the lifetime of the emitters as a function of d (Fig. 1), we show that the behavior is in agreement with a universal scaling law following a d-4 dependence predicted for purely two-dimensional materials. We employ the term universal since we find that the distance dependence of the decay rate is material independent and is governed only by fundamental constants, similar to graphene's universal light absorption reported in ref. 3. Another important aspect that rises from these measurements is that the energy transfer efficiency between the emitters and graphene can reach up to 99% at short distances, making graphene an extraordinary energy sink with promising outcomes for photodetection, energy harvesting and nanophotonics applications.

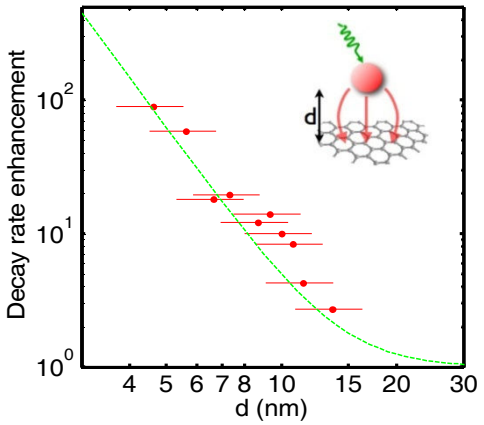

Figure 1. Decay rate enhancement obtained from lifetime measurements of emitters as a function of graphene-emitter distance, yielding up to a factor 90. The green dashed line represents the analytical model with weighted average over emitter dipole orientations. Insert: schematic representation of the energy transfer between a photo-excited emitter and graphene at a distance d.

References

[1] Koppens, F. H. L., Chang, D. E. and de Abajo, F. J. G., Nano Lett., 11 (2011) 3370.

[2] L. Gaudreau, K. J. Tielrooij, G. E. D. K. Prawiroatmodjo, J. Osmond, F. J. Garcia de Abajo, F. H. L. Koppens, Nano Lett. 13 (2013) 2030.

[3] Nair, R., Blake, P., Grigorenko, A., Novoselov, K., Booth, T., Stauber, T., Peres, N. and Geim, A., Science, 320 (2008) 1308.

Stiffening Pristine Graphene by Controlled Defect Creation

Cristina Gómez-Navarro[1], Guillermo López-Polín[1], Vincenzo Parente[2], Francisco Guinea[2], Mikhail I. Katsnelson[3], Francesc Pérez-Murano[4] and Julio Gómez-Herrero[1,5]

cristina.gomez@uam.es

[1]Departamento de Física de la Materia Condensada, UAM, Madrid, Spain
[2]Instituto de Ciencia de Materiales, CSIC, 28049, Madrid, Spain
[3]Radboud University Nijmegen, Institute for Molecules and Materials, Nijmegen, The Netherlands
[4]Instituto de Microelectrónica de Barcelona, CSIC, Bellaterra, Spain
[5]Centro de Investigación de Física de la Materia Condensada, UAM, Madrid, Spain

Defect-free graphene sheets have been shown to exhibit superior mechanical properties: they are very flexible, stiff, and strong [1]. Unfortunately mechanical cleavage of graphene is not a scalable technique, and the current procedures to generate graphene in large amounts still do not yield high quality crystalline graphene. For graphene produced by CVD and chemical reduction of graphene oxide their stiffness and strength are significantly lower than that of pristine graphene [2, 3] and point toward a strong dependence of mechanical properties with defect content in graphene. Unfortunately, the fact that these defects are created during sample preparation in an uncontrolled manner hinders systematic studies. Reliable structure-properties relationship can be obtained starting with a pristine graphene sheet obtained by micro-exfoliation of natural graphite, and subsequently introducing a known quantity of defects.

In this work we focus on the variation of mechanical properties of suspended graphene with a controlled density of defects created by ion irradiation. Stiffness and strength are experimentally determined by indentation experiments with an AFM probe on graphene drumheads. Counter intuitively, we find that the stiffness of graphene increases with defect content up to a vacancy content of ~0.2%, where it doubles its initial value. For higher density of vacancies the elastic modulus slowly decreases with defects inclusion. The initial increase in stiffness can be explained in terms of a power law dependence of the elastic coefficients with the momentum of flexural modes predicted for 2D membranes [4]. In contrast to the elastic trend, the fracture strength decreases with defect density according to standard fracture continuum models.

References

[1] C. Lee, X. D. Wei, J. W. Kysar, J. Hone, Science 321, 385 (2008).
[2] C. S. Ruiz-Vargas et al., Nano Letters 11, 2259 (2011).
[3] C. Gomez-Navarro, M. Burghard, K. Kern, Nano Letters 8, 2045 (2008).
[4] J. A. Aronovitz, T. C. Lubensky, Physical Review Letters 60, 2634 (1988).

Quantifying the quasi-static dielectric response of nano-objects by imaging electrostatic forces

Gabriel Gomila

ggomila@ibecbarcelona.eu

Institut de Bioenginyeria de Catalunya, Baldiri i Reixac 11-15, Barcelona, Spain
Universitat de Barcelona, Marti i Franquès 1, Barcelona, Spain

Understanding long-range interaction forces between small objects is of fundamental importance in materials science and nanotechnology. In particular, electrostatic forces are related to the intrinsic dielectric properties of materials and are essential for assembling molecular electronic devices. However, quantitative detection and interpretation of electrostatic forces remains extremely difficult, particularly for dielectric nano-objects, because they are inherently weak and primary sensitive to geometric effects (shape and size) of the objects. Our group has dedicated all its efforts in recent years to achieving this goal, and succeeded in resolving the dielectric constants on the nanoscale for flat and large insulating films [1-4] using scanning force microscopy techniques. But for small dielectric objects, it is a much more challenging task because the signal is significantly weaker in front of an increased geometrical impact.

Here we present the experimental demonstration that the dielectric constant ε_r - the permittivity in quasi-static regime - of small dielectric objects can be precisely measured from electrostatic forces probed by scanning force microscopy operated in electrostatic mode (EFM) [5]. By precisely quantifying the electrostatic forces, we resolved the intrinsic dielectric response of small insulating nano-objects, biomolecular membranes and macromolecular complexes that cannot be measured in bulk due to their complexity or softness. These results open new possibilities for non-destructive, in-situ and quantitative characterization of dielectric proprieties of nano-dielectrics and macromolecules that have so far remained inaccessible. Extension of this approach to measurements in the liquid environment [6,7] will be also discussed.

References

[1] Fumagalli, L., Ferrari, G., Sampietro, M. and Gomila, G. Dielectric-constant measurement of thin insulating films at low frequency by nanoscale capacitance microscopy. Appl. Phys. Lett. 91 (2007) 243110.

[2] Gramse, G., Casuso, I., Toset, J., Fumagalli, L. and Gomila, G. Quantitative dielectric constant measurement of thin films by DC electrostatic force microscopy. Nanotechnology 20 (2009) 395702.

[3] Fumagalli, L., Ferrari, G., Sampietro, M. and Gomila, G. Quantitative nanoscale dielectric microscopy of single-layer supported biomembranes. Nano Lett. 9 (2009) 1604.

[4] Fumagalli, L., Gramse, G., Esteban-Ferrer, D., Edwards, M. A. and Gomila, G. Quantifying the dielectric constant of thick insulators using electrostatic force microscopy. Appl. Phys. Lett. 96 (2010) 183107.

[5] Fumagalli, L., Esteban Ferrer, D., Cuervo, A., Carrascosa, J. & Gomila, G. Label-free identification of single dielectric nanoparticles and viruses with ultraweak polarization forces. Nature Materials, 11 (2012) 808.

[6] Gramse, G., Edwards, M., Fumagalli, L. & Gomila, G. Dynamic electrostatic force microscopy in liquid media. Appl. Phys. Lett., 101 (2012) 213108.

[7] Gramse, G., Dols-Pérez, A., Edwards, M., Fumagalli, L. & Gomila, G. Nanoscale Measurement of the Dielectric Constant of Supported Lipid Bilayers in Aqueous Solutions with Electrostatic Force Microscopy. Biophysical Journal, 104, (2013) 1257.

Assembly and manipulation of single functional molecules

Leonhard Grill

Chemistry Department, University of Graz, Heinrichstrasse 28, 8010 Graz, Austria

leonhard.grill@uni-graz.at

In order to obtain detailed understanding of physical and chemical processes at the single molecule level, the controlled manipulation of molecules on surfaces with a scanning tunneling microscope (STM) is used. Important aspects are on the one hand the influence of the molecular adsorption and configuration on the function and on the other hand the controlled linking of molecules to larger functional networks. In this presentation, the assembly and manipulation of single molecules and polymers with various molecular functions is presented. A prototype of a functional molecule is a molecular switch that can exist in various stable states with different optical/electronic properties. Single molecules can be switched on a surface by different stimuli and it turns out that the atomic-scale environment plays a fundamental role for the activity of the optical switching function, leading to surface-defined periodic switching [1]. In order to create functional polymers that act as “molecular wires”, the controlled covalent assembly of molecules by “on-surface-synthesis” is used, allowing the bottom-up construction of stable molecular networks with pre-defined topology and shape [2]. The shape of the molecular structures can be precisely tuned via the chemical structure of the initial building blocks, even enabling a hierarchical growth mode [3]. To characterize the charge transport through “molecular wires”, they are pulled off the surface with the STM tip to measure their conductance as a continuous function of the electrode-electrode distance. The conductance curves give detailed insight into the charge transport through the polymer and its mechanical properties [4]. For the case of graphene nanoribbons, the conductance of individual molecular wires could be correlated with their electronic structure and configuration [5]. The results reveal very efficient charge transport if the electron energy matches the molecular electronic states that are delocalized along the molecular wire.

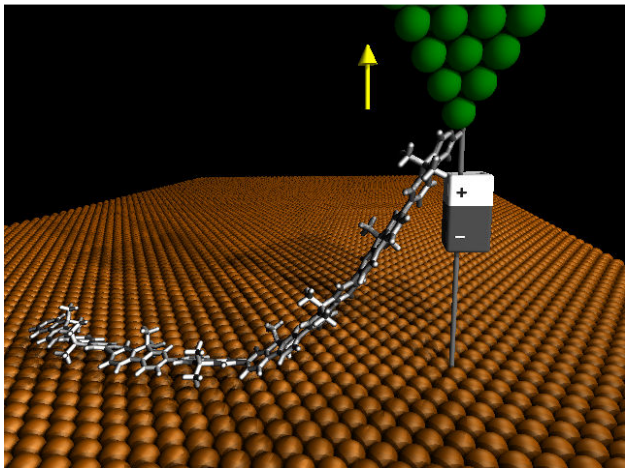

References

[1] C. Dri et al., Nature Nanotech. 3 (2008) 649.
[2] L. Grill et al., Nature Nanotech. 2 (2007) 687.
[3] L. Lafferentz, Nature Chem. 4 (2012) 215.
[4] L. Lafferentz et al., Science 323 (2009) 1193.
[5] M. Koch et al., Nature Nanotech. 7 (2012) 713.

Layered double hydroxide nanoparticle-based anti-restenotic drug delivery system

Zi Gu[1], Barbara E. Rolfe[2], Anita C. Thomas[3], Julie H. Campbell[2], Max Lu[1] and Zhi Ping Xu[1]

[1]ARC Centre of Excellence for Functional Nanomaterials, Australian Institute of Bioengineering and Nanotechnology, The University of Queensland, Brisbane, Australia
[2]Centre for Research in Vascular Biology, Australian Institute of Bioengineering and Nanotechnology, The University of Queensland, Brisbane, Australia
[3]Bristol Heart Institute, University of Bristol, Bristol, United Kingdom

z.gu@uq.edu.au
gordonxu@uq.edu.au

The biological and medical applications of layered double hydroxide (LDH) nanoparticles have attracted wide interest. LDHs consist of brucite-like layers and the exchangeable anions-containing gallery space. The present abstract reported that an anti-restenotic drug, low molecular weight heparin (LMWH), was intercalated into LDH interlayers which enhanced the biological and therapeutical effects of LMWH *in vitro* and *in vivo*. Results from powder X-ray diffraction and transmission electron microscopy demonstrated successful intercalation of LMWH into LDH interlayers by observation of enlarged LDH interlayers [1]. LMWH-LDH presented a hexagonal plate-like shape with ~90 nm in size [1]. Under physiological conditions, the intercalated LMWH was released from LDH in a sustained manner, resulting from the diffusion of LMWH from LDH and the dissolution of LDH layers [1]. The biological examination on cultured rat smooth muscle cells (SMCs) demonstrated the low cytotoxicity of LDH nanocarriers [2]. Comparison of the effects of unconjugated LMWH and LMWH-LDH conjugates showed the enhanced inhibitive effects of LMWH on SMC proliferation and migration (Figure 1A) [2]. The cellular uptake of LMWH by SMCs was also increased (more than 10 times) by conjugation to LDH nanoparticles [2,3]. After internalization by SMCs, LMWH-LDH was found to undergo the endocytic pathway (Figure 1A), and (unlike unconjugated LMWH) escape from endosomal compartment, thus avoiding biodegradation of LMWH [3]. Compared with unconjugated LMWH, LMWH-LDH enhanced suppression of mitogen-activated protein kinas signal transduction, probably due to the sustained release and improved cellular uptake of LMWH-LDH; the enhanced suppression of MAPK signal transduction is associated with enhanced inhibition of SMC proliferation and migration [3]. To target deliver LMWH-LDHs to the site of arterial injury, LMWH-LDH was conjugated with a targeting moiety (an antibody to XLF) and examined in a rat model (Figure 2A) [4]. Our preliminary results showed that targeted delivery of LMWH-LDH with anti-XLF effectively limited restenosis and thrombus formation (Figure 2B), which suggested the potential of this technique for clinical application [4].

References

[1] Gu Z, Thomas AC, Xu ZP, Campbell JH, Lu GQ, Chemistry of Materials, 20 (2008) 3715-3722.
[2] Gu Z, Rolfe BE, Xu ZP, Thomas AC, Campbell JH, Lu GQM, Biomaterials, 31 (2010) 5455-5462.
[3] Gu Z, Rolfe BE, Thomas AC, Campbell JH, Lu GQ, Xu ZP, Biomaterials Biomaterials, 32 (2011) 7234-7240.
[4] Gu Z, Rolfe BE, Xu ZP, Campbell JH, Lu GQ, Thomas AC, Advanced Healthcare Materials, 1 (2012) 669-673.

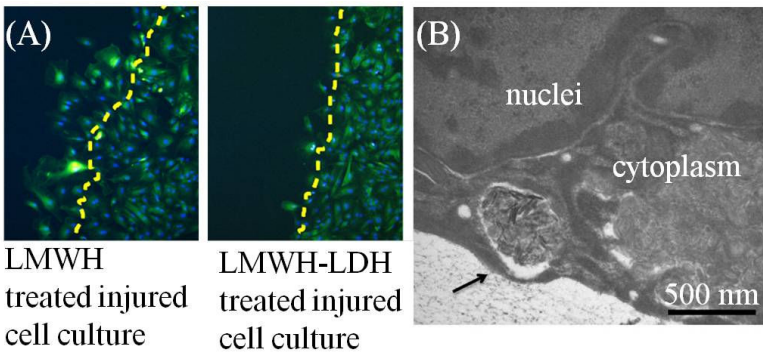

Figure 1. (A) LDH carrier enhanced the inhibitory effect of LMWH on rat vascular smooth muscle cell migration. (B) LMWH-LDH nanoparticles internalized by the endosomal compartment (indicated by the arrow).

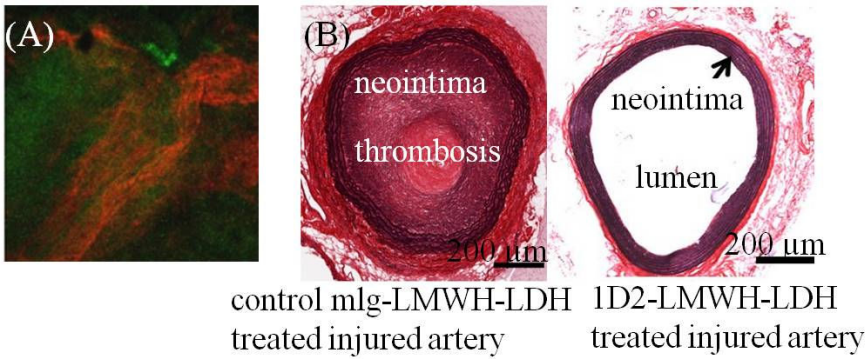

Figure 2. (A) *En face* confocal microscopic images of injured rat arteries (green) treated with red fluorescence labeled antibody-LMWH-LDH. (B) Typical cross-sections of injured artery showing antibody-LMWH-LDH reduced neointimal formation and thrombosis.

Intrinsic electrical conductivity of nanostructured metal-organic polymer chains

[1]Departamento de Química Inorgánica, UAM, Madrid, Spain
[2]Departamento de Física de la Materia Condensada, UAM, Madrid, Spain
[3]Instituto Nicolás Cabrera, UAM, Madrid, Spain
[4]Instituto de Ciencia Molecular, Parque Científico de la Universidad de Valencia, Paterna, Valencia, Spain
[5]Condensed Matter Physics Center (IFIMAC), UAM, Madrid, Spain

Cristina Hermosa[1,2], José Vicente Álvarez[2,3,5], Mohammad-Reza Azani[1], Carlos J. Gómez-García[4], Michelle Fritz[2], José M. Soler[2,5], Julio Gómez-Herrero[2,5], Cristina Gómez-Navarro[2], Félix Zamora[1,5]

cristina.hermosa@uam.es

One-dimensional materials have given rise to great expectations because of their potential utility in the emerging technology of flexible and transparent electronics [1]. Molecular materials have shown promising electronics properties at the macroscale but just recently it has been demonstrated that they can be assembled to nanostructures exhibiting outstanding conductivity [2]. However, despite years of research on the macro- and nano-scale, structural disorder represents the major hurdle in achieving high conductivities [2,3]. Moreover, a good understanding that relates the properties observed at the nano and macro scale is still missing.

Here we focus on the electronic transport properties of nano and macrostructures of a coordination polymer $[Pt_2(dta)_4I]n$ (*dta*= dithioacetate) named as MMX [4]. We report [5] measurements of highly ordered metal-organic nanoribbons, with inherent metallic character, whose intrinsic (defect free) conductivity is found to be 10^4 Sm^{-1}, three orders of magnitude higher than that of our macroscopic crystals. This magnitude is preserved for distances as large as 300 nm. Above this length, the presence of structural defects gives rise to an inter-fibre-mediated charge transport similar to that of macroscopic crystals.

The well-ordered 1D nanostructures have been isolated on SiO_2/Si substrate by direct sublimation from monocrystals of $[Pt_2(dta)_4I]n$ under high vacuum conditions. The electrical transport properties of the nanomaterials were characterized by Conductive Atomic Force Microscopy (C-AFM) at room temperature [6]. The first direct experimental evidence of the gapless electronic structured predicted [7] is also found by Field Effect Transistor configuration measurements.

In summary, to overcoming low conductivities and to clarify the charge transport mechanisms at the nano and macroscale (and their contributions), disorder should be reduced until the studied sizes are in a range where it can be ignored. To reverse this situation, we have simultaneously achieved a high structural order and electrical characterization at the nanometre scale, as well as at the macroscale, allowing us to make a comprehensive approach about the electrical properties that govern this MMX polymer. This was possible due to the excellent processability of these metal organic polymers [8], which show the exceptional feature of undergoing reversible depolymerization/repolymerization during sublimation.

This work constitutes a unique case of study of the influence of a small concentration of defects in metal-organic systems with high electrical anisotropy and the ideas and methodology presented here are expandable to other similar polymeric compounds and can be applied to the study of the emerging nanostructured metal-organic polymer family.

Finally, the experimental results postulate metal-organic molecular wires as good metallic interconnectors in nanodevices.

References

[1] Ju, S. Y. et al., Nature Nanotechnology, 2 (2007) 378.

[2] Welte, L. et al., Nature Nanotechnology, 5 (2010) 110.

[3] Tuccitto,N.. et al., Nature Materials, 8 (2009) 41.

[4] a) Bellito, C. Et al., Inorganic Chemistry, 22 (1983) 449. ; b) Kitagawa, H. et al., Journal of the American Chemical Society, 121 (1999) 10068.

[5] Hermosa, C. et al., Nature Communications, 4 (2013) 1.

[6] de Pablo, P. J. et al., Physical Review Letters, 3 (2002) 36804.

[7] Calzolari,A. et al., Journal of the American Chemical Society, 130 (2008) 5552.

[8] Welte, L. et al., Advanced Materials, 20 (2009) 2025.

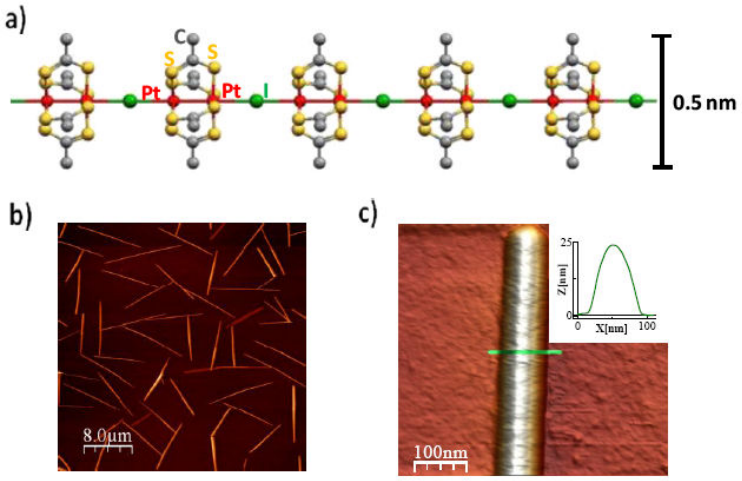

Figure 1. Growth of nanoribbons with high degree of order by crystal sublimation (a) Structure of a $[Pt_2(dta)_4I]n$ (dta= dithioacetato) single fibre. (b,c) AFM images of nanoribbons on a SiO_2 substrate where the straightness and height homogeneity can be appreciated. The inset in c is a profile acquired on the green line of the corresponding image, where the cross-section of the ribbons can be determined (Typical dimensions of the nanoribbons are 10 µm_100 nm_20 nm).

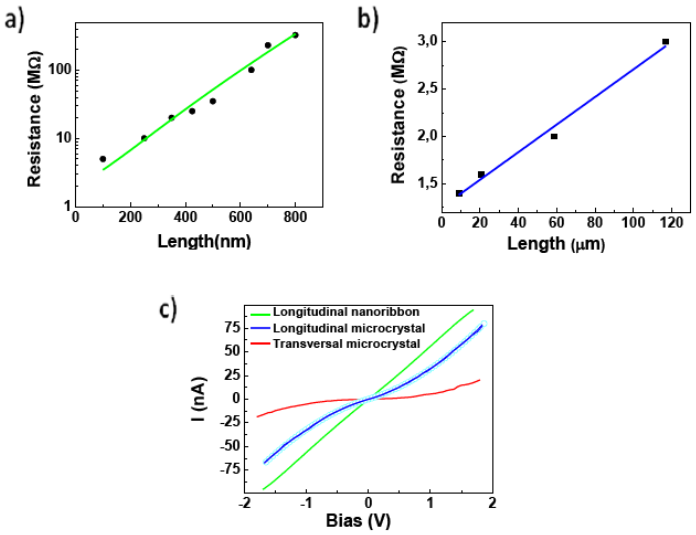

Figure 2. Electrical characterizations by conductive AFM of (a) MMX nanoribbons and (b) MMX crystals. The plots display Resistance versus length curves in a semi log (a) and in a linear scale (b). (c) Experimental I/V curves obtained for nanoribbons (green), and crystals both for longitudinal transport (blue) and for transversal transport (red).

Antiferromagnetic Topological Insulator: Theory and Material Design

Xiao Hu

International Center for Materials Nanoarchitectonics (WPI-MANA), NIMS, Japan

By using staggered electric potential, antiferromagnetic exchange field and spin-orbit coupling, we can control the spin, valley and sublattice degrees of freedom of electrons on honeycomb lattice, and achieve a novel topological insulator with simultaneous finite charge and spin Chern numbers. With first-principles calculation we demonstrate that the scheme can be realized in a sandwich of $[LaCrO_3]_n/La_2Au_2O_6/[LaCrO_3]_n$ along [111] direction of the perovskite structure. The d8 electrons of Au^{+3} hop on a buckled honeycomb lattice and exhibit Dirac behaviors, which feel the antiferromagnetic exchange field from bulk $LaCrO_3$, a Mott insulator with G-type antiferromagnetic order. The staggered electric potential on d8 electrons is provided by an electric field along [111] direction taking advantage of the buckling structure of honeycomb lattice. Due to the orbit hybridization, spin-orbit coupling is enhanced to 30meV, which hopefully makes the topological state stable even up to room temperature. In a finite system, there appears a quantized edge current with full spin polarization, while the total magnetization is compensated to zero. In this topological half-metallic antiferromagnet (HMAFM), the spin polarization of the dissipationless edge current can be inverted by gate voltage, which is a tremendous advantage in spintronic applications.

This work is based on collaboration with Qi-Feng Liang and Long-Hua Wu.

References

[1] Q.-F. Liang, L.-H. Wu and X. Hu: NJP 15, 063031 (2013)

[2] X. Hu: Adv. Mater. 24, 294 (2012).

Towards nanoscale DFT calculations with SIESTA and PEXSI

Georg Huhs, Alberto Garcia, Lin Lin, Miguel Pruneda and Chao Yang

Barcelona Supercomputing Center, Nexus II Building
c/ Jordi Girona, 29, 08034 Barcelona, Spain

georg.huhs@bsc.es

In computational nanoscience the desire to treat large structures as accurately as possible conflicts with the huge computational effort first principles electronic structure computations demand. This effort grows with the system size N like $O(N^3)$.

The availability of more and more powerful supercomputers allows in principle studies of systems with hundreds or thousands of atoms, but the developments in high performance computing can not overcome the $O(N^3)$ scaling. Moreover, the parallel algorithms currently applied can use only a number of processors far below the capabilities top supercomputers provide.

Thus it is clear that new algorithms are needed. One representative of a new class of algorithms is PEXSI, which stands for "Pole EXpansion and Selected Inversion". Its main advantages are the ability to use thousands of cores efficiently and, notably, the reduction of the computational cost for calculating the density matrix to

- $O(N^2)$ for 3D systems
- $O(N^{3/2})$ for (quasi-) 2D systems
- $O(N)$ for (quasi-) 1D systems

The method does not imply any additional simplifications or assumptions, thus it is general and exact. The reduction of order is based on having a sparse density matrix, so only a suitable DFT implementation can take advantage of this feature.

SIESTA is a DFT code using strictly localized basis sets, implying that it works with sparse matrices. This is particularly efficient for systems with a lot of vacuum, like nanotubes and two-dimensional problems.

In this talk we show how using PEXSI in SIESTA enhances the performance for large systems and even allows dealing with 2D systems, like stacked layers of graphene and BN, in the 10nm scale. We also demonstrate that PEXSI can use a much larger number of processors than Scalapack efficiently. As a result this method pushes the size of the systems that can be solved in reasonable time to the range of tens of thousands of atoms.

References

[1] Lin Lin, Jianfeng Lu, Lexing Ying, and Weinan E., Chinese Ann. Math. Ser. B, 30 (2009), 729-742

[2] J. M. Soler, E. Artacho, J. D. Gale, A. García, J. Junquera, P. Ordejón, and D. Sánchez-Portal, J. Phys.: Condens. Matter, 14 (2002), 2745–2779

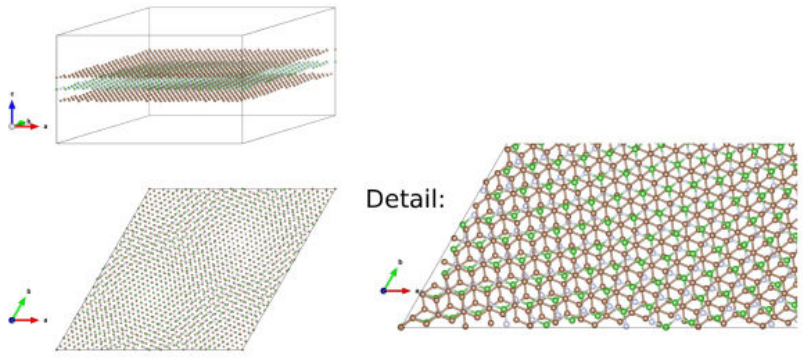

Figure 1. An example for quasi 2D systems under consideration: a layer of BN sandwiched between two graphene sheets. The Moire patterns emerging from the differing atomic distances need large unit cells. This example, consisting of about 2500 atoms, is still rather small compared to those SIESTA + PEXSI can deal with.

Plasmonic Brownian Ratchet

Paloma A. Huidobro[1], S. Ota[2], X. Yang[3], X. Yin[2,4], F.J. García-Vidal[1] and X. Zhang[2,4]

[1]Departamento de Fisica Teorica de la Materia Condensada and Condensed Matter Physics Center (IFIMAC), Universidad Autonoma de Madrid, 28049, Spain.
[2]National Science Foundation Nanoscale Science and Engineering Center, 3112 Etcheverry Hall, University of California at Berkeley, Berkeley, CA 94720, USA
[3]Department of Mechanical and Aerospace Engineering, Missouri University of Science and Technology, Rolla, Missouri 65409, USA.
[4]Materials Sciences Division, Lawrence Berkeley National Laboratory (LBNL), 1 Cyclotron Road, Berkeley, CA 94720, USA

paloma.arroyo@uam.es

The motion of nanoscopic objects in a liquid is generally dominated by thermal noise: the random collisions with the solvent molecules result in Brownian motion of the objects [1]. In agreement with the second law of thermodynamics, this temperature-governed fluctuating forces originate no net motion in the large scale at equilibrium. However, by driving an anisotropic system out of thermodynamic equilibrium, work can be performed out of thermal noise even in the absence of large scale thermal gradients. This is the working principle of the so-called Brownian ratchets [2, 3].

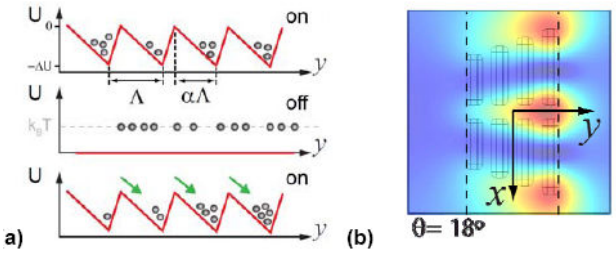

Figure 1. (a) Ratchet concept: by periodically turning on and off an external potential the Brownian diffusion of an ensemble of particles is biased into one direction. (b) The norm of the electric field generated by the plasmonic structure when illuminated at λ = 1.5μm is plotted at z = 90nm.

In this work, we present a proof of principles demonstration of a light-driven nanoscale Brownian motor based on plasmonic interactions (see Fig. 1). This Brownian ratchet makes use of plasmonic-based optical forces [4], that first enable the trapping of nanoscopic particles and then drives them a long distance displacement in a single device at room temperature. By means of an array of optical antennas with broken spatial symmetry, we generate an anisotropic trapping potential for an ensemble of dielectric beads (see Fig. 2). This trapping potential can be repeatedly excited by turning on and off a laser field, thus taking the system out of equilibrium and yielding a directed drift of the particles into one direction. We demonstrate the ratchet mechanism by means of a Molecular Dynamics simulation, showing the rectified Brownian motion of a sub-micrometer bead in the absence of any external bias (see Fig. 3).

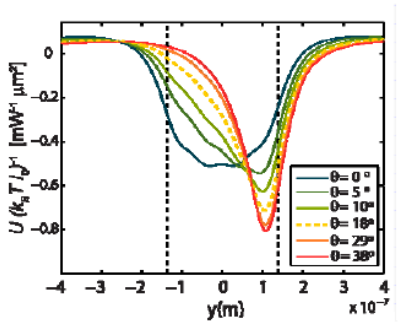

Figure 2. Variation of the anisotropic trapping potential experienced by the PS bead for several values of the geometrical asymmetry.

References

[1] A. Einstein, Ann. Phys., 17 (1905) 549. Authors, Journal, Issue (Year) page.
[2] R. P. Feynmann, R. B. Leighton and M. Sands, Feynmann Lectures in Physics (Addison-wesley, Reading,1966).
[3] P. Hanggi and F. Marchesoni, Rev. Mod. Phys., 81 (2009) 387.
[4] M. L. Juan, M. Righini and R. Quidant, Nat. Photon. 56 (2011) 5.

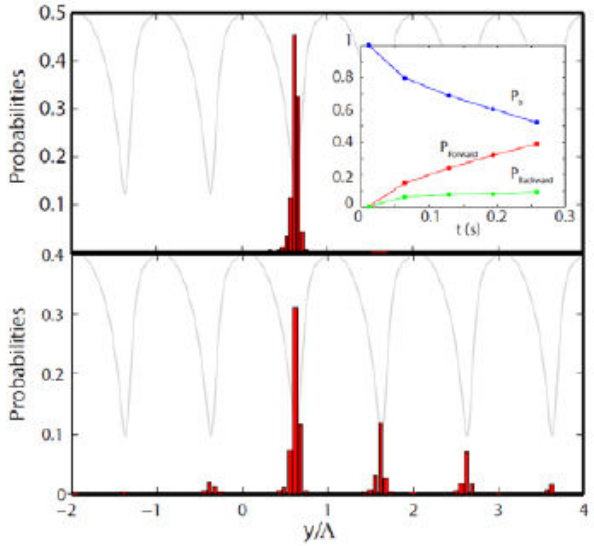

Figure 3. Dynamics for a Plasmonic Brownian Motor for N = 4000 realizations of the system. One PS bead (radius 50 nm, density 1050 kg/m^3) is solved in water (viscous coeffcient 10^{-3} kg/(m s)) at room temperature (T = 300 K). (a) Initial situation: the particle probability distribution is centered at the trapping position of the nanotweezer. Inset panel: time evolution of the probabilities for the particles to move forward (PF), backward (PB) or to remain in the initial unit cell (P0). (b) Final situation: after 16 onoff cycles, the probability for the particle to show a directed motion in the forward direction is 40%. The black gray line represents the plasmonic potential in arbitrary units.

Plasmon-polariton propagation in metallic nano-chains for subdiffraction circuits

W. A. Jacak

witold.aleksander.jacak@pwr.wroc.pl

Institute of Physics, Wroclaw University of Technology, Wyb. Wyspianskiego 27, 50-370 Wroclaw, Poland

Hybridized states of surface plasmons on metal-dielectric interface with photons result in plasmon-polaritons [1, 2], which are of high interest for applications in photonics and microelectronics [1, 3], in particular, for subdiffraction transportation of converted light energy and information in metallic modified structures in nano-scale [2, 4, 5], for sensors, plasmonic antennas, in electrochemistry, plasmon microscopy, plasmon litography and others. The formation of plasmon-polariton consists in reducing the wave-length of corresponding mode, due to lower group velocity in comparison to light velocity, and related concentration of the e-m field along the interface. The remarkable property is that the ideal surface plasmon-polaritons have ca. 10 times lower wave-length, thus larger momentum in comparison to photons with the same energy (thus they allow to enhance subdiffraction optics critical solutions, eg. in the area of nano-opto-electronic interfaces). On the other hand, it is impossible to excite plasmon-polaritons by enlightening metal surface, as well as the e-m irradiation of plasmon-polaritons is quenched. Inclusion of additional periodicity by grating or folding of the surface or introducing periodic nanostructure allow, however, matching momentum and energy conservation in interaction of plasmon-polaritons with free photons.

In the present paper collective wave type plasmon-polariton self-modes in the metallic (Au, Ag) nano-chain were determined and analyzed with respect to the nano-sphere size and chain-separation parameters in the framework of a previously developed analytical theory [6]. At some regions for parameters the undamped modes were identified when the interaction had been assumed as the near-field-zone dipole coupling [7]. These modes were found on the rim of stability of the linear theory, which indicates artifact of the model of near-field coupling. Inclusion of the medium- and far-field zone contributions to dipole interaction removes, however, instability and allows for fully analytical demonstration of quenching of irradiation losses of plasmon-polaritons in the chain to the level of only Ohmic attenuation (the metallic nano-chain behaves thus like an ideal wave-guide for plasmon-polaritons suitable for arrangement of subdiffraction circuits). The plasmon-polariton dispersion and the group velocity of plasmon-polariton wave packets were examined with respect to nano-sphere and chain parameters and mode polarization. Previous numerical results [8] related to long range plasmon-polariton propagation in the chain were transparently reinterpreted within the analytical approach.

References

[1] S.A. Maier, Plasmonics: Fundamentals and Applications, Springer, Berlin (2007).
[2] A.V. Zayats, I.I. Smolyaninov, A.A. Maradudin, Phys. Rep. 408, 131 (2005).
[3] F.J.G. de Abajo, Rev. Mod. Phys. 82, 209 (2010).
[4] S.A. Maier, P.G. Kik, H.A. Atwater, Phys. Rev. B 67, 205402 (2003).
[5] P.A. Huidobro, M.L. Nesterov, L. Martin-Moreno, F.J. Garcia-Vidal, Nano Lett. 10, 1985 (2010).
[6] W. Jacak, et al., Phys. Rev. B 82, p. 035418, (2010).
[7] W. Jacak, et al., J. Appl. Phys. 108, p. 084304, (2010).
[8] V. A. Markel, A. K. Sarychev, Phys. Rev. B 75, p. 085426 (2007).

Ultra fast asymmetric MIM diode structure employing Vertical MWCNT

Jae Eun Jang and Jeong Hee Shin

jang1@dgist.ac.kr

Department of Information & Communication Engineering, Daegu Gyeongbuk Institute of Science & Technology (DGIST), Daegu 711-873, Korea

The ultra fast driving diode structure can be a key technology as basic electrical unit for those various applications [1]. *p-n* junction diode structure has been used generally to convert alternating current (AC) signal to direct current (DC) signal. The structure is also a core technology of Si based transistor, which is employed widely to various electrical components. However, the working mechanism is not suitable for high-speed driving since the speed limit is induced by the mobility of hole and electron in semiconductor. [2] Schottky barrier effect can make a much faster rectifying speed than that of *p-n* junction due to one side depletion formed by just hole or electron movement. [3,4] But, the estimated driving frequency limit is still less than ~ THz. Additionally, the thermionic injection mechanism leads to a poor power efficiency regarded as important in mobile devices. [5] On the issues, all metallic structure and tunneling mechanism can be a key solution factors. However, if we make tunneling diode using all metallic electrodes or even using semiconductor materials, the high reverse current level is an inevitable consequence, which results in a low conversion efficiency and much heat production causing driving speed retardation. [6,7] Here we report a tunneling diode structure using metallic materials as electrode structures with high contrast between the reverse and the forward current. The structural asymmetric effect [8,9] makes a large difference of the tunneling probability, the barrier height and width for the forward and the reverse bias state, respectively. Applying the structural asymmetric effect to MIM diodes, better electrical asymmetric characteristic was achieved in the lateral MIM and the MIC structure. Especially in the MIC diode, high contrast ratio between on- and off-current is as high as about forthorder at room temperature. Its temperature dependence is quite good up to 423K, compared to the other results. The structural sharpness of nanometer level from the fabrication process or the originality of material induces the low threshold voltage (~0.2V) and the high forward current value (16.97MA/cm^2) as well as simple fabrication process. The estimated frequency limit is about 4.74 THz.

References

[1] D. Dragoman, M. Dragoman, Prog. Quantum Electron. 2004, 28, 1.
[2] A. S. Sedra, K. C. Smith, Microelectronic circuits, 6rd Edition, Oxford University Press, New York, 2010.
[3] S. O. Kasap, Principles of electronic materials and devices, 3rd Edition, McGraw-Hill New York, 2006.
[4] S. M. Sze, K. K. Ng, Physics of semiconductor devices, 3rd Edition, Wiley-interscience, New York, 2006.
[5] A. M. Ionescu, H. Riel, Nature 2011, 479, 329.
[6] W. M. Reddick, G. A. Amaratunga, Appl. Phys. Lett. 1995, 67, 494.
[7] K. B. Teo, E. Minoux, L. Hudanski, F. Peauger, J.-P. Schnell, L. Gangloff, P. Legagneux, D. Dieumegard, G. A. Amaratunga, W. I. Milne, Nature 2005, 437, 968.
[8] M. Bjork, H. Schmid, C. Bessire, K. Moselund, H. Ghoneim, S. Karg, E. Lortscher, H. Riel, Appl. Phys. Lett. 2010, 97, 163501.
[9] X. Sun, SPIE Newsroom, The International Society for Optical Engineering, s. 1C4 2006.

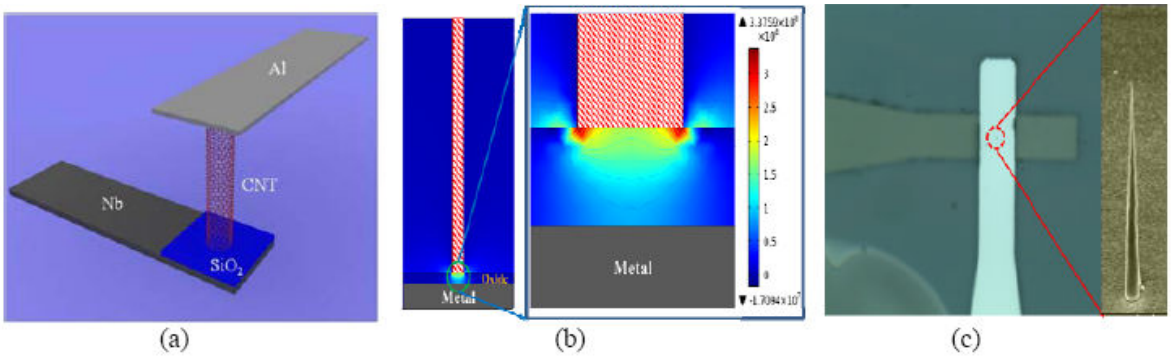

Figure 1. Vertical MIC diode structure a) shematic diagram of the MIC diode composed of Nb-SiO_2- Carbon nanotube on the SiO_2 substrate. b) The simulation of electrical field distribution of the MIC structure. c) The optical photo image of MIC structure. The point inside the red circle is the vertical MWCNT. The inset: 45° tilted view of SEM image for a multi-walled carbon nanotube grown on SiO_2/Nb layers.

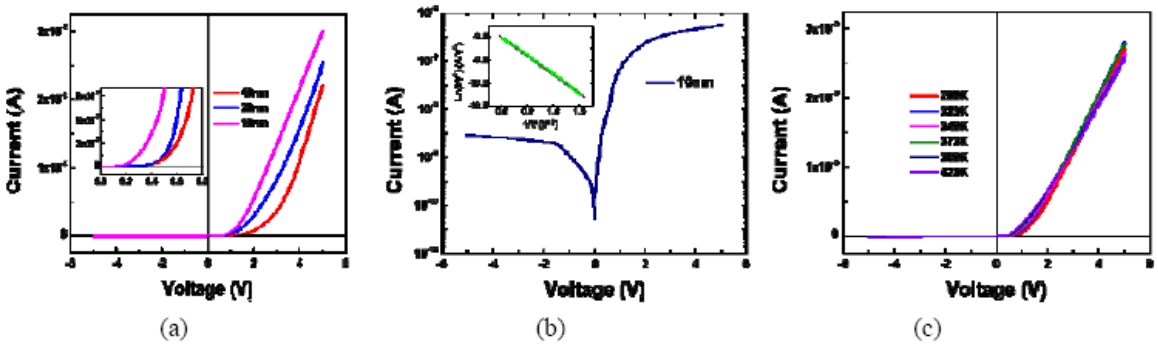

Figure 2. The electrical characteristics of vertical MIC diode structure. a) Currernt-Voltage plots of MIC diodes. The inset of the plots: threshold plots with 10, 20, 40 nm (thickness of SiO_2) MIC diodes with magnified voltage-axis from 0 to 0.8 V. b) Log scale plot for of MIC diode of 10 nm SiO_2 layer and the inset that shows the plot based on Fowler-Nordheim tunneling model. c) The I-V plot of temperaturedependence of MIC diode from 298K to 423K.

Stacking-dependent superstructures and taxonomy at armchair interfaces of bilayer/trilayer graphene

Asieh S. Kazemi, Simon Crampin and Adelina Ilie

Centre for Graphene Science & Department of Physics, University of Bath, Bath BA2 7AY, UK

askss20@bath.ac.uk

We present the first study of quantum interference patterns (QIP) at bilayer-trilayer armchair interfaces, for different stacking sequences [1]. The resulting QIPs allow us to establish a pattern taxonomy for multi-layered graphene systems. Visualization using scanning tunneling microscopy and theoretical calculations (by the embedding method [2], and corroborated with density functional theory) provides direct evidence that near armchair edges electron behavior is dominated by the "hard" edge, where the layer is abruptly truncated, as opposed to the "soft" edges, where layers continue across the boundary. Intervalley reflection causes universal quenching of the wavefunction with a periodicity of three rows of C atoms, while the exact interference patterns depend on the stacking sequence and appear to be robust to disorder and chemical terminations. Lateral interfaces within multi-stacked graphene systems can provide unique system-specific opportunities for wave-function engineering to be exploited in devices employing quantum-interference.

References

[1] A.S. Kazemi, S. Crampin, A. Ilie, Appl. Phys. Lett. 102 (2013) 16311.

[2] J. E. Inglesfield, Comput. Phys. Commun. 137 (2001), 89.

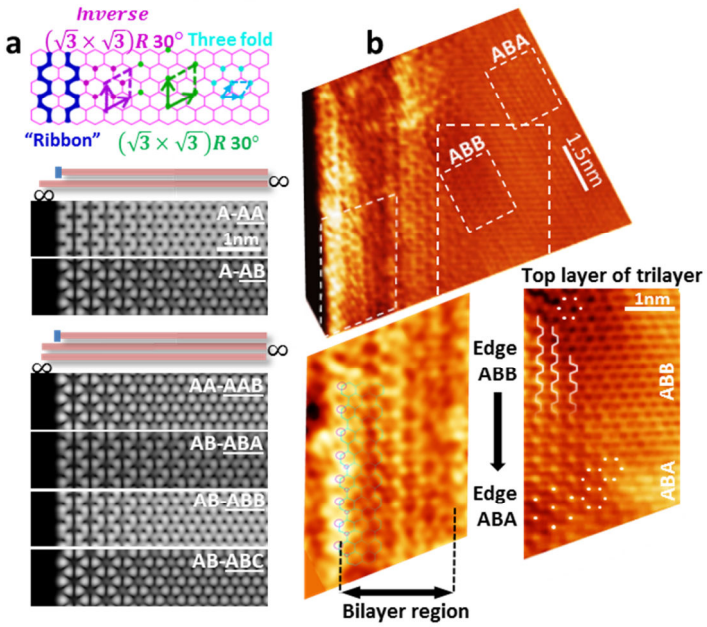

Figure 1. (a) Example of pattern taxonomy for stacked graphene systems at armchair edges/interfaces; STM image simulations of mono-bilayer and bilayer-trilayer armchair interfaces for various armchair edge extents (i.e. finite vs. infinite) within the multi-stack. (b) Experimental STM images at a bilayer-trilayer interface, showing a change in stacking on the top layer of the trilayer side; magnified regions show patterns that are interpreted based on scattering processes and the given taxonomy.

Small is Different: Self-Assembly and Self-Selection of Size, Shape and Form in the Nanoscale

Uzi Landman

School of Physics, Georgia Institute of Technology,
Atlanta, GA 30332 USA

Finite materials systems with dimensions in the nanoscale range are often created through spontaneous, or directed, self-assembly, with self-selection of size (number of atoms), shape (spatial arrangement of the constituents), and form, that is thermodynamic phase (solid, liquid or gas), charge state, and degree of order (e.g., crystalline, disordered or amorphous). In a conversation in 1990 in Atlanta, Heinrich ('Heini') Rohrer (1933-2013) to whose memory this lecture is dedicated, termed this behavior in the nanoscale as "Nature's Way". In this lecture we discuss and demonstrate through computer-based first-principles quantum computations and simulations [1], often in conjunction with laboratory experiments, some of the key physical principles that underlie and govern the properties of materials at the nanoscale, exhibiting discrete quantized energy level spectra and specific structures and morphologies manifested in unique, non-scalable, size-dependent physical and chemical properties. These properties are often of emergent nature - that is, they are not commonly expected, or deduced, from knowledge learned at larger sizes. We focus on the following topics: (i) Formation, atomic arrangements, and properties of self-assembled metal nano-crystals protected by organic monolayers, whose structure and stability originate from superatomic electronic shell-closure [2]; (ii) Size-dependence, structural fluxionality and dimensionality cross over in nanocatalysis [3], and (iii) Shape-transitions and electrocrystallization of liquid droplets brought about by applied electric fields [4].

References

[1] U. Landman, "Materials by Numbers: Computations as Tools of Discovery", Proc. Nat. Acad. Sci. (USA) 102, 6671 (2005).

[2] C. Zeng, et al., "Total Structure of the Golden Nanocrystal $Au_{36}(SR)_{24}$", Angew. Chem. Int Ed. 51, 13114 (2012); "Ultrastable Silver Nanoparticles", A. Desireddy, et al., Nature (in press, August, 2013).

[3] A. Sanchez, et al., "When Gold is not Noble", J. Phys. Chem. A 103, 9573 (1999); S.M. Lang, et al., "$Pd_6O_4^+$: An Oxidation Resistant Yet Highly Catalytically Active Nano-Oxide Cluster", J. Am. Chem. Soc. 134, 20654 (2012); "Dimensionality Dependent Water Splitting Mechanisms on Free Manganese Oxide Clusters" Nano Letters (2013).

[4] W.D. Luedtke, J. Gao, U. Landman, "Dielectric Nanodroplets: Thermodynamics Shape Transitions and Electrocrystallization in Applied Electric Fields", J. Phys. Chem. C 115, 20343 (2011), Feature Article.

Carbon nanotube/enzyme bioelectrodes for implantable glucose/O_2 biofuel cells

Alan Le Goff

alan.legoff@ujf-grenoble.fr

Département de Chimie Moléculaire UMR-5250, ICMG FR-2607,
CNRS Université Joseph Fourier, BP-53, 38041 Grenoble, France

The design of biofuel cells involves the application of enzymes or microorganisms as catalyst for the targeted oxidation and reduction of specific fuel and oxidizer substrates to generate an electrical power output. Biofuels such as glucose can be found in physiological fluids, opening thus the way to energy harvesting from body fluids for supplying biomedical electronic devices [1].We investigated the efficient wiring of enzymes in a carbon nanotube (CNT) conductive matrix for the fabrication of glucose biofuel cells (GBFC). CNTs combine many advantages for designing GBFCs: excellent conductivity, high specific surface, ease of functionalization and strong interactions with redox enzymes [1]. Direct and indirect electron transfer were both investigated for the wiring of laccase and glucose oxidase on CNT electrodes for the respective oxygen reduction and glucose oxidation [2,3]. GBFCs delivered, in vitro, a maximum power density up to 1.3mW cm^{-2} and an open circuit voltage of 0.95 V (50mM glucose, 25 °C, pH 7). Moreover, the GBFC was successfully implanted in rats by surgical insertion into the retroperitoneal space, enabling Glucose and O_2 from the Extracellular Fluid to flow into the GBFC [4]. The implanted GBFC delivered a maximum power density of 0.25mW cm^{-2}, 0.42mW mL^{-1} and an open circuit voltage of 0.85V and has proven to be able to supply small electronic devices.

References

[1] M. Holzinger, A. Le Goff, and S. Cosnier, Electrochimica Acta, 82 (2012) 179.

[2] A. Zebda, C. Gondran, A. Le Goff, M. Holzinger, P. Cinquin, and S. Cosnier, Nat Commun, 2 (2011) 370.

[3] B. Reuillard, A. Le Goff, C. Agnès, M. Holzinger, A. Zebda, C. Gondran, K. Elouarzaki, and S. Cosnier, Phys. Chem. Chem. Phys. 15 (2013) 4892.

[4] A. Zebda, S. Cosnier, J.-P. Alcaraz, M. Holzinger, A. Le Goff, C. Gondran, F. Boucher, F. Giroud, K. Gorgy, H. Lamraoui, and P. Cinquin, Sci. Reports (2013) 3.

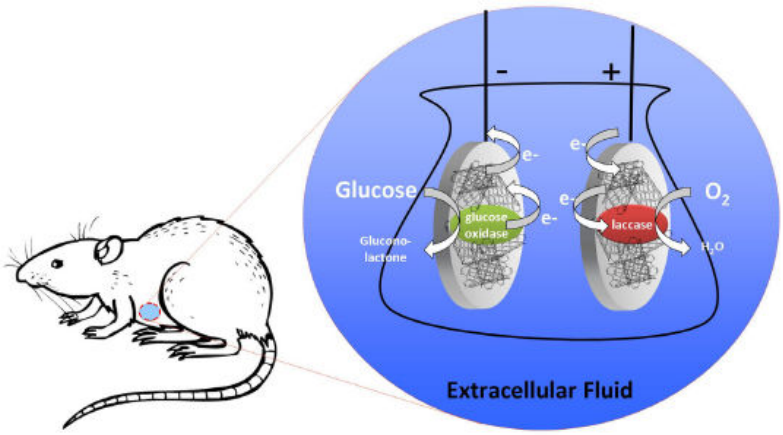

Quantum Hall Effect in Chemically Functionalized Graphene: Oxygen Adsorption Fingerprints

Nicolas Leconte, Frank Ortmann, Alessandro Cresti, Jean-Christophe Charlier, and Stephan Roche

Université catholique de Louvain (UCL), Institute of Condensed Matter and Nanoscience (IMCN), NAPS, Chemin des étoiles 8, 1348 Louvain la Neuve, Belgium

nicolas.leconte@uclouvain.be

In this work [1], we predict a strong electron-hole asymmetry in the Quantum Hall regime in graphene, due to its functionalization by low concentration of oxygen impurities in epoxy position. The scattering potential induced by these impurities is modeled by tight-binding parameters extracted from *ab initio* calculations [2], which, in turn, are used inside an efficient real space order N method [3] to calculate the dissipative conductivity [4] under high field. Various transport regimes are observed by varying the impurity concentrations from 0.5 to 4.4% and magnetic fields ranging from 1 to 80 Tesla, thus evidencing the complexity of the metal-insulator transition in disordered graphene under high magnetic fields. For lowest concentration of defects (0.5 to 1%), the electronic charge carriers feel substantial localization effects without any Landau levels developing in the spectrum. In contrast, the hole spectrum maintains the anomalous Quantum Hall state with associated Landau levels. Moreover, the conductivity exhibits a double-peak structure, which is associated to magnetic field-induced impurity bound states. The length-dependent conductivity proves the formation of mobility edges separating extended states from localized ones. Increasing even further the impurity concentration (up to 4.4%), we observe a complete disappearance of the quantum Hall effect in oxidized graphene, even for highest magnetic fields.

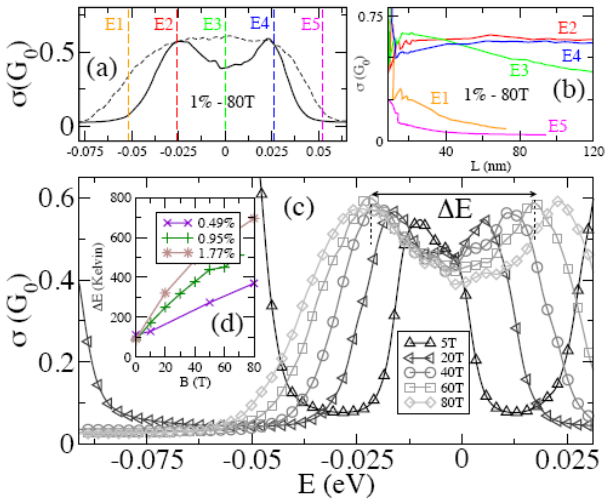

References

[1] N. Leconte, F. Ortmann, A. Cresti, J.-C. Charlier, and S. Roche, submitted (2013)

[2] N. Leconte; A. Lherbier, F. Varchon, P. Ordejon, S. Roche, and J.-C. Charlier, Phys. Rev. B 84 (2011) 235420; N. Leconte, J. Moser, P. Ordejon, H.H. Tao, A. Lherbier, A. Bachtold, F. Alsina, C.M.S. Torres, J.-C. Charlier, and S. Roche, ACS Nano 4 (2010) 4033

[3] H. Ishii, F. Triozon, N. Koboyashi, K. Hirose, and S. Roche, C.-R. Physique 10 (2009) 283

[4] D. Soriano, N. Leconte, P. Ordejon, J.-C. Charlier, J.J. Palacios, and S. Roche Phys. Rev. Lett. 107 (2011) 016602; N. Leconte, D. Soriano, S. Roche, P. Ordejon, J.-C. Charlier, and J.J. Palacios, ACS Nano 5 (2011) 3987

Broadband Carbon Nanotube Photodetectors with Intrinsic Polarimetry

François Léonard

Sandia National Laboratories, USA

Light polarization is used in the animal kingdom for communication, navigation, and enhanced scene interpretation, and also plays an important role in astronomy, remote sensing, and military applications. To date, there have been few photodetector materials demonstrated to have direct polarization sensitivity, as is often the case in nature. In this presentation, I will discuss the realization of macroscopic carbon-based photodetectors, where the polarimetry is intrinsic to the active photodetector material [1,2]. The detectors are based on macroscopic, optically-thick films of aligned single-wall carbon nanotubes (SWCNTs), and are actualized using asymmetric contact electrodes or in p-n junction format. Responsivities as high as 1 V/W were observed in these devices, with a broadband spectral response spanning the visible to the mid-infrared. A combination of experiment and theory is used to demonstrate the photothermoelectric origin of the responsivity and to discuss the performance attributes of such devices.

References

[1] S. Nanot et al, Scientific Reports 3, 1335 (2013).
[2] X. He et al, ACS Nano, DOI: 10.1021/nn402679u.

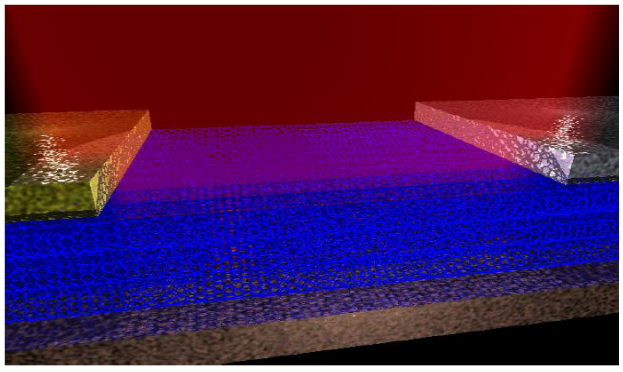

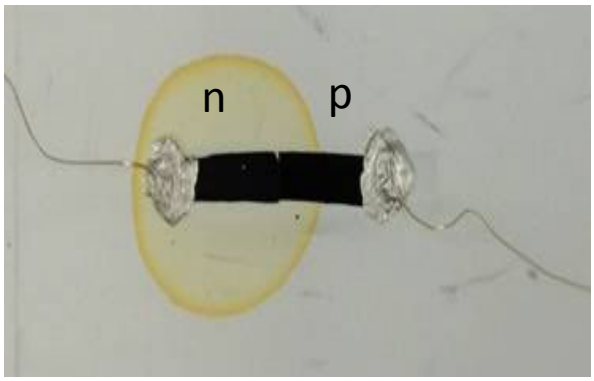

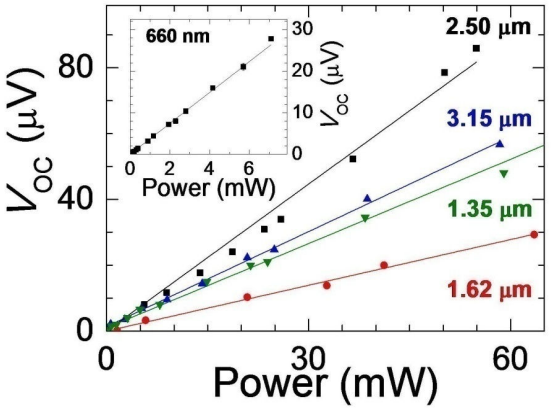

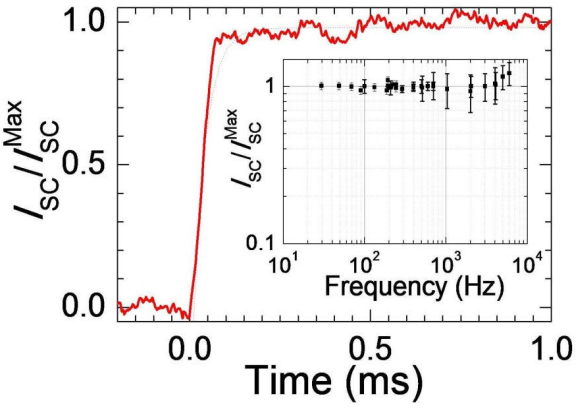

Reactive Nanometer Multilayers – A Versatile Tool for Cold Joining

Andreas Leson[1], Stefan Braun[1], Georg Dietrich[1], Erik Pflug[2] and Maximilian Rühll[2]

[1]Fraunhofer Institut für Werkstoff- und Strahltechnik, Dresden, Germany
[2]Technische Universität Dresden, Institut für Fertigungstechnik, Dresden, Germany

andreas.leson@iws.fraunhofer.de

Established joining techniques like welding, soldering or brazing typically are characterized by a large amount of heat input into the components. Especially in the case of heat sensitive structures like MEMS this often results in stress induced deformation and degradation or even damage of the parts. Therefore, there is an urgent need for a more reliable and reproducible method for joining, which is characterized by a well defined and small heat input for only a short time period. So-called reactive nanometer multilayers offer a promising approach to meet these needs.

Reactive nanometer multilayers consist of several hundreds or thousands of alternating nanoscale layers, which can react with each other. Placing a reactive nanometer multilayer between two surfaces already applied with a solder or brazing metal, it can be used as a controllable local heat source. After activating the chemical reaction by an electrical spark, laser pulse or impact, a self-sustaining intermixing reaction starts, which travels the length of the reactive nanometer multilayer resulting in a stable intermetallic material, such as NiAl. The peak temperature of the reaction can be well above 1000 °C, but it only reaches this temperature for milliseconds. Therefore, the heat remains localized in the solder layers while the components remain at room temperature during the entire process. Besides temperature sensitive components reactive nanometer multilayers are also ideally suited to join parts difficult to access.

The talk will present results in the fabrication of reactive nanometer multilayers by magnetron sputter deposition as well as in the fabrication of free standing and presoldered nanometer multilayers. Furthermore, different application examples for this type of joining will be presented.

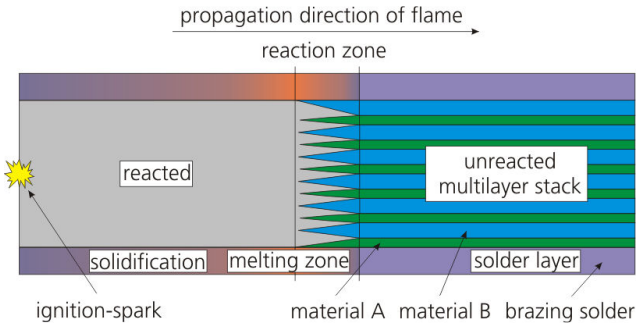

Figure 1. Principle of reactive nanometer multilayers.

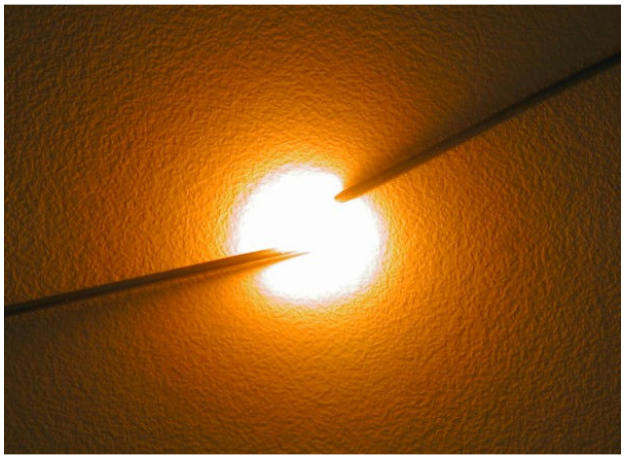

Figure 2. Ignition of a reactive nanometer multilayer by an electrical spark

Optimization of imaging conditions for atomic resolution in Titan TEM to minimize radiation damage and to study low angle boundaries in graphene-like materials

Sergei Lopatin[1] and Andrey Chuvilin[2]

Sergei.Lopatin@fei.com

[1]FEI Electron Optics, Achtseweg Noord 5, 55600KA, Eindhoven, Netherlands
[2]CIC nanoGUNE, Tolosa Hiribidea 76, E-20018, Donostia - San Sebastian, Spain

Recent advances in spherical aberration (Cs) correction for transmission electron microscopes (TEM) in a combination with electron sources of very low energy spread (use of monochromator) enabled imaging of single and bilayer graphene with atomic resolution [1]. Newly developed TEM techniques such as a single atom or single-atomic-column spectroscopy [2, 3] and atomic resolution electron tomography [4] drive the need for increased electron radiation doses to be applied to samples. The radiation damage started to be the key limitation factor for high resolution TEM [5].

For graphene-like (light element) materials [6] the radiation dose limitation is particularly severe for several reasons. First, the knock-on damage cross section is higher for low atomic number elements [7]. Second, the light elements produce less contrast than heavier elements, so that even higher doses are needed to obtain a sufficient signal-to-noise ratio (SNR). Finally, the graphene-like materials appear in the form of low dimensional allotropes that have only one or a few atoms in a typical projection of a high-resolution image. While resolution-wise we are not limited any more by modern TEM systems, there is still a big question about stability of the sample under the beam during the image acquisition.

The optimization of acquisition parameters of TEM systems allows to minimize electron dose and thus reduce possible sample damage. Here we present an extensive study of TEM tuning to obtain high quality HRTEM images of graphene. We used Titan transmission electron microscope (FEI Co) equipped with Cs image corrector, a super-high brightness gun and a monocromator (energy spread of the electron beam better than 0.2eV). Special attention was paid to optimize setting of the Cs corrector.

Tuning of Cs corrector is based on measurement of image defocus (df) and astigmatism while recording so-called Zemlin tableau [8]. It was demonstrated that accounting for Cs of 3rd and 5th order (C3 and C5 correspondingly) and systematic error of C3 measurement results in more than 2 times increase in contrast, meaning more than 4 times decrease in dose for obtaining the same SNR (Fig.1).

The optimal settings found were applied to study low angle boundaries (LAB) in graphene. LAB is a row of edge dislocations, separation of those defining the boundary angle. LABs are not visible directly on the image but can be identified by methods such as geometrical phase analysis (GPA), see Fig.2. Physically LAB may be interesting as they represent a perfect discontinuous layer with periodically spaced singularities.

References

[1] K. W. Urban, Nature Materials, 10 (2011) 165.
[2] P. E. Batson, Nature (London), 366 (1993) 727.
[3] D. A. Muller, L. F. Kourkoutis, M. Murfitt, J. H. Song, H.Y. Hwang, J. Silcox, N. Dellby, and O. L. Krivanek, Science, 319 (2008) 1073.
[4] M. B. Sadan, L. Houben, S. G. Wolf, A. Enyashin, G.Seifert, R. Tenne, and K. Urban, Nano Lett., 8 (2008) 891.
[5] R. F. Egerton, P. Li, and M. Malac, Micron, 35 (2004) 399.
[6] K. S. Novoselov, A.K. Geim, S.V. Morozov, D. Jiang, Y. Zhang, S.V. Dubonos, I.V. Grigorieva, and A. A. Firsov, Science, 306 (2004) 666.
[7] F. Banhart, Rep. Prog. Phys., 62 (1999) 1181.
[8] F. Zemlin, K. Weiss, P.Schiske, W. Kunath, K. -H. Herrmann, Ultramicroscopy 3 (1978) 49.

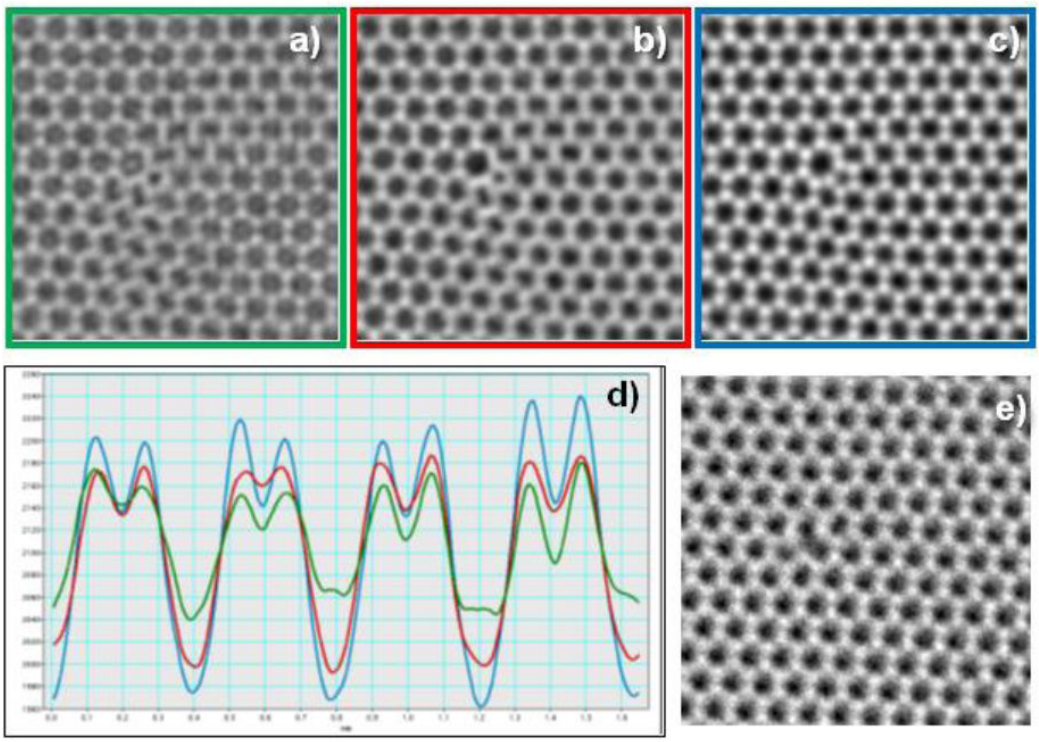

Figure 1. Simulation verification of the impact of optimum conditions: a) Scherzer conditions optimized for 0.1nm transfer; b) C5+C3+df conditions optimized for 0.1nm transfer; c) C5+C3+df conditions optimized for 0.1nm transfer and systematic error from Zemlin tableau is accounted; d) the intensity profiles across simulated images; e) an experimental image acquired at approximately optimum conditions.

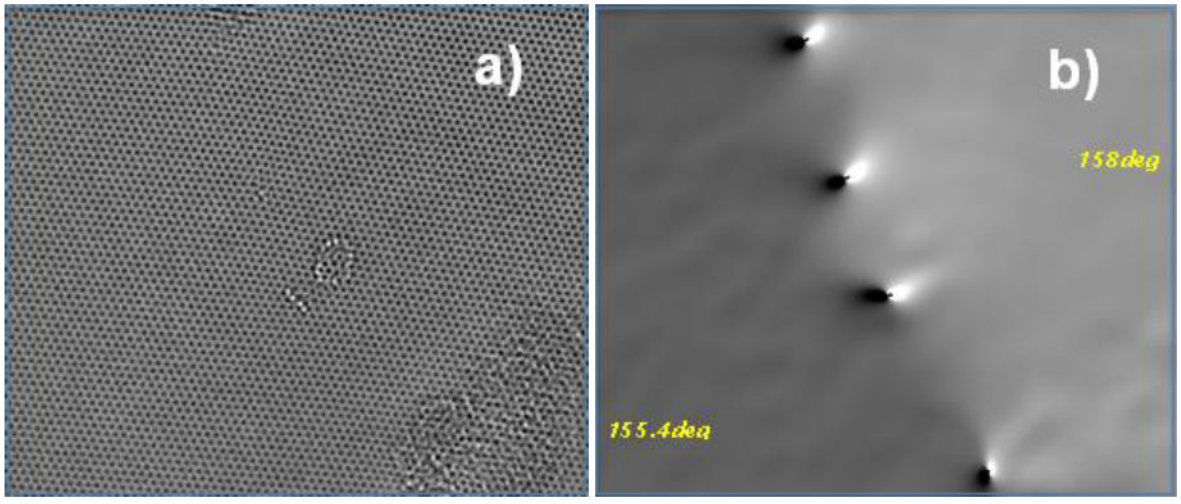

Figure 2. LAB in graphene: a) original HRTEM image; b) dislocations identification by GPA (rotation map).

Development of ultrasensitive bioanalytical assays based on metal and semiconductor nanoparticles

Natalia Malashikhina, Gaizka Garai-Ibabe and Valery Pavlov

nmalashikhina@cicbiomagune.es

CICbiomaGUNE, Paseo Miramon 182, 2009, San Sebastián, Spain

Signal enhancement is an important part in the development of bioanalytical assays. All previously developed strategies for sensitivity improvement in bioanalysis can be devided in molecular biology and nano approaches. In the first category enzyme amplification techniques is widely used to improve sensitivity of several assays. The principle of enzymatic enhancement is based on the presence of primary enzyme label which acts on a substrate whose product catalyses a secondary cycling enzyme reaction. Nano signal amplification methods are based on using of nanomaterials of different nature. Semiconductor and metal nanoparticle (NPs) are extensively used as carriers decorated with recognition molecules or as donor or quencher of FRET pairs. The application of nanomaterials and molecular biology technology for highly sensitive detection of the targets undetectable by traditional methods is of great challenge.

We developed two ultrasensitive analytical assays based on unconventional combination of enzymatic reactions with CdS quantum dots (QDs) and gold NPs.

The first method for the detection of ascorbic acid (AA) is based on DNAzyme cleaving its DNA substrate in the presence of Cu^{2+} and AA [1]. The detection system consists of two DNA strands which bind to each other via Watson-Crick and Hoogsteen hydrogen bonding (Figure 1). The substrate DNA labeled with fluorophore is loaded on the surface of gold NPs and form FRET pair. The cleavage of substrate DNA in close vicinity to the gold surface liberates fluorescein-DNA fragments producing strong fluorescence enhancement. The catalytic function of gold clusters employed in this approach significantly improved detection limit of AA.

The second method for the detection of various analytes (antigens, antibodies) is based on the employing of enzymatically generated CdS QDs in alkaline phosphatase (ALP) immunoassay [2]. p-Nitrophenyl phosphate (pNPP), used as a substrate, in the presence of ALP is catalytically cleaved, giving p-nitrophenol (pNP) and phosphate ions as the products of the reaction (Figure 2). When Cd^{2+} and S^{2-} ions are added to the reaction mixture, phosphate stabilized fluorescent nanocrystals of CdS are formed, giving a rise to the emission. The sensitivity of this novel assay was significantly improved in comparison with the standard method based on colorimetric p-nitrophenyl phosphate assay.

References

[1] N. Malashikhina, V. Pavlov; Biosens. Bioelectron., 33, (2012), 241.

[2] N. Malashikhina, G. Garai-Ibabe, V. Pavlov; Anal. Chem.,(2013), Paper In Press.

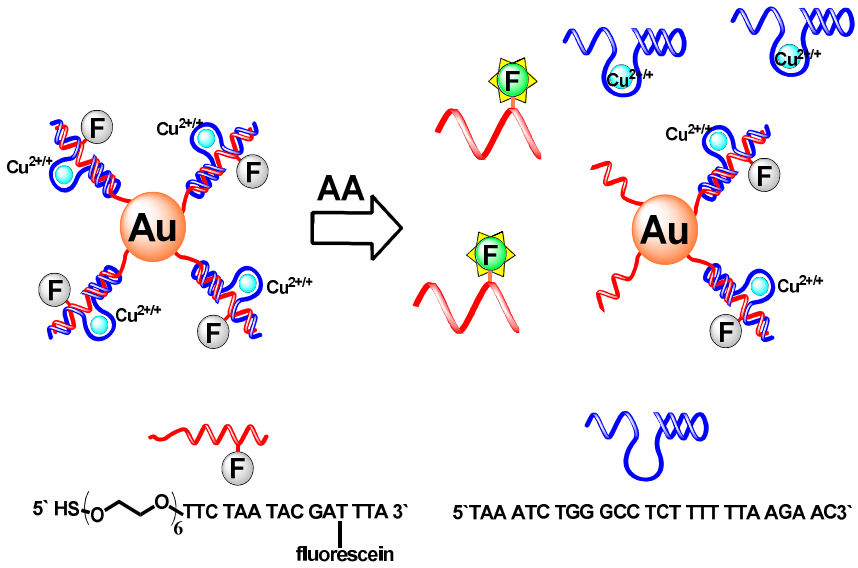

Figure 1. Fluorometric assay for detection of ascorbic acid based on DNAzyme and gold nanoparticles modified with fluorophore labeled DNA substrate.

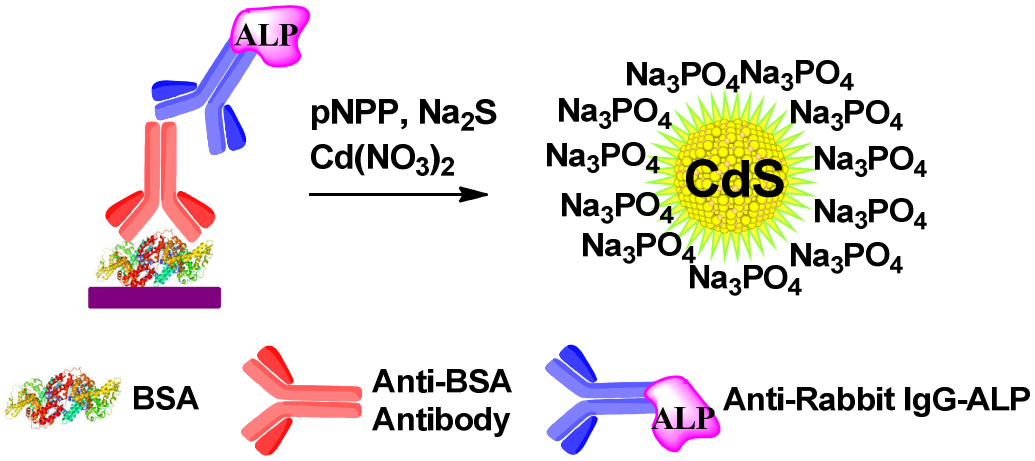

Figure 2. Detection of anti BSA antibody based on enzymatic growth of CdS QDs.

Development of Antifouling Polymer-Coated Nanodiamonds for Biological Applications

L. Marcon and R. Boukherroub

Lionel.Marcon@iri.univ-lille1.fr

Interdisciplinary Research Institute, Parc de la Haute Borne, 50 av. de Halley, 59658 Villeneuve d'Ascq, France

Due to their tunable surface structures and biocompatibility, nanodiamonds (NDs) are promising candidates in a broad range of biomedical applications, including drug delivery and bioimaging [1]. However, NDs produced by detonation have a notable tendency to form tight aggregates in biological media.

In this regard, controlling protein adsorption on NDs via the engineering of adequate antifouling coatings is critical for the design of biologically relevant NDs. We selected click chemistry for the covalent attachment of antifouling polymers on the surface of NDs. The selective cycloaddition of azides to alkynes is highly efficient and can be carried out under aqueous conditions. We investigated in 2011 the antifouling properties of a fluorosurfactant known as Zonyl (M_w 725) having a first block based on a perfluoroalkyl chain followed by a poly(ethylene glycol) block [2]. NDs were functionalized with azide groups using 4-azidobenzoic acid and subsequently coupled with the alkynyl-terminated Zonyl. The adsorption of bovine serum albumin (BSA), which is the most abundant protein in plasma and serum, on NDs was quantified and was found to be reduced by 30% in the presence of the Zonyl layer.

Following this promising result, we conducted further experiments to gain insight about the associated mechanisms of adsorption using standard cell culture medium supplemented with fetal bovine serum as a complex biological fluid [3]. Zonyl and two other polymers, namely a low molecular weight poly(ethylene glycol) (PEG) and a zwitterionic (zwit) sulfobetaine, were attached on NDs. Protein fouling was found to be two-fold lower with Zonyl and zwit coatings, and six-fold lower with PEG coating in comparison with the unmodified particles. These results, along with a modelization of the particleprotein interface, suggest that NDs are covered first by a stabilizing monolayer of high affinity serum proteins, this monolayer being then substituted by proteins of lower affinity.

Future studies will be required to map the dynamic protein bio-corona formed around the NDs since it is known to dictate the overall particle behavior in biological environments.

References

[1] V.N. Mochalin, O. Shenderova, D. Ho and Y. Gogotsi. Nat. Nano. 7 (2012) 11-23

[2] L. Marcon, Z. Kherrouche, J. Lyskawa, D. Fournier, D. Tulasne, P. Woisel and R. Boukherroub. Chem. Commun. 18 (2011) 5178-5180.

[3] Z. Kherrouche, D. Fournier, D. Tulasne, P. Woisel, R. Boukherroub and L. Marcon. Submitted to Biomaterials.

Probing single nanowires with a hard X-ray nanobeam

G. Martínez-Criado[1], J. Segura-Ruiz[1], M.-H. Chu[1], B. Alén[2], J. Eymery[3] and A. Rogalev[1]

[1]Experiments Division, European Synchrotron Radiation Facility, 38043-Grenoble, France
[2]IMM, Instituto de Microelectrónica de Madrid (CNM, CSIC), 28760-Tres Cantos, Spain
[3]CEA-CNRS-UJF group, Nanophysique et Semi-conducteurs, SP2M,
UMR-E CEA/UJF-Grenoble 1, INAC, Grenoble, F-38054, France

Nano X-ray beams are emerging characterization tools with broad implications for semiconductor research. Here we describe how a hard nanometre-sized X-ray beam is used today using reflective optics at the beamline ID22 of the European Synchrotron Radiation Facility to study size-dependent phenomena in single semiconducting nanowires. We show that X-ray microscopy is a key approach for space-resolved determination of structural and time-resolved electronic properties, and for chemical speciation of magnetic doped nanowires, core/multishell heterostructures and crossed nanowire architectures. Selected examples will range from cluster formation to particle contaminations and dopant segregation effects, to phase separations, carrier confinement effects and embedded junction domains.

Structural and electronic properties of graphene grown on Cu(111) and on Au(111) surfaces by ethylene irradiation

Antonio J. Martínez-Galera, Iván Brihuega, José M. Gómez-Rodríguez

gmartine@esrf.fr

Dpto. Física de la Materia Condensada, UAM, E-28049 Madrid, Spain

A novel technique for growing graphene on relatively inert metals is presented in this work [1]. By this route, consisting in the thermal decomposition of low energy ethylene ions irradiated on hot metal surfaces in ultrahigh vacuum (UHV), high quality graphene monolayers have been grown on Cu(111) and, for the first time, on Au(111) single crystals (fig. 1). These samples have been characterized by means of scanning tunneling microscopy (STM), low energy electron diffraction (LEED), and Auger spectroscopy (AES). The results provided by all these techniques reveal the formation, on the Cu(111) and Au(111) surfaces, of carbon monolayers exhibiting a long range ordering in a honeycomb lattice. At this point, it is important to remark that the quality of these graphene monolayers grown on Cu(111) by the method presented here is similar to that obtained by more traditional methods. Additionally, it has allowed the epitaxial growth of graphene monolayers on Au(111), a quite inert surface where graphene had not been grown until now.

Moreover, these graphene monolayers grown on Cu(111) and Au(111) single crystals have served us as a platform for the study of the graphene-metal interaction for both surfaces. The results obtained by STM and scanning tunneling spectroscopy (STS) are compared with existing ones on other graphene like systems where the graphene-substrate interaction is weak [2-4]. In particular, for both noble metal substrates, but specially for Au(111), our STM and STS measurements provide sound evidence of a very weak graphene-metal interaction.

References

[1] Martínez-Galera, A. J.; Brihuega, I.; Gómez-Rodríguez, J. M. Nano Lett. 11, (2011) 3576.

[2] Ugeda, M. M.; Brihuega, I.; Guinea, F.; Gómez-Rodríguez, J. M. Phys. Rev. Lett. 104, (2010) 096804.

[3] Rutter G. M.; Crain J. N.; Guisinger N. P.; Li T.; First P. N.; Stroscio J. A. Science 317, (2007) 219.

[4] Ugeda, M. M.; Fernández-Torre, D.; Brihuega, I.; Pou, P.; Martínez-Galera, A. J.; Pérez, R.; Gómez-Rodríguez, J. M. Phys. Rev. Lett. 107, (2011) 116803.

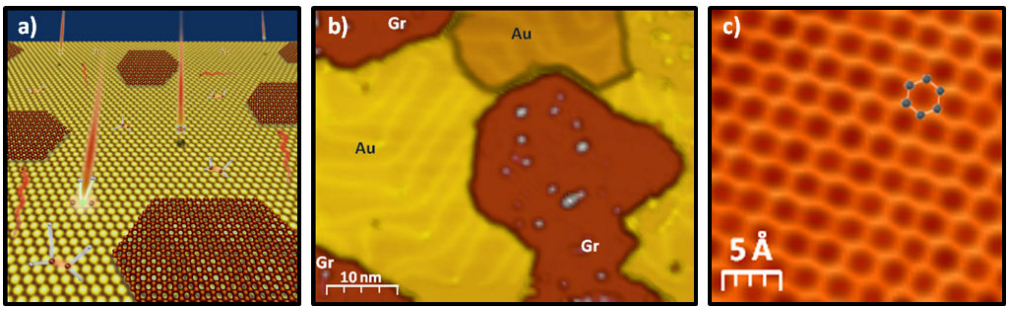

Figure 1. a) Schematic representation of the new method for growing graphene. b) STM image of an area of 53 x 41 nm^2 exhibiting three graphene flakes epitaxially grown on a Au(111) surface. The herringbone reconstruction characteristic of the Au(111) surface can be observed. Tunneling parameters: Vs = 500 mV, I_T = 0.5 nA. c) STM image over a defect-free graphene/Au(111) area displaying the honeycomb structure. Tunneling parameters: Vs = 30 mV, I_T = 21 nA; size: 2.5 x 2.5 nm^2.

Intercalation of Kr atoms into Graphene on SiC(0001)

Tomohiro Matsui[1], Jan Raphael Bindel[1,2], Hiroki Hibino[3] and Hiroshi Fukuyama[1]

matsui@kelvin.phys.s.u-tokyo.ac.jp

[1]Department of Physics, The University of Tokyo, Bunkyo-ku, Tokyo, Japan
[2]II. Institute of Physics B, Physics Center Melaten, RWTH Aachen, Aachen, Germany
[3]NTT Basic Research Laboratories, Kanagawa, Japan

Graphene, a two dimensional hexagonal form of carbon atoms, is attracting a great interest since its experimental finding in 2004. Because the carries, both electrons and holes, in an ideal graphene sheet behave like the massless Dirac fermions, it exhibits a series of new electronic properties such as the anomalously quantized Hall effects, the absence of weak localization, and the existence of a minimum conductivity. In addition, the sp2 bonding of carbon atoms makes it chemically inactive and mechanically robust and flexible. Therefore, Graphene can be an excellent candidate for the next generation of electronic materials. A next step of the graphene research is to find ways to control its physical properties. One of the strategies is to functionalize graphene by depositing atoms or molecules on graphene. For example, it is well known that some adsorbates transfer either electrons or holes into graphene and change the conductance at fixed gate voltage, which can result graphene in a gas sensor. In the case of alkaline atoms as adsorbates, the amount of transferred charge is so much that the Fermi energy (E_F) can reach to the saddle point, the van Hove singularity, which can even lead the superconducting instability. The superstructure of adsorbates, on the other hand, can modify the electronic interaction in graphene which can result in the band gap opening. The chiral symmetry breaking and resultant band gap opening is expected when the adsorbates form (√3x√3)R30° structure.

Here, we report on the effect of Kr atoms deposited on graphene epitaxialy grown on SiC(0001). It is well known that most rare gas atoms adsorb on the surface of graphite in layer-by-layer and form two dimensional (2D) solid. At lower densities, they are adsorbed on the hollow site of the honeycomb lattice of graphite to form (√3x√3)R30° phase.

The surface topography and electronic states of graphene on SiC(0001) are studied with our home designed scanning tunneling microscope, named the ULT-STM, which can work in multi-extreme conditions, i.e. at temperatures down to 30 mK, in high magnetic fields up to 13 T and in ultra-high vacuum (UHV) [1]. The chamber for the microscope is directly connected to the UHV chambers at room temperature, where one can prepare and evaluate the samples and tips for STM. The prepared samples and tips can be transferred to the microscope at T ~ 2 K *in-situ* in UHV quickly within a minute, afterwards the STM with newly installed sample and tip can be cooled down to the base temperature within a few hours.

Kr atoms were deposited onto graphene in a UHV chamber by keeping the temperature of graphene substrate and the partial pressure of Kr for certain time duration (10 minute, in this study). This way of sample preparation worked well in our setup for Kr atoms on graphite [2], where the relation between temperature and saturated vapor pressure of 2D Kr solid had been studied well in various experiments. In the case of graphene as a substrate, however, the P-T phase diagram should be modified reflecting the difference of the adsorption energy of Kr on either graphite or graphene. In general, the adsorption energy on graphene is smaller than that on graphite, and lower temperature or higher pressure is necessary to form the 2D Kr solid on graphene than on graphite. In this study, we have prepared two samples with different areal densities. The sample #1 was prepared at T = 42±0.3 K and P = (8.7±0.3)x10^{-8} Pa, while sample #2 at T = 35±0.05 K and P = (7.2±0.3)x10^{-8} Pa, which means that the density of Kr on sample #1 is smaller than that on sample #2.

As the graphene substrate, monolayer and bilayer graphene epitaxially grown on 6H-SiC(0001) is adopted [3]. It is well known for graphene on SiC(0001) that there is a C-rich buffer layer with 6x6 corrugation in between graphene sheet and the SiC(0001) surface. Because of this buffer layer, graphene sheet shows the 6x6 corrugation together with the honeycomb lattice of C in STM images. The 6x6 corrugation of the surface is getting weaker for thicker graphene when the surface layer is away from the buffer layer. In the I-V spectroscopy, on the other hand, the Dirac point (E_D) is observed at negative voltages as a dip in the dI/dV spectrum suggesting that electrons are doped to graphene from the substrate. And the E_D is getting closer to the Fermi energy (E_F), i.e. zero bias voltage, for thicker graphene.

Throughout this study, we have focused on around a boundary between mono- and bi-layer graphene. In this

study, a boundary of lower and upper terraces is observed with the height difference of 0.16 nm (figure 1(a)), which is about half of interlayer distance of graphite. The 6x6 corrugation of lower and upper terraces are 18 pm and 9 pm, respectively, suggesting that the lower (upper) terrace is mono- (bi-) layer of graphene [4]. The dI/dV spectrum shows a dip feature at -175 mV for lower terrace, while such dip feature is observed at 30 mV higher energy for upper terrace. Though the absolute energies of the dip feature are different from other studies [4], this change of the dip energy depending on the terraces suggests that the upper terrace is thicker than the lower.

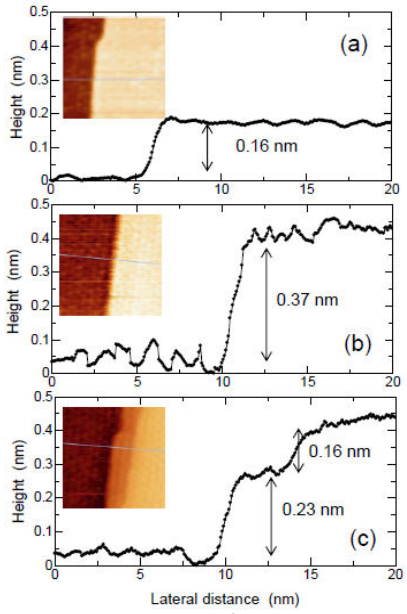

Figure 1. STM images (20 x 20 nm^2) and their line profile (along the line inside STM images) of (a) bare graphene, (b) sample #1 and (c) sample #2. The STM images show the boundary of lower monolayer terrace (left) and upper bilayer terrace (right).

When Kr atoms are deposited on graphene on SiC(0001), no Kr atoms are observed on the surface. It is surprising difference from the behavior on graphite, where each Kr atoms could be observed clearly with STM [2]. However, it does not mean that Kr atoms are not deposited on the graphene sample because some electronic properties are modified by Kr deposition as are discussed below and more during the conference. From the experimental results, one can expect that the Kr atoms are intercalated in graphene or buffer layer instead of adsorbing on the surface.

The effect of the Kr atoms is observed in four measurements. First, it is observed in the amplitude of the 6x6 corrugation. The corrugation is increased to 26 pm and 33pm for lower density sample (#1) and higher density sample (#2), respectively, on monolayer terrace. On the other hand, it is increased to 21 pm and 44 pm for sample #1 and #2, respectively, on the bilayer terrace. The corrugation is increased monotonically by increasing the amount of Kr atoms. This finding suggests that the intercalated Kr atoms are adsorbed commensurate to the 6x6 corrugation of the buffer layer rather than to the honeycomb lattice. It is worth noting that the magnitude correlation of 6x6 corrugation between monolayer and bilayer terraces is reversed for higher Kr density sample (#2).

Figure 1 shows the change of the step height by depositing Kr atoms. It is doubly increased to 0.37 nm for sample #1 (figure 1(b)) from 0.16 nm for the bare graphene (figure 1(a)). Interestingly, the single step is split into two for sample #2, the higher Kr density sample (figure 1(c)). Each step height is 0.23 nm and 0.16 nm, here, the smaller step height is the same as that on the bare sample, and the total height difference is the same as that on sample #1.

The effect of Kr atoms is also observed in I-z spectroscopy. Because the tunnel current is exponentially changed by the distance between the surface and the STM tip, one can extract the decay length of the surface wave function to vacuum from the slope of the I-z relationship. Moreover, one can also deduce the work function from the decay length. In this study, it is observed that the slope of the I-z spectrum on bilayer terrace is steeper than that on monolayer terrace. And the slopes become smoother by increasing Kr density. Considering roughly that the slope is proportional to the work function of the surface, the results suggest that the work function is smaller on monolayer than bilayer, and smaller on higher Kr densities than on lower densities. This tendency that the work function becomes smaller by graphene intercalation is consistent to the study in reference [5].

Finally some changes of the surface DOS are also observed in the dI/dV spectrum. The dip feature in surface DOS is disappeared by the Kr intercalation. It can be because the graphene layers are electronically decoupled from the substrate and E_D is located close to the E_F. However, some theoretical approaches are necessary for better understanding.

The detail of these effects will be discussed in the conference.

References

[1] H. Kambara, T. Matsui, Y. Niimi, and H. Fukuyama, Rev. Sci. Instrum. 78 (2007) 073703.

[2] J.R. Bindel, T. Matsui, and H. Fukuyama, in preparation.

[3] H. Hibino, H. Kageshima, and M. Nagase, J. Phys. D 43 (2010) 374005.

[4] P. Lauffer, K.V. Emtsev, R. Graupner, Th. Seyller, and L. Ley, Phys. Rev. B 77 (2008) 155426.

[5] A. Sandin, T. Jayasekera, J.E. Rowe, K.W. Kim, M.B. Nardelli, and D.B. Dougherty, Phys. Rev. B 85 (2012) 125410.

Towards the control in 2D organization of covalent functionalization of graphene surfaces

Cristina Mattioli[1], Miguel Rubio-Roy[1], Olivier Couturaud[1], Maya Narayanan Nair[2], Laurent Simon[2], Erik Dujardin[1] and André Gourdon[1]

[1]Groupe NanoSciences, CEMES CNRS UPR 8011, BP 94347, 29 rue J. Marvig, 31055 Toulouse, France
[2]Equipe Molecule sur surface-spectroscopie champ proche, Institut de Sciences des Matériaux de Mulhouse, CNRS UMR 7361, 3 bis rue Alfred Werner, Mulhouse, France

mattioli@cemes.fr

Graphene, a monolayer of carbon atoms packed in a two-dimensional honeycomb lattice, has lately become a very interesting material, being endowed with exceptional physical properties [1]. In particular, electronic properties constitute one of the most investigated aspects of graphene, which is considered a zero band gap semiconductor. Great efforts have been devoted to open a band gap into its energetic levels [2] and one of the followed routes is covalent chemical functionalization [3]. Some of the issues related to this strategy are that (1) pristine graphene shows a very low chemical reactivity; (2) if many ways have been proposed to functionalize the surfaces in a "random" fashion, controlled chemical functionalization (i.e. only at specific sites) has not yet been described.

In this context, our attention is focused in getting a control on the patterning of the eventually covalent functionalization of graphene in 2D. The chemistry we apply is that of Diels-Alder cycloaddition reactions [4], offering a better control on the reaction outcome, as for what it is concerned with the composition of the chemisorbed layer, compared to the strategies employing highly reactive radical species [5].

In a first step, we have carried out tests of functionalization of graphite and graphene devices by microwave-activated Diels-Alder reactions with maleimide derivatives. The Raman characterization of the samples has revealed the possibility of activating the reaction at the solid/liquid interphase on different substrates (graphite flakes, graphene on SiO_2).

In a second step, we have synthesised a series of oligo (phenylene-ethynylene) derivatives of different geometries, prone to self-assemble on graphene, characterised by the presence of functionalities potentially reactive with graphene by Diels-Alder reaction. Their self-assembling behaviour has been studied by STM at the liquid/HOPG interphase. In a next step, we will explore the possibility of achieving the controlled chemisorption of the molecules by STM local activation on epitaxial graphene in UHV.

References

[1] Geim, A., Novoselov, K ., Nature Mater., 2007, 6, 183-191
[2] a) Berger, C., Song, Z., Li, X., Wu, X., Brown, N., Naud, C., Mayou, D., Li, T., Hass, J., Marchenkov,A., N., Conrad, E. H., First, P. N., de Heer, W., A., Science, 2006, 312, 1191-1196; b) Han, M. Y., Oezyilmaz, B., Zhang, Y., Kim, P., Phys. Rev. Lett., 2007, 98, 206805
[3] a) Balog R., Jørgensen, B, Nilsson, L., Andersen, M., Rienks, E., Bianchi, M., Fanetti, M., Lægsgaard, E., Baraldi, A., Lizzit, S., Sljivancanin, Z.,Besenbacher, F., Hammer, B., Pedersen, T. G., Hofmann, P., Hornekær, L., Nature Mater., 2010, 9, 315-319; b) Zhang , H., Bekyarova, E., Huang, J.-W., Zhao, Z., Bao, W., Wang, F., Haddon, R. C., Lau, C. N., Nano Lett., 2011, 11, 10, 4047–4051
[4] Sarkar, S., Bekyarova, E., Niyogi, S., Haddon, R. C., J. Am. Chem. Soc., 2011, 133, 3324–3327
[5] Hossain, M. Z., Walsh, M. A., Hersam, M. C., J. Am. Chem. Soc., 2010, 132, 15399-15403

Dynamics of topological defects in the mechanical deformation of curved nanocrystalline shells

M. Carmen Miguel

Departament de Física Fonamental, Facultat de Física, Universitat de Barcelona , Barcelona (Spain)

Crystals must deform to fi ton curved sufaces. The energy cost associated to such deformations consists of both stretching and bending contributions. According to Euler´s theorem and the Euler characteristic of the surface, the minimum energy configuration contains geometrically necessary topological defects, all of which share an elementary building block: the disclination. The elastic cost of a disclination in a crystalline membrane is very high, but buckling and/or the proliferation of boundary scars can reduce it considerably. We briefly discuss the structural transitions of curved nanocrystalline shells as a function of effective bending rigidity, sample size and geometry. The quiasi-static deformation of these structures is characterized by intermittent dynamics with collective particle reorganizations mediated by the proliferation and dynamic delocalization of defects. At large deformations we eventually observe structural failure phenomena such as the melting or the cavitation of the crystal shells.

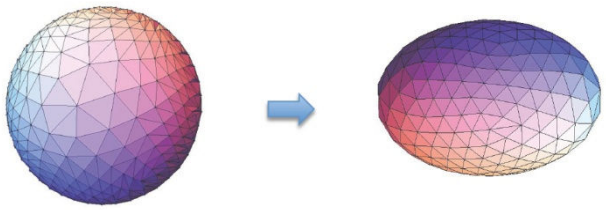

Figure 1: **Squeezing a spherical nanocrystal**: The process involves the nucleation and delocalization of several topological defects. Vacancies and cavities eventually develop at the tips of the spheroid.

Light Absorption and Emission of Nanomaterials in Porous Photonic Structures

Hernán Míguez

hernan@icmse.csic.es

Instituto de Ciencia de Materiales de Sevilla (CSIC-US),
C/Américo Vespucio 49 41092 Sevilla (Spain)

In recent times, several synthetic pathways have been developed to create photonic structures materials of diverse composition that combine accessible porosity and optical properties of structural origin, i.e., not related to absorption. The technological potential of such porous optical materials has recently been demonstrated in various fields such as biological and chemical sensing, photovoltaics, or radiation shielding. In all cases, improved performance is achieved as a result of the added functionality porosity brings on. Also, they offer the possibility to study fundamental light absorption and emission phenomena in materials that could not be integrated in photonic structures before, as well as to develop environmentally responsive coatings with them. In this seminar, a unified picture of this emerging field is provided, special emphasis being put in the opportunities it offers in the fields of energy, sensing and radiation protection.

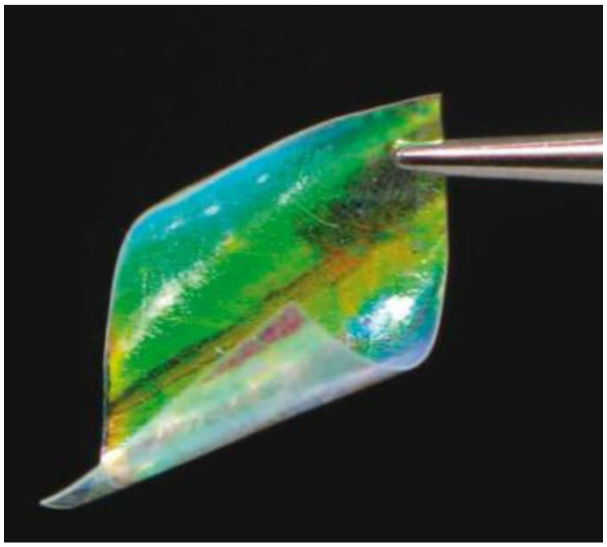

Figure 1. Image of a flexible Bragg mirror made by infiltrating a porous periodic multilayer with a biocompatible polymer.

References

[1] O. Sánchez-Sobrado, G. Lozano , M.E. Calvo, A. Sánchez-Iglesias, L.M. Liz-Marzán, H. Míguez, Adv. Mater. 2011, 23, 2108. “Interplay of Resonant Cavity Modes with Localized Surface Plasmons: Optical Absorption Properties of Bragg Stacks Integrating Gold Nanoparticles”.

[2] S. Colodrero, A. Forneli, C. López-López, L. Pellejà, H. Míguez and E. Palomares, Adv. Func. Mater. 2012, 22, 1303. “Efficient Transparent Thin Dye Solar Cells Based on Highly Porous 1D Photonic Crystals”.

[3] P. Zavala-Rivera, K. Channon, V. Nguyen, E. Sivaniah, D. Kabra, R. H. Friend, S. K. Nataraj, S.A. Al-Muhtaseb, A. Hexemer, M.E. Calvo, H. Míguez, Nature Mater. 2012, 11, 53–57. “Collective Osmotic Shock in Ordered Materials”.

Biomimetic nanofibrous scaffolds for tissue engineering applications

M. Moffa[1,2]
A. Polini[3 †]
A.G. Sciancalepore[1]
L. Persano[1,3] and
Dario Pisignano[1,2,3]

maria.moffa@iit.it

[1] Center for Biomolecular Nanotechnologies @UNILE, Istituto Italiano di Tecnologia,via Barsanti, I-73010 Arnesano, LE, Italy.
[2] Dipartimento di Matematica e Fisica "Ennio De Giorgi", Universit`a del Salento, via Arnesano, I-73100 Lecce, Italy.
[3] National Nanotechnology Laboratory of Consiglio Nazionale delle Ricerche-Istituto Nanoscienze, via Arnesano, I-73100 Lecce,Italy.
[†] Present address: Lawrence Berkeley National Laboratory, Materials Sciences Division, 1 Cyclotron Road, 94720, Berkeley, CA, USA

The multidisciplinary field of tissue engineering has the ultimate aim of repairing and/or replacing damaged tissues or organs by means of a properly designed combination of scaffolding biomaterials and functional cells. Nanomaterials play a pivotal role in stimulating cell growth and guiding tissue regeneration, since they are able to properly mimic the biomimetic features and physio-chemical properties of natural tissues and organs. In particular, electrospinning has emerged as one of the most successful techniques owning to its ability to generate fibers similar to the intricate fibrillar architecture of natural extracellular matrix [1].

Here we review our recent work about the realization of nanofibers with different naturally occurring matrix proteins and synthetic polymers and demonstrate the growth, proliferation and differentiation of different cell lines with the ultimate aim of designing optimized biomimetic scaffolds to support the formation of functional tissues. We explored the various possibilities to articulate the composition and the others proprieties of nanofibers to meet the specific scaffolds demand of the different tissues and /or organs. In particular, we investigate the possibility to improve cellular proliferation, infiltration and functionality using electrospun polymer nanofibers with improved wettability behavior [2]. We also investigate the possibility to engineer electrospun fibrous scaffolds presenting the anisotropy of the specific native tissues. The possibility to improve cell specific adhesion on synthetic nanofibrous mats is also a topic of our works, through the insertion of specific bioactive molecules on electrospun synthetic scaffolds to promote cell adhesion and proliferation. The immobilization of cell recognition motifs leads to controlled interaction between cells and synthetic substrates.

Among other biomedical materials, by virtue of these peculiar advantages polymer nanofibers are rapidly emerging as one of the most promising for an actual industrial application in the field [3].

We acknowledge the support of the Italian Ministry of University and Research through the FIRB Contract RBNE08BNL7 (MERIT Program).

References

[1] A. Polini, et al., D. Pisignano, Soft Matter, 6, (2010)1668-1674.
[2] M. Moffa et al., D. Pisignano, Soft Matter, 9 (2013) 5529-5539.
[3] L. Persano, A. Camposeo, C. Tekmen, and D. Pisignano, Macromolecular Materials & Engineering, 298 (2013) 504-520.

Mapping Intermolecular Force-fields with Sub-Angstrom Resolution

Philip Moriarty

School of Physics and Astronomy, University of Nottingham, Nottingham NG7 2RD, UK

www.nottingham.ac.uk/physics/research/nano

Dynamic force microscopy (DFM, also called non-contact atomic force microscopy) has evolved rapidly into an exceptionally powerful tool for single molecule imaging, spectroscopy, and manipulation. A number of key innovations have enhanced the capabilities of the technique dramatically over the last decade or so: the introduction of the qPlus variant [1], facilitating exceptionally high sensitivity to short range chemical forces; the exploitation of the Pauli exclusion regime of the tip-sample interaction potential for unprecedented levels of resolution [2,3]; and the steady development of sophisticated protocols enabling greater control of the precise structure of the tip apex [2,4].

As a result of these developments, coupled with substantial support from first principles theoretical calculations such as density functional theory (DFT), DFM is now capable of not only characterising reactants and products at the single bond level [5], but of controlling bond conformation on an atom-by-atom basis [6].

I will discuss the application of qPlus DFM to the measurement of intermolecular force-fields and potential energy landscapes for three distinct classes of molecule: fullerenes (specifically, C_{60}) [7], porphyrins (tetra(4-bromophenyl)porphyrin), and NTCDI (see Fig. 1). In each case precise control of the apex of the tip is an essential prerequisite for the acquisition of quantitative force data. In the case of NTCDI this is a particularly acute issue as our primary interest lies in the measurement and exploitation of hydrogen-bonding-derived forces and potentials. Our approaches to ascertaining the chemical termination of the tip via comparison of experimental data with the results of DFT calculations will be described in some detail.

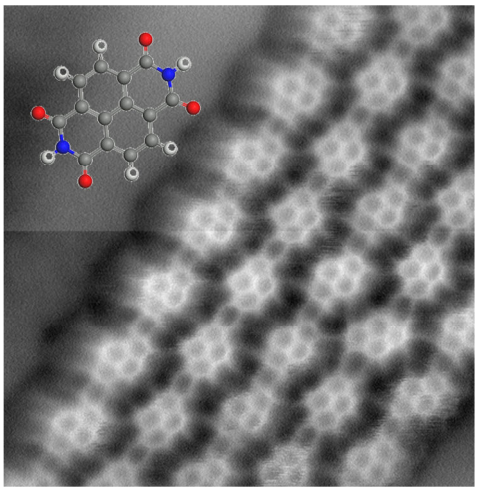

Figure 1. qPlus DFM image of a 2D assembly of NTCDI molecules (structure shown in inset) on the Ag:Si(111)-(√3 x √3)R30° surface.

References

[1] F. Giessibl, Appl. Phys. Lett. 76, 1470 (2000)
[2] L. Gross, F. Mohn, N. Moll, P. Liljeroth, and G. Meyer, Science 325, 1110 (2009)
[3] L. Gross et al., Science 337, 1326 (2012)
[4] J. Welker and F. J. Giessibl, Science 336 , 444 (2012)
[5] D. G. de Oteyza et al., Science 340, 1434 (2013)
[6] A. Sweetman et al., Phys. Rev. Lett. 106, 136101 (2011)
[7] C. Chiutu et al., Phys. Rev. Lett. 108, 268302 (2012)

Electron Transport through Field-induced Quantum Dots in Graphene

Satoshi Moriyama[1]
Yoshifumi Morita[2], Eiichiro Watanabe[3] and Daiju Tsuya[3]

moriyama.satoshi@nims.go.jp

[1] International Center for Materials Architectonics (WPI-MANA), National Institute for Materials Science (NIMS), 1-1 Namiki, Tsukuba, Ibaraki 305-0044, Japan.
[2] Faculty of Engineering, Gunma University, Kiryu, Gunma 376-8515, Japan.
[3] Nanotechnology Innovation Station, NIMS, 1-2-1 Sengen, Tsukuba, Ibaraki 305-0044, Japan

Graphene, a single atomic layer of graphite, and few-layer graphene sheets are one of the attractive two-dimensional conducting materials for a new stage of low dimensional physics. From the application point of view, the ballistic transport and high mobility in graphene make them possible candidates for future electronic quantum devices. Nanostructures on graphene sheets can be fabricated by carving out of the graphene sheets directly, and the spread two-dimensional sheet structure may open a door to realize the integrated quantum nanodevice system. However, carriers in graphene (massless Dirac fermions) cannot be confined by an electrostatic potential due to Klein tunneling [1]. Therefore, in most cases, the formation of graphene quantum-dot (QD) devices relies on the removal of unwanted areas of graphene by etching, thereby resulting in devices with a geometrical confinement [2–4]. We have also demonstrated double quantum-dot devices in triple-layer graphene, which exhibits single-electron transport of two lateral quantum dots coupled in series [5]. Coupled quantum-dot systems have been proposed for various applications as new logic and architectures, such as the quantum computation and the quantum cellular automata. Our results suggest an important step for the realization of the integrated quantum devices in graphene-based nanoelectronics. Although this top–down process enables precise control of graphene device structures on a submicron scale, the graphene-edge shape varies on a nanometer scale. Therefore, the transport properties of graphene QD or nanoribbon devices are often dominated by edge roughness and disorder [6, 7]. The performance of such devices is limited due to the detail of nanoconstriction structures. It is crucially important to develop other methods of creating graphene nanostructures and control the constrictions.

In this paper, we report an alternative device structure for achieving confinement, in which nanostructured graphene islands are perfectly isolated and metallic contacts are directly deposited onto them without constrictions. Such a configuration realizes direct contact with a nanostructured two-dimensional electron gas, and the confinement potential is induced by an electrostatic surface-potential formed by the metal/graphene junction [8]. With this device structure, we demonstrated that the Coulomb blockade evolves under a uniform magnetic field perpendicular to the graphene sheet. As discussed in Ref. [9-11], such a quantum confinement-deconfinement transition is corresponding to the transition between open-to-closed trajectories of Dirac particles in this type of device structure. All trajectories are open for a sufficiently weak magnetic field, which corresponds to a continuum spectrum. At high magnetic fields, closed orbits emerge that correspond to quasi-bound states and coexist with open trajectories. Moreover, the quasi-bound states should be consistent with the Bohr–Sommerfeld condition [9, 12] and lead to a discrete energy spectrum. In addition to that, tunnelling between open and closed trajectories leads to a finite resonance lifetime and QD formation. Our experimental results indicate that a quantum confinement–deconfinement transition is controlled by the magnetic field.

References

[1] M. I. Katsnelson et al., Nature Phys. 2 (2006) 620.
[2] L. A. Ponomarenko et al., Science 320 (2008) 356.
[3] C. Stampfer et al., Nano Lett. 8 (2008) 2378.
[4] J. Güttinger et al., Phys. Rev. Lett. 103 (2009) 046810.
[5] S. Moriyama et al., Nano Lett. 9 (2009) 2891.
[6] K. Todd et al., Nano Lett. 9, (2009) 416.
[7] C. Stampfer et al., Phys. Rev. Lett. 102 (2009) 056403.
[8] B. Huard et al., Phys. Rev. B 78 (2008) 121402(R).
[9] N. Gu et al., Phys. Rev. Lett. 106 (2011) 066601.
[10] G. Giavaras et al., J. Phys.: Condens. Matter 21 (2009) 102201.
[11] P. A. Maksym et al., J. Phys.: Conf. Ser. 245 (2010) 012030.
[12] P.G. Silvestrov and K.B. Efetov, Phys. Rev. Lett. 98 (2007) 016802.

In-situ Raman analysis of possible graphene damage during electron beam or ion beam patterning strategies

J. J. L. Mulders

jjm@fei.com

FEI, Achtseweg Noord 5, 5615GG Eindhoven, The Netherlands

One of the needs in graphene research is to allow characterization of the material once it has been created. This characterization includes for example electrical characterization and therefore it is essential that graphene can be contacted and patterned. Patterning can be based on lithographic processes including resist spinning and removal, but if for example UV exposure or electron beam exposure is applied for the patterning, the graphene may be damaged. This may also occur by residual amounts of resist during development, or any processing for metal deposition and lift-off.

A direct way of patterning can include ion beam irradiation (FIB) or cutting graphene using an electron beam including the use of gas chemistry such as H_2O, O_2 or may be H_2. Also electron beam induced deposition is a method for direct deposition of a metal (for contacts), by exposing the graphene to a precursor gas that is decomposed by the electron beam. Whatever way of patterning is chosen, it is inevitable to check any possible local damage induced by the method itself. Especially the sensitivity of graphene damage related to the required dose for patterning is important to measure. As Raman analysis is considered as a non-destructive method for measuring damage on graphene, a combination of the two techniques is very useful.

In this paper a combination of Raman analysis and DualBeam is proposed as a tool for investigating this. A Raman laser beam coincident with an optical image can be aligned to an area that has been exposed by the electron or ion beam, without breaking the vacuum and without remounting and relocating of the area of interest. Changing from (sequential) exposure to Raman analysis is a matter of seconds and therefore this method is very convenient to understand and relate possible damage to graphene that an ion or electron beam might induce. The practical aspects of the implementation will be discussed, including geometric issues (FIB milling), visibility of graphene for different detectors and examples of high and low kV exposure of graphene and the related damage as a function of the dose.

In a similar way by stage scanning the extent to which the damage is present can be measured with respect to the irradiated area. Possible causes for an extended damage area is the availability of SE type 3, possible Back scatter electrons and in the case of ion beam irradiation re-deposition of (ionic) particles milled away from the substrate.

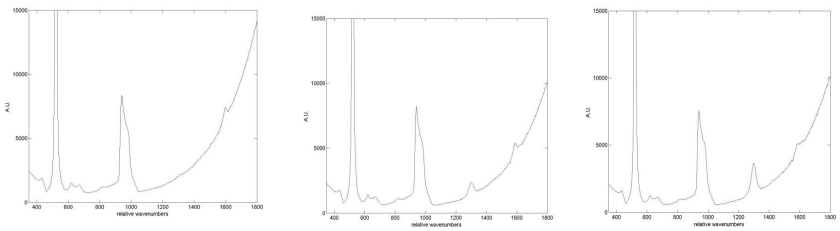

Figure 1 Raman spectra at 785 nm laser line of graphene on SiO_2. Pristine graphene (left) showing a small G and but no D band. After irradiation with an electron beam at 5 kV and a dose of 1.5.10+15 el/cm^2 showing an increase of the D band(middle) and at a cumulative dose of 6.5.10+15 el/cm^2, showing a high D band and a distorted G band. The whole series was made in a time frame of 15 minutes, while the electron beam irradiated area was 10 x 10 um.

Following a Fischer-Tropsch catalyst during reaction with STM and SXRD

[1] Kamerlingh Onnes Laboratory, Leiden University, Leiden, The Netherlands
[2] Beamline ID03, European Synchrotron Radiation Facility, Grenoble, France
[3] Shell Global Solutions International B.V., Amsterdam, The Netherlands

Violeta Navarro[1]
Sander B. Roobol[1], Matthijs van Spronsen[1], Richard van Rijn[1,2], Olivier Balmes[2], Didier Wermeille[2], Andrea Resta[2], Roberto Felici[2], Alexander P. van Bavel[3] and Joost W.M. Frenken[2]

navarro@physics.leidenuniv.nl

Catalyst's surfaces have been largely studied with traditional surface science techniques down to the atomic level. Those techniques are typically applied under vacuum conditions. There is a difference of many orders of magnitude in pressure between those vacuum studies and the industrial conditions at which catalysts work. Even though the studies in vacuum can be very revealing [1], the "pressure gap" leads to dramatic differences between laboratory and industrial conditions in terms of the reaction mechanisms and the changes that may appear in the catalyst during the reaction [2].

We have performed studies with two innovative experimental techniques that approach the conditions at which catalytic reactions take place in industry. Scanning tunneling microscopy (STM) [2,3] and surface X-ray diffraction (SXRD) [4] have been used in-situ to follow catalytic surfaces at high pressures and elevated temperatures. The two techniques are complementary, i.e. real space versus reciprocal space. The STM gives information on local structures on the catalytic surface whereas SXRD detects the periodic structures that appear during the reaction. In both cases we have configured the instruments in the form of small gas flow reactors, inserted inside a UHV chamber in which traditional surface science techniques are used to prepare and characterize the samples. These techniques have allowed us to study the structural changes on the surface of the catalyst while the reaction takes place.

Fischer-Tropsch synthesis (FTS) is the catalytic reaction that leads to the production of hydrocarbons from a mixture of H2 and CO at high temperature and high pressure. In spite of its enormous industrial and economic importance, the fundamental aspects of this reaction are still far from being completely understood on the atomic and molecular scale [5]. In our studies, we have followed a Co(0001) single crystal surface as a model catalyst to detect the changes during the reaction.

Much to our surprise, we find with STM and SXRD that during the reaction, at atmospheric pressures and elevated temperatures, a polycrystalline cobalt phase, i.e. an overlayer of cobalt nanoparticles, rapidly develops on the surface of the single crystal. We attribute this 'powdering' to the formation of a highly defective layer of graphene during the reaction, through which cobalt atoms segregate and coalesce to form particles on top. This scenario has severe consequences for the FTS reaction and for our view on the structure and working mechanisms of this catalyst and also for the potential role of structural promoters.

References

[1] G. Ertl. Angewandte Chemie International Edition, 52, 1 (2013), 52–60.
Y.D.Yin,R.M. Rioux, C.K. Erdonmez, S. Hughes, G.A. Somorjai, A.P. Alivisatos. Science, 304, 5671. (2004) 711-714.
R. Schaub, P. Thostrup, N. Lopez, E. Laegsgaard, I. Stensgaard, J.K. Norskov, F. Besenbacher. Phys. Rev. Lett. 87,(2001) 26
[2] I B.L.M. Hendriksen, et al., Topics in Catalysis, 36, (2005) 1–4.
[3] C.T. Herbschleb et al., to be published.
[4] R. van Rijn et al., Rev. Sci. Instrum. 81, (2010) 014101.
[5] J. Wilson et al., J. Phys. Chem. **99**, (1995) 7860-7866.

Layered and two-dimensional materials explored from first-principles

Pablo Ordejón[1,2]
Jose Angel Silva[1,2] and
Enric Canadell[3]

pablo.ordejon@icn.cat

[1] Institut Català de Nanociència i Nanotecnologia, Campus UAB, 08193 Bellaterra , Barcelona, Spain.
[2] CSIC - Consejo Superior de Investigaciones Cientificas, ICN2 Building , Campus UAB, 08193 Bellaterra, Barcelona, Spain.
[3] Institut de Ciència de Materials de Barcelona - ICMAB-CSIC, Campus UAB, 08193 Bellaterra, Barcelona, Spain.

Three-dimensional crystals with low dimensionality (i.e., small effective electronic interactions in one or two dimensions) have a rich physical behavior that has been the subject of intense study over the last decades. Electronic instabilities in these systems play a crucial role in their properties, and simplified models have been used traditionally to predict and explain these properties. Their structural complexity has usually been an important difficulty for a fully first-principles approach for their study. However, current first-principles methods and computational facilities are now sufficiently powerful and efficient to allow us to attack problems which were formerly too complex to be tackled with these techniques.

Besides, layered materials are experiencing an impressive thrust due to the possibility of obtaining truly atomically-thin two-dimensional layers like in graphene. The unique properties of these layers, and the infinite possibilities offered by the formation of structures obtained from staking multiple layers of different materials, confer these systems a huge potential for devices with new functionalities.

I will describe some of our efforts in attacking some long standing problems in these materials using first-principles simulations. Examples are the prediction of Charge Density Waves in low dimensional metals originated from Fermi level instabilities, the electronic properties of two-dimensional materials like graphene containing impurities and disorder, and the interfaces of two-dimensional layers like graphene and MoS_2

Dynamical aspects of molecular self-assembly at solid surfaces

Roberto Otero

Dep. de Física de la Materia Condensada, Universidad Autónoma de Madrid, Avd. Francisco Tomás y Valiente 7, Madrid, Spain
Instituto Madrileño de Estudios Avanzados en Nanociencia (IMDEA-Nano), c\ Faraday 9, Madrid, Spain

roberto.otero@uam.es

Most of the studies on molecular self-assembly on solid surfaces focus on the thermodynamic driving forces (intermolecular interactions, molecule-molecule interactions, etc) that control the ordering of the molecular species. This is related to the fact that in most cases the energy barriers that control the kinetic processes involved in the assembly (diffusion barrier, rotational barriers, conformational barriers) are much lower than the relevant thermal energy, while the energy gain associated with the nucleation and growth of ordered structures is larger than the thermal energy (at least for a sufficiently large nucleus size). Under such conditions the structure is almost completely determined by thermodynamic reasons and little space is left for kinetic effects.

However, there exist relevant situations in which dynamical effects cannot be disregarded as unimportant. In this presentation we will investigate two of such situations:

- Thermodynamics by itself cannot explain completely the existence of defects. Defects such as vacancies, are however key in controlling mass transport in solids, with implications for mechanical properties and thermal stability. In our first example we will investigate the diffusion of individual vacancies in a self-assembled monolayer of a tetrathiofulvalene derivative (exTTF) on a Au(111) surface. Our experiments allow for a direct identification of the individual vacancies and their thermally induced displacements (see Figure 1), in contrast with other methods that follow tracer atoms that occupy the vacancy sites. A complete analysis of the displacement distribution function shows that correlated jumps of vacancies are actually very frequent, and the rates for long-jump events is inversely proportional to the jump length. We propose that this inverse proportionality is related with the dispersion of the longitudinal phonon bands along the direction of the chains.
- Molecules with different isomeric forms might assemble into different structures corresponding to the different isomers. The growth and self-assembly of such molecules will thus be controlled by the kinetic rate at which the isomerization will take place. We will show that the self-assembly structure of dicyanoquinodiimide (DCNQI) molecules depends on the deposition temperature, being controlled by an isomerization reaction (see Figure 2) which is facilitated by the uptake of one electron from the surface

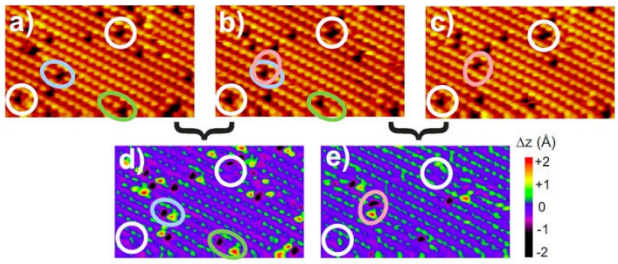

Figure 1. a), b) and c) Consecutive STM images of the same area of (15× 9 nm^2, V_{Bias} = 1.2 V, It = 1 nA) of a self-assembled monolayer of exTTF deposited on Au(111). Two vacancies (white circles) remain in the same position that they occupied in the first frame. Some examples of vacancy diffusion events are marked by blue ovals (single displacement along the a direction), pink ovals (single displacement along b) or green ovals (double displacement along a). d) and e) show the difference between consecutive images, in which the diffusion events can be easily identified. The time interval between the two images is 16 seconds.

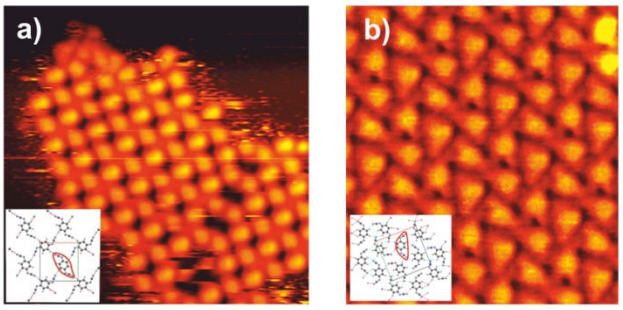

Figure 2. a) STM image (8 × 8 nm^2) of the self-assembled structure obtained by depositing DCNQI molecules with the substrate held at 120 K. The structure and the appearance of the molecules are consistent with DCNQI molecules being in the anti-isomeric state. b) STM image (6 × 5 nm^2) of the structure obtained after RT deposition, which can only be explained by assuming that the molecules are now all of them in the syn-isomeric state.

Charge transfer and screening behaviour of bilayer graphene devices

Vishal Panchal[1,2] Arseniy Lartsev[3], Rositza Yakimova[4], Alexander Tzalenchuk[1] and Olga Kazakova[1]

olga.kazakova@npl.co.uk

[1] National Physical Laboratory, Hampton Road, Teddington, TW11 0LW, UK
[2] Royal Holloway, University of London, Egham Hill, Egham, Surrey, TW20 0EX, UK
[3] Chalmers University of Technology, Göteborg, S-412 96, Sweden
[4] Linköping University, Linköping, S-581 83, Sweden

Graphene is a two-dimensional material comprised of only carbon atoms closely packed in a honeycomb crystal structure. Devices fabricated out of epitaxial graphene grown on SiC have shown great promise for commercialization [1,2]. However, due to the complicated growth procedure, even the best epitaxial samples contain ~95% mono-layer (1LG) and ~5% bi-layer (2LG) graphene coverage [3]. Due to the differences in the band structure of different graphene layer thicknesses, such samples have been shown to exhibit a work function difference of ~120±15 meV between 1LG and 2LG [4-6], which can affect the transport properties of graphene devices.

Our study of the *bulk* electrical properties of 1LG and 2LG devices reveals the carrier density for 1LG and 2LG to be n^{1LG} ~ 2×10^{12} cm^{-2} and n^{2LG} ~ 9×10^{12} cm^{-2}, respectively, in a dark environment at ambient conditions. Further, we investigate the *local* electrical properties of 1LG device with isolated 2LG islands by measuring the longitudinal (V_{xx}) and transverse voltage (V_{xy}) response to an electric field produced by a local scanning gate (Fig. 1a). Scanning gate microscopy (SGM) is performed using an electrically conductive probe to locally gate the double-cross graphene Hall bar at a constant 15 nm lift height, while a DC bias voltage (V_{probe}) is applied to the probe. V_{xx} and V_{xy} maps of the current biased device (I_{bias}) are obtained by measuring and recording the signal, pixel by pixel, with a lock-in amplifier referenced to the mechanical resonance of the cantilever. Spectroscopy is a point measurement performed by sweeping V_{probe} and measuring V_{xx} at well-defined positions.

SGM V_{xx} map of the entire device was obtained at I_{bias} = 10 µA and V_{probe} = –3 V (Fig. 1b). The image shows that gating in the central part of the device on the 1LG increases V_{xx}, whereas gating on the 2LG decreases V_{xx}. Spectroscopy measurements on 1LG, isolated 2LG and background conducted by sweeping V_{probe} and measuring $R_4 = V_{xx} / I_{bias}$ (Fig. 1c), shows that local gating on 1LG with V_{probe} = –5 V *increases* the total resistance of the channel by R_4 ~0.75 Ω. The latter can be described by the electron-electron repulsion between the probe and the sample decreasing the carrier density, thereby increasing the resistance. However, gating on the isolated 2LG *decreases* the total resistance by R_4 ~0.25 Ω, which is a result of an increase in the carrier density. This gives indication of a charge transfer occurring to/from the isolated 2LG islands in the presence of an electric field. Such effect is impossible to observe with uniform top gates, where the small inverse behaviour of the 2LG islands would be masked by the much larger contribution from the 1LG part of the device.

In addition, we study the effects of isolated 2LG islands on the V_{xy} of the Hall device (Fig. 2). Comparing the V_{xy} contrast of the 2LG island (location 1) to the SiC background (location 2), the V_{xy} map indicates that isolated 2LG islands can screen the local electric field, affecting the transport measurements of the Hall sensor. However, the screening efficiency will depend on geometry of 2LG domains and their exact position with respect to the leads. Local electric field applied at location 3 clearly shows a significantly larger response in comparison to locations 1 and 2. These measurements allow investigating the possible effect of decoupling between individual layers of graphene.

In summary, we studied the bulk and local transport properties of graphene nanodevices as

well as the effects of local electric fields applied to continuous 1LG and isolated 2LG islands on the total resistance of the device. We show that the local resistance and, hence the carrier density change of the 2LG island are sensitive to the sign of the gate voltage, giving indication of charge transfer occurring to/from the isolated 2LG islands in the presence of a local electric field. In addition, in the transverse voltage measurements we also observe the effect of local screening of the electric field by the 2LG island. These nanoscale effects of isolated 2LG islands can significantly affect the performance of graphene devices. SGM techniques are ideal for observing these nanoscale effects, which otherwise are difficult to detect with bulk transport measurements alone

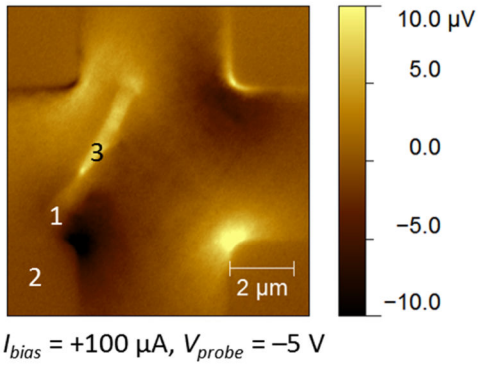

Figure 2. SGM V_{xy} mapping of the right cross of the device shown in Fig. 1a. V_{xy} at location 1 is comparable to the background (location 2), whereas the response at location 3 is significantly larger than location 1

References

[1] C. Dimitrakopoulos et al., J. Vac. Sci. Technol. B, 28 (2010) 985-992.
[2] Y. -M. Lin et al., Science, 327 (2010) 662.
[3] V. Panchal et al., 12th IEEE Conf. on Nanotechnology (2012).
[4] O. Kazakova et al., Crystals, 3 (2013) 191-233.
[5] Y.-J. Yu et al., Nano Letters, 9 (2009), 3430–3434.
[6] T. Filleter et al., Applied Physics Letters 93 (2008), 133117.

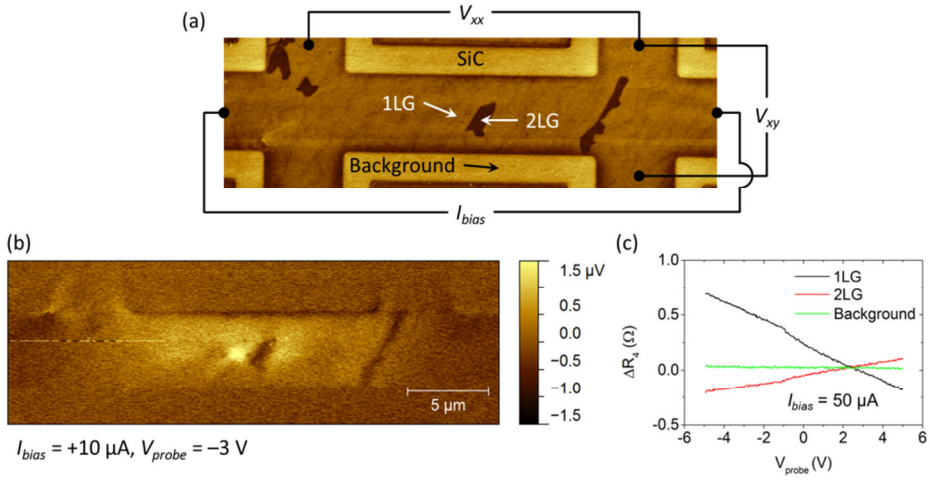

Figure 1. (a) Electrostatic force microscopy map of the 1LG device with patches of 2LG islands. Colour scale: phase range of 0.8°. Electrical scheme of the experiment is shown. (b) SGM V_{xx} mapping of the entire device taken with I_{bias} = 10 μA and V_{probe} = −3 V. (c) Spectroscopy measurement performed by sweeping V_{probe} and recording V_{xx} at the three locations indicated by the arrows in (a).

Novel Pd based catalyst with high performance for Carbon-Carbon coupling reactions

I. Pastoriza-Santos[1]
G. Zheng[1], K. Kaefer[1],
J. Pérez-Juste[1] and
L. M. Liz-Marzán[1,2]

pastoriza@uvigo.es

[1] Departamento de Química Física, Universidade de Vigo, 36310 Vigo, Spain
[2] BNP Laboratory, CIC biomaGUNE, Paseo de Miramón 182, 20009 Donostia, Spain

Palladium-catalyzed cross coupling reactions are the most powerful and versatile methods for carbon–carbon bond formation impacting a broad spectrum of the chemical sciences.[1] The C-C coupling reaction could proceed through a homogeneous or heterogeneous catalysis. Homogeneous cross-coupling reactions, however, have several shortcomings such as limited reusability of the expensive catalyst, which impacts cost, and palladium contamination in the product. In order to address these problems, heterogeneous Pd catalysis is a promising option. We therefore propose a novel heterogeneous catalyst based on the immobilization of pre-synthetized Pd nanoparticles on a paper filter (see Figure 1A) which have a low cost and is available in a variety of forms. The catalytic efficiency of the paper based Pd catalyst was tested for the Ulmann cross-coupling reaction (see Figure 1B). The reaction can be followed by UV−visible spectroscopy and provides a convenient reaction to test catalytic systems under representative aerobic reaction conditions. Such kinetic studies allow the most accurate and honest quantification of recovery of catalytic activity.

References

[1] L. Yin, J. Liebscher, Chem. Rev. 107, 133, (2007).

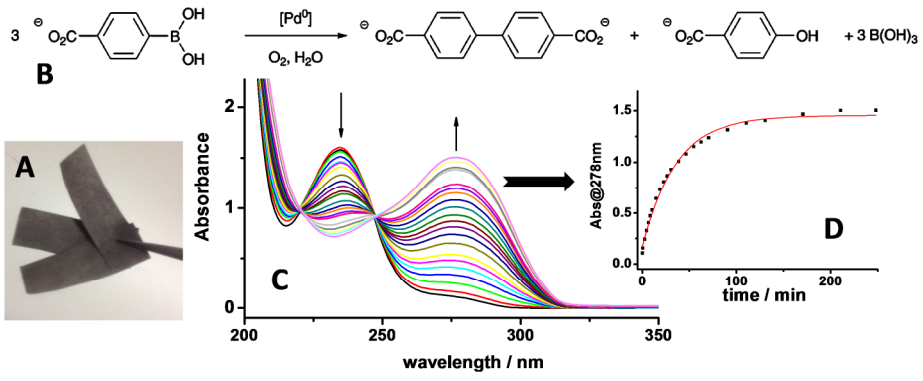

Figure 1. (A) Aqueous aerobic oxidative homocoupling reaction. (B) Photograph of the Pd based catalyst. (C) Time evolution spectra of the reaction. (D) Time variation of absorbance at 278nm.

Optical properties, transport and sensing in metal-molecular aggregate hybrid nanostructures

Olalla Pérez-González[1,2]
Nerea Zabala[1,2] and
Javier Aizpurua[2]

olalla_perez@ehu.es

[1]Department of Electricity and Electronics, University of the Basque Country (UPV-EHU), Leioa, Spain.
[2]Centre of Materials Physics and Donostia International Physics Center (DIPC), Donostia, Spain.

Following the emerging connection between the fields of molecular electronics and plasmonics, we have studied theoretically the optical properties of gold nanoparticle (NP) dimers linked by a molecular bridge [1,2]. In a first approach, we have modelled the linker as a pure conductor with real conductivity. The main resonances governing the optical spectrum are the Bonding Dimer Plasmon (BDP), the Screened BDP (SBDP) and the Charge Transfer Plasmon (CTP) modes, depending on the conductance through the linker. The BDP and the SBDP modes arise from the hybridization of the dipolar modes of the individual NPs, whereas the CTP resonance involves a net current through the junction. This simple model allows us to establish thresholds of conductance for the activation of the SBDP and CTP modes, indicating when the transport through the linker starts to affect the optical properties of the dimer.

In a second step, we have incorporated the excitations of the individual molecules by introducing a Drude-Lorentz model for the dielectric response of the linker [3]. In this case, the BDP and the Bonding Quadrupolar Plasmon (BQP) resonances, with the BQP arising from the hybridization of the quadrupolar modes of the individual NPs, couple to the molecular excitonic transition. In spite of the complexity introduced in the dielectric response, we find that the concept of conductance threshold for the emergence of the CTP mode previously introduced for metallic linkers is still valid. We have performed a deep analysis of the effects of the excitation energy and the density of the molecular aggregates on the optical spectroscopy of the hybrid structures.

Finally, we have explored the efficiency of the new mixed states for LSPR sensing, showing that the CTP mode is a good candidate for shift-based sensing. Furthermore, for the BDP-exciton mixed states, we have observed an interesting behaviour for sensing based on the change of the relative intensity of the resonances, thus introducing a new framework for sensing based on the evolution of plexcitonic intensities rather than on spectral shifts.

References

[1] O. Pérez-González, N. Zabala, A.G. Borisov, N.J. Halas, P. Nordlander and J. Aizpurua, Nano Lett. 10, (2010) 3090.
[2] O. Pérez-González, N. Zabala and J. Aizpurua, New J. Phys. 13, (2011) 083013.
[3] O. Pérez-González, J. Aizpurua and N. Zabala, Opt. Exp. (2013) (accepted).

TiO_2-SiO_2 nanocomposite photoactive mesoporous materials for self-cleaning applications

Luís Pinho,
María J. Mosquera

luis.pinho@uca.es

TEP 243 Nanomaterials Group, Campus Universitario Río San Pedro, Puerto Real, Cádiz, Spain

Mesoporous TiO_2-SiO_2 composites that have photocatalytic activity have been synthesized by mixing ethoxysilane oligomers and TiO_2 nanoparticles in the presence of a non-ionic surfactant (*n*-octylamine) [1]. The products synthesized have a clear practical application because they can be employed outdoors by means of a simple and low-cost process. The resulting nanomaterials give self-cleaning properties and create crack-free effective adhesive coatings for porous building materials. In addition, they improve the mechanical resistance of the substrate. Another important advantage of these nanocomposites is that they substantially improve protection against salt crystallization degradation mechanisms [2].

The use of N_2 physisorption, atomic force microscopy and electron tomography, together with 3D reconstructions, permits us to conclude that the texture of the nanocomposites synthesized is a key parameter to control the photocatalytic activity. Specifically, we find that *n*-octylamine creates a mesoporous SiO_2 structure in which TiO_2 nanoparticles are embedded, and that TiO_2 and SiO_2 are present in separate domains in the bulk of the material. The mesoporous structure enhances the activity of the material by improving access to photoactive sites [3].

We optimize the effectiveness of these photocatalysts on stone by varying loading and particle size of TiO_2. We find that the integration of around 4% w/v content of TiO_2 nanoparticles into the SiO_2 network significantly improves their effectiveness due to a higher availability of photoactive sites. For a higher TiO_2 loading (10% w/v), photoactivity decreases because the porous volume is drastically reduced and subsequently, a more difficult access to photoactive sites is produced. Regarding to the particle size effect, we observe that larger and sharper TiO_2 nanoparticles enhance the photoactivity effect [4].

References

[1] L. Pinho, M. J. Mosquera, J Phys Chem C, 115 (2011) 22851.
[2] L. Pinho, F. Elhaddad, D. Facio, M.J. Mosquera, Applied Surf Sci 275 (2013) 389.
[3] L. Pinho, J.C. Hernández-Garrido, J.J. Calvino, M.J. Mosquera, Phys Chem Chem Phys 15 (2013) 2800.
[4] L. Pinho, M.J. Mosquera, Appl Cat B: Environmental 134-135 (2013) 205.

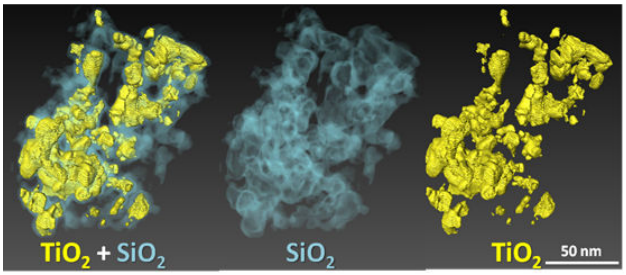

Nanopatterning on atomically thin TaS2 conducting layers

E. Pinilla-Cienfuegos, E. Coronado, A. Forment-Aliaga, E. Navarro-Moratalla and S. Tatay

elena.pinilla@uv.es

Instituto de Ciencia Molecular (ICMol). Universidad de Valencia. Catedrático José Beltrán Martínez nº 2, 46980, Paterna, Spain

Since the discovery of graphene, a lot of effort has been made to integrate atomically thin layers in the fabrication of ultrathin, transparent and flexible electronic devices [1]. The fundamental advance in this area has been feasible thanks to the micro-mechanical exfoliation methods. [2] In this context, 2D crystals such as transition metal dichalcogenides have shown excellent exfoliation mechanism and offer a wide variety of properties that could match or even outweigh the properties of graphene.

In this work we will first report on the controlled chemical modification of ultrathin TaS_2 layers by means of AFM Local Oxidation Nanolithography (AFM-LON). TaS_2 crystals were exfoliated by a novel technique based on the controlled application of shear forces between the 2D crystal and the substrate. Atomically thin TaS_2 layers, which are metallic at room temperature and superconducting at low temperatures, were conveniently nanopatterned with an unprecedented precision and reproducibility achieved thanks to the development of a new LON modality, named by us as static-tip LON. This possibility opens the door for the nanofabrication of devices and furthermore, for the fundamental study at low temperature of the physical consequences derived from the confinement at the nanoscale of this layered superconductor. It was also found unseen rippled mound morphologies in the oxidation process of TaS_2 flakes. This behaviour is novel and may be inferred from the peculiar Fermi surfaces of these bidimensional systems.

References

[1] K. S. Novoselov, A. K. Geim, S. V. Morozov, D. Jiang, Y. Zhang, S. V. Dubonos, I. V. Grigorieva, A. A. Firsov, Science, 306 (2004), 666.

[2] K. S. Novoselov, D. Jiang, F. Schedin, T. J. Booth, V. V. Khotkevich, S. V. Morozov, A. Geim, K. Proc. Natl. Acad. Sci. U.S.A., 102 (2005), 10451.

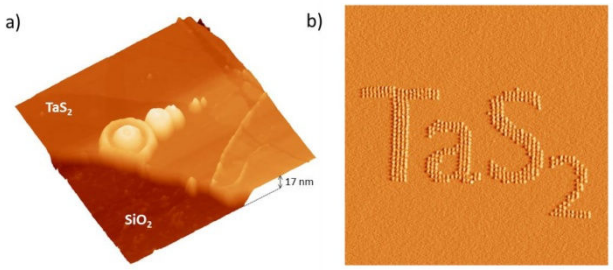

Figure 1. a) 3D representation of an array of 5 rippled mound patterns oxidized on a 17 nm thick flake. Image size: 2.5 µm x 2.5 µm. b) Static-tip AFM-LON performed on the surface of TaS_2 flake. Image size: 3.5 µm x 3.5 µm.

Charge Transport in single DNA-Based Molecules

Danny Porath

Institute of Chemistry and Center for Nanoscience and Nanotechnology,
The Hebrew University of Jerusalem, 91904 Israel

danny.porath@mail.huji.ac.il

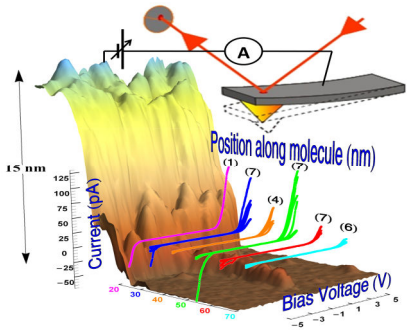

DNA has been in the center of the scientific research for decades. In particular, DNA was considered as one of the attractive candidates for molecular electronics and an excellent system to study charge transport in 1-D polymers. In spite of intensive efforts the results varied between experiments due to changes in the measured molecules, measurement methods and environment. Recently we were able to measure length dependent electrical transport in G4-DNA attached to a hard surface in a controlled way and get an insight to the mechanism governing the charge transport in these molecules. I will report on these results and on our measurement efforts with additional methods.

This work was supported by FOM and the EU FP7 program under the Grant Agreement ELFOS.

References

[1] "Direct measurement of electrical transport through DNA molecules", Danny Porath, Alexey Bezryadin,Simon de Vries and Cees Dekker, Nature 403, 635 (2000).

[2] "Charge Transport in DNA-based Devices", Danny Porath, Rosa Di Felice and Gianaurelio Cuniberti, Topics in Current Chemistry Vol. 237, pp. 183-228 Ed. Gary Shuster. Springer Verlag, 2004.

[3] "Direct Measurement of Electrical Transport Through Single DNA Molecules of Complex Sequence", Hezy Cohen, Claude Nogues, Ron Naaman and Danny Porath, PNAS 102, 11589 (2005).

[4] "Long Monomolecular G4-DNA Nanowires", Alexander Kotlyar, Nataly Borovok, Tatiana Molotsky, Hezy Cohen, Errez Shapir and Danny Porath, Advanced Materials 17, 1901 (2005).

[5] "Electrical characterization of self-assembled single- and double-stranded DNA monolayers using conductive AFM", Hezy Cohen et al., Faraday Discussions 131, 367 (2006).

[6] "High-Resolution STM Imaging of Novel Poly(G)-Poly(C)DNA Molecules", Errez Shapir, Hezy Cohen, Natalia Borovok, Alexander B. Kotlyar and Danny Porath, J. Phys. Chem. B 110, 4430 (2006).

[7] "Polarizability of G4-DNA Observed by Electrostatic Force Microscopy Measurements", Hezy Cohen et al., Nano Letters 7(4), 981 (2007).

[8] "Electronic structure of single DNA molecules resolved by transverse scanning tunneling spectroscopy", Errez Shapir et al., Nature Materials 7, 68 (2008).

[9] "A DNA sequence scanned", Danny Porath, Nature Nanotechnology 4, 476 (2009).

[10] "The Electronic Structure of G4-DNA by Scanning Tunneling Spectroscopy", Errez Shapir, et.al., J. Phys. Chem. C 114, 22079 (2010).

[11] "Energy gap reduction in DNA by complexation with metal ions", Errez Shapir, G. Brancolini, Tatiana Molotsky, Alexander B. Kotlyar, Rosa Di Felice, and Danny Porath, Advanced Maerials 23, 4290 (2011).

[12] "Quasi 3D imaging of DNA-gold nanoparticle tetrahedral structures", Avigail Stern, Dvir Rotem, Inna Popov and Danny Porath, J. Phys. Cond. Mat. 24, 164203 (2012).

Engineered nanoparticles for improved neuropeptide biomedical applications: immunotargeting and control of autoinmune diseases

David Pozo

david.pozo@cabimer.es

University of Seville-Andalusian Center for Molecular Biology and Regenerative Medicine (CABIMER), Seville, Spain
Andalusian Center for Nanomedicine and Biotechnology (BIONAND), Malaga, Spain

Engineering nanoconjugates constitute an extensive field of research due to its translational potential for biomedical applications. These conceptual advances can represent a lifeline for some of the limitations shown by translational neuropeptide research despite overwhelming evidence for key physiological roles. A neuropeptide is a small protein-like molecule -regardless of whether it is secreted by neurons or nonneural cells that expresses the same genetic information and undergoes identical processes of synthesis and transport, and binds to similar families of receptors, in order to act on specific target cells. Among these neuropeptides, sustained interest in therapeutic applications of vasoactive intestinal peptide (VIP) include areas related to neuroprotection, inflammation and autoimmune disorders. In this keynote lecture, we will summarized and update our ongoing research effort related to nano-applications that use VIP as surface ligands in order to induce antigen-specific regulatory T cells, increase its effectiveness, and achieve a smart manipulation of the immune system. In this sense, special attention will be paid to the interaction of nanoparticles with immunocompetent cells.

References

[1] Cejudo-Guillén M, Ramiro-Gutiérrez ML, Labrador-Garrido A, Díaz-Cuenca A, Pozo D. Acta Biomater. 2012. 8:4295-303.
[2] Klippstein R, Pozo D. Nanomedicine NBM. 2010. 6:523-9.
[3] Fernandez-Montesinos R, Castillo M, Klippstein R, Gonzalez-Rey E, Mejias JA, Zaderenko AP, Pozo D. Nanomedicine. 2009. 4:919-30.
[4] Pozo D, Anderson P, Gonzalez-Rey E. J Immunol. 2009; 183:4346-59.
[5] Castillo PM, Herrera JL, Fernandez-Montesinos R, Caro C, Zaderenko AP, Mejías JA, Pozo D. Nanomedicine. 2008. 3:627-35.

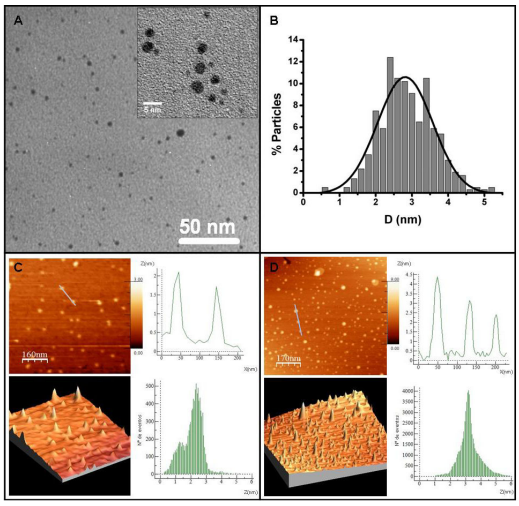

Figure 1. Characterization of VIP-gold nanoparticles. (A) TEM image of AuNPs, scale bar; 50 nm. The inset shows a higher magnification image, scale bar; 5 nm. (B) Statistical analysis of colloid diameter, as evaluated from TEM image. (C) TM-AFM image of tiopronin AuNPs and (D) TM-AFM image of VIP AuNPs.

Fabrication of robust spin-OLEDs: Towards the control of emitted light with an external magnetic field

H. Prima-Garcia
E. Coronado and
J.P. Prieto-Ruiz

Helena.prima@uv.es

Instituto de Ciencia Molecular, Universidad de Valencia,
Catedrático José Beltrán 2, 46980 Paterna (Valencia)

The fabrication of a spin-polarized electroluminescent device has been one of the major topics of organic spintronics in the last years. Still, only one report has been recently published which is based on the fabrication of an organic light emitting diode (OLED) with ferromagnetic electrodes [1]. The electrons and holes form two types of excitons (singlet and triplet) in a ratio 1:3. As the electroluminescence arises from the singlet excitons it is expected to control the emitted light by modulating the singlet:triplet ratio through the application of a magnetic field on the device [2-3].

In this contribution we present an approach based on the use of a HyLED (Hybrid Ligth Emitting Diode) structure which works simultaneously as a spin valve and an electroluminescent device at low temperatures. The main difference respect to OLED structures is the use of metallic oxides as electron injectors. This responds to the need of using an electrode which works as a cathode with a low work function [4]. In this way it is avoided the use of reactive metals giving more stability to the HyLED configuration respect to OLED one. Moreover this kind of configuration exhibits lower working voltages being energetically more efficient. We have fabricated a HyLED structure using Fe or LSMO and Co as ferromagnetic electrodes in order to inject spin-polarized carriers in the active medium [5]. This new approach provides a real alternative for the fabrication of organic luminescent device with light emission modulated with external magnetic fields.

References

[1] T. Nguyen, E. Ehrenfreud, Z. Valy Vardeny, Science, 2012, 337, 204-208.

[2] G. Salis et al., Physical Review B, 70, 085203 (2004).

[3] J. Camarero, E. Coronado, J. Mater. Chem. 2009, 19, 1678–1684.

[4] M. Sessolo, H.J. Bolink, 2011, Advanced Materials, 23, 1829-1845.

[5] "Opto-spintronic device and its fabrication method".E.Coronado Miralles, H. Prima García, J.P. Prieto Ruiz. Spanish National Patent. Ref. 201300083, 2013, Spanish Office of Patents and Trademarks. Ministry of Industry, Energy and Tourism.

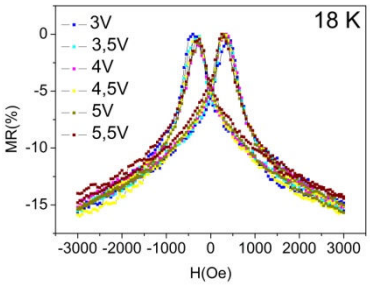

Figure 1. MR loops of the LSMO-Co device at 18 K for high voltages.

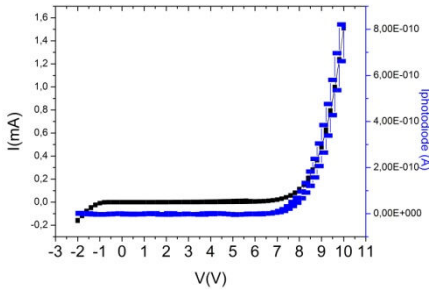

Figure 2. IVL characteristics of the LSMO-Co device measured at 13 K.

Towards electroactive carbon nanoforms: chemical modification and propeties

Laura Rodríguez-Pérez[1] Raúl García[1], Jaime Mateos-Gil[1], Mª Ángeles Herranz[1] and Nazario Martín[1,2]

laura.rodriguez.perez@quim.ucm.es

[1] Organic Molecular Materials Group, Organic Chemistry Department, Complutense University of Madrid, 28040 Madrid, Spain.
[2] IMDEA Nanoscience, Cantoblanco Campus, 28049 Madrid, Spain.

Since the discovery of fullerenes, the hollow cylindrical multiple and single wall carbon nanotubes (SWCNTs) and, more recently, the one atom thick layer sheet of graphite known as graphene, the research on different carbon nanoforms has attracted the attention of the scientific community in all fields and has been in continuous evolution. Among carbon nanostructures, SWCNTs and graphene present outstanding mechanical and electronic properties and their versatility as integrative building blocks in electron-donor-acceptor structures is an important issue to be considered for the preparation of optoelectronic devices.[1]

However, for pursuing practical applications, one major drawback is the difficult processability and/or dispersibility of these nanoforms of carbon, which decrease the overall yields of usable material and interfere with most of their desired properties. So, the chemical functionalization is the required first step in order to have materials easy to be handled. Two strategies are generally used: i) the supramolecular modification relies on interactions that are affected by many parameters (concentration, solvent,..) but has the advantage of preserving the electronic structure. In contrast,.ii) the covalent modification of SWCNTs and graphene can alter their inherent properties if it is not controlled, but the improving in the stability of the nanoconjugates makes it suitable for practical applications.[2]

Carbon nanostructures are good electron-acceptor, which have been combined with donors of different nature. In this regard, the remarkable gain of aromaticity and planarity that π-extended TTF (exTTF) derivatives reveals upon oxidation renders them an interesting donor unit that has been extensively used in the preparation of different donor-acceptor ensembles.[3] Interestingly, the electron-donor character of SWCNTs and graphene has been scarcely explored. Good electron-acceptor systems are those based on tetracyanoanthraquinodimethane derivatives (TCAQ), which have been investigated with respect to their charge-transfer interactions with conjugated polymers and fullerenes.[4]

In the present work, we will present our recent results on the covalent and supramolecular functionalization of SWCNTs and graphene with exTTF electron-donors or TCAQ electron-acceptor moieties (Figure 1). The synthesis and characterization of the new nanostructures will be discussed in detail.

References

[1] a) P. Singh, S. Campidelli, S. Giordani, D. Bonifazi, A. Bianco, M. Prato, Chem. Soc. Rev. 38, (2009), 2214. b) V. Sgobba, D. M. Guldi, Chem. Soc. Rev. 38, (2009), 165. c) J. Malig, N. Jux, D. M. Guldi, Acc. Chem. Res., 46, (2013), 53.

[2] L. Rodríguez-Pérez, M. A. Herranz, N. Martín, Chem. Commun. 49, (2013), 3721.

[3] C. Romero-Nieto, R. García, M. A. Herranz, C. Ehli, M. Ruppert, A. Hirsch, D. M. Guldi, N. Martín, J. Am. Chem. Soc. 134, (2012) 9183. F.G. Brunetti, J.L. Lopez, C. Atienza, N. Martin, J. Mater. Chem. 22, (2012), 4188.

[4] J. Santos, E.M. Pérez, B.M. Illescas, N. Martín, Chem. As. J. 6, (2011), 1848.

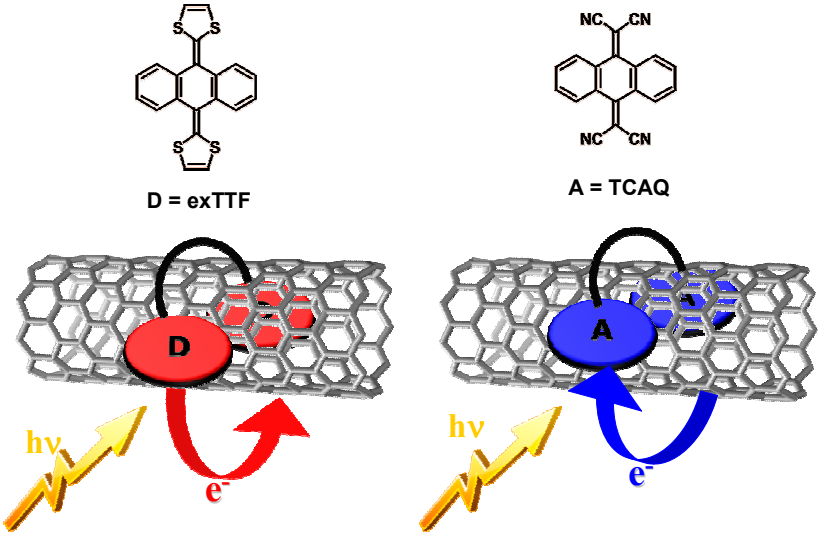

Figure 1. Supramolecular modification of SWCNTs with electron-donor (exTTF) and electron-acceptor (TCAQ) molecules.

Recent developments on functional nanoarchitectures based on clay silicates: from supported graphenes to bionanocomposites

Eduardo Ruiz-Hitzky

eduardo@icmm.csic.es

Instituto de Ciencia de Materiales de Madrid (ICMM), CSIC,
c/ Sor Juana Inés de la Cruz, 3, Cantoblanco, 28049 Madrid, Spain

The synthesis of nanoarchitectures based on silica and silicates belonging to the clay family, is an achievement emerged in recent years that procures functional materials of interest in various advanced applications [1]. Layered and fibrous clays, i.e. smectites and sepiolite, can be regarded as extremely versatile silicates presented as nanosized solids with structural and textural features that allow their assembling as building units with diverse organic or inorganic components. Bottom-up approaches involving diverse type of clay particles and components of different origin able to introduce a modulated functionality have been used for that assembly [2]. In this way alkoxides, nanoparticles and biopolymers are typical examples of those components able to give rise to complex nanostructured systems as diverse as magnetic nanoplatforms, ultra light-weigh monolits, selective heterogeneous catalysts or active phases of chemical sensors.

This communication will illustrate several examples of clay-based nanoarchitectures. The first one will focus on the preparation of conductive supported graphenes from natural resources, such as sucrose or gelatin, used as precursors in this green way synthetic approach of graphenes [3]. The resulting carbon-clay nanocomposite materials exhibit electrical conductivity, inherent to the in situ synthesized graphenes, together with the properties of the clay silicate [e.g., ion-exchange ability; elevated porosity & specific surface area] which allow their applications as components of electrochemical devices (supercapacitors, lithium-batteries and ion-sensors). The second example will introduce superparamagnetic adsorbents prepared by infiltration of clays with ferrofluids based on magnetite nanoparticles that lead to nanostructured materials of interest for the easy uptake of pollutants in water, including pesticides and radionuclides [4]. The third example will describe inorganic-organic biohybrid systems consisting of layered or fibrous clay particles assembled to biopolymers and other components of biological origin [5,6]. These biohybrids represent an interphase between living bodies and inorganic silicates that may give rise to materials provided of bioactivity introduced by the incorporated bio-components.

Acknowledgements

Financial support from CICYT (Spain, MAT2012-31759) and COST (EU, MP1202) is gratefully acknowledged

References

[1] K. Ariga (Editor), Manipulation of Nanoscale Materials: An Introduction to Nanoarchitectonics, Royal Society of Chemistry, Cambridge, UK (2012).

[2] E. Ruiz-Hitzky, P. Aranda, M. Darder, M. Ogawa, Chem. Soc. Rev. 40, (2011) 801.

[3] E. Ruiz-Hitzky, M. Darder, F. M. Fernandes, E. Zatile, F. J. Palomares and P. Aranda, Adv. Mater. 23 (2011) 5250.

[4] Y. González-Alfaro, P. Aranda, F.M. Fernandes, B. Wicklein, M. Darder and E. Ruiz-Hitzky, Adv. Mater. 23 (2011) 5224.

[5] E. Ruiz-Hitzky, K. Ariga, and Y. Lvov (Editors). Bio-inorganic Hybrid Nanomaterials: Strategies, Syntheses, Characterization and Applications, Wiley-VCH, Weinheim (2008).

[6] E. Ruiz-Hitzky, M. Darder, P. Aranda, K. Ariga, Adv Mater. 22, (2010) 323.

Cleanup: new heterogeneous catalysts based on a new functionallization process of porous material with supercritical CO_2

Jordi Rull
Guillaume Nonglaton and Caroline Marchi-Delapierre

Jordi.RULL-BARRULL@cea.fr

CEA-Grenoble LETI/LCBM, Bat. 42, 17 rue des Martyrs, Grenoble, France

Supercritical carbon dioxide ($scCO_2$) is an attractive solvent alternative for a variety of chemical and industrial processes, especially because it is plentiful and inexpensive. [1]

The advantages of using $scCO_2$ have been numerous, like an excellent solvent for alkoxysilanes. With a density close to the liquid, but a very low viscosity and a surface energy close to zero, the $scCO_2$ easily diffuses into porous materials. [2] In addition, the diffusion coefficients and high self-diffusion allow very rapid transfer of reagents. [3] The other advantage is that treatment with $scCO_2$ is a process called soft and considered as a method of green chemistry. [4] $ScCO_2$ is also non- toxic, non-flammable, easily recyclable and chemically neutral. Finally, after the rinsing step, the $scCO_2$ will simply evaporate thus avoiding the inconvenience of drying, including treatment degradation or nanostructures.[5] The supercritical phase deposition (SFD) is mainly used for the preparation of chromatographic stationary phases [6] including the functionalization of porous silica beads with different fluoroalkyl- or mercapto-silanes. [7]

In this project we have synthetized two new catalytic systems, 1 and 2. Both catalytic systems have been prepared from a new grafting method in supercritical CO_2 path of bio-inspired iron based catalysts [8] on porous substrates, such as silica beads and carbon nanotubes, in order to activate oxygen as the oxidant.

We fully studied the optimum SFD for grafting a monolayer of new synthesized ligands into silica beads and carbon nanotubes and the coordination with iron species.

These catalysts have been tested in the oxygen degradation of naphtlene and promotion of methane, giving excellent results. Work is in progress to give more applications.

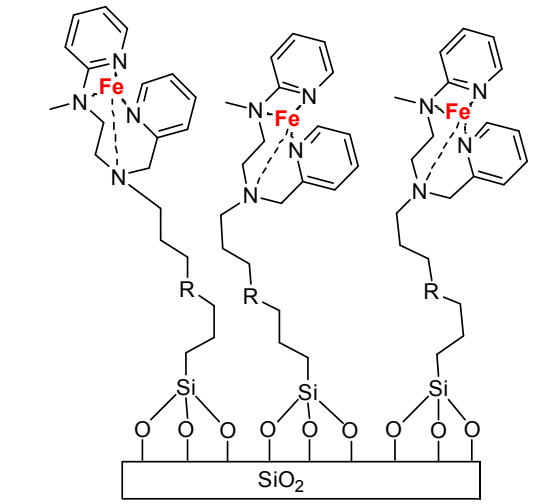

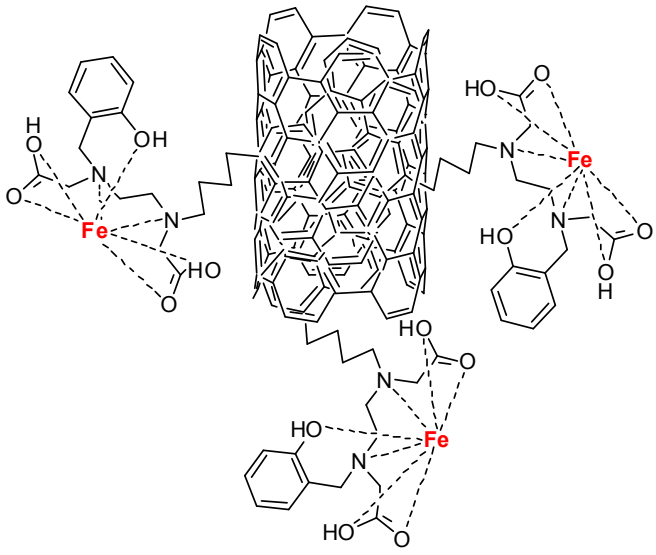

References

[1] R. Elghanian, J. J. Storhoff, R. C. Mucic, R. L. Letsinger and C. A. Mirkin, Selective colorimetric detection of polynucleotides based on the distance-dependent optical properties of gold nanoparticles, Science, 5329, (1997) 1078-1081

[2] W. P. Hall, S. N. Ngatia and R. P. Van Duyne, LSPR Biosensor Signal Enhancement Using Nanoparticle-Antibody Conjugates, Journal of Physical Chemistry C, 5, (2011) 1410-1414

[3] H. X. Li and L. Rothberg, Colorimetric detection of DNA sequences based on electrostatic interactions with unmodified gold nanoparticles, Proceedings of the National Academy of Sciences of the United States of America, 39, (2004) 14036-14039

[4] J. R. Waldeisen, T. Wang, B. M. Ross and L. P. Lee, Disassembly of a Core-Satellite Nanoassembled Substrate for Colorimetric Biomolecular Detection, Acs Nano, 7, (2011) 5383-5389

[5] M. C. Daniel and D. Astruc, Gold nanoparticles: Assembly, supramolecular chemistry, quantum-size-related properties, and applications toward biology, catalysis, and nanotechnology, Chemical Reviews, 1, (2004) 293-346

[6] L. Guerrini and D. Graham, Molecularly-mediated assemblies of plasmonic nanoparticles for Surface-Enhanced Raman Spectroscopy applications, Chemical Society Reviews, 21, (2012) 7085-7107

Mask effect: an actor in graphene oxide size dependent modulation of cellular activity and internalization

Julie Russier[1], Emanuele Treossi[2], Alessia Scarsi[3], Francesco Perrozzi[4], Hélène Dumortier[1], Luca Ottaviano[4], Moreno Meneghetti[3], Vincenzo Palermo[2] and Alberto Bianco[1]

j.russier@ibmc-cnrs.unistra.fr

[1] CNRS, Institut de Biologie Moléculaire et Cellulaire, Immunopathologie et Chimie Thérapeutique/Laboratory of Excellence Medalis, Strasbourg, France.
[2] CNR-ISOF, Bologna, Italy
[3] Dipartimento di Scienze Chimiche, Università di Padova, Padova, Italy
[4] Dipartimento di Fisica, Università dell'Aquila, L'Aquila, Italy

Graphene oxide (GO) is one of the most studied graphene-based nanomaterial, due to its extraordinary chemical and physical properties [1,2] and especially because of its good dispersibility in aqueous media [3]. Indeed, GO gathered an ever-growing interest in fields such as electronics, optics, energy, catalysis and biomedicine in the last few years [4-6]. As for other nanomaterials, this intense research activity on its potential applications imperatively needs to be associated to the assessment of its safety profile.
In particular, not much is known about the possible impact of the lateral dimensions of the GO sheets on their effects towards biological substrates in vitro, especially on human primary cells. In an attempt to address this issue, we evaluated whether GO samples constituted of large, small and very small flakes would differently affect primary human or murine macrophages. Our data revealed that GO sheet size had a significant impact on different cellular parameters (i.e. cellular viability, ROS generation, and cellular activation). Indeed, the more lateral dimensions of GO were reduced, the higher were the cellular internalization and the effects on cells. Interestingly, it was also possible to observe that these effects were more or less pronounced based on the cellular type as human cells resulted less sensitive and less responsive to the GO samples in comparison to murine macrophages in our conditions. Our study also suggested a possible correlation between the particular interaction of GO with the cellular membrane, surrounding and somehow masking it, with the subsequent internalization of graphene sheets and the following impact on cellular parameters. This intrinsic characteristic of GO, and in particular the mask effect, could be further developed and tuned to modulate or deplete cells. Together with the possibility of targeting specific cells via functionalization, this approach could open the way for new graphene-based therapeutic applications.

References

[1] Novoselov KS, Fal'ko VI, Colombo L, Gellert PR, Schwab MG, Kim K, Nature, 490 (2012) 192.
[2] Park S, Ruoff RS, Nat Nanotechnol, 4 (2009) 217.
[3] Park S, An J, Jung I, Piner RD, An SJ, Li X, Velamakanni A, Ruoff RS, Nano Lett, 9 (2009) 1593.
[4] Dreyer DR, Park S, Bielawski CW, Ruoff RS, Chem Soc Rev, 39 (2010) 228.
[5] Kim H, Namgung R, Singha K, Oh IK, Kim WJ, Bioconjug Chem, 22 (2011) 2558.
[6] Yang K, Wan J, Zhang S, Tian B, Zhang Y, Liu Z, Biomaterials, 33 (2012) 2206.

Interfacial electron transfer kinetics at single CCVD multiwalled carbon nanotubes

Jean-Paul Salvetat,
Paul Vincent and
Jean-Pierre Aimé

salvetat@crpp-bordeaux.cnrs.fr

CRPP, CBMN, France

The understanding of charge transfer processes between nanomaterials and solvated molecules is a long-standing goal that concerns many applications, as diverse as biosensing, catalysis, energy production and storage, etc. Despite the enormous amount of data on electrochemistry with CCVD multiwalled carbon nanotubes, there remains a controversy about the origin of mechanisms involved in the charge transfer kinetics. Dealing properly with this problem necessitates controlling the geometry of the device under test to analyze the quasi-reversible regime and discriminate between kinetic and diffusion effects in the steady state [1]. The faster the reaction, the smaller the device surface.

We report here on new experiments of redox outer-sphere electron transfer between single multiwalled carbon nanotubes and two species, 1-1'-ferrocene dimethanol (FeDM) and Ru(NH3)63+, in aqueous solutions. To minimize contamination effects, we have elaborated a new process where single MWCNTs are connected to etched gold tips by fast electrical breakdown, the adhesion being ensured by van der Walls forces only (fig. 1). After attachment of the MWCNT, the electrode is mounted on a micromanipulation stage under optical control. Cyclic voltammograms and chronoamperometry curves were recorded at various immersion depths in a home-made liquid cell. MWCNTs show quasi-reversible quasi-steady-state reactions with FeDM and Ru(NH3)6+, and kinetic parameters are estimated using simple geometrical models. CVs were analyzed in the framework of the Butler-Volmer kinetic equation.

$$i = \frac{i_{\lim}}{\left(1 + e^{\frac{F(E-E^{0'})}{RT}} + \frac{1}{\Lambda^*} e^{-\frac{F(1-\alpha)(E-E^{0'})}{RT}}\right)} \qquad (1)$$

where i_{lim} is the diffusion limited current, which is proportional to the area of active sites, F the Faraday constant, R the molar gas constant, $E^{0'}$ the formal potential of the redox-couple, α the transfer coefficient, and Δ* the dimensionless heterogeneous rate constant that depends on geometry and k^0[3]. It appears that MWCNTs behave as partially blocked microcylinders, with moderate heterogeneous rate constant ($<k^0>$=0.2 cm/s). An anomalous transfer coefficient (>0.7) is measured systematically (fig. 2). We discuss the origin of this behavior in the framework of microscopic models adapted to nanometer-sized electrodes [3].

References

[1] Bond AM, Oldham KB, Zoski CG, Anal. Chim. Acta 216 (1989) 177.
[2] Amatore CA, Deakin MR, Wightman RM, J. Electroanal. Chem. 206 (1986) 23.
[3] Liu Y and Chen S J., Phys. Chem. C 116 (2012) 13594.

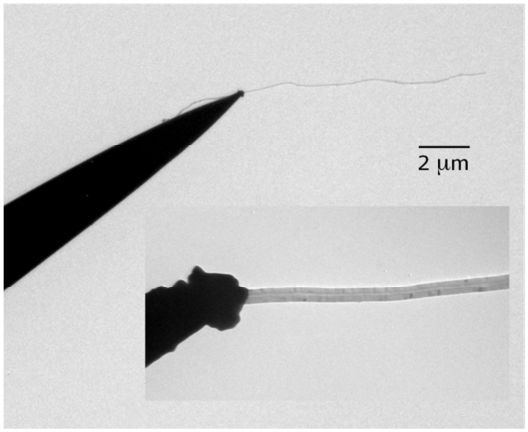

Figure 1. TEM image of a 70-nm diameter MWCNT connected to an etched gold tip.

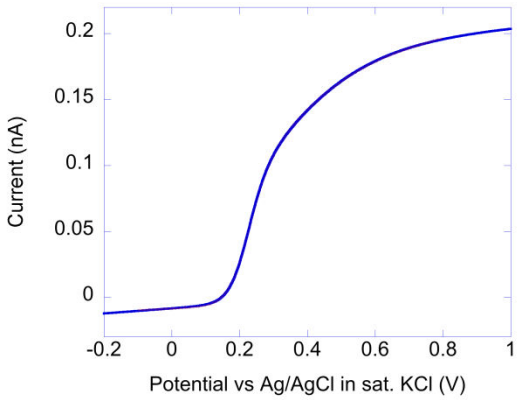

Figure 2. Cyclic voltammogram of a 60-nm MWCNT, immersion depth 4 µm, in 1mM FeDM + 0.5 M KCl. Scan rate 0.1 V/s. Data were fitted by Butler-Volmer equation (blue line masks data points). The rate constant was 0.4 cm/s and transfer coefficient 0.84.

Gradient and uneven nano-patterns distributions for cell adhesion and differentiation studies

A. Lagunas and **J. Samitier**

Institut de Bioenginyeria de Catalunya
Baldiri Reixac, 10-12, 08028 Barcelona, Spain

Cell adhesion onto bioengineered surfaces is affected by a number of variables, including the former substrate derivatisation process. Cells can sense and respond to their immediate surroundings. The information arising from this environmental sensing is integrated into the cell machinery through receptor proteins located at the cell membrane. We have studied the correlation between cell adhesion and cell–adhesive ligand surface gradient concentration. Similar procedure has been used to systematic *in vitro* screening of the effects of different concentrations of immobilized Bone Morphogenetic Protein (BMP-2). For this purpose, gradient surfaces were created on poly(methyl methacrylate) substrates by continuous hydrolysis and were then grafted with biotin-PEG-RGD molecules or BMP-2 molecules. In addition, nanopatterning of arginine-glycine-aspartic acid (RGD)-tailored dendrimers has been used to obtain uneven distributions of cell-adhesive motives. Cell adhesion studies reveal that first adhesion events are dictated by the surface layout and reinforced by a narrow interligand spacing and high local ligand densities.. This is a simple, all-organic nano-patterning approach that can be easily scaled up to large surface areas. The biocompatible and biodegradable nature of dendrimers also opens for biomaterial applications.

Multitechnique Characterization of Atomically Precise Graphene Nanoribbons

Carlos Sanchez[1]
Juan R. Sanchez-Valencia[1], Jinming Cai[1], Hajo Söde[1], Pascal Ruffieux[1], Richard Denk[2], Michael Hohage[2], Peter Zeppenfeld[2], Xiliang Feng[3], Klaus Müllen[3], and Roman Fasel[1]

carlos.sanchez@empa.ch

[1] Empa, Swiss Federal Laboratories for Materials Science and Technology, nanotech@surfaces Laboratory, Überlandstrasse 129, 8600 Dübendorf, Switzerland.
[2] Institute of Experimental Physics, Johannes Kepler University Linz, Altenbergerstr. 69, 4040 Linz, Austria
[3] Max Planck Institute for Polymer Research, Ackermannweg 10, 55124 Mainz, Germany

Graphene nanoribbons (GNRs) – narrow stripes of graphene [1] – are predicted to be semiconductors with an electronic band gap that sensitively depends on the ribbon width [2]. The electronic properties of GNRs also depend strongly on the arrangement of the carbon atoms in the ribbon structure. For armchair GNRs (AGNRs) the band gap is inversely proportional to the ribbon width. On the other hand, zigzag GNRs (ZGNRs) are predicted to present spin polarized edges. Their gap opens thanks to an unusual antiferromagnetic coupling between the magnetic moments at opposite edge carbon atoms.

These versatile characteristics allow the design of GNR-based structures with widely tunable electronic properties, but require highest (i.e. atomic) structural precision. With our recently developed bottom-up approach the fabrication of atomically precise AGNRs [3] can be achieved using specifically designed precursor monomers. The monomers are sublimed in ultrahigh vacuum (UHV) and deposited onto metallic substrates such as Au or Ag. Substrate catalyzed dehalogenation of the monomers induces the formation of linear polymers that are subsequently cyclodehydrogenated to form the desired GNRs. With this approach, we have fabricated ultra-narrow GNRs and related graphene nanostructures for experimental investigations of their structural and electronic properties [3-10]. For the case of N=7 AGNRs (7-AGNRs), the electronic band gap and dispersion of the occupied electronic bands have been determined with high precision [9].

In this talk, we will show how different GNRs have been characterized following a multitechnique approach. The desired atomic precision obtained by this surface-assisted GNR fabrication method has been demonstrated by high-resolution Scanning Tunneling Microscopy (STM). Electronic properties like band dispersion and gap of GNRs have been determined by means of Scanning Tunneling Spectroscopy (STS), Angle Resolved Ultraviolet Photoemission Spectroscopy (ARUPS) and X-Ray Photoelectron Spectroscopy (XPS). Optical characterization of GNRs has been performed by means of in-situ Reflectance Difference Spectroscopy (RDS) [11]. Finally, we have characterized the vibrational properties of the GNRs by Raman spectroscopy, obtaining valuable information about the ribbon nanostructure

References

[1] A. K. Geim, Science, 324 (2009) 1530.
[2] V. Barone et al., Nano Lett., 6 (2006) 2748.
[3] J. Cai et al., Nature, 466 (2010) 470.
[4] M. Bieri et al., Chem. Commun., (2009) 6919.
[5] M. Bieri et al., J. Am. Chem. Soc., 132 (2010) 16669.
[6] S. Blankenburg et al., Small, 6 (2010) 2266.
[7] M. Treier et al., Nature Chemistry, 3 (2011) 61.
[8] S. Blankenburg et al., ACS Nano, 6 (2012) 2020.
[9] P. Ruffieux et al., ACS Nano, 6 (2012) 6930.
[10] L. Talirz et al. JACS, 135 (2013) 2060.
[11] M. Hohage et al. Appl. Phys. A, 80 (2005) 1005.

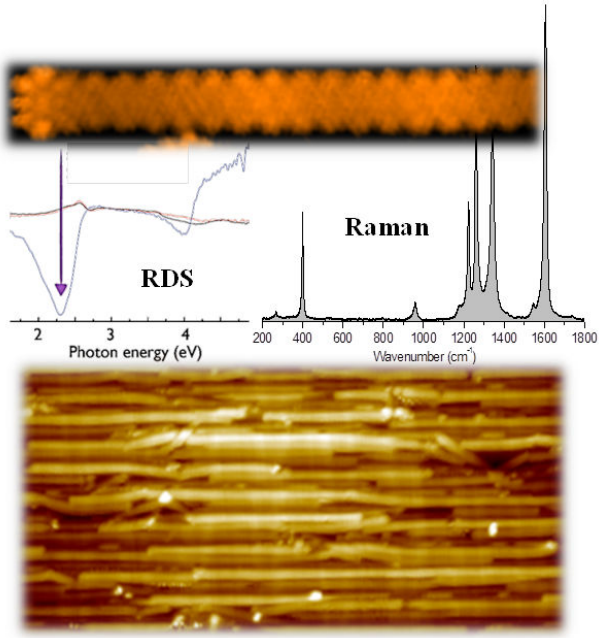

Figure 1. STM pictures of a 7-AGNR with one visible terminus (top) and aligned ribbons on the Au(788) surface (bottom). RDS (middle, left) reveals characteristic absorption features that are directly related to the electronic band structure of 7-AGNRs. Raman spectroscopy (middle, right) reveals the expected intensity distribution on G- and D-modes and the width-dependent characteristic radial breathing like mode (RBLM) at ~400 cm^{-1}.

Manipulating and visualising the local density of states at the nanoscale

Riccardo Sapienza

Department of Physics, Kings College, London, Strand, London WC2R 2LS, UK

Numerous optical technologies and quantum optical devices rely on the controlled coupling of a local emitter to its photonic environment, which is governed by the local density of optical states (LDOS). Light spontaneous emission, absorption and scattering are all related to the LDOS that can be engineered in dielectric and metallic nano structures. I will present how a nano-sized light probe can illuminate complex materials and shed light on their optical properties and modes.

I will report nanoscale mapping of the local density of states by cathodoluminescence microscopy, a combination of electron-beam scanning and optical spectroscopy [1]; it relies on scanning a transient dipolar emitter induced by electron beam bombardment with respect to its photonic environment while measuring the total emitted power. Each individual electron traversing the photonic structure generates a nanoscale transient dipole by the accelerated charge that we exploit as a local probe of the LDOS. With unprecedented resolution (~10 nm) we image localized photonics crystal cavity modes in a nanostructured silicon nitride membrane, over the visible spectrum into the near-IR. We identify individual cavity modes that are spatially different and we map their LDOS. Also, our measurements reveal extended Bloch modes that are delocalized over the crystal and periodically modulated. Moreover, by momentum spectroscopy, we resolve the angular emission pattern of the radiation emitted, which exhibits complex diffraction patterns [1].

In addition, we image the LDOS for random gold films as their topology approaches percolation. Thanks to the high-resolution imaging we are able to observe single-particle resonances localized at the gold particle transforming into extended modes when the cluster merge into a network. We report a study of the rich spectral dynamics of the localhot-spot of the LDOS through all the visible range. We also observe a long-tailed distribution of the LDOS at percolation.

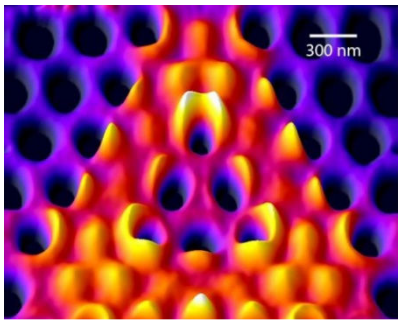

Figure 1. Experimental deep-subwavelength imaging of the optical local density of state in a nanostructured photonic membrane.

I will also discuss our recent studies of fluorescence from a nano-sized emitter embedded in complex photonic media, such as photonic crystals and random powders. By fluorescence dynamics we measure LDOS distributions in 3D disordered dielectric powders. We observe a surprisingly long-tailed distribution of the LDOS with Purcell factor up to ~10 [2]. I will discuss how our experimental results fed the ongoing discussion on the dependence of the C0 correlation function on macroscopic disorder parameters

References

[1] R. Sapienza, et al. Deep-subwavelength imaging of the modal dispersion of light, Nature Materials 11, 781–787 (2012).

[2] R. Sapienza, et al. Long-Tail Statistics of the Purcell Factor in Disordered Media Driven by Near-Field Interactions, Phys. Rev. Lett. 106, 163902 (2011).

Disordered photonic materials derived from three dimensional hyper uniform point patterns

Frank Scheffold

Frank.Scheffold@unifr.ch

Physics Department and Fribourg Center for Nanomaterials
Soft Matter and Photonics Group
University of Fribourg- Perolles
CH-1700 Fribourg (Switzerland)

We discuss the mesoscale fabrication and characterization of (polymeric) templates for isotropic photonic materials derived from hyperuniform point patterns using direct laser writing in a polymer photoresist. We study experimentally the microscopic structure by electron microscopy and small angle light scattering. Reducing the refractive index mismatch by liquid infiltration we find good agreement between the scattering data and numerical calculations in the single scattering limit. We are able to fabricate templates with the typical structural length scale of the seed pattern from a = 3.3 micron to a = 2micron, fairly close to the technologically relevant fiber-optic communications wavelength range around 1.5 micrometer. We have employed scanning electron microscopy coupled with focused ion beam cutting to look inside the bulk of the samples of different height. Moreover we demonstrate the use of laser scanning confocal microscopy to assess the real space structure of the samples fabricated by direct laser writing. We address in detail question about scalability, finite size effects and geometrical distortions. We also study the effect of the lithographic voxel shape, that is the ellipsoidal shape of the laser pen used in the fabrication process. To this end we employ detailed numerical modelling of the scattering function using a discrete dipole approximation scheme.

References

[1] J. Haberko, N. Muller and F. Scheffold, Direct laser writing of three dimensional network structures as templates for disordered photonic materials, submitted to Phys. Rev. A

[2] J. Haberko and F. Scheffold, Fabrication of three-dimensional disordered photonic materials from hyperuniform point patterns, Optics Express, Vol. 21, Issue 1, pp. 1057-1065 (2013)

Graphene Technology Platform at BASF

Matthias Schwab

matthias.schwab@basf.com

BASF SE
GVM/I – J 550
Carl-Bosch-Straße 38, D-67056 Ludwigshafen Germany
Phone: +49-(0)621-6022986

Graphene as an emerging material has recently spurred the interest of scientific research both in academia and industry. At BASF graphene and graphene materials are currently being studied for several potential fields of application. We have set up a graphene technology platform aiming at the systematic investigation of this new carbon material fabricated either by top-down or bottom-up procedures. Owing to its appealing electrical conductivity, graphene can be used for conductive formulations and coatings as well as for polymer composite materials with antistatic properties. Also, graphene may serve as a new carbon material thus replacing or complementing traditional carbon black additives in lithium-ion batteries as well as activated carbons in supercapacitor devices. It is also intended to evaluate graphene-based transparent conductive layers for their use in displays, organic solar cells and organic light emitting diodes. On a longer perspective the semi-conducting properties of graphene nanoribbons fabricated from chemical bottom-up approaches shall be explored. The talk will focus on the recent activities of BASF in the field of graphene and provide an evaluation of this promising material from an industrial point of view.

Graphene: new venues for spintronics

P. Seneor[1]
B. Dlubak[1,3], M.-B. Martin[1], H. Yang[1], R. Weatherup[3], M. Sprinkle[2], B. Servet[1], S. Xavier[1], C. Berger[2], W. de Heer[2], S. Hoffman[3], J. Robertson[3], C. Deranlot[1], R. Mattana[1], A. Anane[1], F. Petroff[1] and A. Fert[1]

[1] Unité Mixte de Physique CNRS/Thales, Palaiseau, France, & Université Paris-Sud, Orsay, France
[2] GeorgiaTech, Atlanta/Institut Néel and
[3] University of Cambridge

Spintronics is a paradigm focusing on spin as the information vector in fast and ultra-low-power non volatile devices such as the new STT-MRAM. Beyond its widely distributed application in data storage it aims at providing more complex architectures and a powerful beyond CMOS solution. The recent discovery of graphene has opened novel exciting opportunities in terms of functionalities and performances for spintronics devices. We will present experimental results on the impact and potential of graphene for spintronics. We will show that unprecedented highly efficient spin information transport can occur in graphene [1] leading to large spin signals and macroscopic spin diffusion lengths (~100 microns), a key enabler for the advent of envisioned beyond-CMOS spin-based logic architectures. Furthermore, we will show that a thin graphene passivation layer can prevent the oxidation of a ferromagnet, enabling its use in novel humide/ambient low-cost processes for spintronics devices, while keeping its highly surface sensitive spin current polarizer/analyzer behavior and adding new enhanced spin filtering property[2]. These different experiments unveil promising uses of graphene for spintronics.

References

[1] B. Dlubak et al., Nature Physics 8, 557 (2012); P. Seneor, et al., MRS Bulletin 37, 1245 (2012).
[2] B. Dlubak et al., ACS Nano 6, 10930 (2012); R. Weatherup, et al., ACS Nano 6, 9996 (2012).

Modeling the mechanisms for formation of helices and perversions in elastic nanofilaments through molecular dynamics

J.P.T. Lopes[1],
F. Vístulo de Abreu[2,3]
and **Ricardo Simoes**[1,2,4]

rsimoes@dep.uminho.pt
rsimoes@ipca.pt

[1]Institute for Polymers and Composites - IPC/I3N, University of Minho, Campus de Azurém, 4800-058 Guimarães, Portugal,
[2]I3N-Institute for Nanostructures, Nanomodelling and Nanofabrication, Portugal
[3]Department of Physics, University of Aveiro, Portugal
[4]Polytechnic Institute of Cávado and Ave, Campus do IPCA, Barcelos, Portugal

Helices made of elastic filaments have been the target of considerable and growing interest in past years [1-3]. The formation mechanisms for such helices are still not well understood, but recent results have indicated they may be due to buckling instabilities that naturally emerge when primary interactions strength vary asymmetrically across the filament's cross-section. Several different treatments (e.g. thermal, friction or radiation), can induce such asymmetry, which means this can be easily obtained in practice [4-5]. In addition, these effects can be observed on filaments at different length scales; both micro-filaments and nano-filaments also form this sort of structure.

Figure 1. Initial fiber configuration.

Figure 2. Final simulation configuration, exhibiting one perversion (D=5, L/D=100).

Figure 3. Final simulation configuration, exhibiting several perversions (D=3 L/D=200).

In this work, we present coarse-grained molecular dynamics (MD) simulations performed using the LAMMPS (Large-scale Atomic/Molecular Massively Parallel Simulator) platform. We will also discuss in detail how perversions - regions where the helical handedness changes - occur. The simulations show it is possible to replicate the formation of helices and perversions, within certain conditions. Finally, we show how the helical radius can depend on the strength and the asymmetry of the interactions used, the filament's aspect ratio, and the recovery velocity.

The occurrence of a perversion has attracted considerable interest in a number of theoretical works, in which they are shown to occur in the stationary solutions of Kirchoff's equations [6-7]. However, the possibility of creating more than a single perversion has been given much less attention [8]. Understanding and being able to control the formation mechanisms of helices and perversions could enable many different practical applications. As next-generation nano-mechanical systems can be obtained by nano-patterning of soft materials, these simulations can provide importance input for the design of such systems

References

[1] Gerbode S. J., Puzey J. R., McCormick A. G., Mahadevan L., Science, 337 (2012), 1087-1091.

[2] Shariatpanahi S.P., Irajizad A., Abdollahzadeh I., Shirsavar R., Bonn D., Ejtehadi R., Soft Matter, 7 (2011), 10548-10551.

[3] Godinho M.H., Canejo J.P., Feio G., Terentjev E.M., Soft Matter, 6(2010), 5965-5970.

[4] Godinho M.H., Trindade A.C., Figueirinhas J.L., Melo L.V., Brogueira P., Deus, A.M., Teixeira P.I.C., The European Physical Journal E, 21 (2006), 319–330.

[5] Wilson D.K., Kollu T., Textile Progress, 21:3 (1991), 1-42.

[6] McMillen T., Goriely A., Journal of Nonlinear Science, 12 (2002), 241-281.

[7] Goriely A., Nizette M., Journal of Mathematical Physics, 40 (1999), 2830.

[8] Domokos G., Healey T. J., International Journal of Bifurcation and Chaos, 15 (2005), 871.

Observation of the Quantum Hall Effect in Hydrogenated Graphene

T. Szkopek[1]
G. Gervais[1], R. Martel[2] and M. Siaj[3]

[1] McGill University
[2] Université de Montréal
[3] Université du Québec à Montréal,Montréal, Canada

The quantum Hall effect (QHE) is observed in a two-dimensional electron gas formed in millimeter-scale hydrogenated graphene, with a mobility less than 10 cm^2/Vs and corresponding Ioffe-Regel disorder parameter $(k_F\lambda)^{-1}$ ~ 500. Our observations with hydrogenated graphene push the limit of disorder where the QHE can still be attained in a strong magnetic field, suggesting that the QHE might be robust to arbitrarily large disorder. The strongly temperature dependent electrical resistance and high thermal resistance of hydrogenated graphene may further find potential applications in thermometry and bolometry.

Hydrogenated graphene samples were prepared from pristine, large-area, monolayer graphene samples grown by chemical vapour deposition (CVD) on Cu foils. The graphene was controllably hydrogenated by exposure to a beam of atomic hydrogen in a UHV chamber. *In-situ* measurement shows an exponential growth in graphene sheet resistance versus hydrogen dose. We find hydrogenated graphene to exhibit a strong temperature dependent resistance consistent with variable range hopping. We measured the 2-point resistance of hydrogenated graphene at low temperatures in magnetic fields of up to 45T, Fig. 1. A colossal negative magnetoresistance was observed, with a dramatic transition from a highly resistive state of R_{2pt} = 250 h/e^2 at zero field to a quantized resistance R_{2pt} = 12 962Ω at 45T, which is within 0.5% of $h/2e^2$. The quantized resistance corresponds to a QHE state with ν=−2 filling factor, $R_{2pt} \approx |R_{xy}| = h/2e^2$, and R_{xx} = 0. The high field resistance versus charge carrier density is consistent with the opening of an impurity-induced gap in the density of states of graphene. The mean spacing between point defects induced by hydrogenation was estimated to be λ_D = 4.6 ± 0.5 nm via Raman spectroscopy. The rapid collapse of resistance and emergence of a QHE state is observed to occur when the magnetic length $\ell_B = (\hbar/eB)^{1/2}$ is comparable to the mean point defect spacing λ_D. The interplay between electron localization by defect scattering and magnetic confinement in two-dimensional atomic crystals will be discussed. Preliminary work on the application of hydrogenated graphene's electrical and thermal properties to thermometry and bolometry will also be discussed.

This work was made possible with the support of NSERC, FRQNT, the LNCMI (Toulouse) and the NHMFL (Tallahassee).

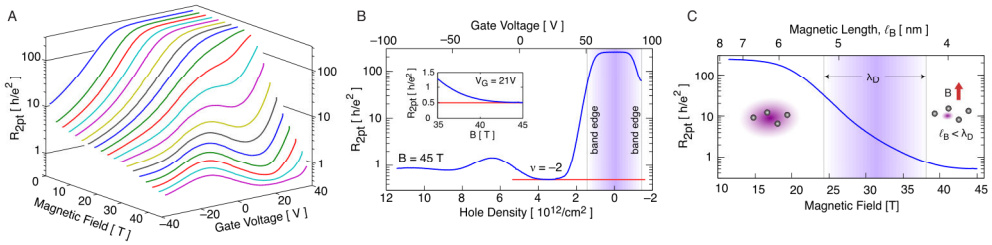

Figure 1. A) The two-point resistance of a hydrogenated graphene sheet versus magnetic field and gate voltage. All data were taken at a temperature of 575±25 mK. B) At 45T, the resistance versus gate voltage and hole density, with the red line indicating a Hall plateau at R2pt = h/2e2. C) Resistance of the hydrogenated graphene versus both the magnetic field B and magnetic length ℓB = (ħ/eB)1/2. The shaded region indicates the estimated point defect spacing extracted from the Raman spectra.

A Reconfigurable Architecture Based on Spin MOSFET

T. Tanamoto
H. Sugiyama, T. Inokuchi, S. Ishikawa, and Y. Saito

Toshiba Corporation, Japan

Spintronics is expected to provide wide variety of application of next generation circuit. Here we present one of promising application of spin MOSFET as Field Programmable Gate Array (FPGA) (spin FPGA). Spin MOSFET is composed of MOSFET whose source and drain are contacted with ferromagnetic materials[1]. Magnetization directions affect current through spin-torque transfer[2]. We model the spin MOSFET by describing a high resistive magnetic state with smaller mobility in SPICE parameters. SRAMs in Look-up table (LUT) and those attached to pass transistors other than multiplexers are replaced by spin MOSFET. This reduces the number of transistors and makes LUT and switching box(SB) smaller resulting in faster and smaller FPGA. Spin FPGA are benchmarked over 20 circuits by modifying VPR[3] with Monte Carlo method. Performance is improved for smaller transistors (Fig.1). For 22nm transistors, area is reduced averagely by 16% and speed (critical path delay) is improved by 24%. As MR ratio increases, operation margin increases, and as transistor size decreases, impedance of wire part increases relatively. These result in better performance of spin FPGA[4].

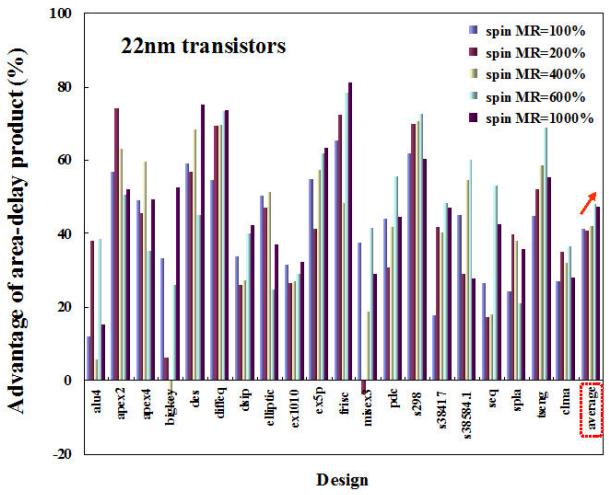

Figure 1. Benchmark calculation of the advantage of spin FPGA over 20 circuits (area-delay product). Leftmost data shows average over 20 circuits. As MR increases, spin FPGA shows better performance.

References

[1] S. Sugahara and M. Tanaka. ACM Transaction on Storage Vol 2 (2006) 197.
[2] T. Marukame, T. Inokuchi, M. Ishikawa, H. Sugiyama and Y. Saito, IEDM 2009-215.
[3] V. Betz, J.Rose and A. Marguardt, “Architecture and CAD for Deep-Submicron FPGAs”, Kluwer Academic Publishers, 1999.
[4] T. Tanamoto, H. Sugiyama, T. Inokuchi, T. Marukame, M. Ishikawa, K. Ikegami and Y. Saito: J. Appl. Phys. 109, 07C312 (2011)

Surface Science studies of FeS_2 for catalytic N_2 reduction

Israel Temprano, Tao Liu, Stephen J. Jenkins, David A. King, Stephen M. Driver

Department of Chemistry, University of Cambridge, UK.

Ammonia synthesis is reckoned to account for over 1% of the world´s consumption of man-made power, driven predominantly by the production of fertilizers and pharmaceuticals [1]. Of all the classic catalytic reactions, ammonia synthesis is arguably the instance for which tuning catalytic efficiency is most urgently required. Intriguingly nitrogenase (found in symbiotic and free-living diazotrophs) catalyses the reduction of nitrogen to ammonia, under ambient conditions, in lively contrast with the energy-consuming industrial Haber-Bosch reaction. Efforts of protein crystallography have gradually unveiled that the active site of nitrogenase is essentially a FeS_x nanocluster, with a central light atom and a Mo atom [2,3].

In the light of the above understanding, we decided to investigate the interaction of N_2, H_2 and NH_3 on the surface of naturally grown single crystal FeS_2{100}. The adsorption of nitrogen species was studied using both background dosing and activated N_2 species directed to the pyrite surface [4]. The synthesis of ammonia from hydrogenation of adsorbed nitrogen species was subsequently studied [5]. The gas-surface interactions were investigated under a wide range of conditions to evaluate the particularities of NH_3 synthesis on pyrite single crystals

References

[1] Schlögl, R. Angewandte Chemie International Edition 2003, 42, 2004-2008.

[2] Spatzal, T.; Aksoyoglu, M. g.; Zhang, L.; Andrade, S. L. A.; Schleicher, E.; Weber, S.; Rees, D. C.; Einsle, O. Science 2011, 334, 940.

[3] Lancaster, K. M.; Roemelt, M.; Ettenhuber, P.; Hu, Y.; Ribbe, M. W.; Neese, F.; Bergmann, U.; DeBeer, S. Science 2011, 334, 974-977.

[4] Liu, T.; Temprano, I.; Jenkins, S. J.; King, D. A.; Driver, S. M. Physical Chemistry Chemical Physics 2012, 14, 11491-11499.

[5] Liu, T.; Temprano, I.; Jenkins, S. J.; King, D. A.; Driver, S. M. The Journal of Physical Chemistry C -In press.

Molecular engineering of graphene, carbon nanomembranes and their heterostructures for nanotechnology applications

Andrey Turchanin

turchanin@physik.uni-bielefeld.de

Faculty of Physics, University of Bielefeld, Universitätsstr. 25, 33615 Bielefeld, Germany

Bottom-up approaches via molecular self-assembly have high potential to facilitate the use of carbon-based free-standing two-dimensional (2D) in nanotechnology. In this talk it will be demonstrated how self-assembled monolayers (SAMs) of aromatic molecules can be employed to this end. By electron or photon irradiation these organic monolayers are converted into dielectric carbon nanomembranes (CNMs) with a thickness of one molecule. CNMs possess their structural integrity and similar to graphene or BN sheets can be separated from their original substrates and transferred onto various other substrates, fabricated as suspended sheets or stacked into multilayer films with precise control over their thickness and atomically sharp boundaries. By annealing CNMs in vacuum or at atmospheric pressure they are converted into graphene. This approach makes possible both scalable production of high-electronic-quality graphene and CNMs as well as direct writing of their nanostructures on various technologically relevant substrates. Layer-by-layer assembly of the CNM/graphene heterostructures opens many doors to the engineering of novel materials for optics, electronics, biofunctional coatings and nanosensors. Physical and chemical properties of these materials, obtained by state-of-the-art spectroscopy, microscopy, electric and magneto-transport measurements, their nanopatterning and functional applications will be presented. Implementation of CNM/graphene heterostructures in novel field-effect devices aiming to improve electronic performance of the integrated graphene sheets (electric-field gating, environmental stability, mobility of the charge carriers) will be shown.

References

[1] D. G. Matei et al.: Adv. Mater. (2013), Functional single-layer graphene sheets from aromatic monolayers, DOI: 10.1002/adma.201300651.

[2] P. Angelova et al.: A universal scheme to convert aromatic molecular monolayers into functional carbon nanomembranes. ACS Nano (2013) accepted.

[3] A. Turchanin and A. Gölzhäuser: Carbon nanomembranes from self-assembled monolayers: Functional surfaces without bulk. Prog. Surf. Sci. 87 (2012) 108-162.

[4] A. Turchanin et al.: Conversion of self-assembled monolayers into nanocrystalline graphene: structure and electric transport. ACS Nano 5 (2011) 3896-3904.

[5] C.T. Nottbohm et al.: Mechanically stacked 1 nm thick carbon nanosheets: Ultrathin layered materials with tunable optical, chemical, structural and electrical properties, Small 7 (2011) 874-883.

[6] Z. Zheng et al.: Janus nanomembranes: A generic platform for chemistry in two dimensions, Angew. Chem. Int. Ed. 49 (2010) 8493-849.

[7] A. Beyer et al.: Fabrication of metal patterns on free-standing graphenoid nanomembranes, J. Vac. Sci. Technol. B 26 (2010) C6D6-C6D10.

[8] A. Turchanin et al.: One nanometer thin carbon nanosheets with tunable conductivity and stiffness. Adv. Mater. 21 (2009) 1233-1237.

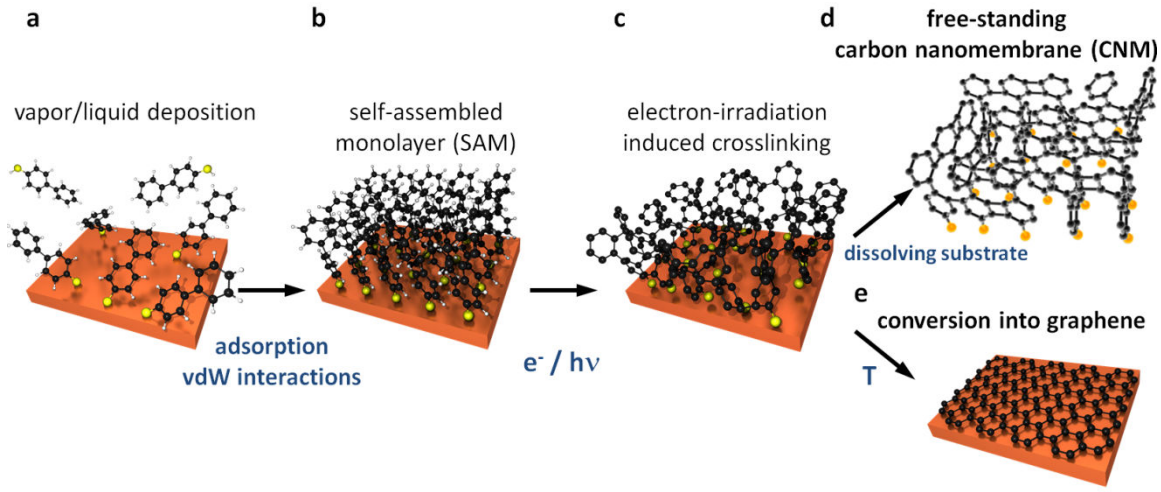

Figure 1. Schematic of the fabrication route to carbon nanomembranes (CNMs) and graphene from aromatic self-assembled monolayers (SAMs): **a**, Deposition of molecules on a substrate; here, vapor deposition of biphenyl-thiols (BPT). **b**, Formation of a SAM. **c**, Electron/photon-irradiation-induced crosslinking of the BPT SAM into a carbon nanomembrane (CNM).**d**, Formation of a free-standing CNM by dissolving the substrate. **e**, Conversion of a CNM into graphene by annealing [1-4, 8].

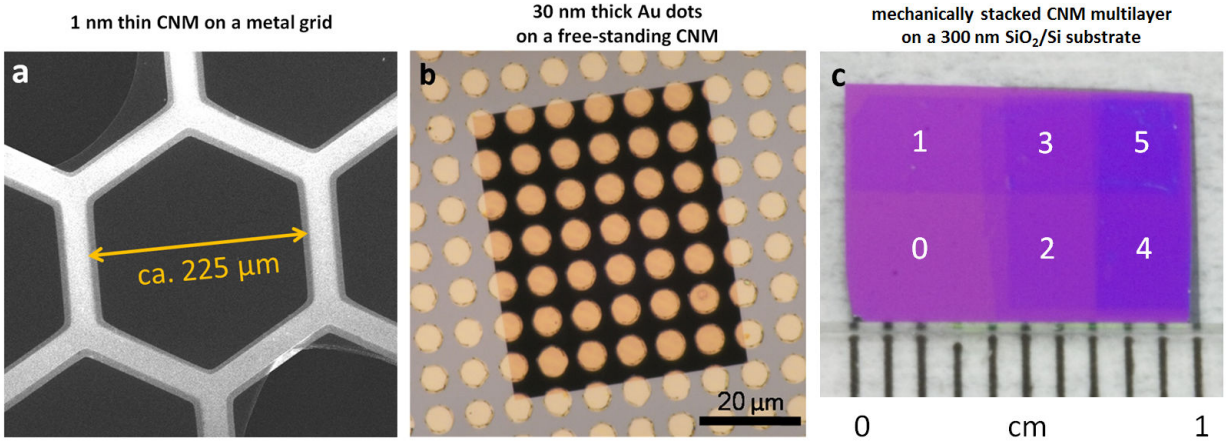

Figure 2. Free-standing CNMs and CNM stacks. a, SEM image of the 1 nm thin free-standing BPT-based CNM on a metal grid. **b**, Optical image of the free-standing CNM with an evaporated metal pattern. **c**, Optical image of the mechanically stacked CNMs on a SiO2/Si wafer (1 to 5 layers) [3, 5, 7-8].

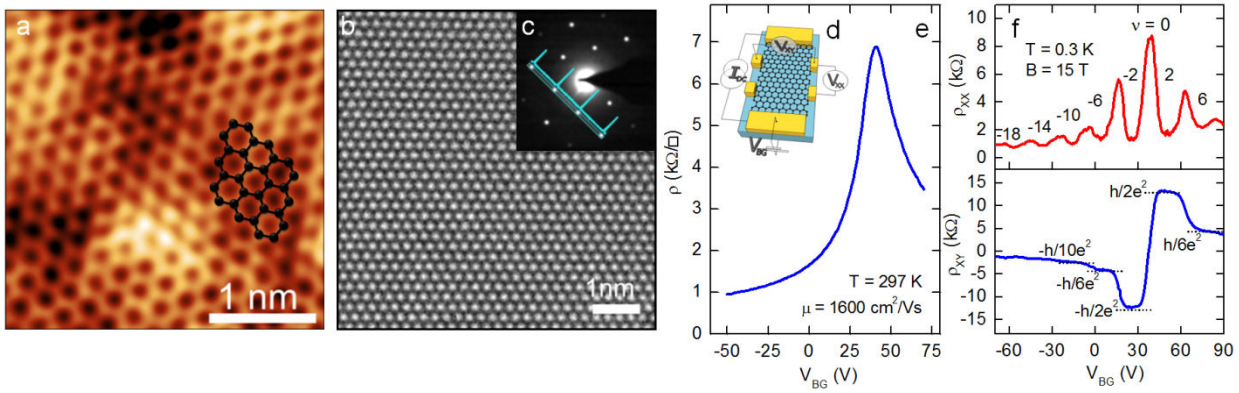

Figure 3. Single-layer graphene (SLG) formed by conversion of biphenyl-thiol SAMs on Cu. a, HR STM image on Cu(111). **b,** HRTEM image and diffraction pattern **(c)** of a free-standing SLG produced from the BPT SAM on a Cu foil and **(d-f)** its electric and electro-magnetic transport properties [1].

Charge Transfer in Carbon Nanotubes-Supported Nanoparticles

Béatrice Vanhorenbeke[1,2], Delphine Bouilly[2], Richard Martel[2,3], Sophie Hermans[1]

[1] Institute of Condensed Matter and Nanosciences (IMCN), Université catholique de Louvain, Place Louis Pasteur 1, 1348 Louvain-la-Neuve, Belgium.
[2] Département de Chimie and ‡Département de Physique, Université de Montréal, C.P. 6128 Succursale Centre-Ville, Montréal QC H3C 3J7, Canada.
[3] Regroupement Québécois sur les Matériaux de Pointe (RQMP)

beatrice.vanhorenbeke@uclouvain.be

Due to their outstanding mechanical and electrical properties, carbon nanotubes (CNTs) are being considered as promising materials in various fields such as electronic, material engineering, sensor design and catalysis. A potential application of carbon nanotubes consists of using them as support of nanoparticles for heterogeneous catalysis.[1] Aiming this, we chose mixed-metal clusters as precursors of bimetallic catalysts from which a synergic effect between constituting metals is expected. Moreover, the size and composition of the activated metallic nanoparticles can be easily controlled by selecting the appropriate starting cluster. More specifically, we synthesized the $[Ru_5PtC(CO)_{14}COD]$ cluster compound as nanoparticle precursor.[2]

As previously reported, interactions between support and precursors are of critical importance in the preparation of heterogeneous catalysts.[3] A chemical modification of the nanotubes allows to introduce anchoring groups on their surfaces. Among the carbon nanotubes covalent functionalization pathways, diazonium salts are widely used as radical reagents. This type of compounds is used for the covalent grafting of phenyl derivatives on the carbon nanotubes surface. Subsequent modification of those grafted moieties allows the bimetallic cluster compound to be anchored securely. In this work, we developed a four-step functionalization pathway of single-walled carbon nanotubes (SWNTs): (i) covalent functionalization of carbon nanotubes by diazonium salt; (ii) derivatization of the functionalized nanotubes in order to anchor a ligand for cluster coordination; (iii) cluster coordination; and eventually (iv) thermal activation (Figure 1). At the end of this process, we obtained 'naked' Ru-Pt nanoparticles of 1-2 nm size supported on carbon nanotubes (Figure 2), which are expected to exhibit catalytic activity.[4].

Those nanoparticles-decorated carbon nanotubes can be used to study the charge transfer between nanotubes and nanoparticles. In order to do this, individual single-walled carbon nanotubes field-effect transistors (SWNT-FETs, Figure 3a) were prepared by dispersion and deposition of SWNTs on n-doped SiO_2/Si, followed by conventional optical lithography and lift-off techniques.[5] These devices were used to measure the electrical response of nanotubes-supported nanoparticles. Drain-source current (Ids) was measured while varying gate voltage (Vg) for pristine-, functionalized- and nanoparticles decorated- carbon nanotubes.

Measurement of functionalized-carbon nanotubes revealed a high loss of conductance (70 to 80 %) compared with pristine-CNTs. This result is due to the covalent nature of the functionalization step, which alters the aromaticity of the nanotube.[6] Modification of the grafted moieties does not change the electrical characteristics, since the tube is not further altered by these steps. During thermal annealing, activated nanoparticles are deposited on the carbon nanotube surface. After this activation step, carbon nanotubes recover about 60 % of their initial conductance. Moreover, these measurements show evidence of a charge transfer from the nanotube to the nanoparticle, as revealed by the p-doping of the carbon nanotubes (Figure 3b). This charge transfer is of significant relevance for catalytic applications, since the nanoparticle can be viewed as an electron sink.

In summary, we have covalently grafted Ru5Pt clusters on single-walled carbon nanotubes. After thermal activation, we obtained bimetallic nanoparticles-decorated carbon nanotubes. Electrical characterization of those nanohybrids revealed a charge transfer between nanoparticles and carbon nanotubes as evidenced by p-doping of CNTs. Those materials are expected to exhibited catalytic activity

References

[1] P. Singh, S. Campidelli, S. Giordani, D. Bonifazi, A. Bianco, M. Prato, Chem. Soc. Rev., 38 (2009) 2214.1300651.

[2] S. Hermans, T. Khimyak, B. F. G. Johnson, J. Chem. Soc. Dalton Trans., (2001) 3295.

[3] C. Willocq, A. Delcorte, S. Hermans, P. Bertrand, M. Devillers, J. Phys. Chem. B, 109 (2005) 9482.

[4] a) R. Raja, T. Khimyak, J. M. Thomas, S. Hermans, B. F. G. Johnson, Angew. Chem. Int. Ed., 40 (2001) 4638; b) Y.-L. Yao, Y. Ding, L.-S. Ye, X.-H. Xia, Carbon, 44 (2006) 61; c) J. Li, Y. Liang, Q. Liao, X. Zhu, X. Tian, Electrochim. Acta, 54 (2009) 1277.

[5] a) R. Martel, T. Schmidt, H. R. Shea, T. Hertel, Ph. Avouris, Appl. Phys. Lett., 17 (1998) 2447;b) S. J. Tans, A. R. M. Verschueren, C. Dekker, Nature, (1998) 49.

[6] J. Cabana, R. Martel, J. Am. Chem. Soc., (2007) 2244.

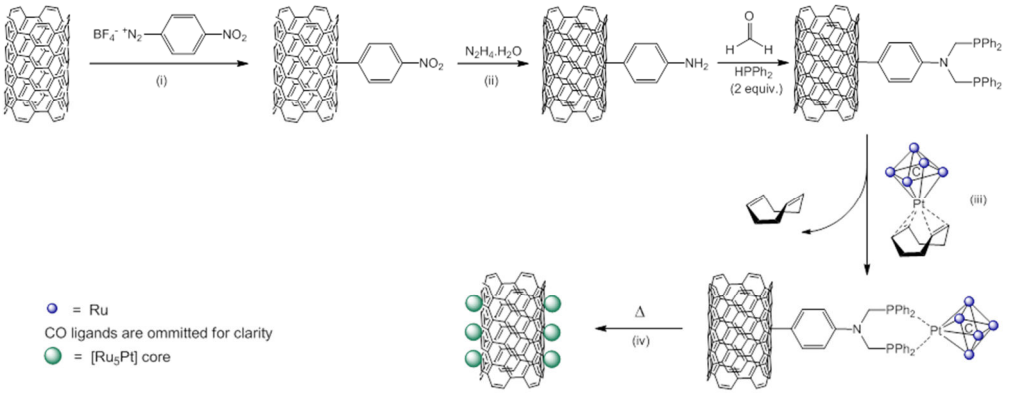

Figure 1. Reaction scheme of the functionalization pathway developed for the formation of [Ru5Pt] nanoparticles on carbon nanotubes.

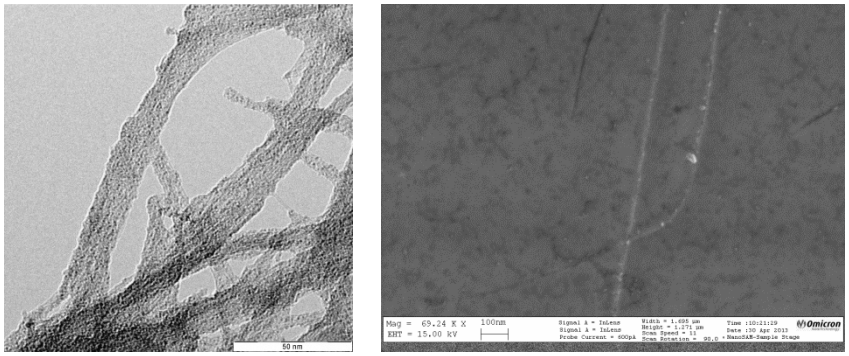

(a) (b)

Figure 2. (a) TEM image of SWNTs supported nanoparticles; (b) HR-SEM image of Si-supported nanoparticles-decorated SWNTs.

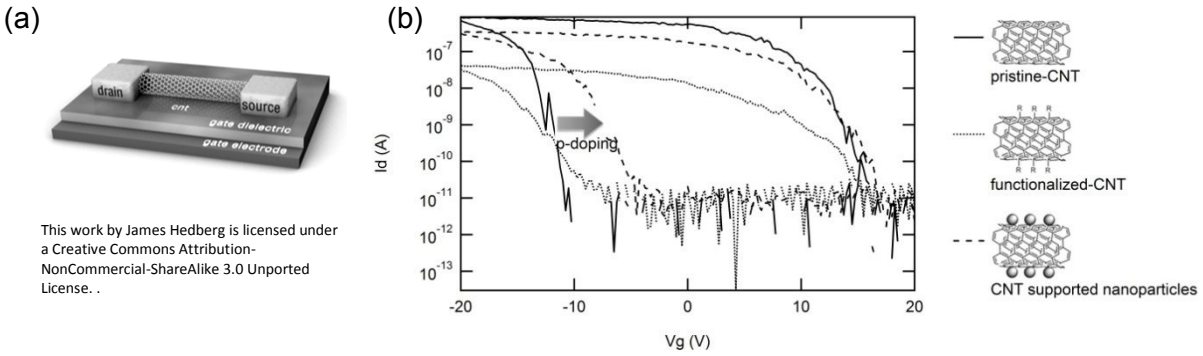

Figure 3. (a) Schematic representation of a CNT-FET; (b) Charge transfer in carbon nanotubes supported nanoparticles.

Responsive polymersomes and nanocapsules as robust and tunable carrier systems

Brigitte Voit[1,2]
Dietmar Appelhans[1],
Jens Gaitzsch[1,2],
David Gräfe[1,2] and
Xin Huang[1]

voit@ipfdd.de

[1] Leibniz-Institut für Polymerforschung Dresden e.V., Hohe Strasse 6, D-01069 Dresden, Germany
[2] Technische Universität Dresden, Organische Chemie der Polymere, D-01062 Dresden, Germany

In the recent years organic nanoparticles based on synthetic macromolecules have found significant interest especially in the area of biotechnology, biomedicine and synthetic biology as various carrier molecules. This comprises core-shell and hydrogel nanoparticles, dendritic structures, defined aggregates as well as polymersomes and polymeric (hollow) nanocapsules.1-4 For defined up-take and release as well as for use as bionanoreactors, responsiveness has to be introduced into the various nanocarriers. Here we would like to present different synthetic strategies for the preparation of responsive nanocarriers. Synthetic details can be found in the references.5-7

We prepared in one strategy UV-crosslinkable polymersomes based on the self-assembly of amphiphilic block copolymers. We combined this cross-linking with a well-known pH sensitive polymer to give a highly stable polymersome with strictly controlled trans-membrane diffusion by reversible pH switches. Polyethylenglycole (PEG) was used as a biostable hydrophilic block, which is combined with the pH sensitive polydiethylaminoethyl-methacrylate (PDEAM) and photocross-linkable poly-dimethyl-maleic imidobutyl methacrylate (PDMIBM) as hydrophobic components (Scheme 1)5. The content of the PDMIBM is high enough to provide effective cross-linking after 30 s of UV irradiation, while the pH sensitivity remains. While pH sensitive polymersomes usually disassemble upon acidification, ours show a definite swelling, since the cross-linked membrane remains intact. This swelling is reversible as well as reproducible, indicating a highly stable cross-linking. These vesicles provide a very good basis for a synthetic bionanoreactor. While the membrane is not open for diffusion traffic in the basic state, small molecules are able to diffuse inside in an acidic state. Thus, cascade enzyme reactions could be carried out under pH control using polymersome-encapsulated enzymes in a one-pot arrangement (Scheme 2).

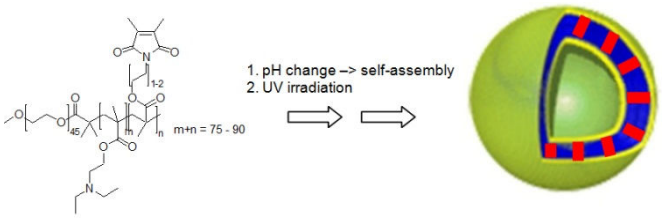

Scheme 1. Block copolymer structure forming photo-crosslinkable polymersomes.

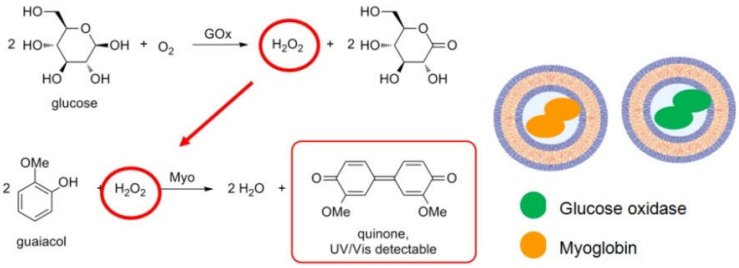

Scheme 2. pH controlled cascade enzyme reaction carried out by polymersome enclosed enzymes glucose oxidase and myoglobin.

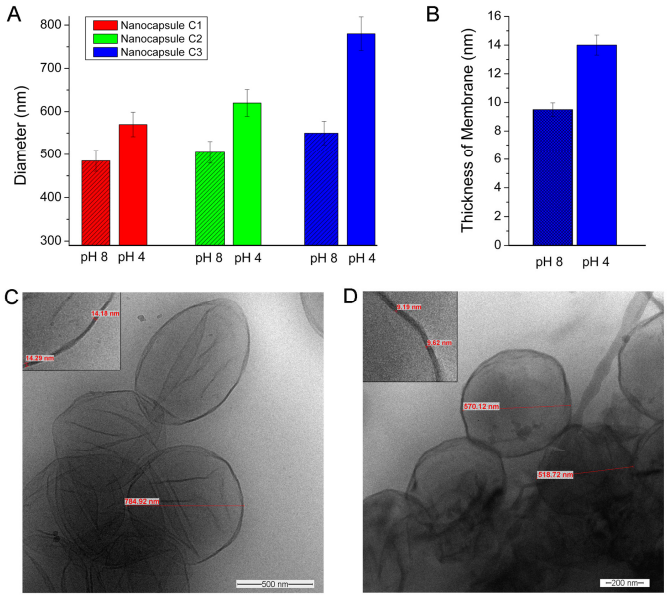

Figure 1. (A) diameter of nanocapsules C1 to C3 (by the template method using three different crosslinker) in pH 4.0 and 8.0 buffer solution, respectively, measured by DLS, (B) thickness of the membrane of nanocapsules C3 at pH 4.0 and pH 8.0, (C) and (D) Cryo-TEM images of nanocapsules C3 in pH 4.0 and pH 8.0 solution.

References

[1] Blanazs, A.; Armes, S.P.; Ryan, A.J. Macromol. Rapid Commun. 2009, 30, 267.

[2] Hendrickson, G.R.; Smith, M.H.; South, A.B.; Lyon, L.A. Adv. Funct. Mater. 2010, 20, 1697.

[3] Wang, Y.; Angelatos, A.S.; Caruso, F. Chemistry of Materials 2007, 20, 848-858. C.

[4] van Hest, J.C.M.; Kim, K.T.; Zhu, J.H.; Meeuwissen, S.A.; Cornelissen, J.J.L.M.; Pochan, D.J.; Nolte, R.J.M. J. Am. Chem. Soc. 2010, 132, 12522.

[5] Gaitzsch, J.; Appelhans, D.; Grafe, D.; Schwille, P.; Voit, B. Chem. Commun. 2011, 47, 3466.

[6] Gaitzsch, J.; Appelhans, D.; Wang, L.; Battaglia, G.; Voit, B. Angew. Chem. 2012, 51, 4448.

[7] Huang, X.; Appelhans, D.; Formanek, P.; Simon, F.; Voit, B. Macromolecules 2011, 44, 8351. [8] Huang, X.; Appelhans, D.; Formanek, P.; Voit, B, ACS Nano 2012, 6, 9718.

Absorption engineering in stacked Au-SiO_2-Pd nanostructures

Carl Wadell,
Tomasz J. Antosiewicz and Christoph Langhammer

Department of Applied Physics, Chalmers University of Technology, SE-412 96 Göteborg, Sweden

carl.wadell@chalmers.se

Nonradiative decay of localized surface plasmon resonance (LSPR), i.e. *absorption,* leads to the formation of energetic electron-hole pairs and, if not otherwise utilized, subsequent decay into heat. In a photocatalysis application such energetic electrons can be used to enhance a chemical reaction on the surface of the plasmonic nanoparticle [1]. This concept has been demonstrated in a number of studies but is to date focused entirely on Au or Ag particles, owing to their favourable plasmonic properties. This greatly limits the number of possible reactions since Ag and Au surfaces are catalytically not very active (exceptions exist). Other classical metals in catalysis with high activity, e.g. palladium (Pd), have not been considered since they show rather weak LSPR in the UV-visible spectral range [2], due to a strong presence of interband transitions.

In this work [3, 4] we combine the strong LSPR of Au with a more catalytically active metal, Pd, in order to "make use of the best from both worlds" by exploiting a novel *generic absorption engineering strategy*. Our model structure, to demonstrate the effect, is a stack consisting of Au and Pd nanodisks separated by a SiO_2 spacer layer, see Fig. 1. As we show, by varying the spacer layer thickness, the coupling strength between the plasmonic excitations in the Au and Pd disks can be tailored and the dissipation of the absorbed energy *locally* optimized in the structure.

For our experiments amorphous arrays of Au-SiO_2-Pd sandwich structures with various spacer thicknesses are fabricated using hole-mask colloidal lithography [5]. Their optical properties are evaluated using a spectrophotometer with integrating sphere detector, allowing for both extinction and absorption measurements. The experimental data are compared to electrodynamic simulations obtained using the FDTD method and analyzed qualitatively by an analytical coupled-oscillator/dipole model. In our analysis we put particular focus on "dissecting" the structure to identify *where* in the stack light absorption is taking place.

As the main result of our study we find that the local light absorption in the Pd in the stack arrangement is significantly enhanced. Assuming a flat light intensity profile and integrating the total light absorption in the range 400 – 900 nm we find an enhancement of ca. two. For a specific wavelength the maximum absorption enhancement is six-fold. We attribute this novel effect of *absorption enhancement*, in a mechanistic picture, to the fact that the Au disk in the stack is an efficient antenna, which captures energy from the incoming light. Due to the coupling and the specific damping mechanisms in the Au and Pd disks this energy is dissipated predominantly in the Pd disk.

We argue that our absorption engineering concept constitutes a general blueprint for optimization of light absorption in heterometallic plasmonic structures. As the key feature one element in such a structure is an efficient plasmonic antenna; such as Au, Ag or Al; and the other one is "lossy", i.e. features interband transitions in the visible range; such as Pd, Pt, Ni, Ru, Re, Co, or Fe. We predict that this novel concept will facilitate LSPR-enhanced chemical reactions on a wide range of metal catalysts beyond Au or Ag.

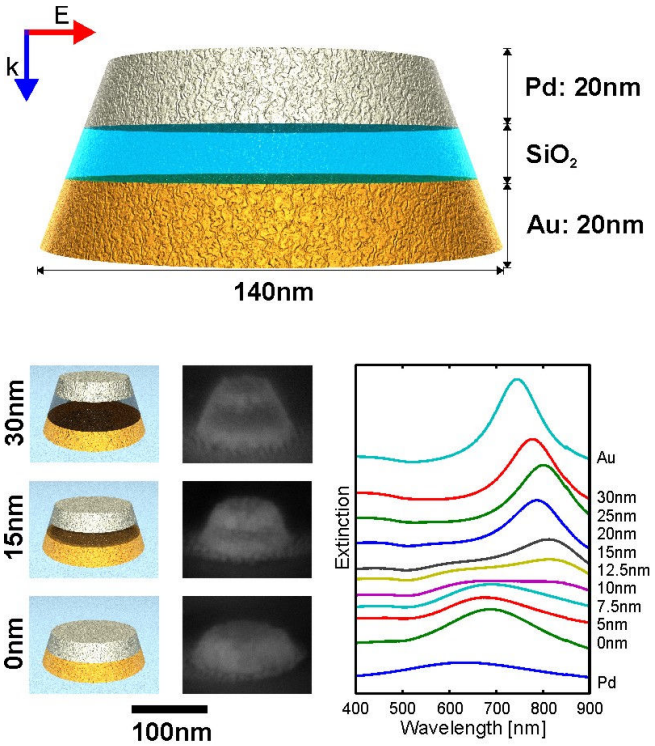

Figure 1. Sketch of the Au-SiO_2-Pd structures used in this work. Also shown are extinction spectra for structures with different spacer thicknesses, as well as for the individual Au and Pd disks. Figure from [3].

References

[1] S. Linic et al., Nat. Mater. 10 (2011) 911.
[2] C. Langhammer et al., J. Chem. Phys. 126 (2007) 194702.
[3] C. Wadell et al., Nano Lett. 12 (2012) 4784.
[4] T.J. Antosiewicz et al., J. Phys. Chem. C 116 (2012) 20522.
[5] H. Fredriksson et al., Adv. Mater. 19 (2007) 4297.

Nanogenerators as new energy technology and piezotronics for functional systems

Zhong Lin Wang[1,2]

zlwang@gatech.edu

[1] School of Materials Science and Engineering, Georgia Institute of Technology, Atlanta USA
[2] Beijing Institute of Nanoenergy and Nanosystems, Chinese Academy of Sciences, Beijing

Developing wireless nanodevices and nanosystems is of critical importance for sensing, medical science, environmental/infrastructure monitoring, defense technology and even personal electronics. It is highly desirable for wireless devices to be self-powered without using battery. Nanogenerators (NGs) have been developed based on piezoelectric, trioboelectric and pyroelectric effect, aiming at building self-sufficient power sources for mico/nano-systems. The output of the nanogenerators now is high enough to drive a wireless sensor system and charge a battery for a cell phone, and they are becoming a vital technology for sustainable, independent and maintenance free operation of micro/nano-systems and mobile/portable electronics. This talk will focus on the fundamentals and novel applications of NGs.

For Wurtzite and zinc blend structures that have non-central symmetry, such as ZnO, GaN and InN, a piezoelectric potential (piezopotential) is created in the crystal by applying a strain. Such piezopotential can serve as a "gate" voltage that can effectively tune/control the charge transport across an interface/junction; electronics fabricated based on such a mechanism is coined as piezotronics, with applications in force/pressure triggered/controlled electronic devices, sensors, logic units and memory. By using the piezotronic effect, we show that the optoelectronc devices fabricated using wurtzite materials can have superior performance as solar cell, photon detector and light emitting diode. Piezotronics is likely to serve as a "mechanosensation" for directly interfacing biomechanical action with silicon based technology and active flexible electronics. This lecture will focus on the fundamental science and novel applications of piezotronics in sensors, touch pad technology, functional devices and energy science

References

[1] "Nanogenerators for self-powered systems", http://hdl.handle.net/1853/39262.
[2] "Piezotronics and Piezo-phototronics", Z.L. Wang, Springer, 2013.

Negative Optical Force: Tractor Beam, Light Escalator, and Interface

Cheng-Wei Qiu

Department of Electrical and Computer Engineering, National University of Singapore, 4 Engineering Drive 3, Republic of Singapore 117576

Recently tractor beam which can pull the object has been receiving intensive attention. In this presentation, we will first unveil the fundamental physics and origin of the general pulling force by using multiple beams and even a single gradientless beam. Nevertheless that cannot be called a “tractor beam” per se, as long as the light pulling effect is ultrasensitive to the object’s material and size, a perturbation of which will ruin pulling effect. We therefore investigate the universality condition for Bessel beam to be a material-independent and size-independent tractor beam in dipolar regime. These universal pulling effects and conditions are discussed in association with insight on modified far-field scattering, scattering resonances, and induced polarizabilities. It is still too stringent to achieve pulling light with nonparaxial Bessel beam in practice. Hence we propose another schematic to transform normal plane waves into a light escalator, which can change the sign of the optical force on the object and gear it up and down using light. A non-magnetic levitating “train” can thus be possible then like Fig.1. A liquid interface is also presented and experimentally verified to be efficient to make a plane wave into a “tractor beam” based on linear photon momentum transfer

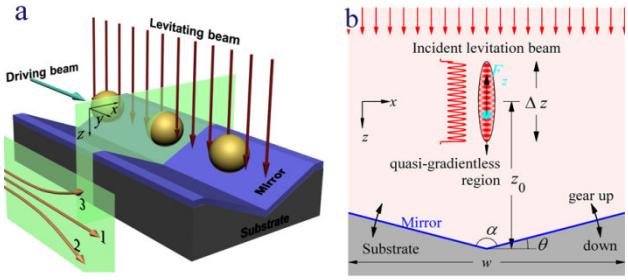

Figure 1. Telescope-based escalator (a) and its levitating/descending region (b).

Nanomechanical Membrane-type Surface Stress Sensor

Genki Yoshikawa

World Premier International (WPI) Research Center, International Center for Materials Nanoarchitectonics (MANA), National Institute for Materials Science (NIMS), 1-1 Namiki, Tsukuba, Ibaraki 305-0044, Japan

YOSHIKAWA.Genki@nims.go.jp

The demands for new sensors are rapidly growing in various fields; medicine (e.g. rapid detection of biomarkers at the very early stage or non-invasive diagnostics by breath), security (e.g. detection of drugs, explosives, and land mines), and environment (e.g. monitoring of pollution in air, soil, water, and indoor). Nanomechanical sensors have potential to contribute to these global demands owing to their intrinsic versatility—detecting fundamental parameters, such as "volume" or "mass". Since all molecules have "volume" and "mass", nanomechanical transduction of them into detectable signals can realize label-free and real-time measurements of virtually any kind of target specimen. Based on the newly developed platform "Membrane-type Surface stress Sensor (MSS)" (Fig. 1) [1], we are now trying to realize useful nanomechanical sensors which can fulfill the practical requirements, such as portability, low-cost, ease of use, in addition to the basic specifications e.g. high sensitivity.

To demonstrate the capability of MSS for the multi-dimensional array, we fabricated the second generation MSS (2G-MSS) with a two dimensional array (Fig. 2. (a)) [2]. In addition, the implementation of various modifications in design and microfabrication led to further enhancement of sensitivity, reaching a limit of detection of ~0.1 mN/m, which is even better than that of common optical read-out cantilever sensors (0.15~0.90 mN/m) [2].

For practical applications, one of the major issues of nanomechanical sensors is the difficulty in coating receptor layers on their surface to which target molecules adsorb or react [3]. The MSS also provides an effective solution to this coating issue by means of double-side coating [4]. While a cantilever-type sensor requires a single-side coating to have measurable deflection, MSS has been found to yield reasonable signals even with double-side coatings, allowing almost any kind of coating technique, including dip-coating methods. As the double-side coating is compatible with batch protocols, such as dip coating, the double-side-coated MSS represents a new paradigm of "one-chip-one-channel (channels on a chip are all coated with the same receptor layers)" shifting from the conventional "one-chip-multiple-channel (channels on a chip are coated with different receptor layers)" paradigm [4].

As for the measurement system, the latest version of the MSS setup can be operated all by USB-connected/powered devices. This setup provides an opportunity for anybody to start nanomechanical sensing with high sensitivity and stability, including the coating of MSS chips by e.g. simple hand-operated dip-coating.

References

[1] G. Yoshikawa, T. Akiyama, S. Gautsch, P. Vettiger, and H. Rohrer, Nano Lett. 11, 1044 (2011).
[2] G. Yoshikawa et al. Sensors 12, 15873 (2012).
[3] G. Yoshikawa, Appl. Phys. Lett. 98, 173502 (2011).
[4] G. Yoshikawa et al. Langmuir (2013) published online DOI: 10.1021/la3046719.

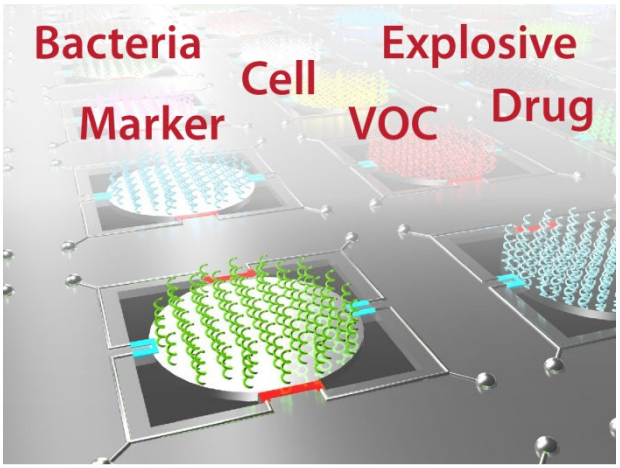

Figure 1. Membrane-type Surface stress Sensor (MSS) in array and the examples of possible targets.

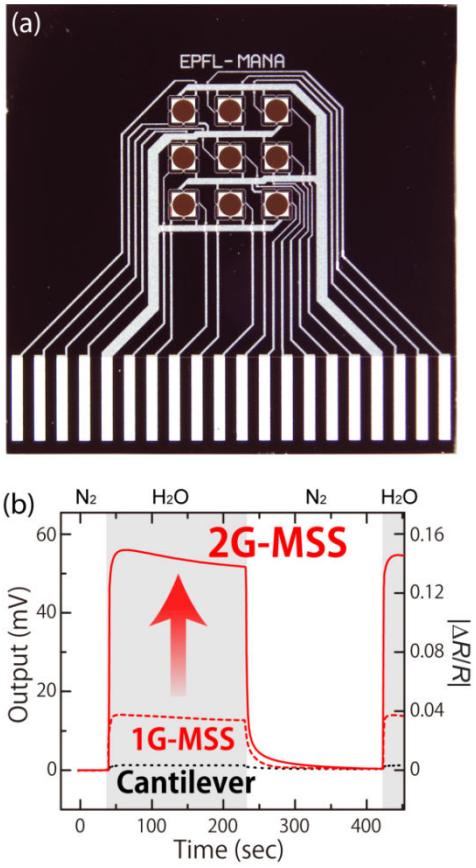

Figure 2: (a) Photograph of the fabricated 2G-MSS chip with a 2D array. (b) Obtained output signals from each sensor.

(001)-oriented anatase TiO_2 nanosheets as a photoanode material for dye-sensitized solar cell

Marketa Zukalova[1]
Barbora Laskova[1], Ladislav Kavan[1], Paul Liska[2], Jacques E. Moser[3] and Michael Grätzel[2]

marketa.zukalova@jh-inst.cas.cz

[1] J. Heyrovský Institute of Physical Chemistry, v.v.i., Academy of Sciences of the Czech Republic,Dolejškova 3, CZ-18223 Prague 8, Czech Republic
[2] Laboratory of Photonics and Interfaces, Institute of Chemical Sciences and Engineering, Swiss Federal Institute of Technology, CH-1015 Lausanne, Switzerland
[3] Photochemical Dynamics Group, Institute of Chemical Sciences and Engineering, Swiss FederalInstitute of Technology, 1015 Lausanne, Switzerland

Dye-sensitized solar cell (DSC) is one of the most promising photovoltaic technologies for production of renewable, clean, and affordable energy [1]. Since its invention by Graetzel et al. in 1985 [Ref. 2] it has been permanent subject of interest of research teams all over the world. One of the key issues in optimization of the Graetzel cells consists in the morphological engineering of the TiO2 photoanode. High surface area and crystallinity predetermine nanocrystalline TiO2 to work effectively as photoanode in DSC [3]. Among others, an increase of the open-circuit voltage (UOC) of DSC via tuning of the photoanode material is a pathway towards an improvement of the device performance. (001)-oriented anatase exhibits enhanced Li insertion activity [4] as compared to (101)-oriented one due to synergic contributions of faster interfacial charge transfer and facile Li transport within a more open structure of the anatase lattice. Since material and structural requirements for both Li insertion electrode and DSC photoanode are similar and charge transport in the anatase skeleton controls the overall efficiency of both processes, the performance of “reactive” (001)-oriented anatase photoanode in DSC was examined [5]. Although the (001) face adsorbed a smaller amount of the used dye sensitizer (C101), it provided a larger open-circuit voltage of the solar cell. The negative shift of flatband potential is suggested to be responsible for the observed enhancement of UOC.

Acknowledgment. Financial support of the Grant Agency of the Czech Republic (P108/12/0814) is gratefully acknowledged.

References

[1] K. Kalyanasundaram, Ed., Dye-Sensitized Solar Cells, CRC Press Taylor & Francis, Boca Raton 2010, pp. 45-81.
[2] J.Desilvestro, M.Grätzel, L.Kavan, J.Moser and J.Augustynski, J.Am.Chem.Soc., 107 (1985), 2988.
[3] Kavan L (2012) Chem Rec 12:131–142.
[4] Bousa M, Laskova B, Zukalova M, Prochazka J., Chou A., Kavan L., J. Electrochem. Soc., 157 (2010)(10), A1108-A1112.
[5] Laskova B., Zukalova M., Kavan L., et al., J Solid State Electrochem.,16 (2012):2993–3001.

Future Applications of Graphene

Amaia Zurutuza

Graphenea S.A.
Donostia-San Sebastian, E-20018, Spain
www.graphenea.com

Graphene has emerged as a new material with a very bright future. It is predicted that it could be applied in many different fields ranging from energy, electronics, optoelectronics, aerospace, lighting, and up to biotechnology to mention a few. Some of these applications will be covered during this talk such as the use of graphene in future light harvesting devices [1], optical transistors [2], organic light emitting diodes and flexible batteries [3].

However, unique properties are not the only requirement that has to be fulfilled in order to be successful in the marketplace [4]. There are other important factors that have to be taken into consideration such as the availability of suitable industrial production methods, market readiness/awareness, industrial readiness of value chains, an effective technological progress, etc. Therefore, I will also try to shed some light into the industrial future of this material.

References

[1] J. Tielrooij, J. C. W. Song, S. A. Jensen, A. Centeno, A. Pesquera, A. Zurutuza Elorza, M. Bonn, L. S. Levitov, and F. H. L. Koppens, Nature Physics, 248 (2013).

[2] J. Chen, M. Badioli, P. Alonso-González, S. Thongrattanasiri, F. Huth, J. Osmond, M. Spasenović, A. Centeno, A. Pesquera, P. Godignon, A. Zurutuza Elorza, N. Camara, F. J. García de Abajo, R. Hillenbrand, and F. H. L. Koppens, Nature 487, 77 (2012).

[3] D. Wei, S. Haque, A. Piers, J. Kivioja, T. Ryhänen, A. Pesquera, A. Centeno, B.Alonso, A. Chuvilin, and A. Zurutuza, Journal of Materials Chemistry A 1, 3177 (2013).

[4] H. Alcalde, J. de la Fuente, B. Kamp and A. Zurutuza, Proceedings of the IEEE 101, 1793 (2013).

Evokinetics: A software tool for the analysis of CVD growth of novel 2D materials?

Miguel A. Gosalvez

Center of Materials Physics (CSIC-UPV/EHU)
Donostia - San Sebastián, Gipuzkoa, Spain

Planar synthesis technologies, such as Chemical Vapor Deposition (CVD), are currently attracting increasing attention as an alternative to mechanical exfoliation in order to supply a complete, new generation of atom-thick materials, including semi-metals (graphene, $NiTe_2$, VSe_2,...), semiconductors (WS_2, WSe_2, MoS_2, $MoSe_2$, $MoTe_2$, TaS_2, $RhTe_2$, $PdTe_2$,...), insulators (hexagonal-BN, HfS_2,...), superconductors (NbS_2, $NbSe_2$, $NbTe_2$, $TaSe_2$,...) and topological insulators (Bi_2Se_3, Bi_2Te_3, Sb_2Te_3). During CVD growth, however, many flakes of the 2D material are nucleated at different locations, leading to the formation of a polycrystalline 2D sample, characterized by the presence of numerous grain boundaries, which deteriorate the electronic, thermal and mechanical properties of the material. Therefore, control over the actual shape and size of the flakes before coalescing is essential in order to enable tailor production and quality management of the grown 2D materials by both researchers and CVD synthesis industries.

By showing that the shape and size of the flakes are dominated by the relative kinetics of different atomistic processes, such as adsorption, desorption, dissociation, nucleation, terrace/perimeter diffusion, etc..., the talk presents the idea that a software tool can possibly be used in the near future in order to analyze the atomistic kinetics by directly extracting information from microscopy images of the surface morphology during growth. Refered to as Evokinetics, we show that the approach, is able to describe the activation energies of the various atomistic processes, simultaneously providing clear information about which atomistic processes are relevant (i.e. active) and which are accessory, implicitly describing the effect of temperature, partial pressures, inlet fluxes and other experimental parameters.

This autonomous determination of the kinetic competition between atomistic processes can possibly be performed in a wide range of fields, including heterogeneous catalysis, chemical synthesis, wet etching and epitaxial growth. In the same way as researchers currently may try to optimize manually surface-mediated processes by varying the experimental conditions, measuring total yields and analyzing morphology images, Evokinetics offers the possibility to automatize and speed up such a search while making it completely objective. In this manner, Evokinetics may perhaps be used in the future in order to accelerate/optimize the setup/development of CVD equipment for the synthesis of novel 2D materials.

graphene 2014

May 06-09, 2014
Toulouse (France)
www.graphene2014.com

graphene
International Conference

PHANTOMS foundation
UCL Université catholique de Louvain
ICN2 Institut Català de Nanociència i Nanotecnologia
cnrs